Synthesising Complex Chiral Amines Through Resolution-Racemisation-Recycle

Nisha Pooja Becherlal Pokar

Submitted in accordance with the requirements for the degree of Doctor of Philosophy

The University of Leeds

School of Chemistry

September 2022

Acknowledgements

Abstract

Chiral amines building blocks are present in 40% of pharmaceuticals, though synthesis remains a challenge. Traditional methods involving kinetic resolution and diastereomeric crystallisation are limited by low maximum yields (50%) which lead to costly and wasteful disposal of unwanted enantiomers. Coupling of in *situ* racemisation of undesired enantiomers can increase theoretical yield to 100%, although harsh conditions required for racemisations are incompatible with relatively mild conditions required for resolution.

The Resolution-Racemisation-Recycle (R^3) process overcomes the traditional limitations of diastereomeric crystallisation through spatial separation of resolution and racemisation steps. The diastereomeric resolution is conducted at optimal crystallisation temperatures (room temperature and below) and the racemisation at elevated temperatures (80 ºC). The process employs a continuous flow set-up coupling a continuously-stirred tank reactor (CSTR) for crystallisation and packed-bed reactor (PBR) containing immobilised iridium-based racemisation catalyst. Investigation of each process independently is required prior to coupling the two. Successful epimerisation conditions for a novel amino acid ester salt were demonstrated, and investigation of a mixture of sertraline diastereomers under unoptimised R^3 conditions generated solid, of which 75% was sertraline.

The mechanism of chiral amine racemisation using homogeneous iodo-iridium complex $[IrCp*I_2]_2$ was explored *on-line* using flowNMR, allowing real-time reaction monitoring. Coupled with mass spectrometry data, an iridium-hydride intermediate validating the originally proposed inner-sphere mechanism was observed. Triply bridged mono, di and trihydride dinuclear iridium intermediates were evidence through mass spectrometry, believed to be off-cycle species. An updated mechanistic cycle was proposed.

Exploration of amine racemisation is often impeded by the need for analytical methods and enantiopure amine. Development of a hydrogen borrowing methodology, involving hydrogen-deuterium exchange, allowed circumvention of these issues. Iridium-catalysed generation of an imine or enamine intermediate followed by re-hydrogenation, or racemisation, with deuterium was investigated using ^1H NMR and mass spectrometry. The integration decrease at α-chiral and adjacent β-centres, coupled with narrow isotopologue distribution patterns with sufficient mass difference to the non-deuterated amine was demonstrated for a number of pharmaceutically complex chiral amines.

List of Abbreviations

AS3PC	Auto-Seeded Polythermic Programmed Preferential Crystallisation
ASPreCISE	Auto-Seeded Preferential Crystallisation Induced by Solvent Evaporation
ATR	Attenuated Total Reflection
CALB	Candida Antarctica lipase B
CD	Cyclodextrin
Cee	Crystal enantiomeric excess
CIDT	Crystallisation Induced Diastereomeric Transformation
Cp	Cyclopentadienyl complex
Cp*	Pentamethylcyclopentadiene
CSP	Chiral Stationary Phase
CSTR	Continuous stirred-tank reactor
CTR	Continuous Tubular Crystalliser
DBTA	Dibenzoyl-L-tartaric acid
DCM	Dichloromethane
DKR	Dynamic Kinetic Resolution
DMF	Dimethylformamide
DTTA	Di-p-toluyl-tartaric acid
Ee	Enantiomeric excess
ESI	Electrospray Ionisation
FT-IR	Fourier Transform-Infra Red
GC	Gas Chromatography
GMP	Good Manufacturing Practice
HPLC	High Performance Liquid Chromatography
HRMS	High-resolution mass spectrometry
I.D.	Inner diameter
IPA	Isopropyl alcohol
IPAc	Isopropyl acetate

IR	Infrared
KR	Kinetic Resolution
LAH	Lithium Aluminium Hydride
MA	Mandelic acid
ML	Mother liquor
MSMPR	Mixed-Suspension Mixed-Product Removal
MTBE	Methyl tert-butyl ether
O.D.	Outer diameter
PBR	Packed-bed reactor
PFR	Plug Flow Continuous Crystalliser
PTFE	Polytetrafluoroethylene
Rpm	Revolutions per minute
SIPC	Seed Isothermal Preferential Crystallisation
SMB	Simulated Moving Bed
SOAT	Second-Order Asymmetric Transformation
TMB	True Moving Bed
TMB	1,3,5-trimethoxybenzene
TOF	Turnover frequency

Table of Contents

1 Introduction

1.1 Chiral Amines in Organic Chemistry

Chirality is used to describe molecules which are non-superimposable on their mirror image, Figure 1.1. Chiral molecules are commonly a result of 4 unique substituents attached to an asymmetric, or chiral carbon centre. The resultant non-identical mirror images are referred to as enantiomers.
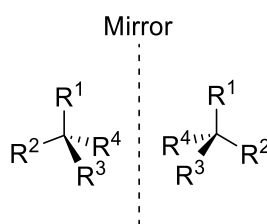
Figure 1.1. Non-superimposable mirror images

Chiral amines are the result of a nitrogen atom with a neighbouring (or α) stereogenic carbon atom. The nitrogen atom can be primary, secondary, tertiary or quaternary. By necessity, the stereogenic carbon can only be secondary or tertiary, Figure 1.2.[1]
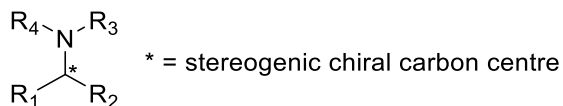
Figure 1.2. The general structure of a chiral amine.

1.1.1 Importance

There are many cases in which the importance of synthesising enantiomerically pure chiral amines has been emphasised. Possibly the most infamous example is that of thalidomide, Figure 1.3, which was sold as a racemic mixture in the 1960s. Whilst the *(R)*-enantiomer possessed a sedative effect in parturient women, the *(S)*-enantiomer had teratogenic effects which resulted in birth defects. Due to this disaster, the targeted manufacture of one stereoisomer was introduced as a strict requirement in 1992 by the US Food and Drug Administration (FDA).[2]

R-Thalidomide
(sedative)

S-Thalidomide
(teratogenic)
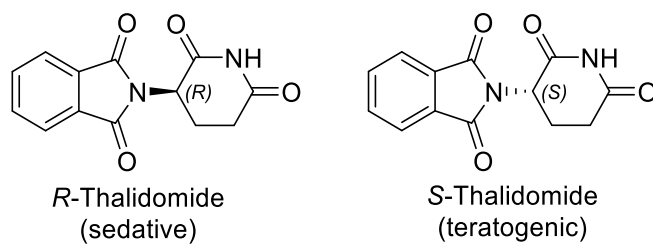
Figure 1.3. The (R)- and (S)-enantiomers of thalidomide with a tertiary amine chiral centre.

The different biological responses produced by each thalidomide enantiomer is one of many examples of chiral amine mixtures which would otherwise have a catastrophic effect if sold as a racemic mixture. An example of a chiral secondary amine is ethambutol, the D enantiomer of which has anti-tuberculosis properties, whereas L-ethambutol has been shown to cause blindness. L-DOPA, a chiral primary amine used against Parkinson's disease, has an isomer which reduces white blood cell levels leading to infection susceptibility.[3] This is summarised in Figure 1.4. For these reasons, the synthesis of enantiopure drug molecules is vital for controlling the number of side effects a patient may experience.

D-Ethambutol
(anti-tuberculosis)

L-Ethambutol
(causes blindness)

L-DOPA
(Parkinson's disease drug)

D-DOPA
(cause of white blood cell deficiency)
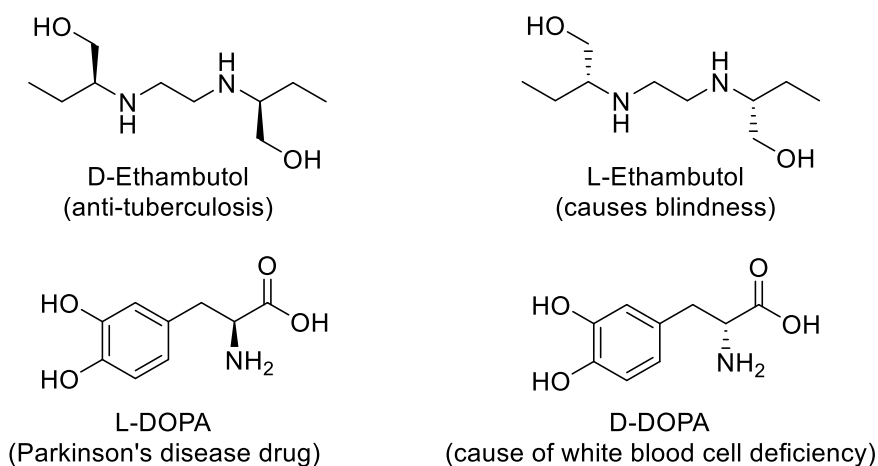
Figure 1.4. The differing biological effects of each ethambutol and DOPA enantiomer

1.2 Synthesis of Chiral Amines

Chiral amine building blocks are powerful pharmacophores in the synthesis of novel pharmaceutical drugs due to their intrinsic ability to hydrogen bond. Despite this, and the estimated fact that 40% of pharmaceuticals contain a chiral amine in their structural motif, synthesis remains a challenge.[1,2]

The main approaches in synthesising enantiopure amines are summarised in Scheme 1.1 and will be detailed in the following sections.
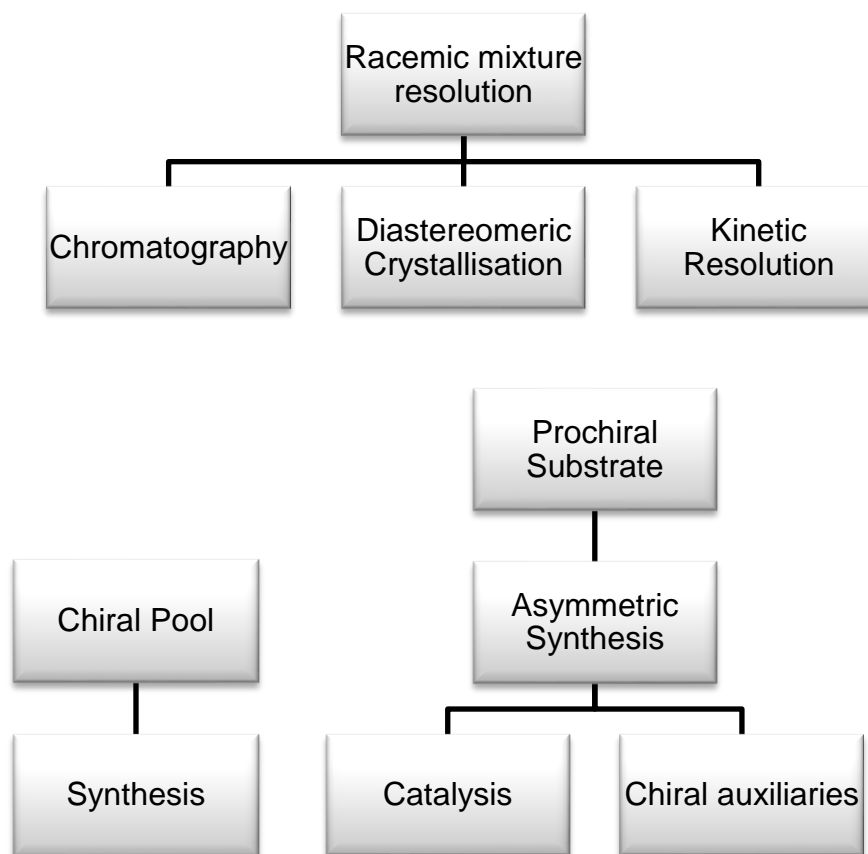
Scheme 1.1. Methods in synthesising enantiopure chiral amines.

1.2.1 Chiral Pool

The chiral pool refers to naturally abundant and enantiopure molecules found in nature, and can be used to synthesise molecules of interest. For example, Tamiflu® **2** is synthesised from readily available (-)-shikimic acid **1**, sourced from star anise seeds.[4]
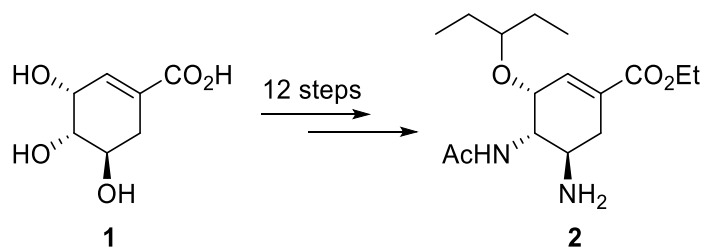
Scheme 1.2. The synthesis of Tamiflu from readily available (-)-shikimic acid

The chiral pool is an efficient way of introducing an asymmetric centre, as it is often cheaper to use a homochiral, naturally occurring reagent than it is to synthesise it. However, the chiral pool can be restrictive, as some molecules only have one commercially available enantiomer, or the other enantiomer is expensive.[5]

1.2.2 Asymmetric Synthesis

Asymmetric synthesis involves using (i) chiral auxiliaries and (ii) chiral catalysts to convert achiral or prochiral substrates into molecules with high enantiomeric excess (ee)

(i)   Chiral Auxiliaries

Chiral auxiliaries are temporary components incorporated into a reaction to control stereochemical outcome. Ellman's sulfinamide **3** is an example of a chiral auxiliary used with Grignard reagents in the preparation of α-branched amines **5**. The steric hindrance as a result of the *tert*-butyl group reduces side reactions, and it is thought that the reaction proceeds through a six-membered transition state **4**, Scheme 1.3.[6,7]
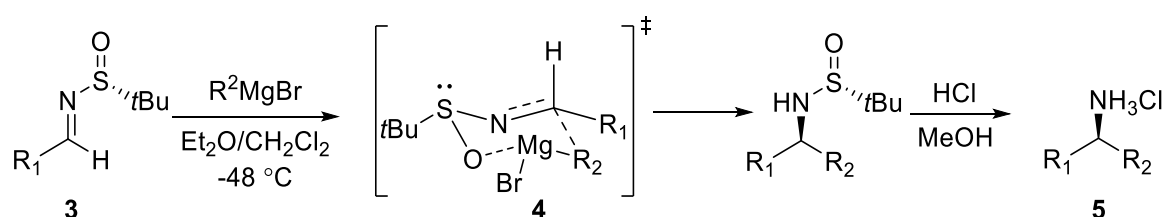
Scheme 1.3. Ellman's auxiliary in the synthesis of α-branched amines.

Due to easy removal and commercial availability, viability of Ellman's auxiliary has been demonstrated in the multikilogram synthesis of sertraline,[8] (*R*)-salsolidine[9] and (*S*)-rivastigmine.[10] Despite wide adoption of auxiliaries, they require a point of attachment and add additional synthetic steps which reduce yield.

(ii)   Chiral Catalysis

Asymmetric catalysis is useful in that small amounts of catalyst can be used, avoiding stochiometric quantities of expensive chiral reagents. The catalyst can be biological, organometallic with chiral ligands or organocatalytic. A key technique employed is enantioselective reductive amination, which was first illustrated by Blaser *et al.* in the synthesis of (*S*)-metolachlor, which was synthesised with low catalyst loading, 99% yield and 76% ee.[11–13] The first industrial scale synthesis of this compound employed hydrogen gas, and preformed and isolated imine **6** to form (*S*)-**7** due to lower catalyst loading, Scheme 1.4.[14]

Scheme 1.4. Enantioselective reductive amination in the industrial synthesis of (S)-metolachlor

Despite the atom efficiency of using hydrogen gas, its use at large scale is potentially catastrophic due to its explosive nature. As a result, research has also focussed on asymmetric transfer hydrogenation. Mwansa *et al.* noted interesting enantiomeric excess profiles in the asymmetric transfer hydrogenation of 6,7-dimethoxy-1-methyl-3,4-dihydroisoquinoline **8**, Figure 1.5.[15] The (R)-**9** initially predominates, however, it decreases significantly throughout reaction. This change in ee was a result of (R)-**9** following pseudo first order kinetics, and (S)-**9** following pseudo zero order kinetics. As a result, rate of formation of (R)-**9** decreases with decrease in imine concentration whilst (S)-**9** remains constant, causing the relative rates of enantiomer formation to change as the reaction progresses.[15,16] The enantiomeric profiles of this reaction demonstrates the need for careful kinetic studies of chiral catalysts, as their enantioselectivities tend to be less reliable than that of auxiliaries. In addition to this, further applications are limited due to high catalyst loading and high cost of metals and or chiral ligands. As a result, catalyst recyclability is important to maintain an economically feasible process.[5,17]

Scheme 1.5. Asymmetric transfer hydrogenation of **8**

1.2.3 Racemic Mixture Resolution

The resolution of compounds is based on the separation of two enantiomers acquired through a non-enantioselective process i.e. the separation of a racemic mixture. Resolution is one of the most common ways to obtain enantiopure compounds due to operational ease and low cost. The method is limited by a maximum yield of 50% and therefore displays poor atom economy. [2,18,19] There are three main approaches in which this can be carried out: chromatography, crystallisation and kinetic resolution.[20]

(a) Chromatography

Chromatography, a traditional method used in chemistry to separate compounds, can be used in the separation of enantiomeric pairs. In this area, efforts have been devoted to investigating suitable chiral derivatising agents to produce diastereomers, separated using traditional chromatographic techniques used for achiral molecule separation. This method does have its drawbacks such as the risk of racemisation and the different rates of transformation of each enantiomer. For preparative purposes, the direct method which omits tedious derivatisations is generally more successful.[21]

Due to the large number of possibilities presented by the adjustment of the stationary and mobile phases, column chromatography on solid stationary phase is seen as a good enantioselective separation technique. With respect to the mobile phase, gases, liquids and supercritical fluids can be applied. In terms of preparative applications, gas chromatography (GC) still holds no importance and is used more for analytical purposes. High-Performance Liquid Chromatography (HPLC) on the other hand can be used for preparative purposes, although suitable methods are usually developed empirically. For this reason, the potential of HPLC in the separation of enantiomers has not yet been fully realised.[21]

When considering an enantiomeric chromatographic separation, it is important to consider which of the two phases should be chiral. The application of a chiral stationary phase (CSP) is the most straight-forward choice for preparative applications. Examples of CSPs include cyclodextrins (CDs) and chiral crown ethers, which are usually adsorbed onto the chromatographic support such as silica shown in Figure 1.5. This method exploits selective interactions at a liquid-solid interface. Selectivity is different to that in a liquid-liquid environment as the solid support has an influence on complexation mechanism. When the sample migrates through the column, the diastereomeric environments formed mean that one enantiomer is strongly retained over another and therefore each enantiomer can be separated, Figure 1.6.[21]
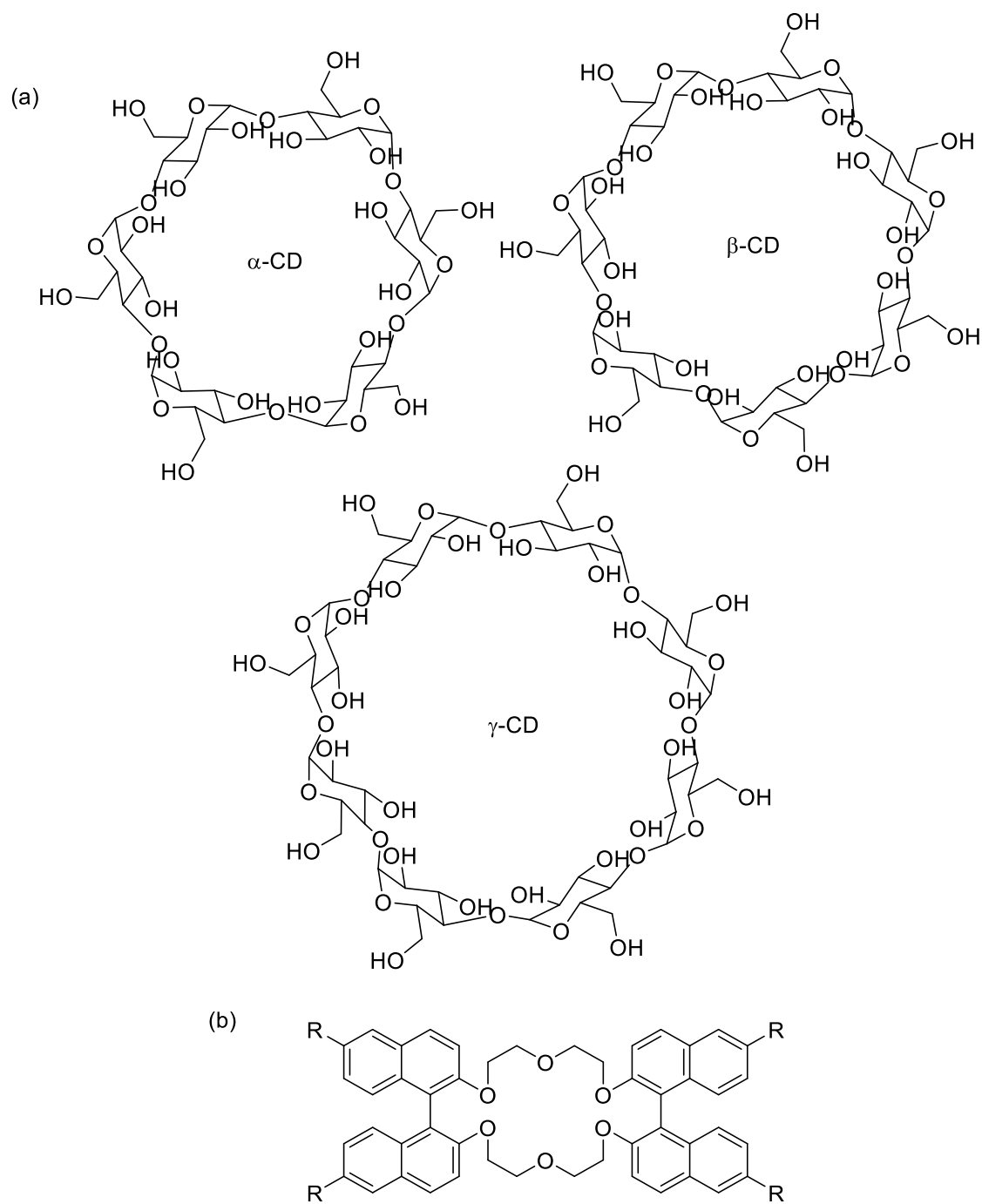
Figure 1.5. Examples of CSPs (a) cyclodexrins and (b) chiral crown ethers. [21]
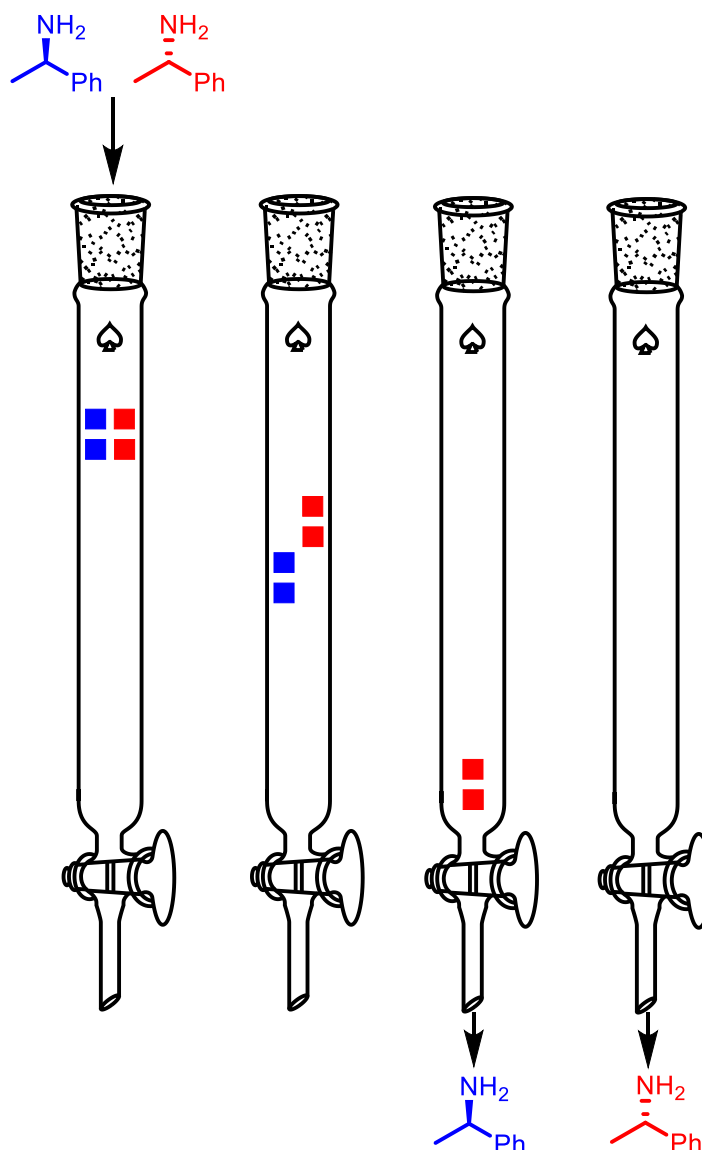
Figure 1.6. A chirally modified column demonstrating that one enantiomer can be more strongly retained than another.

Another type of chromatography which can be used to separate enantiomers is known as Simulated Moving Bed (SMB) chromatography. By applying this multicolumn method, a breakthrough in increasing the productivity of enantiomeric separations was achieved.[21] In the imaginary True Moving Bed (TMB) chromatography, a column filled with resin in a toroidal shape has a continuous flow of eluent (water) in one direction of the loop. The resin in the toroid, on the other hand, is circulating in the opposite direction to the water, Figure 1.7a. If a binary mixture is added to this loop, the component more readily adsorbed by the resin will move with the resin, whereas the component less readily absorbed will stay with the water. In this way, the two components can be separated continuously, Figure 1.7b.[22]

(a) Water circulating in one direction

Resin circulating in a countercurrent direction to water

(b) Extract = more highly adsorbed components stay with resin

Water (eluent) fed continuously

Continuous feed of feed mixture

Raffinate = poorly adsorbed components stay with water
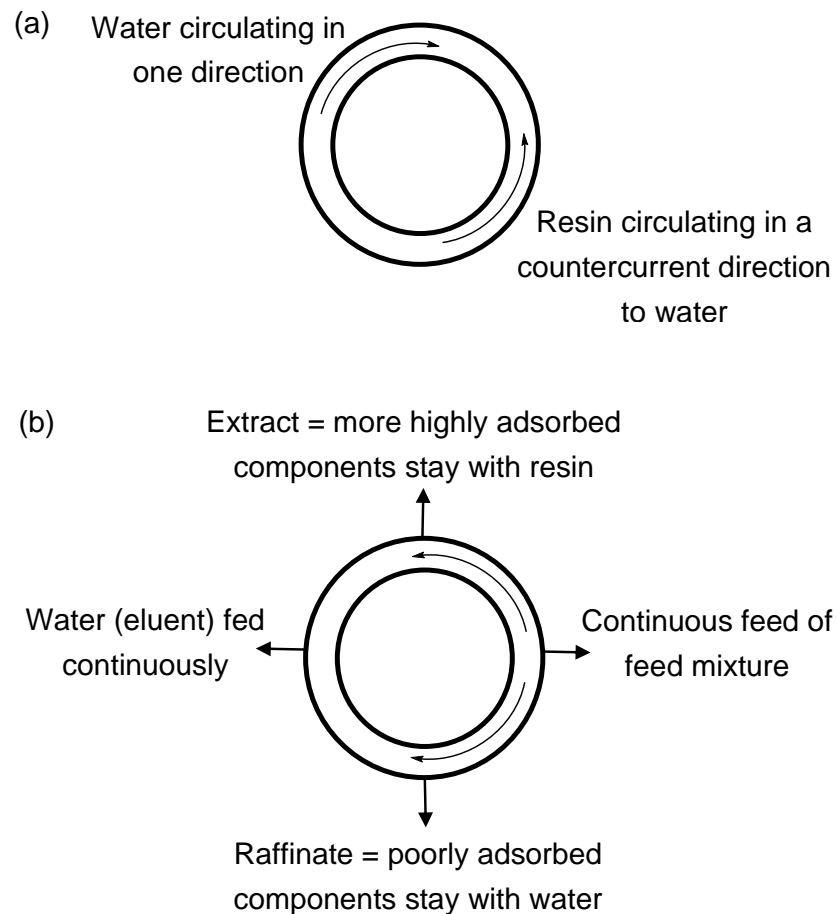
Figure 1.7. Theory of True Moving Bed chromatography. (a) Resin and eluent circulate in opposite directions. (b) Component more highly adsorbed by the resin will move with the resin whereas that less absorbed will stay with the eluent. Figure reproduced and adapted from reference [22].

Since TMB is imaginary, SMB is used to implement a close approximation of TMB. Unlike TMB, the resin resides in a cell and is stationary as there is no way in which it can be moved in a direction opposite to the circulating liquid. The secret of SMB is that the resin movement can be simulated in a direction opposite to the circulating liquid if the feed valve is intermittently changed to the same direction as the liquid flow. The other 3 valves, raffinate, extract and eluent must also move in this way as shown in Figure 1.8. The switching of the valves in SMB is analogous to the resin flow in TMB.
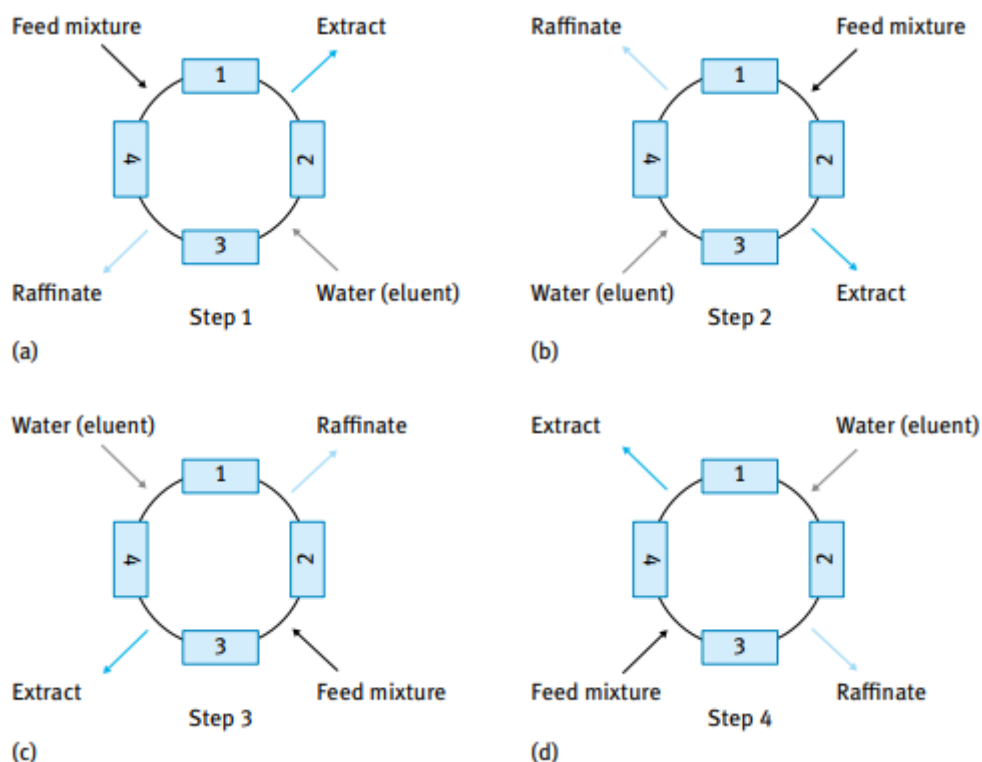
Figure 1.8. The circulating liquid is moving forward whereas the resin is moving back. This is apparent for a person standing in the feed mixture frame of reference.[22]

(b) Crystallisation

In the preparation of enantiopure compounds, resolution through crystallisation remains one of the most important methods.[23] In this section, crystallisation methods which can be used in order to isolate one enantiomer are discussed. The method used generally depends on factors such as the crystal symmetry and lattice. There are three symmetry elements which can be considered:[24]

1. Symmetry about a point (a *centre* of symmetry)
2. Symmetry about a line (an *axis* of symmetry)
3. Symmetry about a plane (a *plane* of symmetry)

When each point on the crystal surface has an identical point on the opposite side to the centre, equidistant from it, a crystal possesses symmetry about a point (a centre of symmetry). A cube, for example, has a centre of symmetry.[24]

A crystal returns to its original position if it is rotated by 360° about a given axis. If the crystal appears to have reached its initial position more than once during its rotation, the axis in question is an axis of symmetry. For example, if a crystal is rotated through 180° before appearing at its original position, this axis is called a diad axis and is one of twofold symmetry. If a crystal must be rotated through 120°, 90° or 60°, the axes are of

threefold (triad axis), fourfold (tetrad axis) and sixfold (hexad axis) symmetry respectively. These axes of symmetry are the only ones possible in the crystalline state. A cube has 13 axes of symmetry: 6 diad axes through opposite edges, 3 tetrad axes through opposite faces and 4 triad axes through opposite corners, Figure 1.9. [24]

| 6 diad axes | 4 triad axes | 3 tetrad axes |
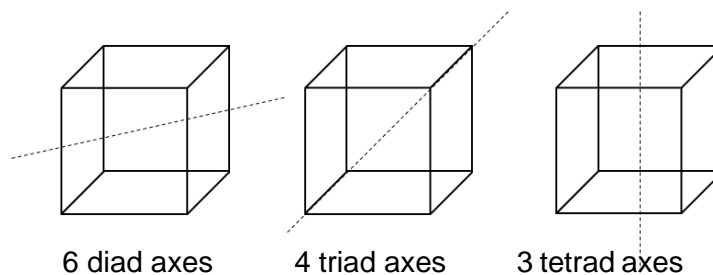
Figure 1.9. The axes of symmetry in a cube.

A plane of symmetry intersects a crystal in a way such that one half of the crystal becomes the mirror image of the other half. This type of symmetry is fairly common. A cube, for example, has 9 planes of symmetry: 3 planes each parallel to two faces and 6 diagonal planes which pass through opposite edges, Figure 1.10. [24]

3 rectangular planes   6 diagonal planes
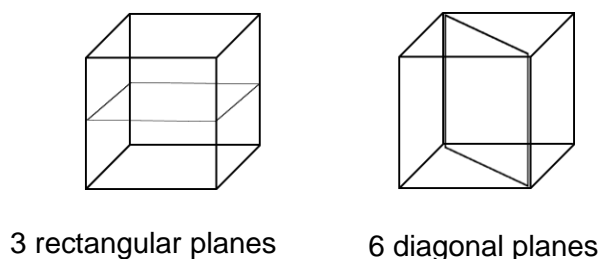
Figure 1.10. The planes of symmetry in a cube.

Enantiomers can crystallise in 3 different forms: as conglomerates (mechanical mixtures of pure (S) and (R) enantiomers with each unit cell containing a sole enantiomer), racemic compounds (both enantiomers exist in a 1:1 ratio in the unit cell), pseudo-racemates (also known as a solid solution, both enantiomers exist in an unordered arrangement in the condensed phase). [25] Conglomerates are amongst the rarest crystal forms, as they account for only 10% of chiral molecules on the occurrence of the rare $P2_1/n$ space group. Each different form enantiomers can crystallise in is summarised schematically in Figure 1.11.
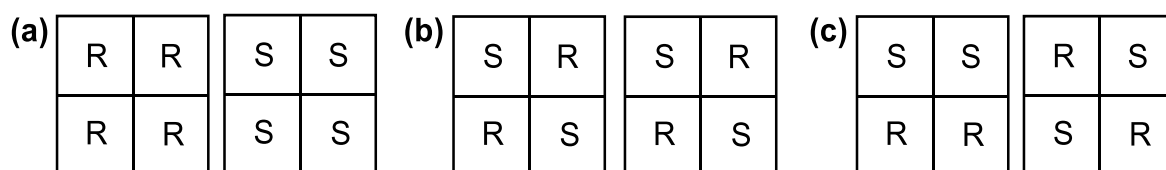
Figure 1.11. Different ways in which enantiomers can crystallise (a) conglomerates, (b) racemic mixture, (c) pseudo-racemates.

Similarly, diastereomers can crystallise in three analogous ways. Commonly, diastereomers produce eutectic mixtures (conglomerate-like behaviour where the molecules are crystallising as distinct entities). Occasionally, they can crystallise as a quasi-racemate (racemic-like behaviour) or as a mixed crystal (also known as a solid solution) where one diastereomer replaces another without impacting the crystal packing.[25]

(i) Diastereomeric Crystallisation

Crystallisation-Induced Diastereomer Transformation (CIDT), otherwise known as Pasteurian Resolution,[26] is a type of resolution where a racemic amine is, by reaction with a chiral acid, transformed into a diastereomeric salt pair which have differing solubilities. Whilst one diastereomer remains in solution, the other can crystallise out. An inherent drawback of CIDT is based on the limited (maximum 50%) yield of each enantiomer, which often leads to disposal of the undesired enantiomer. Several diastereomeric salts must be explored in different solvents to find an ideal chiral resolving agent to allow easy isolation of the desired enantiomer following crystallisation. For this reason, the interaction between chiral agent and desired enantiomer must be non-covalent to allow facile recovery after crystallisation.[26]

An example of diastereomeric crystallisation is demonstrated by chemists at pharmaceutical company Cilag, Scheme 1.6. Their procedure used (1R,2S)-(-)-ephedrine **11** as a basic resolving agent to selectively crystallise (S)-**10** from rac-**10**. The crystalline salt was separated through filtration and treated with acid to give the target amino acid in >98% d.e. and 42% yield.
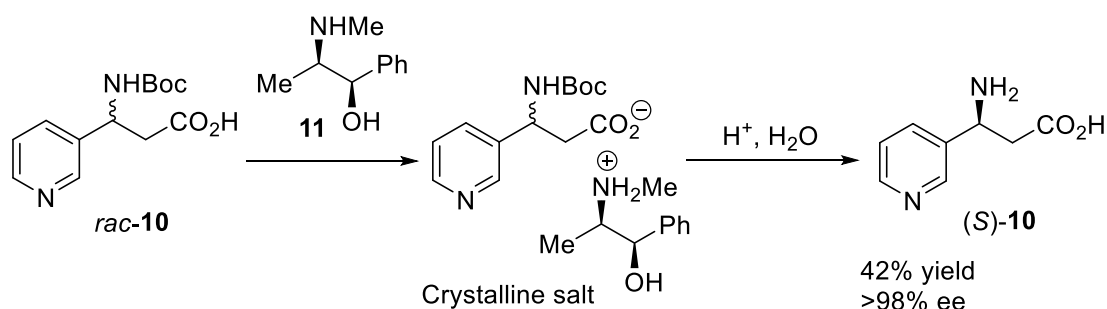
Scheme 1.6. Diastereomeric crystallisation of N-BOC-protected acid using (1R,2S)-(-)-ephedrine

(ii) Preferential Crystallisation

In preferential crystallisation, also known as conglomerate crystallisation, a single enantiomer is crystallised selectively from a racemic supersaturated solution by adding an enantiopure seed crystal, avoiding the need for a chiral auxiliary.[27] Selective crystallisation of one enantiomorph occurs due to the spontaneous nucleation energy

barrier of the non-seeded enantiomer (primary nucleation) being higher than the energy required to grow crystals in the seed (secondary nucleation). The kinetic advantage this energy difference provides, allows crystal propagation of one enantiomer, whilst the other remains fully in solution.

More than one variation of preferential crystallisation exists:[26]

- o Seed Isothermal Preferential Crystallisation (SIPC) involves crystallisation of the pure enantiomer at constant temperature through seeding of a supersaturated solution
- o Auto-Seeded Polythermic Programmed Preferential Crystallisation (AS3PC) where the pure enantiomer is crystallised through application of controlled cooling to a saturated solution
- o Auto-Seeded Preferential Crystallisation Induced by Solvent Evaporation (ASPreCISE) involves the controlled loss of solvent, which induces supersaturation and as a result, drives crystallisation

SIPC, AS3PC and ASPreCISE are advantageous as crystallisation becomes a cyclic process where exceptional recovery of both enantiomers is a result of the recyclability of the mother liquor.[26]

Whilst it's traditionally been thought that this type of crystallisation is only possible with a conglomerate mixture, a study by Brandel *et al.* described the resolution of a racemic compound (diprophylline) using SIPC. This study prompted reconsideration into the conditions that are deemed compulsory for successful enantiomeric separation through preferential crystallisation. [28] Generally, direct resolution of a racemic compound is not possible *via* existing crystallisation techniques. Screening for a conglomerate form can be implemented to overcome this problem, with the hope of identifying a salt, solvate, cocrystal or the like displaying attributes permitting preferential crystallisation.[29]

(c) Kinetic Resolution

Kinetic resolution (KR) refers to a process where two enantiomers within a racemic mixture react with a chiral reagent or catalyst at different rates, Scheme 1.7. As a result, an efficient KR allows recovery of both enantiomers in high yield (maximum 50% yield for each enantiomer) and high enantiopurity.

$$S_R \xrightarrow{\text{Fast}} P_R$$

$+$

$$S_S \dashrightarrow[\text{Slow}]{} P_S$$
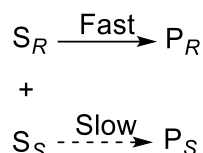
Scheme 1.7. Schematic depiction of a kinetic resolution process.

An example of enzymatic KR is reported by Crawford *et al.*, where Candida antarctica lipase B (CALB) enzyme was used to resolve a racemic tetrahydroquinoline **12** through selective acetylation of the (*R*)-**12**, Scheme 1.8.[30]

12

CALB
EtOAc

Toluene
50 °C
3h - 24h

(*S*)-**12**
45% yield
97% ee

(*R*)-**12**
45% yield
97% ee
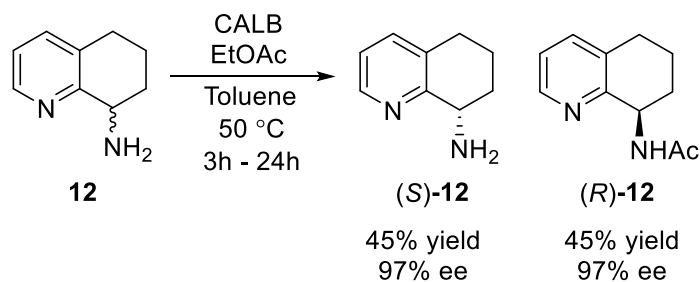
Scheme 1.8. Enzyme catalysed kinetic resolution of *rac*-8-Amino-5,6,7,8-tetrahydroquinoline

Surprisingly, leaving the reaction for 40-48 hours increased the yield above 50%, which was unexpected for a kinetic resolution. Further investigation provided evidence for spontaneous racemisation, which is discussed in the following section.

1.3 Racemisation

Racemisation involves irreversible conversion of an enantiomer to a 1:1 mixture of two enantiomers, otherwise known as a racemic mixture. The process is thermodynamically favourable due to an increase in entropy ($\Delta G° \approx -RT\ln 2$) corresponding to -1.7 kJ mol^{-1} at 25 °C. The inversion of one chiral centre in a molecule containing several stereocentres is known as epimerisation.[31] Consequently, epimerisation is the interconversion of diastereomers, Scheme 1.9.

$(R) \underset{k_{-1}}{\overset{k_1}{\rightleftharpoons}} (S)$

Racemisation
$k_1 = k_{-1}$

$(R)\bullet(S) \underset{k_{-1}}{\overset{k_1}{\rightleftharpoons}} (S)\bullet(S)$

Epimerisation
$k_1 \neq k_{-1}$
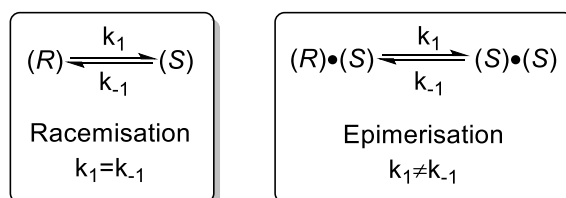
Scheme 1.9. Equilibria representing racemisation and epimerisation

Racemisation is an important technique which can be used in addition to resolution to increase yield above 50%. According to Ebbers *et al.* in 1997, the main methods of racemisation involve thermal racemisation, acid or base catalysed racemisation, Schiff

base formation, enzyme-catalysed racemisation and redox catalysed racemisation.[31] Methods described often require harsh conditions, making them incompatible with highly functionalised compounds.

1.3.1 Iridium-Catalysed Chiral Amine Racemisation

Transition metal catalysis has become one of the most important methods in the racemisation of chiral amines. During metal catalysed racemisation of chiral amines, interconversion between an sp^3 and sp^2 carbon centre occurs through hydrogenation and dehydrogenation. The amine is therefore either in its imine form or in one of its enantiomeric forms. Whilst racemisation in principle is a straight forward process, in reality, side-reactions such as unwanted dimerisations can decrease process efficiency.

The dimeric iodo-iridium complex [IrCp*I$_2$]$_2$ **13**, is an example of an iridium based catalyst which has been used in the racemisation of amines. The half-life racemisation rates of various optically active amines with the SCRAM catalyst **13** are shown in Table 1.1. Preliminary work has shown that compounds with electron donating substituents racemise quicker than those with electron withdrawing substituents (entries 2, 3, 5 and 6). Substrates containing a primary amine were found to give rise to dimeric impurities (entries 1 and 4). This is especially common in the racemisation of primary amines, likely due to the relatively high nucleophilicity of the nitrogen atom, causing it to attack an imine intermediate before hydrogenation and therefore before racemisation can occur, Scheme 1.10.[32]
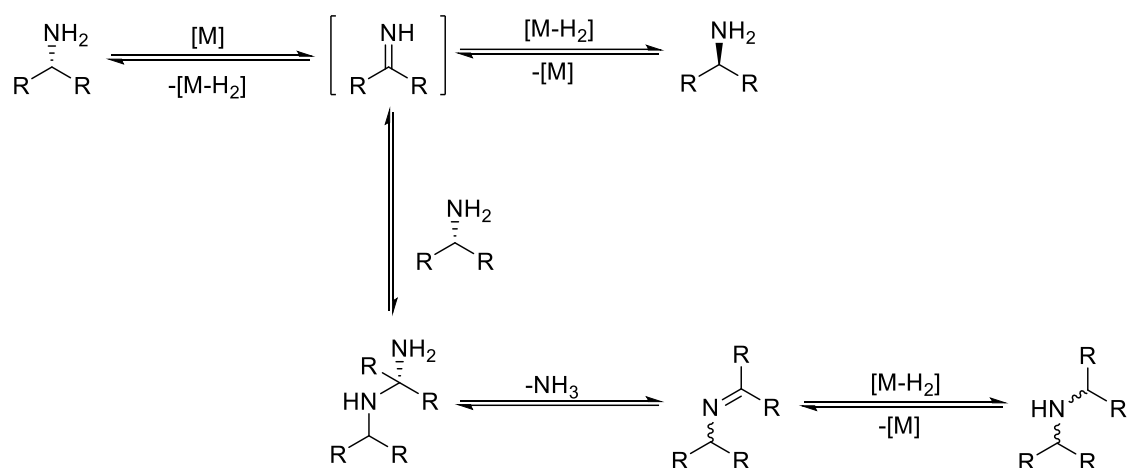
Scheme 1.10. Primary amine racemisation and dimerisation. [M] = metal catalyst.

Entry	Substrate	T (°C)	Racemisation $t_{1/2}$ (min^{-1})
1	NH$_2$	80	Dimeric impurities
2	NHMe	80	45
3	NHBn	80	250
4	NH$_2$	80	Dimeric impurities
5	NHMe	80	900
6	NHBn	80	1400
7		80	>7200
8	NMe$_2$	90	1250
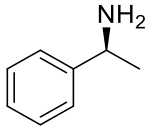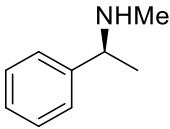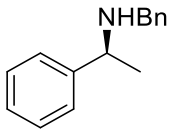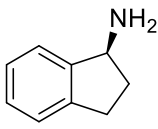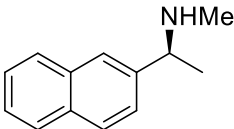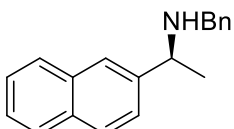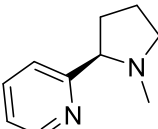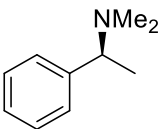
Table 1.1. The half-life ($t_{1/2}$) racemisation of various optically active amines with SCRAM (1.0 mol % catalyst loading).[32]

Surprisingly, one tertiary amine (entry 8) was successfully racemised suggesting a quaternary iminium species can be generated, providing evidence that iminium salts can act as good substrates for hydrogen transfer. Generally, with respect to amine structure, whilst primary amines undergo dimerisation faster than racemisation, tertiary and secondary amines can be racemised by SCRAM catalyst **13**, with the former having a

greater rate of racemisation that the analogous secondary amine. A bidentate tertiary amine was unable to racemise, possibly due to its ligation to the SCRAM catalyst **13**, deactivating it (entry 7).

A reaction mechanism compatible with kinetic isotope effect data for this catalyst has been suggested, as shown in Scheme 1.11.[33] In the presence of reactant amine, the catalytic dimer dissociates to form an 18 electron iridium species **14**. Transfer of a hydride from the amine to iridium generates a negatively charged iridium complex, also 18 electron, but with the newly generated iminium-cation as an ion pair **15**. This ion pair may dissociate prior to or in competition with hydride transfer back to the iminium ion to produce the enantiomeric amine.
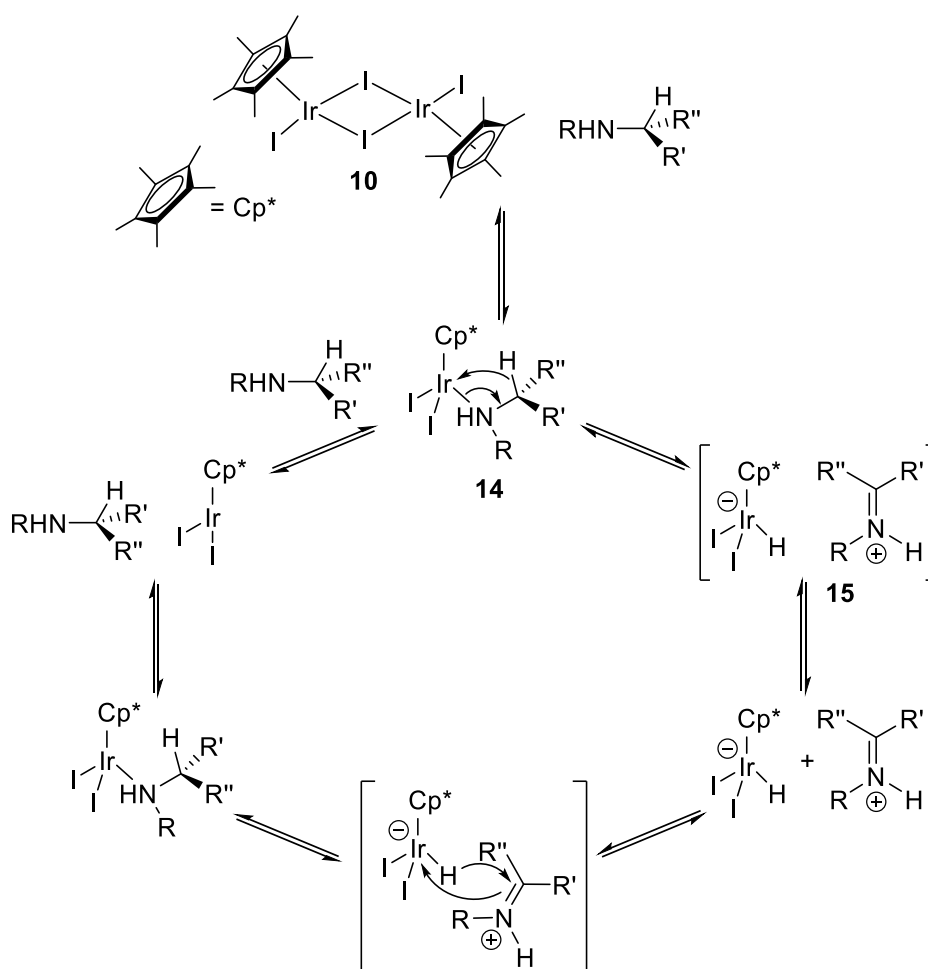
Scheme 1.11. Proposed mode of mechanistic action of the SCRAM catalyst.[33]

Variations of the SCRAM catalyst **13** were investigated in the racemisation of amines. For example, the iodides were replaced with chloride or bromide atoms which resulted in the organo-iridium complexes being much less effective in catalysing the racemisation of amines. The chloride catalyst, for instance, was greater than 3 orders of magnitude less effective in catalysing the racemisation of (*S*)-**9**, in addition to producing a greater

number of impurities. This was quite surprising given the small difference between iodide, chloride and bromide ligands in the racemisation of alcohols using a cyclopentadienylruthenium based catalyst.[34]

An electron withdrawing amide group substitution to SCRAM, **16**, was also investigated. The racemisation rate of (*R*)-**9** and (*S*)-**9** in dichloromethane at 40°C had a second order rate constant of k_{cat} = 0.134M^{-1}s^{-1}, a 7-fold reduction in activity. Under equivalent conditions, but replacing dichloromethane with toluene led to a second order rate constant k_{cat} of 1.37 x 10^{-2}M^{-1}s^{-1} which is around a 10-fold decrease in catalytic activity in comparison to dichloromethane. This demonstrates the implications of using a different solvent and how this can also affect catalytic activity. It is assumed that the amide substituent increases the positive charge density on the iridium in comparison to the iridium in the SCRAM catalyst **13**, although structural changes shown by x-ray crystallography are minor. [33]
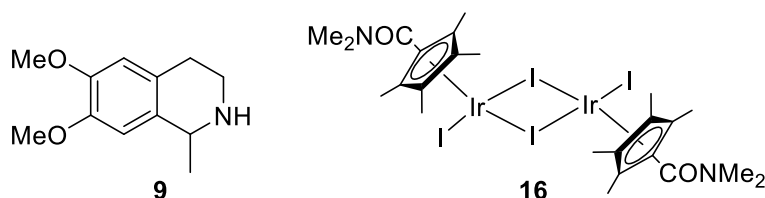
Given the factors which can affect SCRAM **13** activity, the mechanistic mode of SCRAM catalyst action is important to study in order to be able to predict which molecules can be racemised and under which conditions. As a result, the mechanism of catalyst **13** will be discussed further in Chapter 2.

1.4 Deracemisation

Deracemisation is a recent method which allows access to a single enantiomer through recrystallisation of a conglomerate solid coupled to *in situ* solution phase racemisation.[26,29] This method begins with a biphasic saturated solution and a racemic mixture of conglomerate solids. Stirring of the crystalline solid in equilibrium with its saturated liquid phase and a racemising agent allows the increase of enantiomeric excess (ee), giving rise to a single enantiomer.[26] The general principle of racemisation is shown in Scheme 1.12.
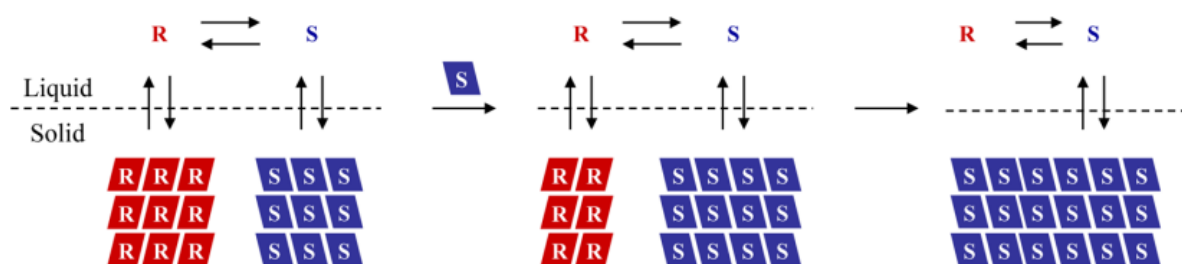
Scheme 1.12. Diagram representing the principle of deracemisation.

Whilst deracemisation in theory is simple, two factors complicate development of methods. First, conversion to a single enantiomer from a racemic mixture is entropically unfavourable and requires additional energy to drive the reaction forwards. The second challenge is due to the inherent equal energy of *R* and *S* enantiomers. Without an exogeneous driving force, a racemic equilibrium of *R* and *S* enantiomers is formed based on the principle of microscopic reversibility.[35]

1.4.1 Viedma Ripening

The concept of deracemisation was first observed by Viedma in 2005. *L* and *D* chiral crystals of $NaClO_3$ when stirred maintained their initial enantiomeric excess even after several days. However, when stirring was commenced in the presence of glass balls, which were added to cause attrition, an increase in crystal enantiomeric excess (CEE) and therefore complete crystal chiral purity was observed. The time required to achieve this depended upon the number of glass balls in the system, and when the number of balls was kept consistent, the agitation speed (related to mechanical energy) became the more important factor. This is summarised in Figure 1.12, where it can be seen that increasing the number of balls or the agitation speed (measured in rpm) leads to a decrease in the time required for deracemisation.[36]
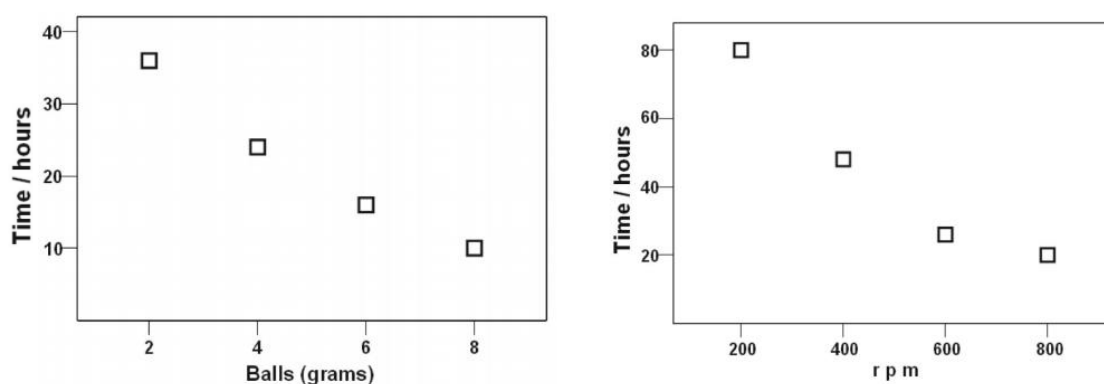
Figure 1.12. The relationship between the time taken to achieve chiral purity and (a) the number of balls in the system (at 600 rpm) or (b) the agitation speed in rpm (using 4 g of balls).[36]

Following 8 hours of the abrasion-grinding process at 600 rpm, a solution with preliminary 5% of *L*-CEE shows 100% *L*-CEE, whereas that of an initial 5% *D*-CEE shows 100% *D*-CEE, Figure 1.13. A racemic mixture of the *D* and *L* crystals show chiral purity after 24 hours at 600 rpm with 4 g of balls. In this case, the handedness varies randomly from *D* to *L*,

Figure 1.14, and it is believed that a small difference between them biases production of one of them, which is a stochastic process.
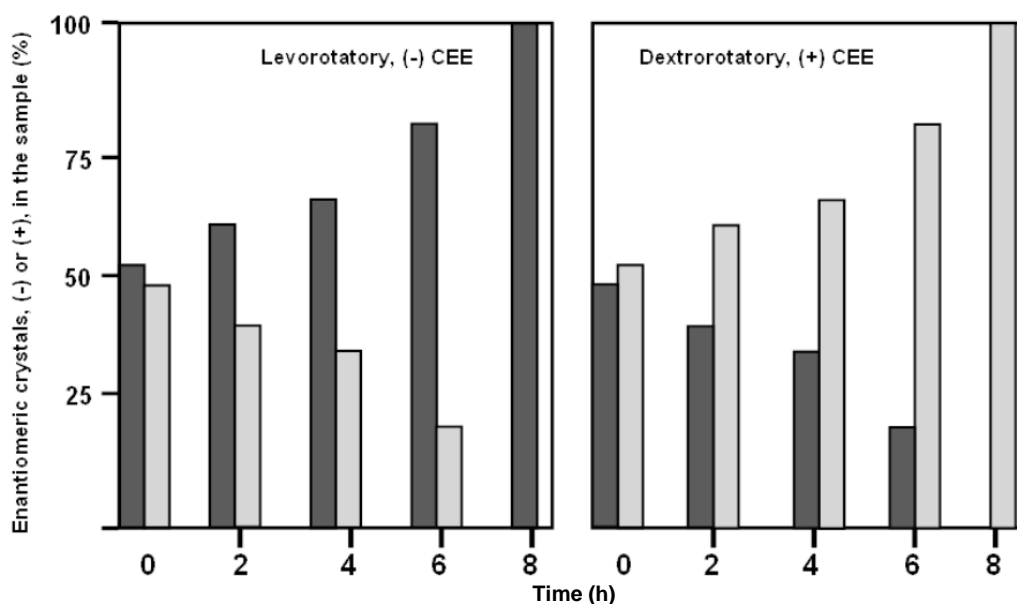
Figure 1.13. In 8 hours, solutions of 5% L-CEE show 100% L-CEE and solutions of 5% D-CEE show 100% D-CEE.[36]
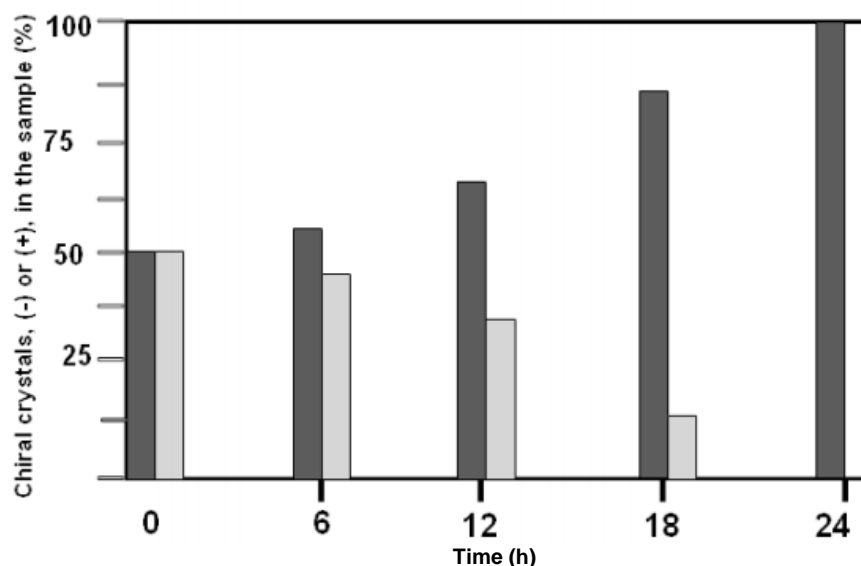
Figure 1.14. Initially racemic mixtures show chiral purity after 24 hours, in this case 100% L-CEE.[36]

Due to the combination of stirring and abrasion-grinding as a result of the glass balls, the opposite enantiomeric forms continuously lose small microcrystallite fragments. [36] It is believed that these small fragments are responsible for secondary nucleation, leading to an autocatalytic feedback mechanism whereby initial enantiomeric excess is augmented exponentially to a pure chiral end state. [37]

A similar study conducted by Hein *et al.* also investigated attrition-enhanced deracemisation. Twenty-four experimental runs carried out under identical conditions led to the conversion of a racemic mixture to 9 sets of homochiral *R*-**17** and 8 sets of homochiral *S*-**17**, with 7 mixtures remaining racemic. This is summarised graphically in Figure 1.15.[38] In this case, it is a difference in crystal-size-induced solubility that causes the conversion of one enantiomorph to the other. This is related to the Gibbs-Thomson rule (larger crystals display lower solubility than smaller crystals) and how crystal growth occurs through Ostwald ripening (larger crystals grow at the expense of smaller crystals). Together, these rules dictate that mechanical grinding, which leads to the breakdown of larger crystals into (relatively more soluble) smaller crystals aids in the growth of larger crystals. Since crystal-size-induced solubility forms the basis of this research, it is somewhat surprising that the crystal area is calculated using a two dimensional (as opposed to three dimensional) parameter using imaging software. Only 5 – 7 randomly selected sections of high resolution were investigated for each sample, for a population size of 11000-17000 particles. The paper also uses chiral conglomerate solids, which only account for 10% of chiral molecules.[39]
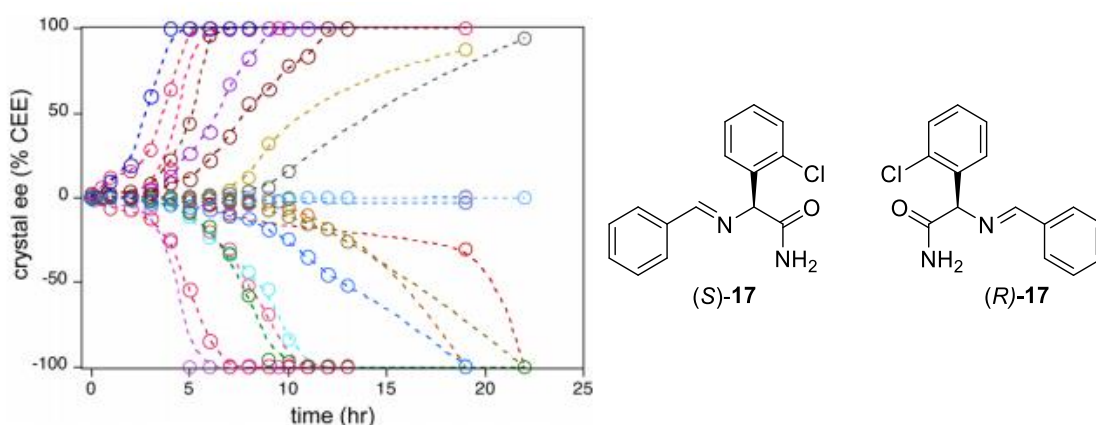
Figure 1.15. A conglomerate derivative of 2-chloro-phenylglycine and the evolution of its crystal enantiomeric excess (% CEE) over 24 deracemisation experiments under identical conditions.[38]

1.4.2 Photochemical Deracemisation

Research into visible light photocatalysis has increased dramatically over the last 15 years. Whilst photochemistry and the use of photocatalysts is not a new concept, combination of advanced reactor technology, relatively powerful light sources and the development of various photocatalysts has led to its exploitation in sectors including large-scale chemical production. Photocatalysts can achieve electronically excited states through absorption of photons, and through subsequent electron transfer with organic molecules.[40,41]

A photochemical deracemisation of hydantoins **27** with various R substituents was recently reported through employment of 5 mol% photocatalyst **28**, Scheme 1.13. In total, 27 hydantoins containing a broad range of hetereoatoms and multiple bonds were synthesised (80-99% ee) including olefins, nitriles, alkynes, ethers, esters and halogen atoms. Upon excitation, a hydrogen atom transfer only occurred at *S*-configured hydantoins **27** but not at *R*-configured hydantoins **27**. Computational studies predicted this preference based on hydrogen bonding between the α-chiral proton and the carbonyl oxygen bridged between two aromatic groups. Unfortunately, the oxidising properties of the photoexcited ketone **28** meant that hydantoins with oxidation sensitive groups such as amines and sulfides were not used or gave low ee.[42]
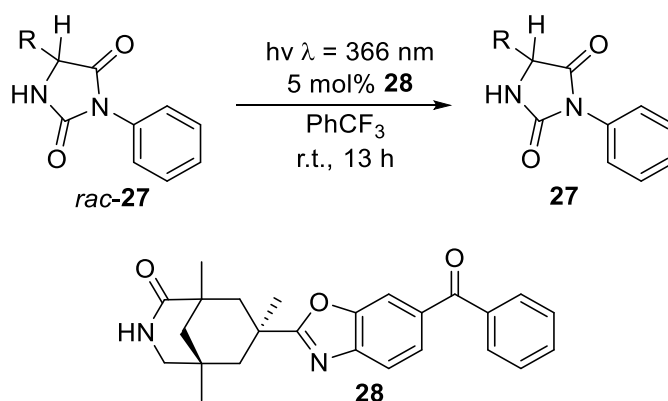
Scheme 1.13. Photochemical deracemisation of *rac*-**27** using photocatalyst **28**.

Investigating racemisation under photochemical conditions is advantageous as it eliminates the need for harsh conditions, high temperatures and or the addition of redox reagents or acids and bases. However, lack of reaction protocol standardisation has led to inconsistent reporting of reaction conditions, and as a result, wide adoption has been limited. Furthermore, proposed mechanisms in the literature often rely on little to no experimental evidence.[40]

1.4.3 Dynamic Kinetic Resolution

Following on from Kinetic Resolution (KR), discussed in Section 1.2.3, Dynamic Kinetic Resolution (DKR) is a method that allows the combination of resolution and racemisation. An equilibrium between two stereoisomers in a racemate can allow the formation of 100% of one enantiomer through enzymatic chemical modification, chiral chromatography or crystallisation.[32] In order for an efficient and rapid DKR process to occur, $k_{Rac} > k_R > k_S$, shown in Scheme 1.14. This is so that the racemisation step is rapid enough to replace reacted SM_R, which reacts quicker than SM_S to form P_R as opposed to P_S. The equilibrium of SM_R and SM_S is then re-adjusted by racemisation of SM_S which is the slower reacting enantiomer. Theoretically, 100% of P_R can be formed this way.

$$SM_R \xrightarrow{\;k_R\;(fast)\;} P_R$$

$$k_{Rac} \Updownarrow$$

$$SM_S \xrightarrow{\;k_S\;(slow)\;} P_S$$
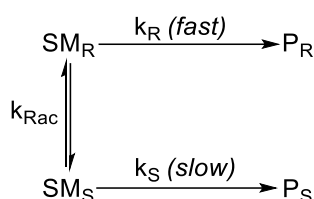
Scheme 1.14. A schematic depiction of the DKR of a racemic mixture where SM_R, SM_S = starting material of each enantiomer, P_R, P_S = enantiomer products, k_R, k_S = rate constants of P_R and P_S formation respectively, k_{Rac} = racemisation rate constant

Performing a DKR under mild conditions is favoured as the harsh conditions required for racemisation are usually incompatible with reagents such as chiral acids and enzymes used in the resolution step.[32]

Papers describing the DKR of alcohols are common, especially those which make use of enzymes due to their high stereoselectivity. For example, Choi *et al.* conducted experiments where Candida antarctica lipase B (CALB) was immobilised on acrylic resin (Novozym 435) as a resolving enzyme. The synthetic scheme for this reaction in addition to the ruthenium catalyst **18** utilised is shown in Scheme 1.15, using 1-phenylethanol **19** as an example substrate. The KO*t*Bu is believed to form the active catalyst and therefore a ruthenium hydride bond. Acetic acid, formed during the DKR from the reaction of acetylated lipase and water, led to the addition of Na_2CO_3 or molecular sieves (MS). Various secondary alcohols were investigated and the majority were isolated in > 90% yield and ee.[43,44]
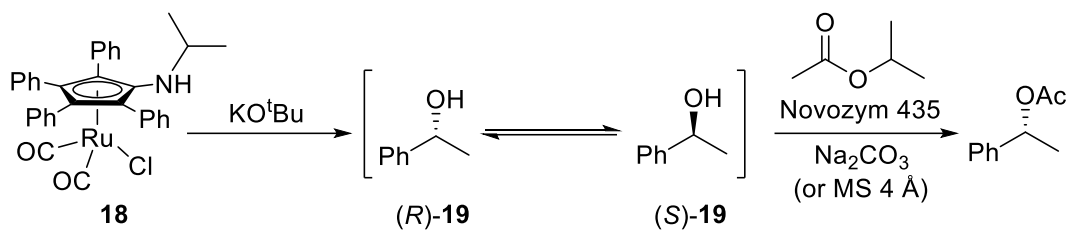
Scheme 1.15. DKR of 1-phenylethanol **19** where MS = molecular sieves.[43]

Previous research has shown that factors which affect the efficiency of an alcoholic DKR include temperature,[43] acyl donor,[43] electron donating or withdrawing groups[45] and various other additives such as Ag_2O.[46]

Amine DKR, on the other hand, is rather more challenging. Protocols for the DKR of amines are fewer in number than that of their alcoholic counterparts due to scarcity of efficient amine racemisation catalysts. The biggest challenges in the DKR of amines are as follows:[47]

> ➢ Amines can behave as strongly coordinating ligands, which can lead to the disruption of catalytic activity
> ➢ High temperatures are usually required to disrupt amine-catalyst coordination, restricting the range of enzymes which can be employed
> ➢ The generated imine is highly reactive and can therefore be subject to unwanted side reactions, such as hydrolysis to the corresponding ketone or reaction with an amine molecule.

High temperatures favour these unwanted reactions, emphasising the need for mild but efficient protocols for amine racemisation.

In 2007, Blacker *et al.* reported the DKR of amine **9** using immobilised enzyme *Candida rugosa* lipase, 3-methoxyphenylpropyl carbonate as acyl donor **20** and [IrCp*I$_2$]$_2$ (SCRAM, **13**) as racemisation catalyst at 40 °C, Scheme 1.16. After 23 hours, there was a 90% conversion to the product carbamate in 96% ee, demonstrating the ability of [IrCp*I$_2$]$_2$ to catalyse a racemisation reaction.[48]
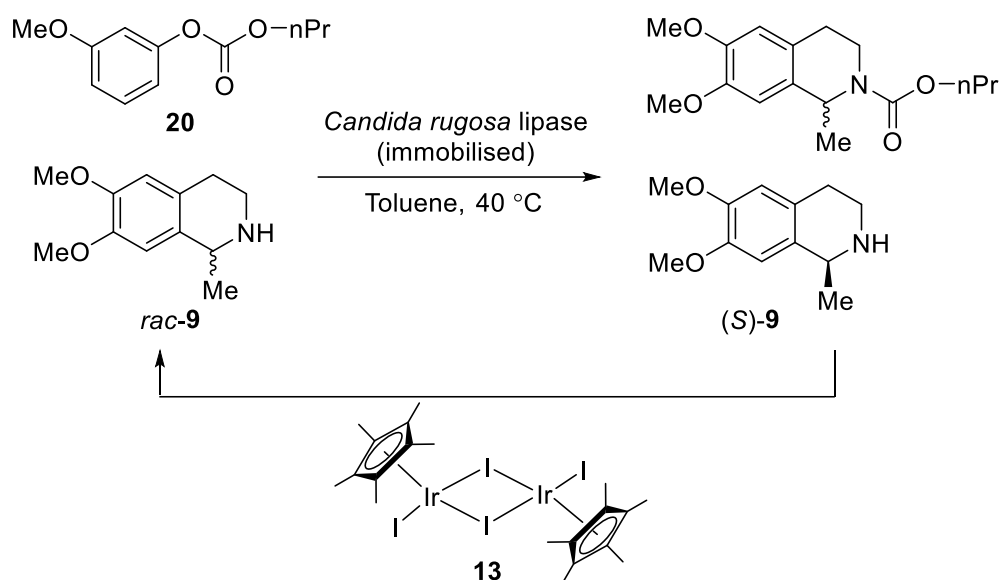
Scheme 1.16. Schematic diagram demonstrating the DKR of rac-**9**.[48]

Under the same conditions, but using 1-methyl-1,2,3,4-tetrahydroisoquinoline **21** as the racemic amine precursor and 3-methoxyphenyl allyl carbonate **22** as acyl donor, *N*-allyl-1-methyl-1,2,3,4-tetrahydroisoquinoline **23** was formed as an impurity. It was proposed that the racemic amine **21** reacts with the carbonate acyl donor **22** to produce the *N*-allyl amine **23**. The reaction itself must be catalysed by the SCRAM catalyst **13** as the *N*-allyl amine **23** is not formed in the resolution of the racemic amine **21** otherwise under identical conditions in the absence of [IrCp*I$_2$]$_2$ **13**.[48] It is surprising that even at this low temperature of 40 °C, an impurity was observed.
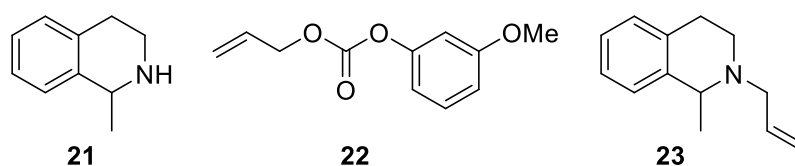
1.4.4 Resolution-Racemisation-Recycle

The compromise between the resolution and racemisation processes in DKR mean that lower temperatures than preferred must be used. Combining these steps to create a resolution-racemisation-recycle (R^3) process may aid in the reduction of impurity and racemisation catalyst influence on crystallisation processes. Although, if additional purification is required, the overall process efficiency would decrease as the amount of solvent waste generated increases in addition to the time taken for each R^3 cycle to take place.

The concept of resolution-racemisation-recycle is best explained using examples from the literature. The synthesis of duloxetine, a potent serotonin and noradrenaline

reuptake inhibitor, was synthesised by Eli Lilly *via* a resolution-racemisation-recycle (R[3]) process. A modified version of this R[3] cycle investigated by Fujima *et al.* is shown in Scheme 1.17. In this modified scheme, the MTBE-EtOH in the original Eli Lilly scheme was replaced by PhMe-MeOH which was more environmentally friendly and economical.[49]
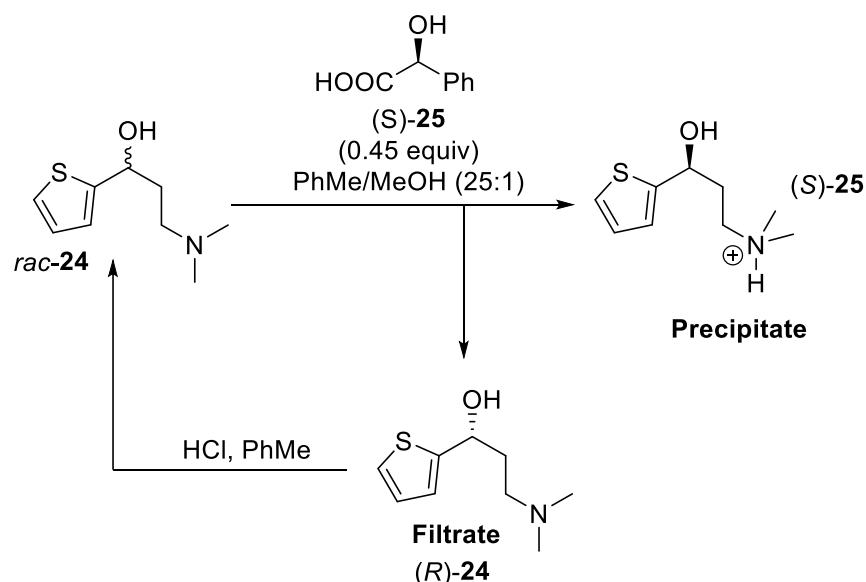
Scheme 1.17. A variation of the R[3] cycle required in the synthesis of duloxetine.[49]

Whilst the mandelate salt of **24** is carried forward in the synthesis, the filtrate was concentrated to recover (*R*)-**24** which would be racemised before being recycled for another round of resolution, hence the term Resolution-Racemisation-Recycle.[49] In this respect, one enantiomer can be formed in high yield and ee, increasing the efficiency of the process.

Another R[3] type process was reported by Blacker *et al.* in 2009, describing a semi-continuous process in the resolution racemisation recycle of sertraline **26**. The selective crystallisation of the (1*S*,4*S*)-diastereomer from a mixture of all 4 diastereomers was achieved in >99% ee and 90-98% de. Whilst the isolated yield of this isomer is 35%, the resolution yield is unimportant since the unwanted isomers are recycled and therefore, in theory, can all be transformed into the required product. This process utilises the [IrCp*I$_2$]$_2$ SCRAM catalyst **13** which can also be recovered and recycled, which is useful as iridium is a precious metal. A simplified scheme of this process is shown in Scheme 1.18, where (*R*)-**25** is used as the resolving agent.[50]
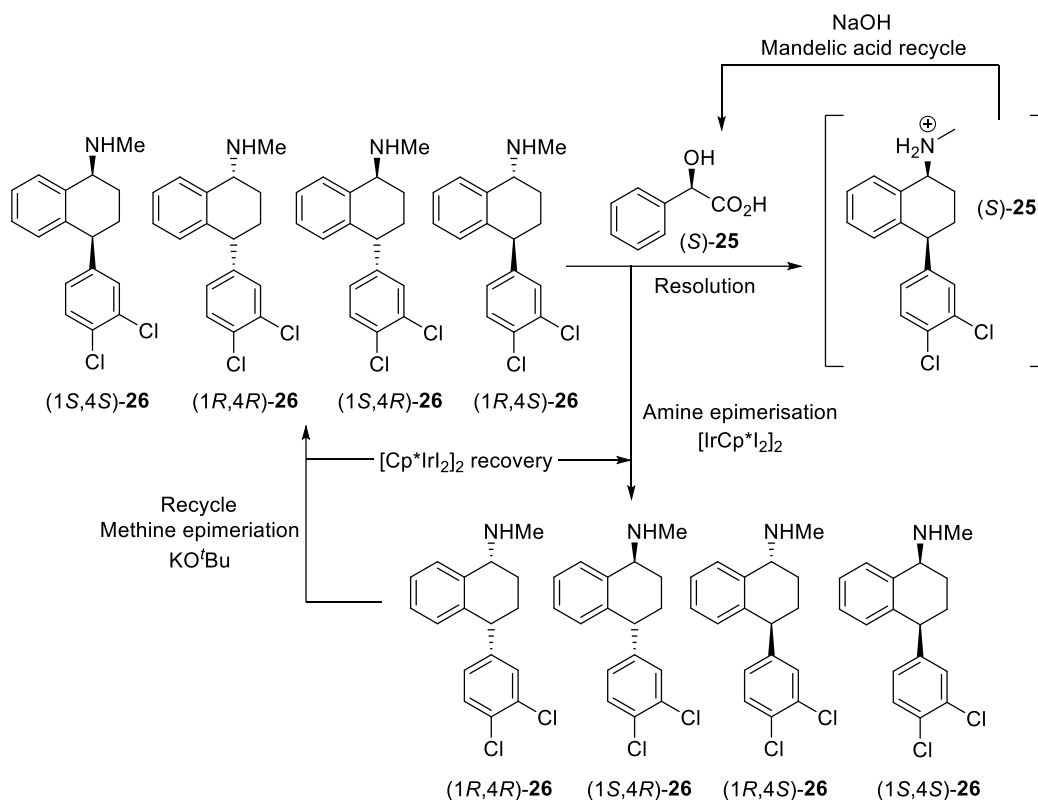
Scheme 1.18. Semi-continuous sertraline R^3 process.[50]

These R^3 processes demonstrate that the problem of a wasteful and low yielding process can be overcome through the recycling of unwanted enantiomers or diastereomers. Moving towards a continuous R^3 process would be economical, decrease user input, and if using recyclable immobilised catalyst, reduce issues associated with metal contaminated product. As a result of these benefits, catalyst immobilisation is discussed further in the following section, and a continuous R^3 process is discussed further in Chapter 4.

1.5 Catalyst Immobilisation

Homogenous metal catalysts often have excellent selectivity and activity when coupled with an extensive set of reactions. The use of homogeneous catalysts in synthesis, however, is uneconomical as the precious metals employed can typically only be used once before deactivation occurs. Given that pharmaceutical compounds must be exceedingly pure, the difficulty in recovering the metal from the reaction mixture is disadvantageous.[51]

By immobilising a catalyst onto a solid support, it has been shown that it is easier to remove the reaction mixture through filtration or decantation. This would ideally allow the catalyst to be recycled, therefore making the process commercially feasible.

Homogeneous catalysts can be attached to supports in two main ways, physically or chemically. Examples of the former method include physisorption, hydrogen bonding and encapsulation, whereas chemical attachment usually involves covalent attachment or ionic bonding. The main problems associated with the use of immobilised catalysts are metal leaching and loss of activity.[51] This explains the use of catalysts with a cyclopentadienyl ligand, as immobilisation via this ligand gives the advantage of a stable η^5 ligand which prevents leaching of the metal.[50]

A recent study by Sherborne *et al*. investigated the activation and deactivation of an immobilised transfer hydrogenation precatalyst, $[Cp^{**}IrCl_2]_2$ (Cp^{**} = immobilised Cp^* ligand) on a Wang resin **29a**. The precatalyst, linked to the support through a η^5-Cp^* ligand, has shown slow and partial deactivation over 26 uses. The immobilised catalyst **29a** and **29b** is illustrated in Scheme 1.19, with corresponding hydrogen borrowing reaction. Evidence suggests the catalyst exists in its monomeric form as opposed to its dimeric form.[52]
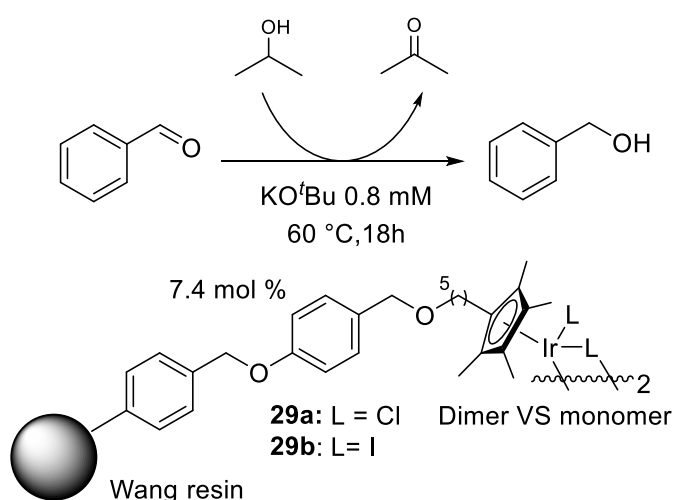
Scheme 1.19. Transfer hydrogenation using immobilised $[Cp^{**}IrCl_2]_2$ **29a** as a precatalyst.

In the experiment, the reaction solution containing KO^{t}Bu was flowed through a flow-cell. A ~50% decrease in chlorine content was observed in conjunction with a minute increase in potassium (chloride) content, using x-ray absorption spectroscopy (XAS) as a monitoring technique. It is thought that potassium chloride was formed either by reaction of HCl with KO^{t}Bu or by the reaction of HCl with the deactivated catalyst containing the potassium cation. The decrease in chlorine but increase in potassium content was found to be consistent with the replacement of a chloride ligand with an alkoxide (O^{i}Pr or O^{t}Bu) to produce $[Cp^{**}IrCl(OR)(S)]$ **30** (R = O^{i}Pr or O^{t}Bu and S = neutral ligand), thought to be the dominant species prior to catalytic turnover, supported by XAS data. Aqueous HCl was pumped through the catalyst in an attempt to 'reactivate'

the catalyst, allowing the catalyst to be used again 3 more times. The proposed deactivated catalyst **31** can explain why this works, as it leads to the protonation of the alkoxide ligands, making them more labile and prone to displacement, allowing temporary restoration of catalytic activity as shown in Scheme 1.20 by **32**.[52]
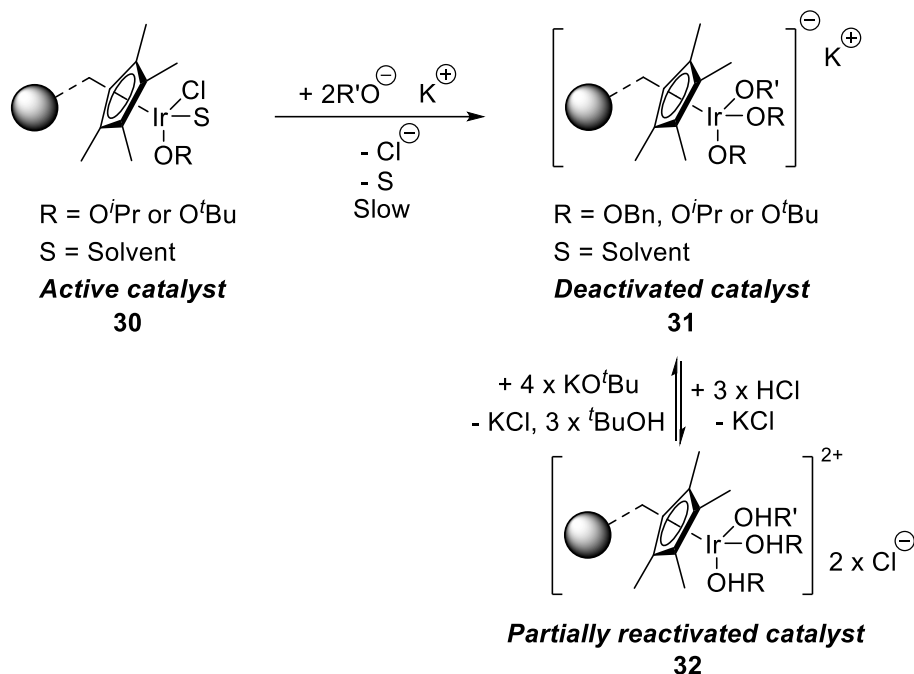
Scheme 1.20. The proposed deactivation and reactivation pathways for the immobilised catalyst.[52]

A study by Lucas *et al.* into the same immobilised catalyst shows that increasing the length of the immobilised catalyst's tether from a 5 carbon chain length to a 14 carbon chain length enhances the % conversion of reactant to product. The initial rate observed (92% conversion after 4 hours) was comparable to that of SCRAM **13** under homogeneous conditions (89% conversion after 4 hours). The 5 carbon chain length showed a 60% conversion after 4 hours in comparison. It is suggested that the longer more flexible tether allows the catalyst to behave more homogeneously, hence its activity is more closely associated with the homogenous SCRAM catalyst **13**.[51] Unfortunately, the longer carbon chain catalyst is relatively unstable.

1.6 Continuous Flow Processing

Due to the reduction of purifications and intermediate isolations, continuous flow techniques have been developed in response to the global demand for chemical production at a lower cost.[53] Flow chemistry involves continuous reactions carried out in microreactors (submillimeter to submicrometer dimensions) with other microscale operations such as heating, cooling, mixing, extraction, concentration and phase

separation. The conventional batch chemistry approach requires isolation and purification of intermediates, whilst modern continuous flow involves a telescopic approach, Figure 1.16.
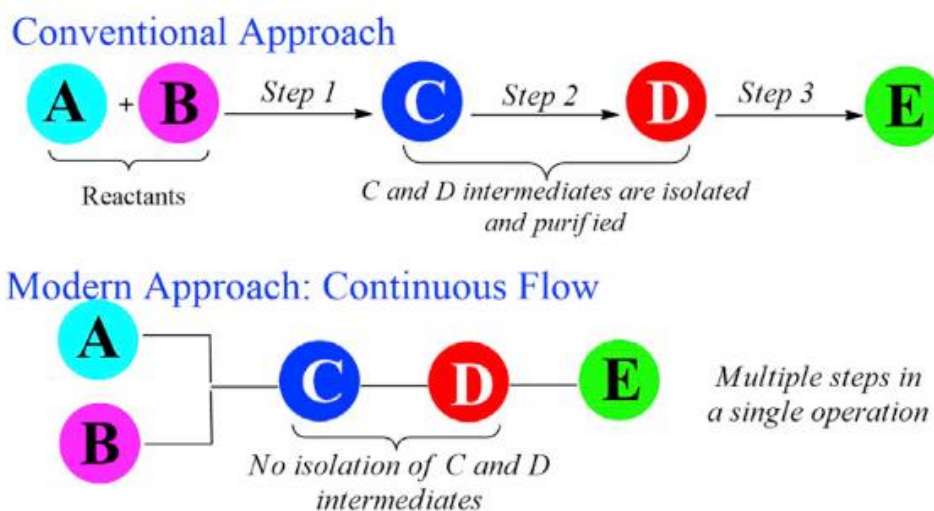
Figure 1.16. Comparison between conventional batch chemistry to modern continuous flow chemistry.

The first end-to-end continuous manufacturing process was demonstrated by the Myerson-Trout team at the Novartis-MIT Centre for Continuous Manufacturing.[54] The process of aliskiren hemifumarate synthesis integrated all reactions, dilutions, washes, separations, crystallisations, drying and formulation steps to produce the final tablet in high purity. As a result of continuous flow chemistry, this process allows for the production of 2.7 million tablets per year in addition to reducing the number of unit operations from 21 to 14 and the residence time to 48 hours, compared to 300 hours for batch.[55–57] This example demonstrates what can be achieved through exploitation of continuous flow chemistry with respect to waste and process cycle time reduction.

In order to benefit from wide application of continuous flow chemistry, reactor design is an important consideration. As many chemical reactions involve multiple phases such as solid-liquid and liquid-liquid, efficient mixing of phases is necessary. In tubular reactors, high flow rates are required to maintain effective mixing which may not be feasible for slow reactions. As a result of poor mixing, biphasic reaction mixtures going through tubular reactions can show segmented or density-separated flow, Figure 1.17.[58,59]

(a) Segmented flow

(b) Density separated flow
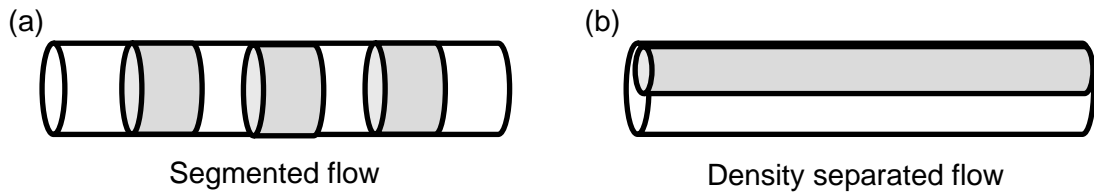
Figure 1.17. Inefficient mixing of biphasic reactions can lead to (a) segmented flow and (b) density separated flow

More recently, industrial crystallisation has been investigated under continuous flow conditions. Whilst traditional batch techniques are still being used, continuous manufacturing has the benefits of being implemented under identical and controlled conditions relative to batch processes. Two important crystalliser types are known as mixed-suspension mixed-product removal (MSMPR) crystalliser, and continuous tubular crystalliser or plug flow continuous crystalliser (CTR, PFR). The selection between each reactor system is guided by kinetics; MSMPR has low conversion and long residence time whilst PFR has high conversion and short residence time.[54]

The MSMPR is a well-mixed crystalliser whereby homogeneous feed solution enters the reactor and generated supersaturation through evaporation leads to crystal growth, Figure 1.18. Due to varying crystal residence time, the withdrawn product slurry displays variation in crystal size distribution. It is also assumed that the withdrawn contents are of the same composition as the reactor contents.[60] An MSMPR system for the crystallisation of cyclosporine investigated by Alvarez *et al.* indicated that crystallisation with recycle gave a 87% yield whilst no recycle gave a yield of 71%. For comparative purposes, the process in batch gave a 74%.[60] The study demonstrates how continuous flow experiments can support movement to more sustainable crystallisation approaches.
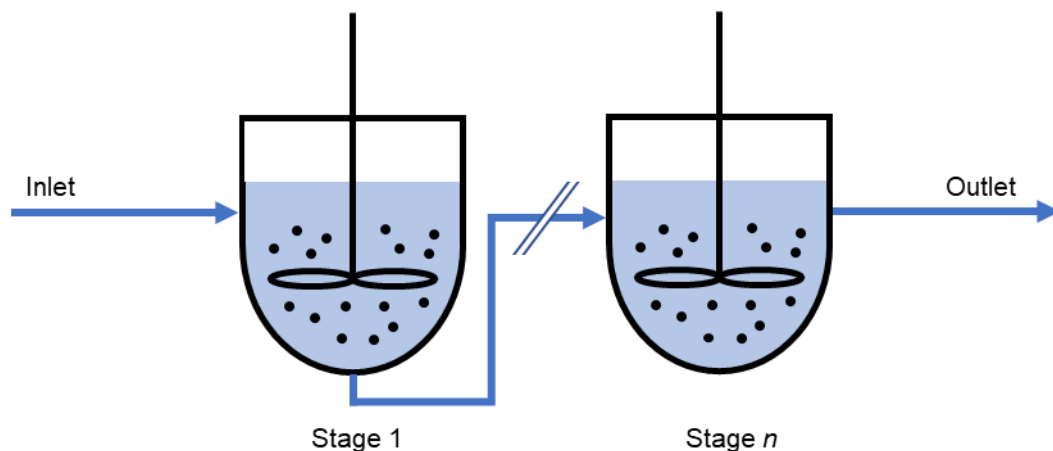
Figure 1.18. Schematic diagram of Mixed-Suspension Mixed-Product Removal (MSMPR) Reactor for continuous crystallisation.

Variations of MSMPR crystallisers have been investigated to meet the chirality requirements in the pharmaceutical industry. For example, Galan *et al.* investigated the first experimental coupling of two MSMPR crystallisers *via* continuous exchange of liquid phases. Through continuous feeding of racemic solutions of D- and L-threonine and withdrawal of liquid phase and solid particles, the process mimics liquid phase racemisation. As a result, the concentration of one enantiomer increases, whilst the other decreases. Under identical conditions, the coupled crystalliser was twice as productive as the single crystalliser and aligned with previous mathematical simulations.[61,62]

In the continuous tubular crystalliser, the solution is fed through an inlet and crystallises through anti-solvent addition or cooling, followed by product crystal withdrawal at the outlet. An infinite number of coupled MSMPR crystallisers is mathematically equivalent to a CTR, Figure 1.19. Due to the difficulty in controlling CTR leading to blockages, these reactors mainly focus on crystal size control.[63]
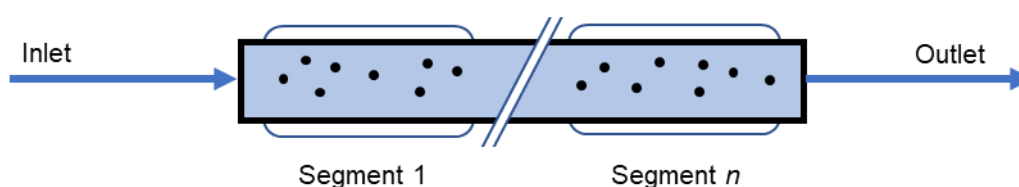
Figure 1.19. Schematic diagram of Continuous Tubular Crystalliser (CTR) for continuous crystallisation.

The immobilisation techniques in the previous section can be utilised in combination with continuous flow techniques. The advantage of this is that the reaction and catalytic separation can be performed simultaneously, decreasing product contamination and increasing catalytic recyclability. In addition to this, no mechanical agitation or stirring is required in flow, meaning that mechanical degradation of the immobilised support leading to shortened immobilised catalyst life-times is avoided.[64] These reasons explain why utilisation of a packed bed reactor is explored in this project. A packed bed reactor is characterised by an entire column being filled with solid material such that the particle movement is restricted. Flow of liquid in this bed is usually plug flow but can be turbulent at a higher flow rate. In a fluidised bed reactor, particles are free-flowing and suspended by turbulent flow, whilst mixed beds are a combination of both packed beds and fluidised beds.[58] As optimal condition investigation for mixed and fluidised beds is time-consuming, this project focusses on using a PBR set-up.
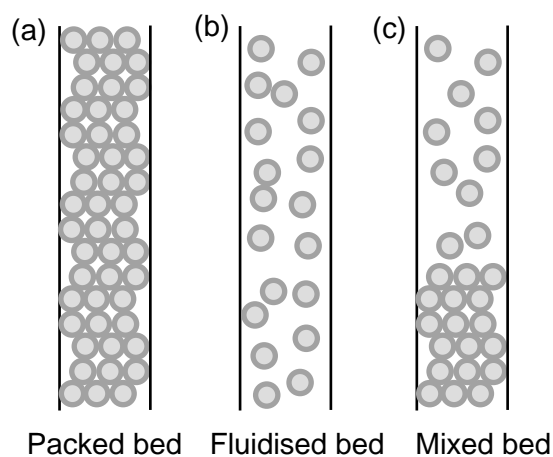
Figure 1.20. Comparison of each solid-liquid reactor bed where (a) packed bed reactor, (b) fluidised bed reactor, (c) mixed bed reactor.

Continuous flow processes are advantageous compared to their batch counterparts for many reasons. For example, on-demand analysis can be integrated into the reaction to allow quick analysis, unstable and hazardous materials can be directly telescoped without isolation and narrower temperature profiles result in a reduction in side reactions[65–68] However, the major drawback of flow processing is that most laboratories are set up for batch reactions, with a large knowledge-base and infrastructure supporting batch chemistry. Furthermore, there is uncertainty in regards to implementation of Good Manufacturing Practice (GMP) and regulatory acceptance.[68]

1.7 Project Objectives

The overall aim of this project was to explore a continuous flow methodology, namely the Resolution-Racemisation-Recycle R^3 process, in the synthesis of complex chiral amines. The initial workflow was set with the intention of investigating the following:

(i) Utilisation of FlowNMR methodology to probe mechanistic pathway of $[IrCp^*I_2]_2$ catalyst (Chapter 1)

(ii) Development of a rapid H/D exchange screening methodology to assess the racemisation/epimerisation of simple and complex chiral amines (Chapter 2)

(iii) Investigation of β-amino-alcohol racemisation as first priority, or α- and β-hydroxy/amino acids, esters and nitriles

(iv) Prior to integration of resolution and racemisation in the R^3 process (Chapter 3):

    a. Investigation of complex chiral amine resolution through diastereomeric crystallisation

    b. Exploration of racemisation using homogeneous $[IrCp^*I_2]_2$ catalyst, using solvent and acid conditions identified for resolution

(v) Develop an understanding of the limitations and scope of the R^3 process (Chapter 3), in addition to understanding how to manipulate the conditions to produce the desired diastereomer

The extent to which these targets were achieved is described in the following chapters, with further investigation required with respect to targets (iii) and (v) as a result of the COVID-19 pandemic.

2 Dynamic Reaction Monitoring Facility

2.1 Introduction

Reaction mechanisms and kinetics can be determined through monitoring the concentration of different species in real-time. A variety of spectroscopic techniques can be used, including Raman, ultraviolet-visible (UV-vis), infrared (IR), mass spectroscopy (MS) and nuclear magnetic resonance (NMR) spectroscopy. By far the most useful, ^{1}H NMR is quantitative and able to give a large quantity of information on molecular structure.

Traditionally, NMR samples are removed from a batch reaction mixture and analysed *off-line*. Monitoring reactions in this way allows reaction conditions to be controlled prior to periodic sampling. However, as samples analysed in this way are often quenched, the data obtained is often unrepresentative of the original reaction mixture. Furthermore, the delays introduced whilst sampling *off-line* expose the sample to different conditions, and lack of agitation in NMR tubes can lead to the acquisition of unreliable kinetic data.[69,70]

The limitations of *off-line* monitoring can be circumvented using *on-line* monitoring techniques, where tubing delivers samples to the desired instrument.[70] Amenable to a range of different conditions, such as heating, cooling and inert gas atmospheres, *on-line* NMR monitoring allows reactions to be performed without ceasing data acquisition. As the reaction is mixed, data is monitored under realistic conditions where reaction kinetics remain unaffected by mass transfer limitations.[70]

The following section contextualises the data presented in this chapter by providing background information on the practicalities and considerations of FlowNMR, as carried out at the Dynamic Reaction Monitoring (DReaM) facility.

2.2 DReaM Facility

The DReaM facility at the University of Bath allows the real-time monitoring of homogenous reactions using FlowNMR.[71–74] Two, one-week sessions were carried out there, to investigate the mechanism of chiral amine racemisation by SCRAM catalyst **13**. The set-up uses a VapourSF-10 pump to circulate reaction mixture to a 5 mm glass tip NMR flow tube, residing in a 500 MHz NMR spectrometer, Figure 2.1. The reaction mixture returns to the reaction vessel after flowing through the InsightMR flow tube in a continuous closed loop. Techniques such as UV-visible spectroscopy, mass

spectrometry, HPLC and polarimetry can be coupled with the flow system, and can be removed and added as required.
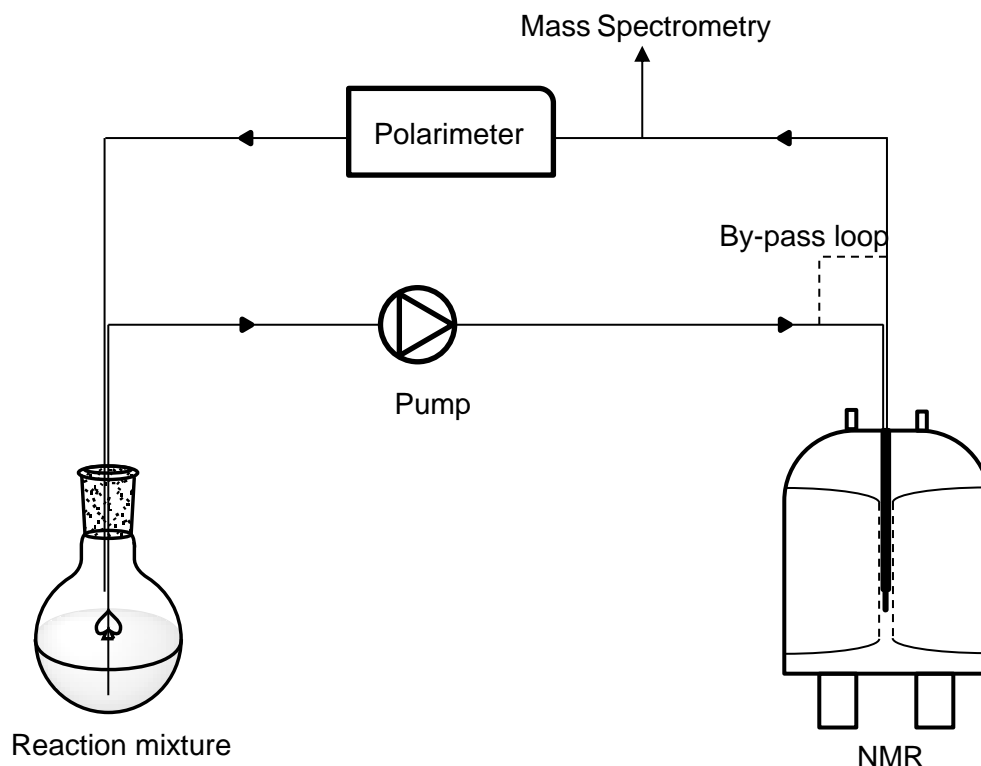
Figure 2.1. FlowNMR reaction monitoring set-up at the DReaM facility

The reaction is conducted in a vessel external to the spectrometer, allowing careful control of reaction conditions, and allows addition of new reagents without ceasing flow. The reaction is continuously stirred for uniform reactant distribution, is monitored without the need to quench and can be run with high temporal resolution (spectra per time).

It is important to consider the intrinsic effects of flow on NMR data quantification. At a standard flow rate of 4 mL min^{-1}, the sample spends approximately 3 seconds within the magnet, followed by 8 seconds in the detector. As a result, signal intensity is underestimated and quantification is impacted, as 3 seconds is less than the relaxation time delay required for the magnetisation of most nuclei ($<5T_1$). Discrepancies at flow rates of 4 mL min^{-1} can be as high as 25%, and if unaccounted for, translate to inaccurate kinetic data. Fortunately, these in-flow effects can be accounted for by recording one flowing spectrum and one static spectrum at the beginning and end of a reaction, or by halting flow upon significant intermediate observation. Similarly, continuous replenishing of magnetised nuclei in the detector with fresh sample, so called out-flow effects, can also be corrected for. Accordingly, a correction factor (CF) may be calculated for each

integral (I), using the simple mathematical formulae below, Equation 2.1 and Equation 2.2.

$$I_{corrected} = CF \times I$$
<div align="right">Equation 2.1</div>

$$CF = \frac{I_{Static}}{I_{Flow}}$$
<div align="right">Equation 2.2</div>

As dust and particulates can block the flow tubing, all solvents and solutions must be filtered beforehand. The operator must also be certain no precipitate will form during the reaction course. Reactions can be carried out in non-deuterated solvents, which are cheaper than their deuterated counterparts and avoid any hydrogen-deuterium exchange. Solvent suppression pulse sequences decrease non-deuterated solvent peak intensity, however, this may still pose an issue if solvent peaks overlap with peaks of interest.

Generated data is often in the range of hundreds to thousands of spectra, therefore automated processing is often used for phasing and baseline correction. Nevertheless, manual parameter refinement is recommended for reduction in data scattering and baseline distortion, which is unreasonable for larger datasets.

2.3 Experimental Overview

The initial racemisation experiments of (R)-N-methyl-α-methylbenzylamine **33** using catalyst **13** were conducted in pure IPA to increase catalyst solubility and simplify analysis. However, polarimetry of these samples suggested no racemisation under these conditions. This was later confirmed using chiral GC, and may be due to the high concentration of IPA pushing the equilibrium towards the amine and preventing imine formation. Modifying the conditions, using a solvent combination of IPA and EtOAc (1:4), the racemisation worked, and decreased the ee of (R)-**33** from 100 to 6%, monitored by chiral GC, Scheme 2.1.[75] However, it was noted the catalyst required 3.5 hours to dissolve. A comparison of the experimental conditions is shown in Table 2.1
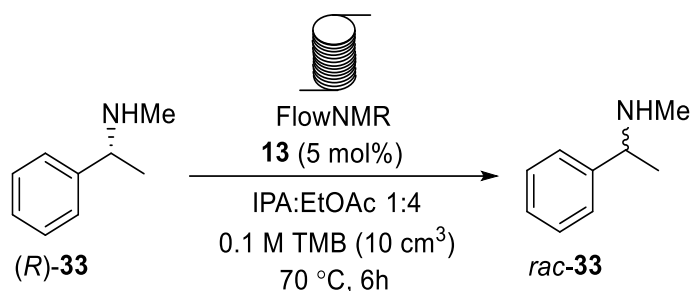
Scheme 2.1. Racemisation of (R)-**33** under flowNMR conditions.

Entry	Solvent	33 (M)	13 (mol %)	Temperature (°C)	Endpoint ee
1	IPA	0.4	0.5	70	100%
2	EtOAc:IPA 4:1	0.5	1	60	6%
3	EtOAc:IPA 4:1	0.25	1	60	55%
4	EtOAc:IPA 4:1	0.25	0.5	70	94%

Table 2.1. Comparison of conditions used to racemise. Data from entry **2** taken from reference 75**.**

Despite the lack of racemisation of **33** in pure IPA, a hydride signal at -15.18 ppm was observed and remained throughout the reaction. Interestingly, when the reaction was repeated using the IPA:EtOAc mixture, a hydride signal was observed at -16.86 ppm which diminished in intensity throughout the reaction, until no longer visible. The difference in chemical shift (1.68 ppm) would suggest that each hydride species is in a distinctly different chemical environment, as a change in chemical shift to this extent was not expected.
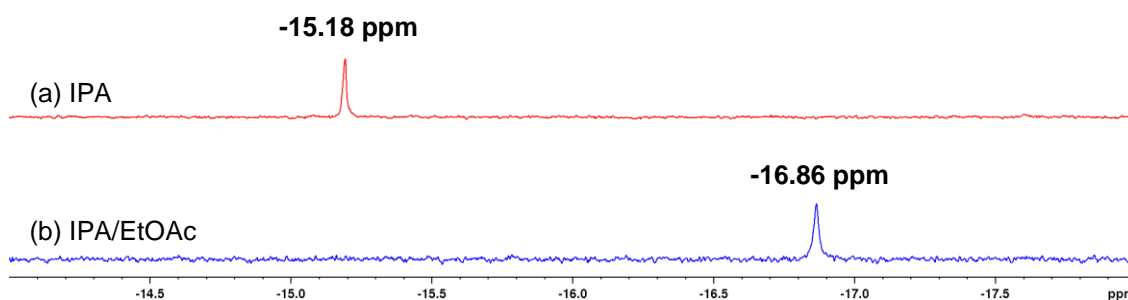
Figure 2.2. Hydride signal observed during (a) attempted racemisation of (*R*)-**33** with SCRAM catalyst in pure IPA and (b) racemisation of (*R*)-**33** with SCRAM **13** catalyst in a 1:4 IPA:EtOAc mixture.

Due to slow dissolution of the catalyst in the IPA:EtOAc (1:4) mixture, an in-line filter was added after 60 minutes, however this may have affected the 3 mL/min flow rate. Due to issues with the polarimeter, the first 160 minutes of datapoints were missed, nevertheless, hydride signals were still observed.

2.4 Results and Discussion

When carried out in EtOAc and IPA 4:1, the on-line polarimeter showed a fall in rotation, suggesting racemisation, however catalyst solid was still seen recirculating. To alleviate this, the reaction was repeated with half the catalyst (Table 2.1, entry 4). Despite more rapid dissolution, no hydride signal was observed and the reason for this is unclear.

Analysis of the results from Table 2.1, entry 3 showed the amine signals remaining constant, whilst an exponential decay of a hydride signal at -16.86 was seen as the reaction progressed, Figure 2.3. The natural log of this gave a straight line fit with $R^2 =$ 0.96, which suggests first-order reaction with respect to the hydride, Figure 2.4. If the catalyst is at steady-state, the hydride signal would be expected to remain at constant intensity, so a first-order decay indicates an off-cycle species. Previous work has shown hydrolysis of the imine intermediate can generate methylamine that coordinates strongly to iridium to produce deactivated catalyst species.[75] It is possible that the hydrido-species is decaying to form a mono-, di-, or tri- methylamino species. No ^{1}H-^{15}N coupling was observed with the hydride signal.

The overall order is zero with respect to aminev, but first order with respect to the *S*-enantiomer. Increasing the concentration of amine or catalyst causes an increase in the rate of reaction.
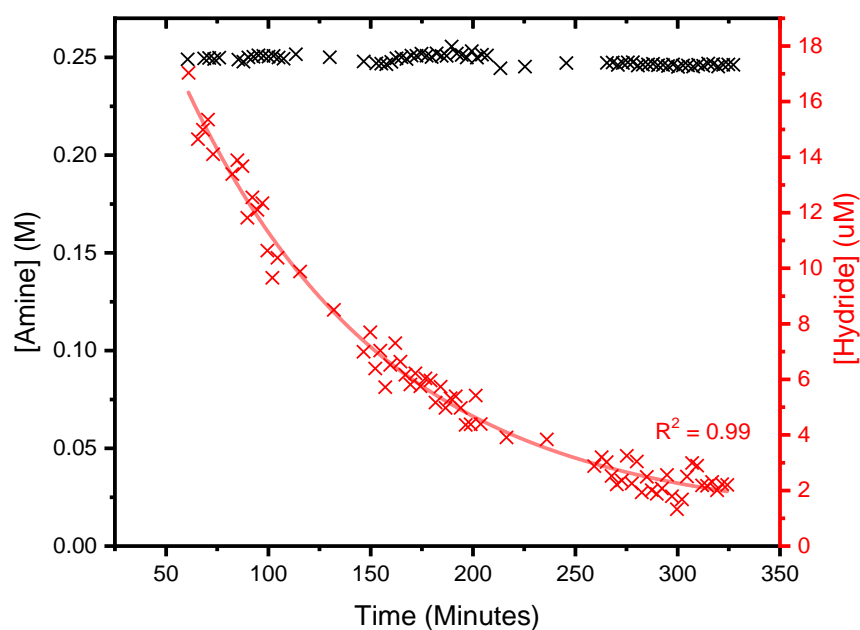
Figure 2.3. A graph to show the change in concentration of hydride and amine using conditions in Table 2.1, entry 3
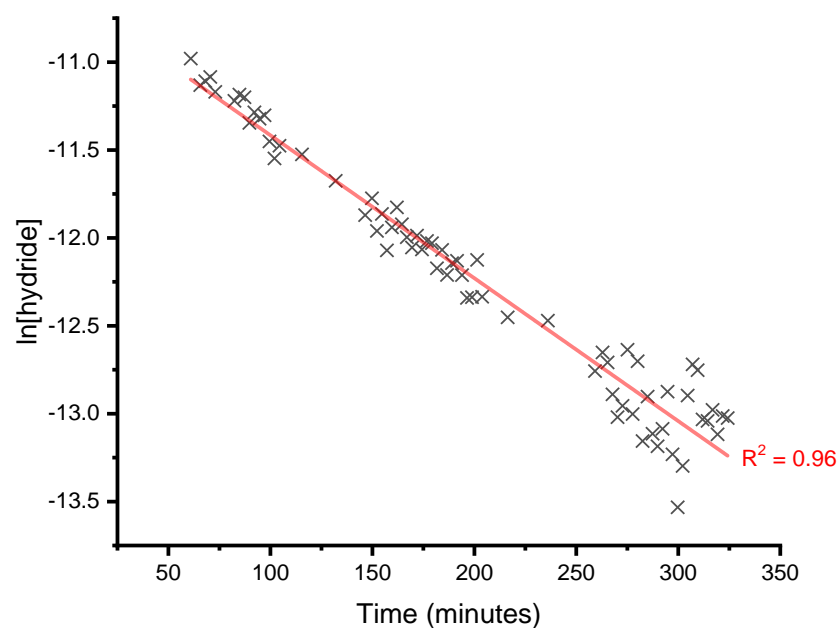
Figure 2.4. The linear change in ln[hydride] with respect to reaction duration showing first-order fit for entry 3, Table 2.1

The polarimetry data showed the enantiomeric excess of (*R*)-**33** in Table 2.1, entry 3 decreasing from 100 to 55% after 5.8 hours, Figure 2.5, with a linear fit R^2 of 0.95. An experiment in batch with 0.5 M amine decreased to approximately 6% ee after a similar time. The higher amine concentration may account for this difference, as its addition increased the solubility of the catalyst. By linear interpolation to time zero, the specific rotation $[\alpha]_D$ is -61.7, giving a starting material of 82% ee instead of 100% ee. This may be accounted for by a more rapid initial racemisation, ie not linear. The racemisation half-life determined polarimetrically in Table 2.1, entry 3 experiment is 10 hours, compared to the 1-2 hour with 0.5 M amine.
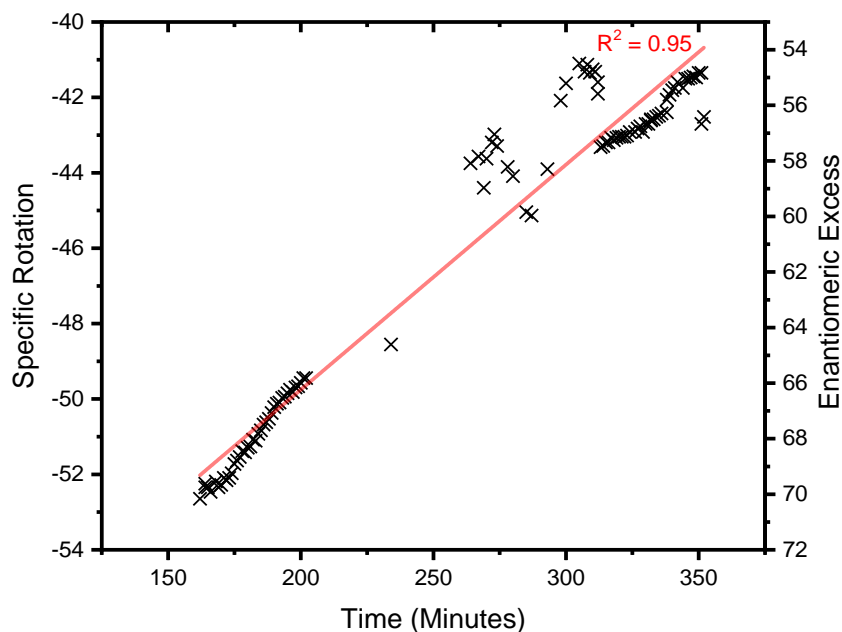
Figure 2.5. Change in specific rotation and enantiomeric excess throughout reaction in entry 3, Table 2.1

2.4.1 Spin-lattice relaxation T_1

The spin-lattice relaxation (T_1) value for a particular hydride gives an indication as to whether that signal is a classical (terminal) or non-classical (η-2 bound) hydride. The T_1 value can be measured using a standard inversion-recovery pulse sequence (180^0-t-90^0) and measuring the time taken for equilibrium magnetisation to be recovered along the direction of applied magnetic field. Dipolar relaxation is the main mechanism through which these inverted spins are recovered, which is influenced by other nearby dipolar nuclei. As a result, the environment around a hydride can lead to different T_1 relaxation times, and therefore provide information about the nature of the hydride.[76] For example, the minimum T_1 value for a classical complex has never been <50 ms and that of a non-classical complex has never been >35 ms at 250 MHz. As a consequence, values associated with either classical or non-classical hydrides do not overlap.[77]

The T_1 value for the hydride in the pure IPA reaction was calculated to be 1.179 seconds, suggesting it could be due to the presence of a terminal hydride. Whilst T_1 values for iridium hydrides are available in the literature, most values found were <520 ms, making it difficult to unequivocally assign this hydride as classical or non-classical.[77–80] The closest T_1 value found was 820 ms for a 7-coordinate iridium pentahydride complex **34**, $IrH_5(PCy_3)_2$.[81] A similar complex **35**, $[IrH_2(H_2)_2(PCy_3)_2]^+$ with two classical and two non-

classical hydrides, gave T_1 values of 76 ms and 48 ms respectively which indicates the extent to which the T_1 value can vary with change in environment.[82] The full skeletal structure of these complexes with corresponding T_1 values are shown in Figure 2.6.

34 **35**
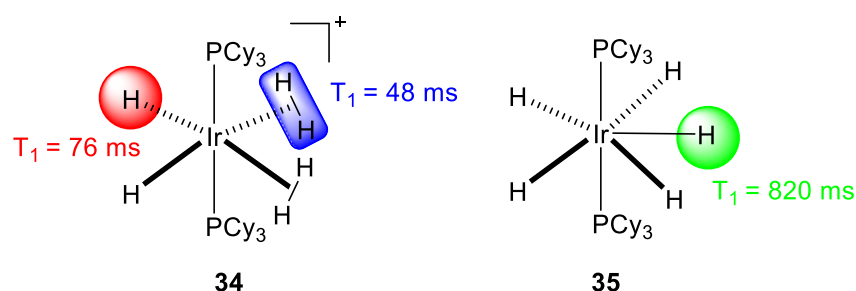
Figure 2.6. T_1 values for iridium polyhydrides **34** and **35** found in the literature.[81,82]

Unfortunately, due to time constraints at the facility, a T_1 value for the EtOAc/IPA reaction could not be calculated. However, future calculation of the T_1 value under conditions where *N*,α-Dimethylbenzylamine **33** racemises would be useful for comparative purposes.

2.4.2 Mass Spectrometry Data

Mass spectrometry is a useful technique in reaction mechanism elucidation based on its speed, sensitivity, and ability to capture transient, low concentration species.[83–85] As a result, monitoring the relative intensity throughout reaction duration proved to be useful in determining which species may be present during the amine racemisation. It is important to note that mass spectrometry can only monitor how well a particular species ionises, and not how much of the species is truly present. The relative increase and decrease of different species can provide insight into possible reaction mechanism.

Of the detected masses, two species corresponding to m/z 723.1799 and 725.1883 reached relative intensities of around 75,000 and 100,000 respectively. Compared to other masses detected, these values were relatively high. Both species' signal intensity changed proportionally, Figure 2.7.
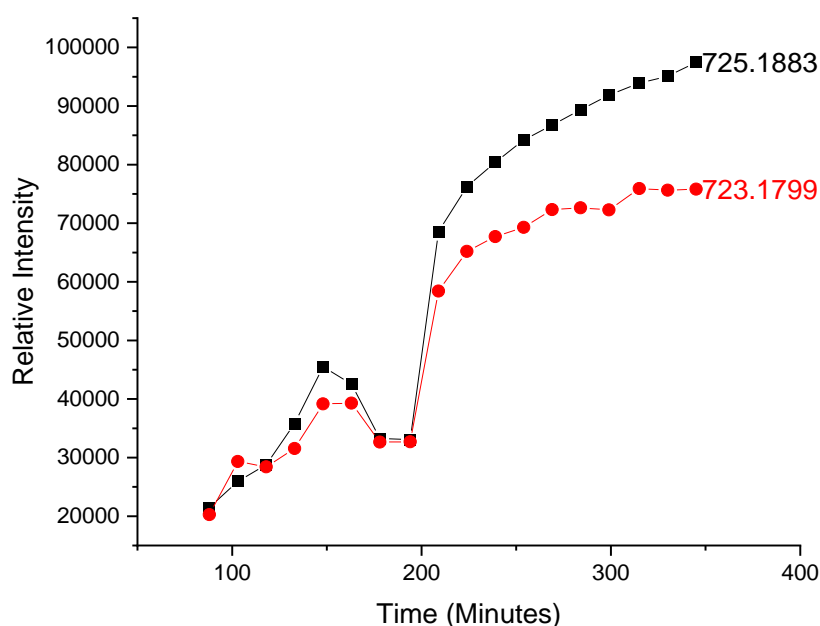
Figure 2.7. Change in relative intensity of m/z 723.1799 and 725.1883 during racemisation of *N*,α-Dimethylbenzylamine **33** (Table 2.1, entry 3)

Comparison of the observed and simulated mass patterns enabled a possible structure of each species to be proposed. For m/z 723.1799, a positively charged iridium (V) complex **36** with was proposed. Ir(V) complexes have previously been proposed as intermediates in transfer hydrogenation reactions.[86–89] The chemical formula of this species was used to simulate a mass spectrum for comparison to the observed mass spectrum, Figure 2.9. With respect to relative peak intensity, the simulated and observed patterns were similar, with the exception of the peak at m/z 725.1886, which was relatively intense in comparison to nearby peaks. This is likely due to the overlap of fragmentation patterns corresponding to both the m/z 723.1799 and 725.1883 species. Comparison of the expected exact mass to the observed mass gave a mass error of - 7.30 ppm.

The proposed structure **37** for the m/z 725.1883 species, Figure 2.9, is similar to that in Figure 2.8. Both the observed and simulated mass spectra are comparable with respect to relative peak intensity and m/z, with a mass error of 4.28 ppm.
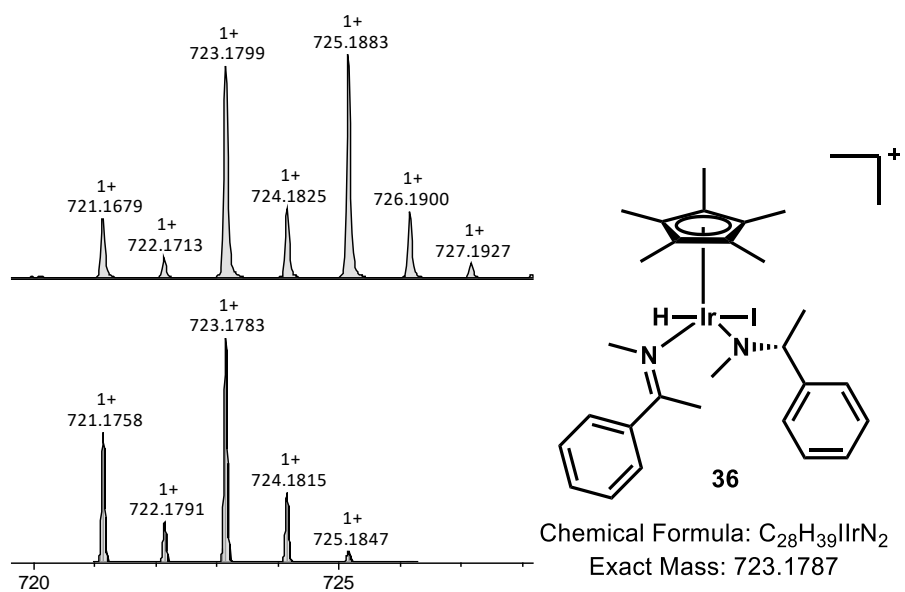
Figure 2.8. Top: partial HRMS for entry 3 in Table 2.1. Bottom: Simulated pattern for [$C_{28}H_{39}IIrN_2$]$^+$. Right: proposed structure **36**.
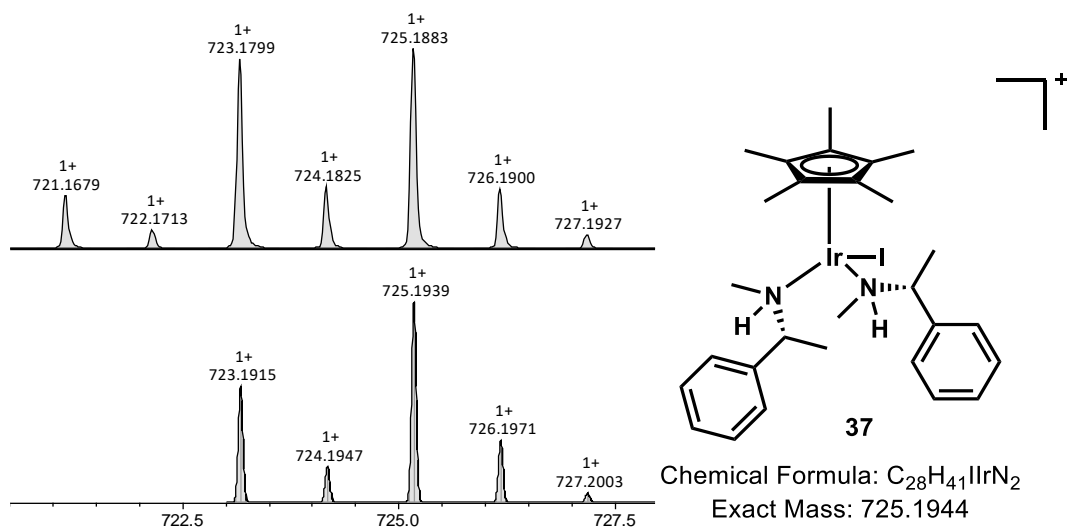
Figure 2.9. partial HRMS for entry 3 in Table 2.1. Bottom: Simulated pattern for [$C_{28}H_{41}IIrN_2$]$^+$. Right: proposed structure **37**.

The relative intensities of m/z 659.1787, 785.0758 and 910.9720 were also plotted with respect to time, demonstrating a correlation, Figure 2.10.
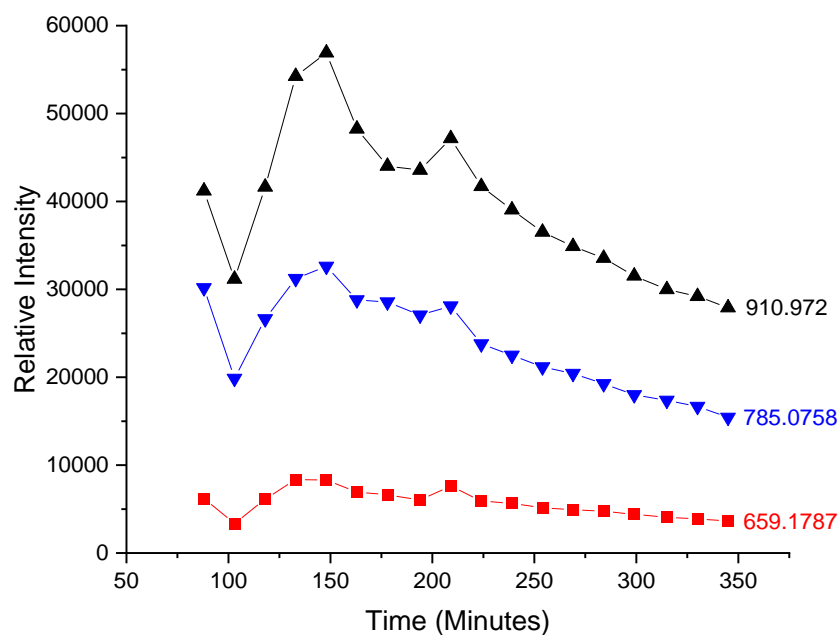
Figure 2.10. Change in relative intensity of m/z 659.1787, 785.0758 and 910.9720 during racemisation of *N*,α-Dimethylbenzylamine **33** (Table 2.1, entry 3)

Bridging monohydride **38**, dihydride **39** and trihydride **40** species of SCRAM catalyst **13** were proposed as possible structures, Figure 2.10, with the relative intensity of each species inversely correlating with increasing number of hydrides.

38

Chemical Formula: $C_{20}H_{31}I_2Ir_2$
Exact Mass: 910.9774

39

Chemical Formula: $C_{20}H_{32}IIr_2$
Exact Mass: 785.0807

40

Chemical Formula: $C_{20}H_{33}Ir_2$
Exact Mass: 659.1841
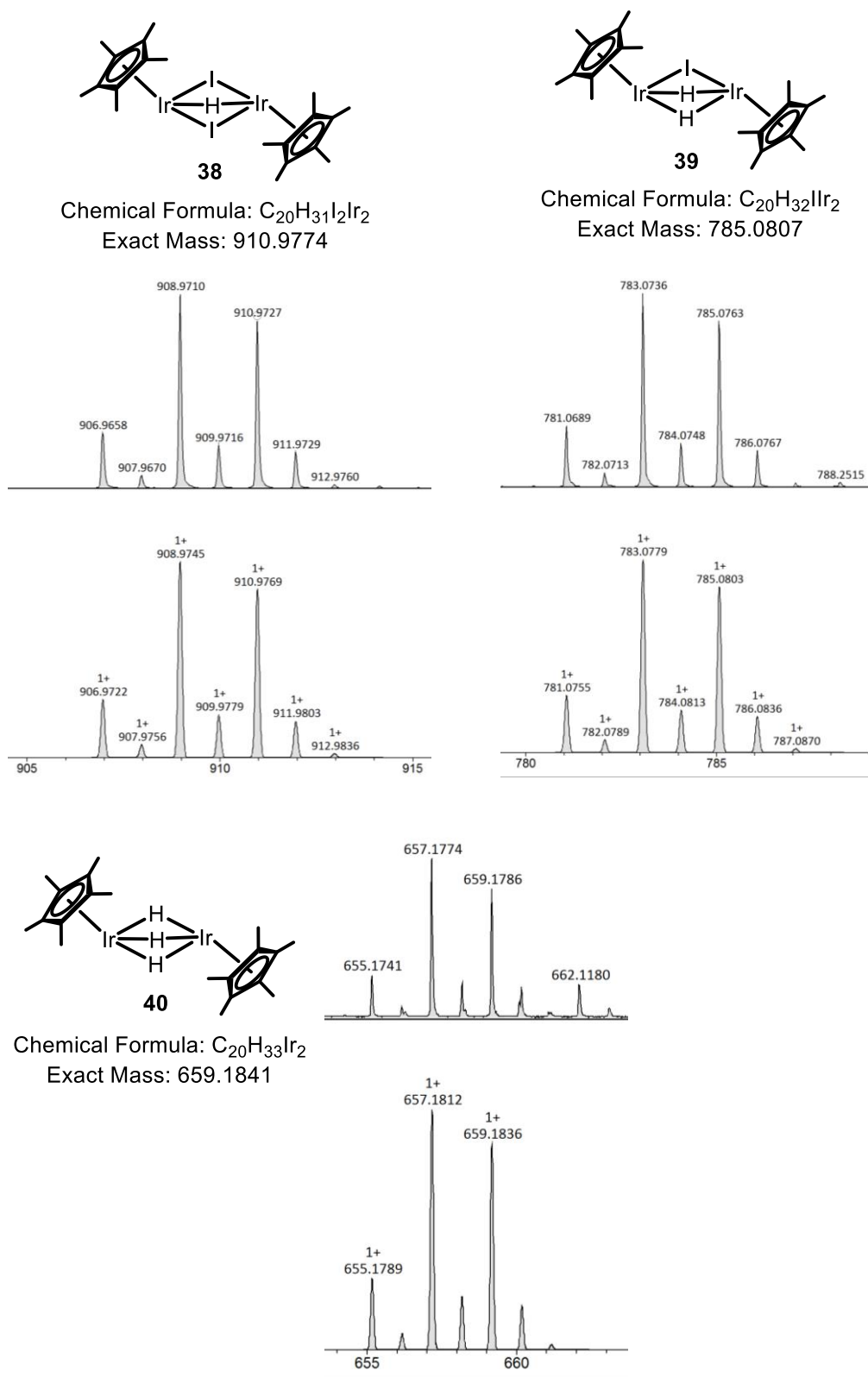
Figure 2.11. Top pattern: partial HRMS for entry 3 in Table 2.1. Bottom: Simulated pattern for triply bridging hydrides. Proposed structures **38**, **39**, **40** adjacent to corresponding pattern.

Perhaps due to the temperature at which the racemisation was conducted (70 °C), a chemical shift value comparable to the detected hydrides (at -15.18 and -16.86 ppm, Figure 2.2) could not be found in the literature. However, a trihydride structure **41** $[IrH_5(PPh_3)_4]^+$ similar to the proposed structure in Figure 2.11 was found, with ^1H NMR δ -6.9 ppm (H_a), -8.4 ppm (H_b), -23.9 ppm (H_c) at -80 °C in deuterated acetone. At room temperature, coalescence of the H_a and H_b signals were observed, likely due to rotational fluxionality on the NMR timescale.[90,91]

41
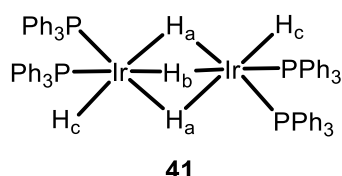
Based on the mass spectrometry data in Figure 2.10, it is possible that rotational fluxionality leads to the appearance of the single hydride signals at 15.18 and -16.86 ppm in IPA and EtOAc/IPA respectively, Figure 2.12. This is despite the proposed hydrides being in at least two distinct chemical environments.
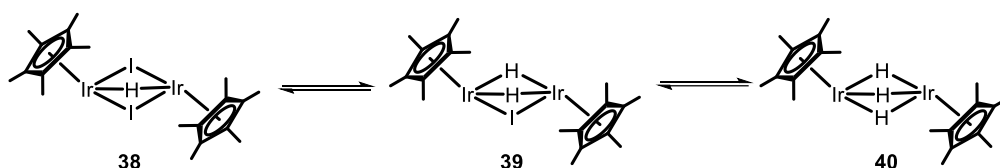
Figure 2.12. Proposed equilibrium between iridium-hydride species **38**, **39** and **40**.

To confirm this, variable temperature NMR experiments could be carried out. It would be interesting to do this in both IPA and the EtOAc/IPA mixture, and subsequently compare any resolved chemical shift values to those in the literature. Based on a study by Morris *et al.* it is possible that their trihydride $[IrH_2(\mu\text{-}H)_3L_4]^+$ (Where R = PPh_3, $PMePh_2$) is the result of two separate iridium hydride complexes coordinating and, in their study, leading to irreversible deactivation.[92] However, due to the change in intensity of all proposed species in Figure 2.10, our study suggests that if the trihydride species is formed, it is likely reversible. Furthermore, the observed and simulated fragmentation patterns for the three proposed species are similar with respect to relative intensity, Figure 2.11. The mass error for the monohydride, dihydride and trihydride are small, -5.16, -5.60, -8.34 ppm respectively.

2.4.3 Proposed Catalytic Cycle

The original proposed mechanism, Scheme 1.11, shows the dissociation of SCRAM catalyst **13** to its monomer which interacts with (*R*)-**33** to form an iridium hydride bond and iminium ion. This ion-pair may dissociate prior to, or at a rate competitive with hydride transfer back to the iminium ion, regenerating the $IrCp*I_2$ monomer.[33] Complex **14** signifies a neutral species, and as such, does not appear in our mass spectrometry data.

Through comparison of the original mechanism and data presented in this chapter, an updated catalytic cycle is proposed, Figure 2.15. The formation of analogous positively charged diamine **41** species is shown undergoing β-Hydride elimination to form Ir(V) species **42**, the formation of which is supported by previous observations of Ir(V) complexes by Heinekey *et al.*[93,94] Original cross-over experiments suggest **42** likely exists in equilibrium with its ion-pair, the imine counterpart **43** of which can dissociate and interact with a separate iridium-hydride species.[33] As a result, imine reduction can occur once again to form **44**, which, in addition to amine counterpart **46**, is evidenced through observed and simulated mass spectra, Figure 2.13 and Figure 2.14 respectively. The dissociated iridium counterpart **45** is shown reducing imine **43**, demonstrating catalytic intermediate ability to associate and dissociate with imine. Previously reported triply bridged dinuclear iridium complexes **38, 39, 40** are shown forming as off cycle species, and are likely formed through interaction of active catalytic intermediates.[95–97]

Chemical Formula: $C_{19}H_{28}IIrN^+$
Exact Mass: 590.0890
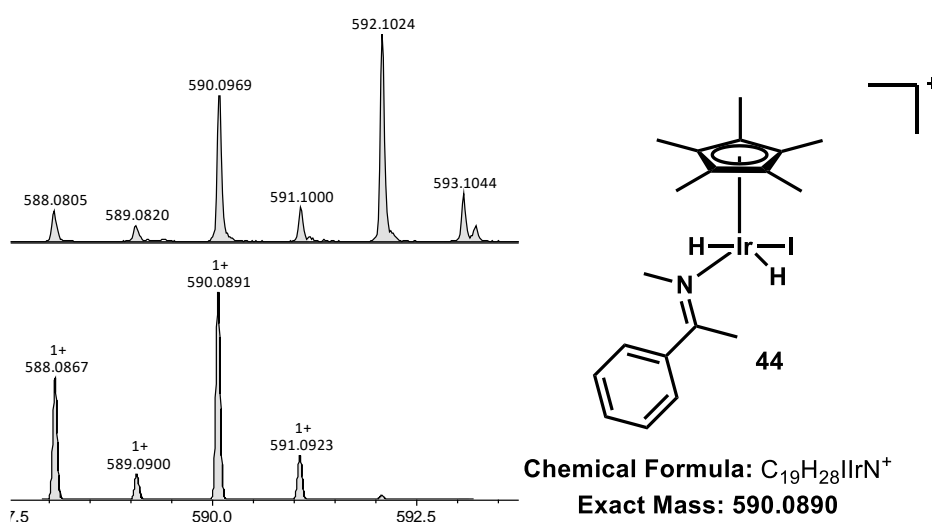
Figure 2.13. Top: partial HRMS for entry 3 in Table 2.1. Bottom: Simulated pattern for $[C_{19}H_{28}IIrN]^+$. Right: proposed structure **44**.
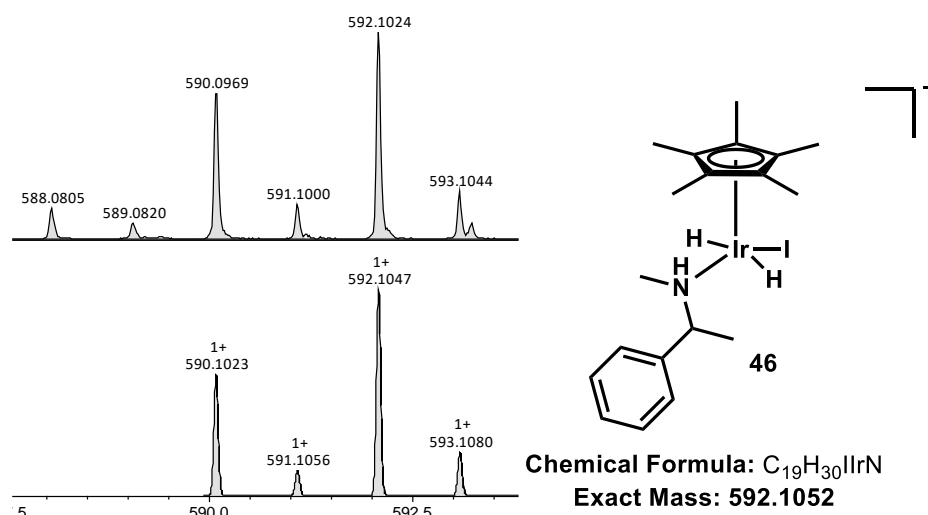
Figure 2.14. Top: partial HRMS for entry 3 in Table 2.1. Bottom: Simulated pattern for $[C_{19}H_{30}IIrN]^+$. Right: proposed structure **46**, not explicitly included in the proposed catalytic cycle.

2.4.3.1 Limitations

Whilst the proposed cycle in this chapter reflects the mass spectrometry data obtained during flowNMR experiments, it is not without limitation. The transition between species **41** and **42** does not account for the loss of protons from the amine species and or respective counteranion formation. It is possible that iodide ions from SCRAM catalyst **13** provide a source for hydrogen iodide formation or behave as counteranions to the formed iridium complexes, however, there are not enough of these iodide ions to support the provided mechanism. Removing or introducing protons to the amines changes the ligand from L- to X-type or visa versa. As a result, this changes not only the oxidation state of the iridium complex but also the electron count. The proposed cycle has therefore been proposed in a way which supports mass spectrometry data and previously observed iridium complex oxidation states with an 18 electron count. Further research under flow conditions would be required to refine this catalytic cycle and substantiate elements of the cycle which have already been proposed.

Figure 2.15. Updated catalytic cycle combining the original proposed cycle and data achieved through FlowNMR investigations.

2.5 Conclusion and Future Work

In combination with flowNMR, other *on-line* spectroscopic techniques such as HRMS and polarimetry can be used to deduce catalytic mechanisms. The otherwise problematic effects of incomplete magnetisation under flowNMR conditions are accounted for through calculation of a correction factor, unique to each NMR signal. As a result, accurate kinetic data can be calculated.

The SCRAM **13** catalysed racemisation of (*R*)-*N*-methyl-α-methylbenzylamine **33** was investigated in both IPA and IPA/EtOAc (1:4), leading to observation of an iridum-hydride signal through ^{1}H NMR. The chemical shift difference between the signals suggests each signal is associated with a different iridium-based catalytic intermediate, which is unsurprising as racemisation only occurred in the IPA/EtOAc (1:4) mixture, confirmed through polarimetry data ($t_{1/2}$ = ~10 hours). The concentration of hydride in the racemising mixture decreased exponentially throughout reaction observation, and as a result, the data indicated it was first-order with respect the hydride. Consequently, this suggested formation of an off-cycle species, which may be due to well-established catalytic poisoning through methylamine ligation.[98] However, there was no evidence for this in the HRMS data.

The spin-lattice relaxation (T_1) value for the non-racemising reaction in IPA was determined to be 1.179 seconds. Due to time constraints, a value for the racemising mixture was not determined. Based on the T_1 value in the non-racemising solution, the hydride signal is associated with a terminal hydride. However, compared to literature values, this value was very high. For comparative purposes, any future work at the facility should ensure derivation of the T_1 value for a racemising solution.

Mass spectrometry data collected every 15 minutes supported proposition of iridium-based catalytic intermediates. An Ir(V) complex containing an iridium-hydride bond and an Ir(III) complex with two ligated amines were proposed. The chemical formula of each proposed species was used to generate a simulated mass spectrum which aligned with observed HRMS data. Furthermore, HRMS data provided evidence for mono-, di- and tri-hydride dinuclear iridium species. ^{1}H NMR and HRMS data suggest these species may exist in equilibrium with each other through molecular fluxionality, although similar structures have been reported to lead to irreversible deactivation.[92] As a result of the data in this chapter, the original catalytic cycle was considered in comparison to the data collated at the DReaM facility and a new, adapted catalytic cycle was proposed.[33]

Further research at the DReaM facility would first require preliminary investigation into the solubility of SCRAM catalyst in a range of different solvents and temperatures. As a result, no solubility issues will be encountered upon a subsequent visit to the facility. Furthermore, catalyst solubility will allow for circulation of homogeneous mixture containing only catalyst under flowNMR conditions prior to amine addition.

Investigation of *N*-methyl-α-methylbenzylamine **33** racemisation under batch solvent and temperature conditions with pre-solubilised SCRAM catalyst will allow for the best conditions to be selected and further investigated at the facility. For optimal understanding of substrate racemisation in batch, the kinetics of chosen conditions should be investigated at different concentrations of amine and catalyst.

After thorough investigation of these conditions, it is recommended that flowNMR experiments investigate the effects of $MeNH_2$ and D_2O addition to the reaction mixture. As $MeNH_2$ (formed through hydrolysis) is a known catalyst poison, findings would assist in understanding the deactivation mechanism. Repeating the reaction with imine rather than amine and observing whether hydride formation and or racemisation occurs would also be interesting. In addition to this, investigating the reaction with the chloride analogue of the catalyst, $[IrCp*Cl_2]_2$ which is able to racemise alcohols but not amines, would allow for further investigation into the importance of the iodide ligands. The experiment may be repeated with the addition of potassium iodide to generate $[IrCp*I_2]_2$ in *situ* which has been shown to racemise amines, but not as effectively as isolated SCRAM catalyst.[99]

3   Development of a rapid screening method for determining racemisation

3.1   Background

Traditional methods for determining homochiral amine racemisation require an analytical method for monitoring the concentration of both amine isomers. Synthesis of both enantiomers can be laborious, and development of a chiral HPLC, GC or NMR method is time-consuming.[100] Therefore, a rapid microwave-assisted ^{1}H NMR and HRMS screening technique was developed to quickly assess chiral amine racemisation.[75,101] The use of a deuterated hydrogen donor (d_8-isopropyl alcohol) allows deuterium incorporation into the intermediate imine, and observation of the point of addition using ^{1}H NMR.[102] Importantly, this allows the use of racemic amines, which are usually readily available and less costly, avoiding enantiomer synthesis. Furthermore, microwave irradiation increases reaction rate and has been explored extensively for deuterium labelling.[103–105] The general procedure involves heating a mixture of chiral amine, d_8-IPA **47**, d_8-toluene **48**, SCRAM catalyst **13** and suitable internal standard at 110 ºC under microwave conditions for 4 hours, Scheme 3.1. The cooled sample can be analysed directly by ^{1}H NMR or HRMS, and monitored as a function of time if it is repeatedly reheated and reanalysed.
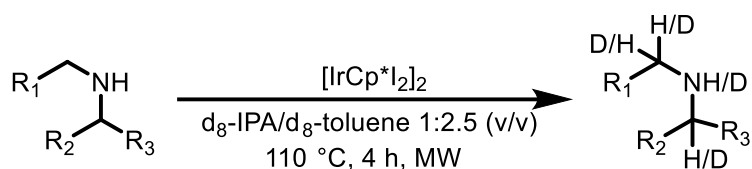
Scheme 3.1. General deuteration procedure of chiral amines with d_8-IPA **47**, catalysed by [IrCp*I$_2$]$_2$ **13**.

The amine under investigation **49**, and the d_8-IPA **47**, interact with SCRAM catalyst **13** to form an imine **50**, and carbonyl group **51** respectively, Scheme 3.2.[33,98] The products can remain coordinated, and also exist in equilibrium with their enamine **52** and enol **53** counterparts due to tautomerisation. Reaction of the iridium-deuteride in **51** with imine **50** leads to deuteration at the α-centre and reaction of enamine **52** with enol **53** leads to β-centre deuteration. As such, the d_8-IPA **47** can act as both a source of deuteride (D⁻) and deuteron (D⁺), the former of which can attack either face of the imine indicating racemisation.
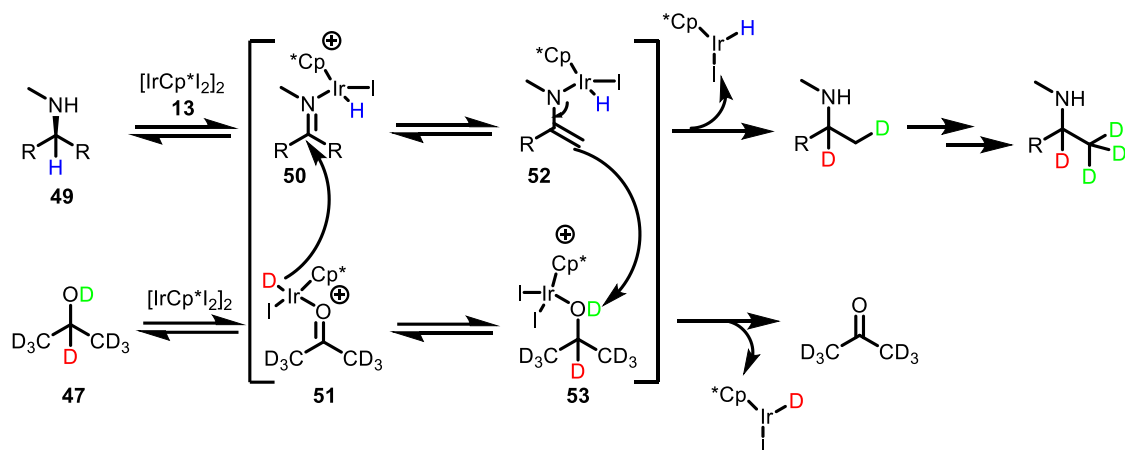
Scheme 3.2. The proposed deuteration mechanism of a general secondary amine, *via* the catalysed formation of imine and enamine intermediates and their interaction with deuteride (D-) and deuteron (D+) respectively.

In this chapter, a series of simple chiral amines, both primary and secondary in nature were examined. The study scope was broadened through investigation of pharmaceutically relevant compounds (including those with more than one chiral centre) and diastereomeric salts.

3.2 Simple aromatic amines

3.2.1 *N*-Methyl-α-methylbenzylamine

Racemisation of *N*-methyl-α-methylbenzylamine **33** was previously investigated in the group,[75,101] and was investigated in the previous chapter. As a result, investigation of the mechanistic pathway was further expanded through comparison of reactions conducted with d_8-IPA **47** and OD-IPA **54**, Scheme 3.3. Using different extents of deuterated IPA, the points of deuterium incorporation could be further investigated.
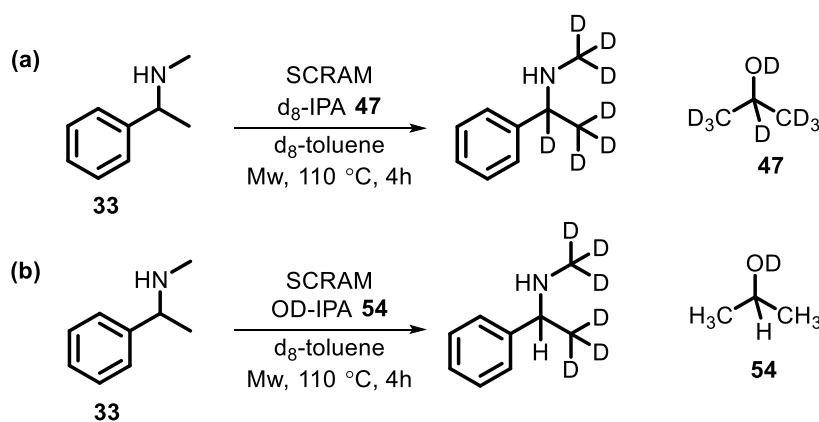
Scheme 3.3. Possible deuteration sites of **33** in the H/D exchange reaction with (a) d_8-IPA **47** (b) OD-IPA **54**, catalysed by SCRAM catalyst **13**

The data for **33** and its reaction with **47** suggests racemisation. Both the α (H1) and β (H2) ^{1}H NMR signals decrease, the majority of the decrease in the first hour of heating. Furthermore, both proton signals suffer from a clear loss of spectral resolution after one hour, Figure 3.1. The sharper decrease in the H2 peak relative to the H1 peak can be attributed to the relatively faster incorporation of deuteron (D[+]) over deuteride (D[-]). This may be because the hydrogen-deuterium exchange at the H2 position relies only on nucleophilic attack between the enamine H2 centre and the D[+] of the deuterated IPA. Exchange at the H1 centre, on the other hand, relies on association with SCRAM catalyst **13** to abstract the H1 proton, forming the imine, followed by dissociation and re-association with a catalytic monomer which has already incorporated a nucleophilic iridium deuteride bond. As anticipated, the proton integration of *N*-Me signal decreases only slightly, due to the unfavourable formation of the high energy and positively charged quaternary enamine. The data for this compound can be seen summarised graphically in Figure 3.2.
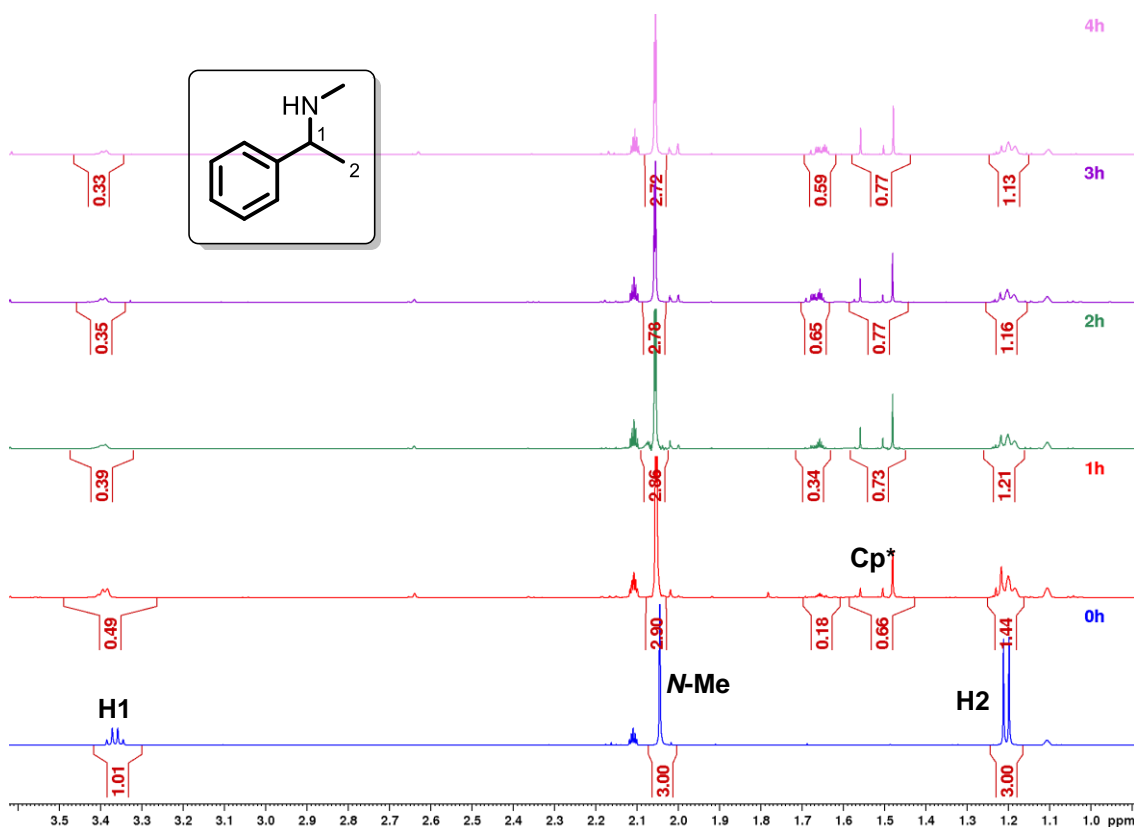
Figure 3.1. ^{1}H NMR spectra for the H/D exchange reaction of **33** with d$_8$-IPA **47**, catalysed by SCRAM catalyst **13**
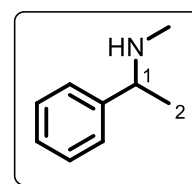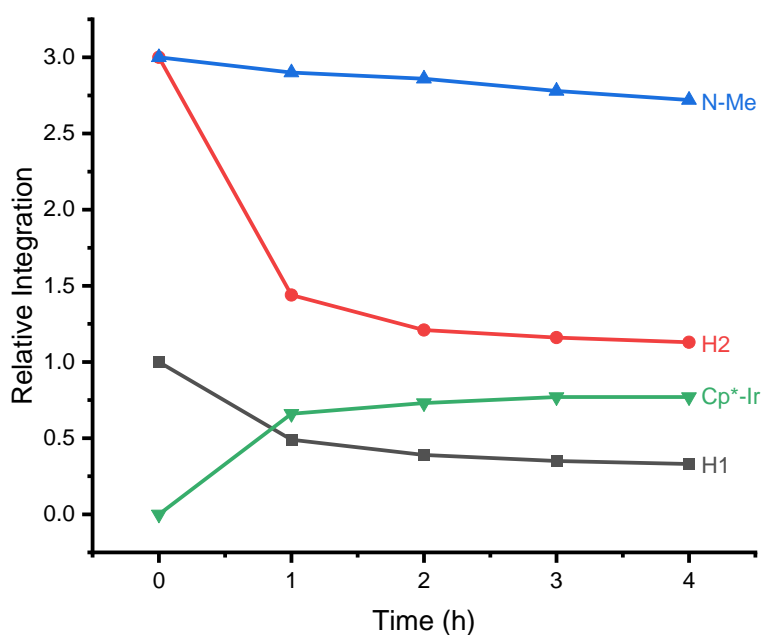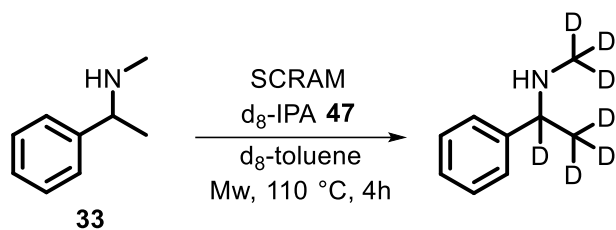
Figure 3.2. Decrease in ^{1}H NMR integration of **33** for the H/D exchange reaction with d_8-IPA **47**, catalysed by SCRAM catalyst **13**

The data for the reaction which utilises OD-IPA **54** over d_8-IPA **47** also shows a decrease in integration of the H1 and H2 signals, albeit a slower decrease for H2, Figure 3.3. The slower rate of H2 decrease may be explained by a secondary kinetic isotope effect. The O-D bond strength may differ between OD-IPA **54** and d_8-IPA **47** upon reaction with different extents of deuterated amine. Mechanistically, the decrease in the H1 proton integration was somewhat surprising, as there was no source of deuteride to allow any form of exchange with H1. However, in both experiments, the decrease of H1 mirrors the increase of Cp* signals associated with methylamine poisoned SCRAM catalyst. It is possible that the decrease in H1 is predominantly due to imine formation and subsequent hydrolysis, rather than hydrogen deuterium exchange. HRMS data supports formation of the imine intermediate, but provides no evidence for hydrogen-deuterium exchange. As racemisation of **33** using SCRAM catalyst **13** is well established, it is

possible that racemisation occurs through an alternative mechanism. Further investigation is required to address these unanswered questions.
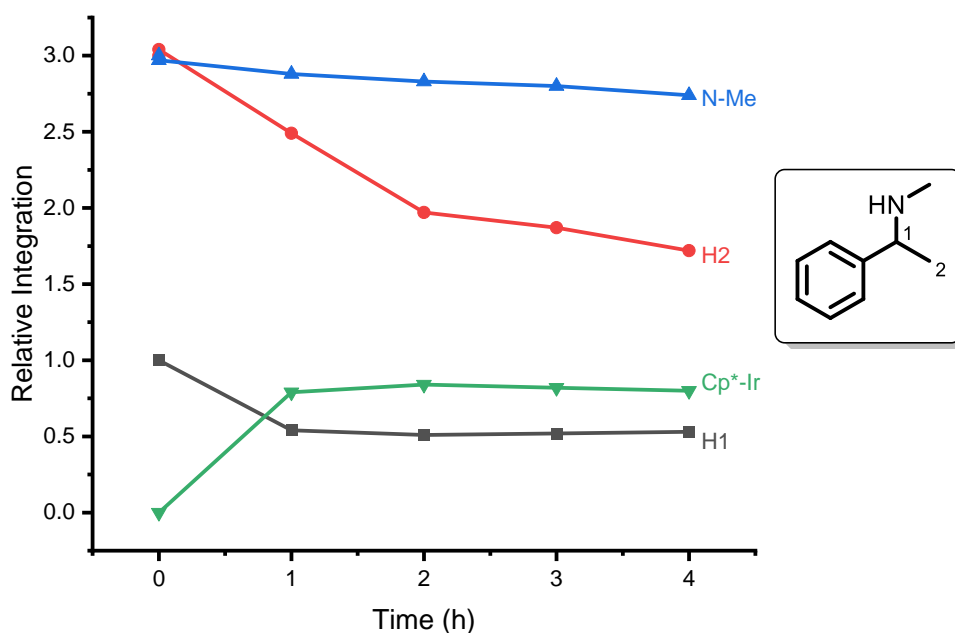
Figure 3.3. Decrease in ^{1}H NMR integration of **33** for the H/D exchange reaction with OD-IPA **54**, catalysed by SCRAM catalyst **13**

3.3 Simple chiral amines

3.3.1 *S*-1-Cyclohexylethanamine

S-1-cyclohexylethanamine **55** was investigated as it was cheap, readily available and an example of a primary amine to broaden the scope of our study, Scheme 3.4.
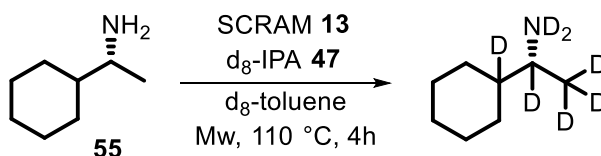
Scheme 3.4. Possible deuteration sites of **55** in the H/D exchange reaction with d_8-IPA **47**, catalysed by SCRAM catalyst **13**

Investigation of hydrogen-deuterium exchange in this compound suggested the formation of impurities, in addition to the possibility of some deuteration. The overall decrease in the α H1' proton integration of 76 %, and the β H1, H2' integration decrease

of 11 % over the course of 4 hours, suggests deuteration, as demonstrated in Figure 3.4. However, there is an increase in integration of protons attached directly to the cyclohexane ring. The overall fall in proton integration (omitting only alpha proton H1') is 4.5 %. This suggests that whilst some signals are decreasing with respect to their integration, that there are signals increasing in an inversely proportional manner. Integration change is summarised in Figure 3.5, where α (H1) and β (H1, H2') amine signals are shown decreasing.
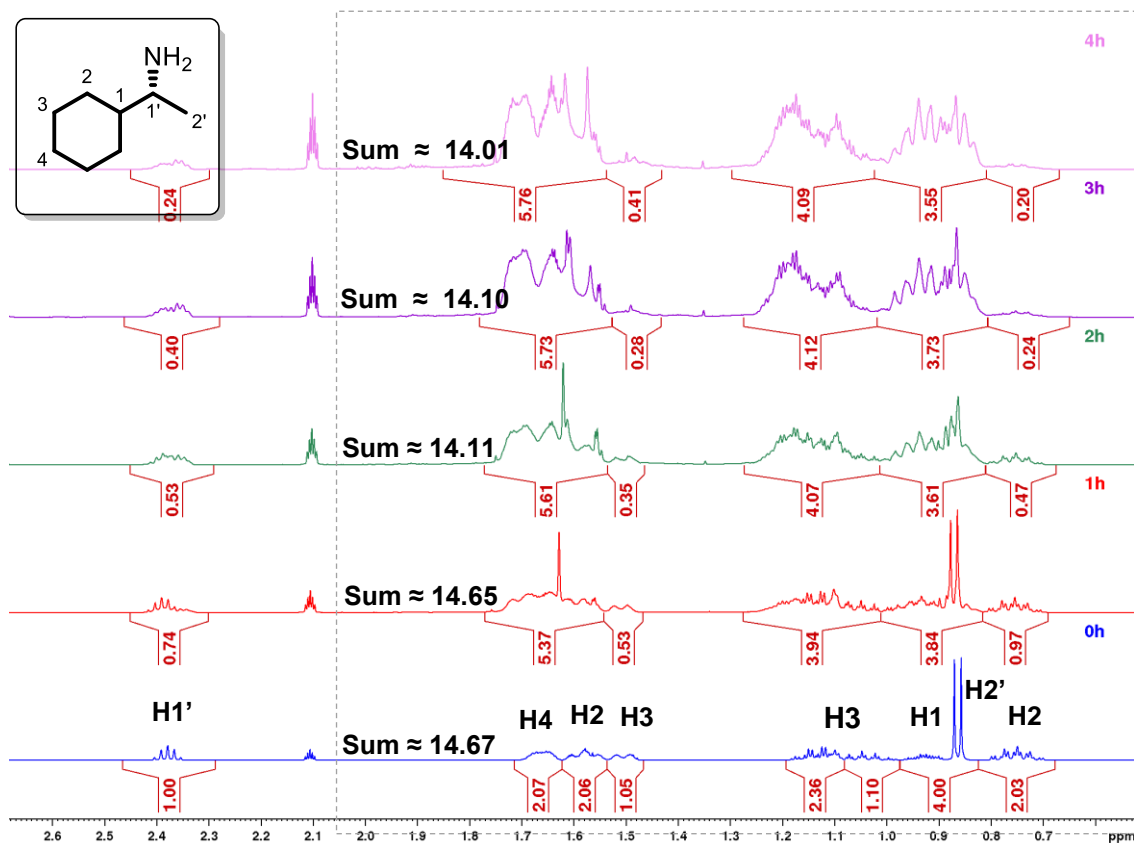
Figure 3.4. ^{1}H NMR spectra for the H/D exchange reaction of **55** with d_8-IPA **47**, catalysed by SCRAM catalyst **13**. Sum indicates the integral total of all protons except H1'.
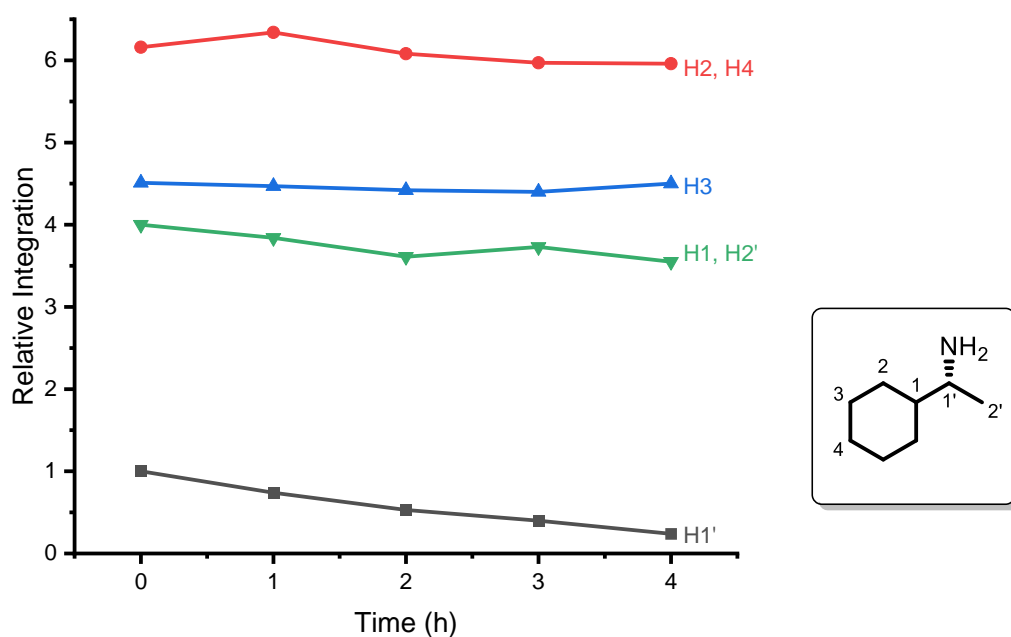
Figure 3.5. Decrease in ^{1}H NMR integration of **55** for the H/D exchange reaction with d_8-IPA **47**, catalysed by SCRAM catalyst **13**

HRMS data suggests presence of both imine **56** (formed through reaction of **55** with d^6-acetone, Figure 3.6) and deuterated dimer **57**, Figure 3.7. As anticipated, both of these species are absent prior to placement for reaction, as indicated by the 0 hour mass spectrum.
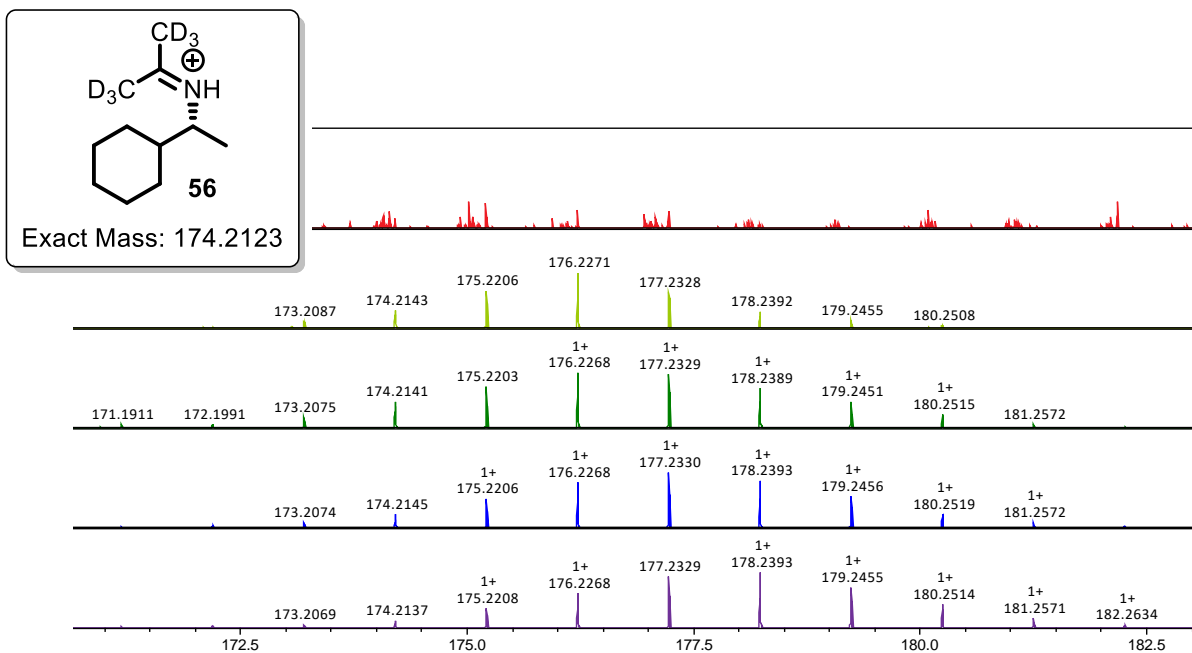
Figure 3.6. HRMS data indicating M+1 peaks of **56** in the H/D exchange reaction of **55** with d_8-IPA **47**, catalysed by SCRAM catalyst **13**. Top to bottom: 0 hours – 4 hours.
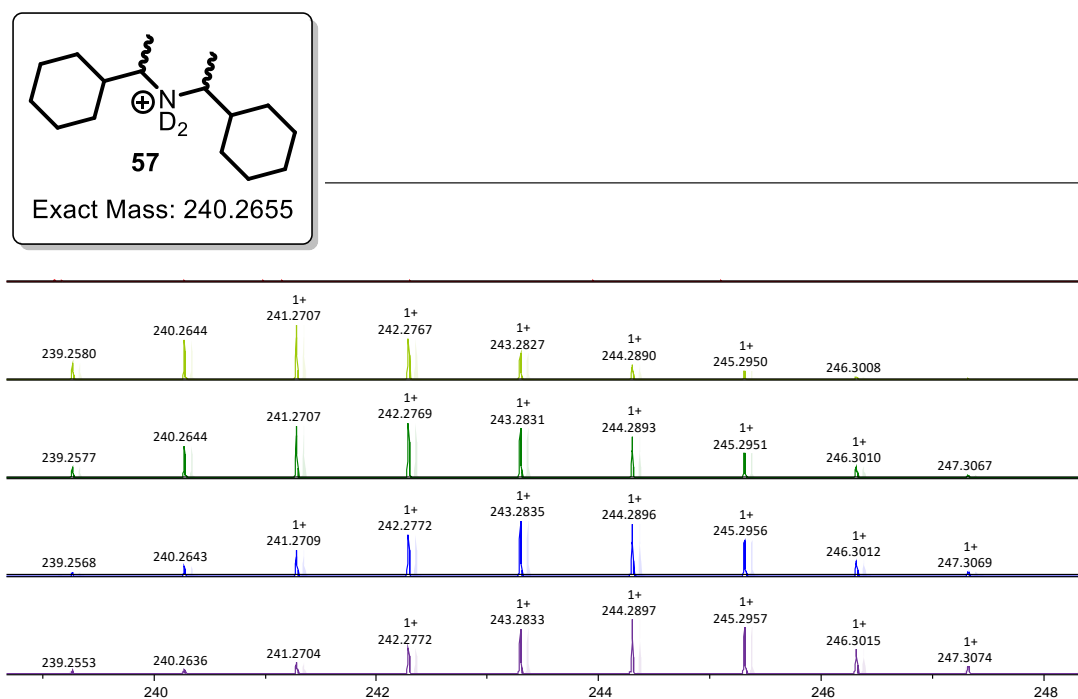
Figure 3.7. HRMS data indicating M+1 peaks of **57** in the H/D exchange reaction of **55** with d_8-IPA **47**, catalysed by SCRAM catalyst **13**. Top to bottom: 0 hours – 4 hours.

3.3.2 3-Methylmorpholine

Morpholine heterocycles have long been explored in medicinal chemistry due to their advantageous metabolic, physiochemical and biological properties, including anti-inflammatory, antioxidant and anticancer activity.[106] As a result, a simple morpholine, 3-methylmorpholine **58** was investigated, Scheme 3.5. The reaction suggested racemisation due to the decrease in integration of the α and β protons, specifically the 36% and 54% decrease of two separate peaks corresponding to H3, H5 and a 35% decrease for 3-Me suggested racemisation, Figure 3.9. This was in addition to mass spectrometry data which also suggested racemisation due to the presence of +1 peaks, insinuating deuteration, Figure 3.10.
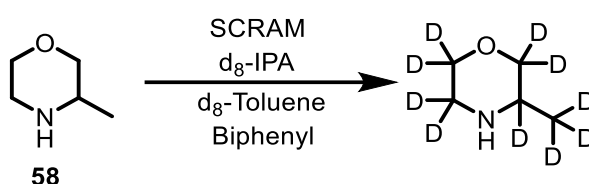
Scheme 3.5. Possible deuteration sites of **58** in the H/D exchange reaction with d_8-IPA **47**, catalysed by SCRAM catalyst **13**
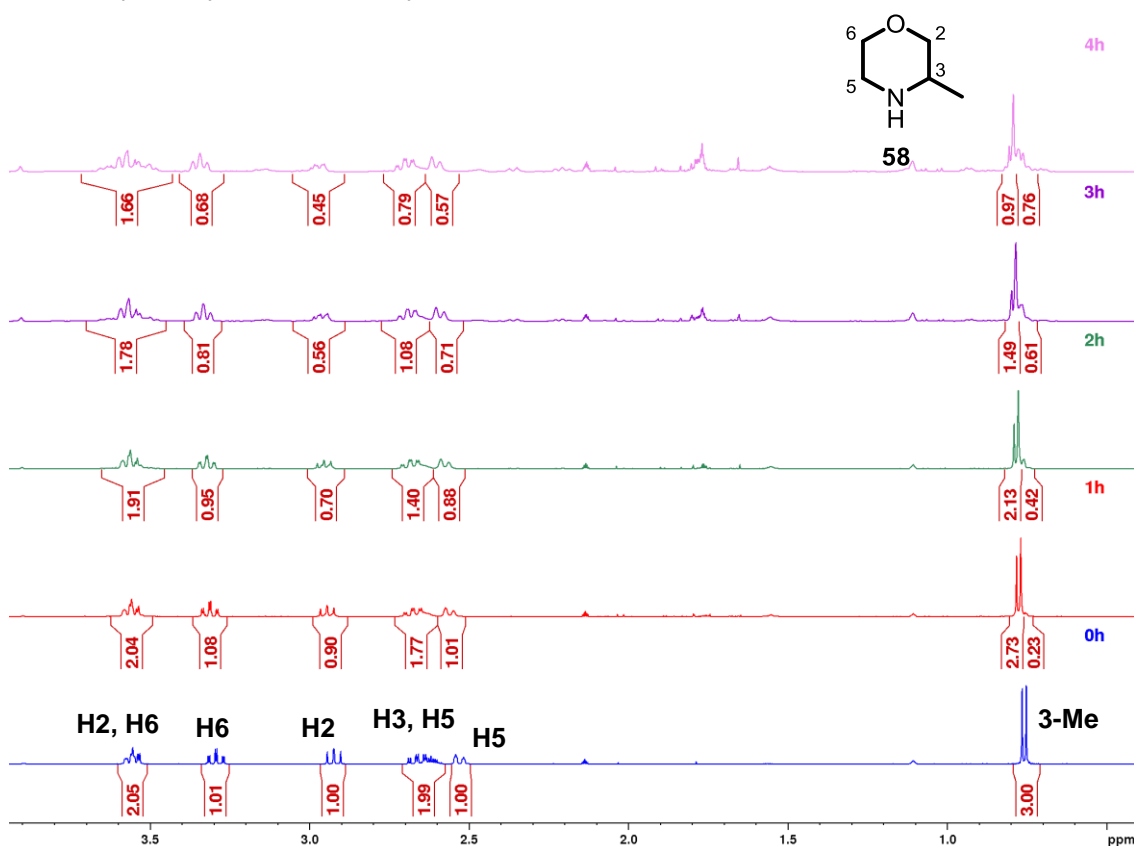
Figure 3.8. ^{1}H NMR spectra for the H/D exchange reaction of **58** with d_8-IPA **47**, catalysed by SCRAM catalyst **13**
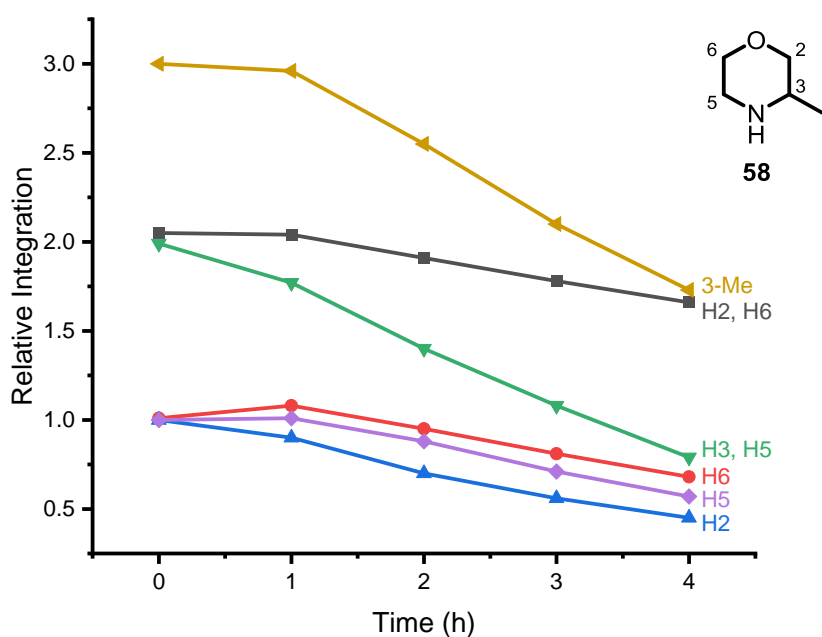
Figure 3.9. Decrease in ^{1}H NMR integration of **58** for the H/D exchange reaction with d_8-IPA **47**, catalysed by SCRAM catalyst **13**
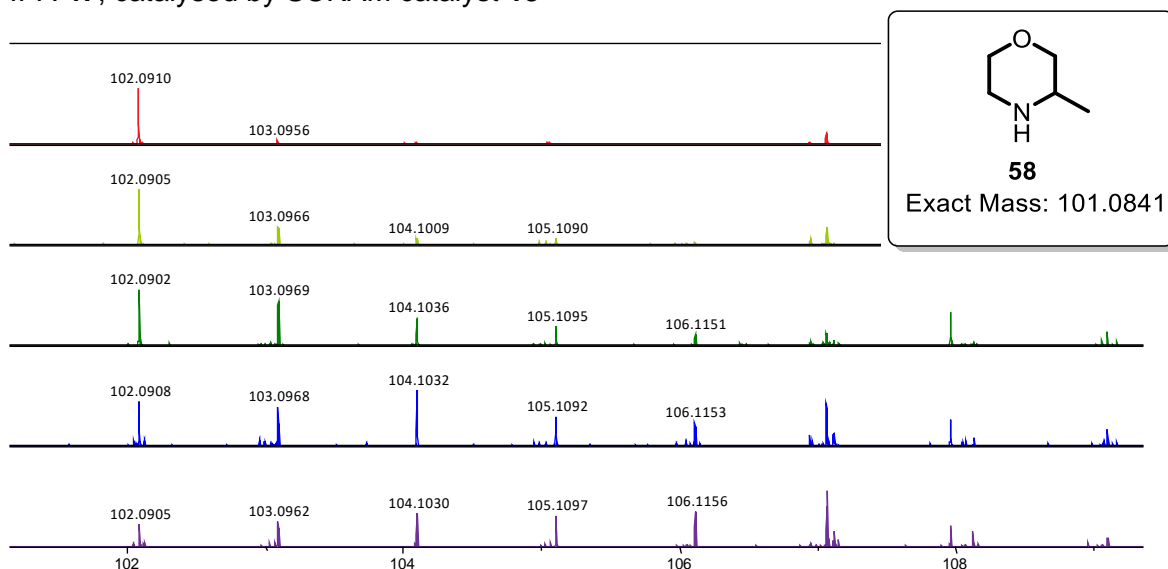
Figure 3.10. HRMS data indicating M+1 peaks of **58** in the H/D exchange reaction with d_8-IPA **47**, catalysed by SCRAM catalyst **13**. Top to bottom: 0 hours – 4 hours.

However, when the experiment was conducted in the absence of SCRAM catalyst, a decrease in integration of all the protons was also observed and suggested that impurities were formed, independent of the SCRAM catalyst. This control experiment is summarised graphically in Figure 3.12
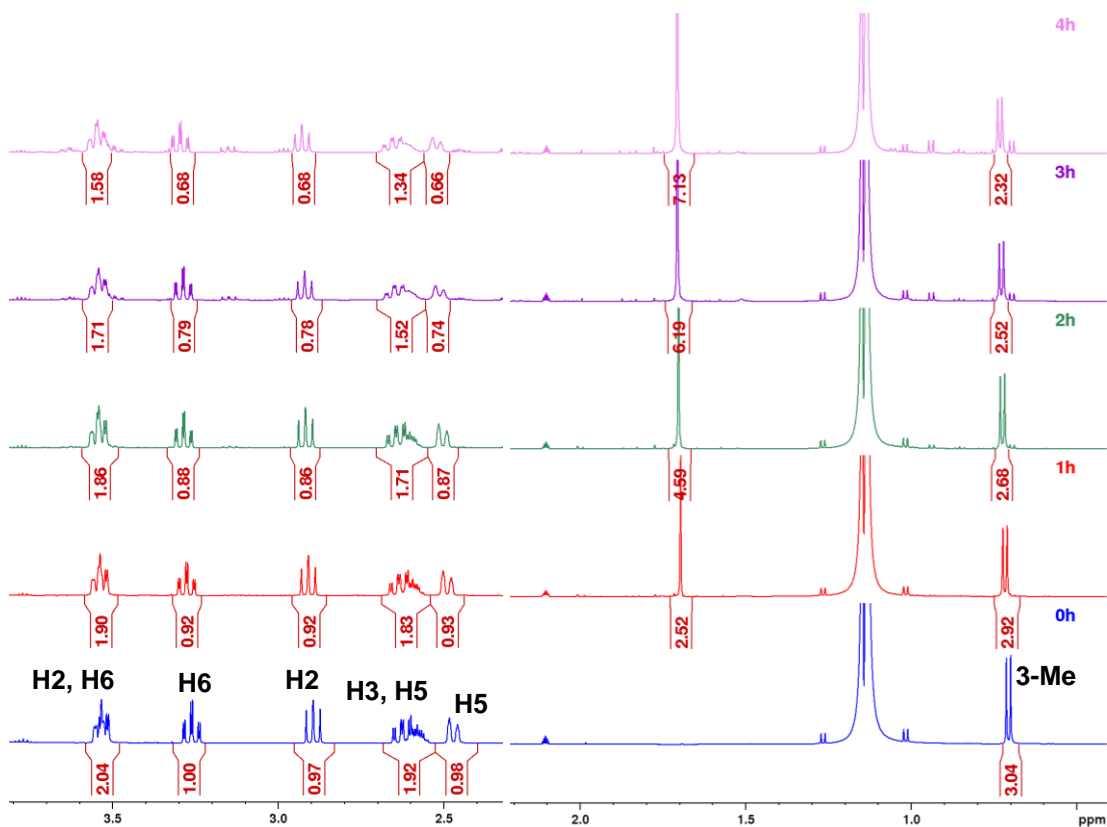
Figure 3.11. ^{1}H NMR spectra for the control reaction of **58** with IPA, in the absence of SCRAM catalyst **13**
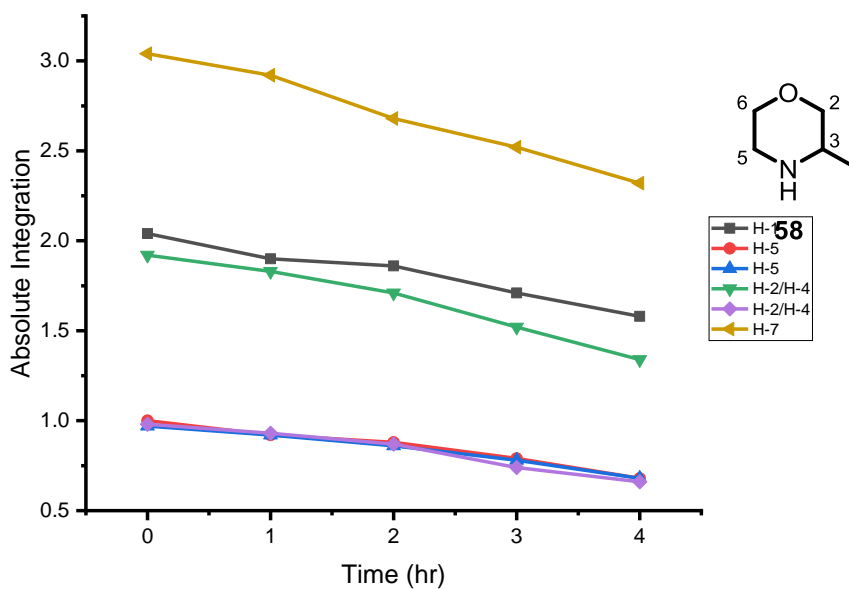
Figure 3.12. Decrease in ^{1}H NMR integration of **58** in a control reaction with IPA, in the absence of SCRAM catalyst **13**

Comparing both the reaction with d^8-IPA and the reaction with normal IPA suggests the presence of side reactions
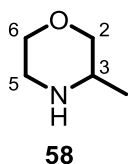
	% decrease (d8-IPA)	% decrease (IPA)
H2,H6	19.0	22.5
H6	32.7	32.0
H2	55.0	29.9
H3,H5	60.3	30.2
H5	43.0	32.7
3-Me	42.3	23.7

58

When comparing the decrease at each proton position between the experiment using deuterated IPA and the experiment using hydrogenated IPA, it is clear that some positions are deuterated favourably over others. From the data, it is clear that all positions are deuterated, apart from the H6 position. This is unsurprising as the enamine **59** is more stable than the enamine **60** due to the inductive effect of the methyl group, Scheme 3.6. Furthermore, it is clear that deuteration at position H2 is more likely than positon H6 as the enamine required for the former is more stable and therefore more likely to exist favourably
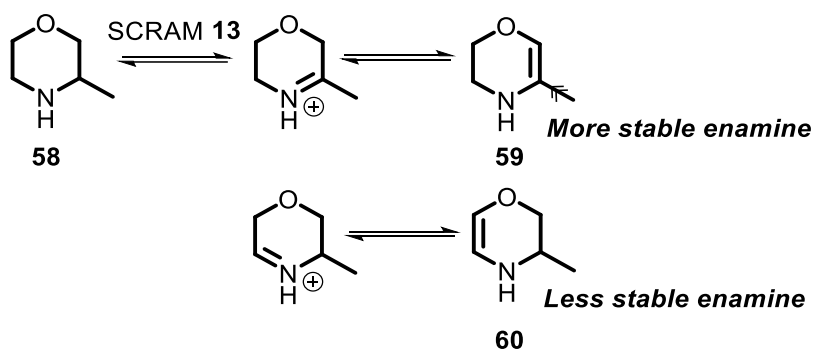
Scheme 3.6. 3-methylmorpholine **58** interaction with SCRAM **13**, to form relatively more and less stable enamines, **59** and **60** respectively.

3.4 Complex chiral substrates and salts

3.4.1 Ethyl (2*R*,4*R*)-4-methylpiperidine-2-carboxylate

The carboxylic acid analogue of (2*R*, 4*R*)-**61** is a key structural intermediate in the synthesis of anti-tumour agents, and thrombin inhibitors such as Argatroban®.[107,108] The (2*R*, 4*R*)-**61** derivative was chosen for investigation to prevent issues associated with bidentate coordination to iridium.[109–111] The scheme for epimerisation shows possible deuterium incorporation sites, Scheme 3.7.
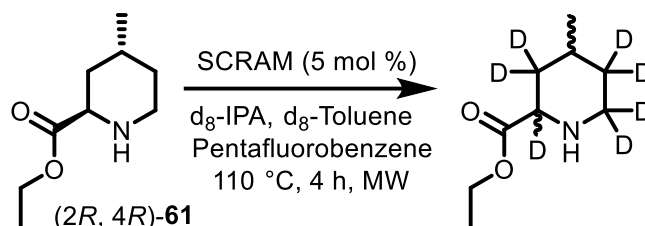
Scheme 3.7. Possible deuteration sites of **61** in the H/D exchange reaction with d$_8$-IPA **47**, catalysed by SCRAM catalyst **13**

Since the H4-Me protons are both unlikely to exchange, and remote from the reaction protons in the NMR spectrum, these were used as an internal standard. As the reaction progressed, new signals, adjacent to or overlapping with the ester signals (Figure 3.13, C*H$_2$*C*H$_3$*, H1'and H2' respectively) and internal standard H4-Me signal, began to form. The evolution of these suggested the formation of diastereomers, and therefore epimerisation. The decrease in α- (H2, H6) and β- (H3, H5) protons also suggest hydrogen-deuterium exchange and therefore epimerisation. The decrease of the α- and β-proton integrations is shown graphically in

Figure 3.14.
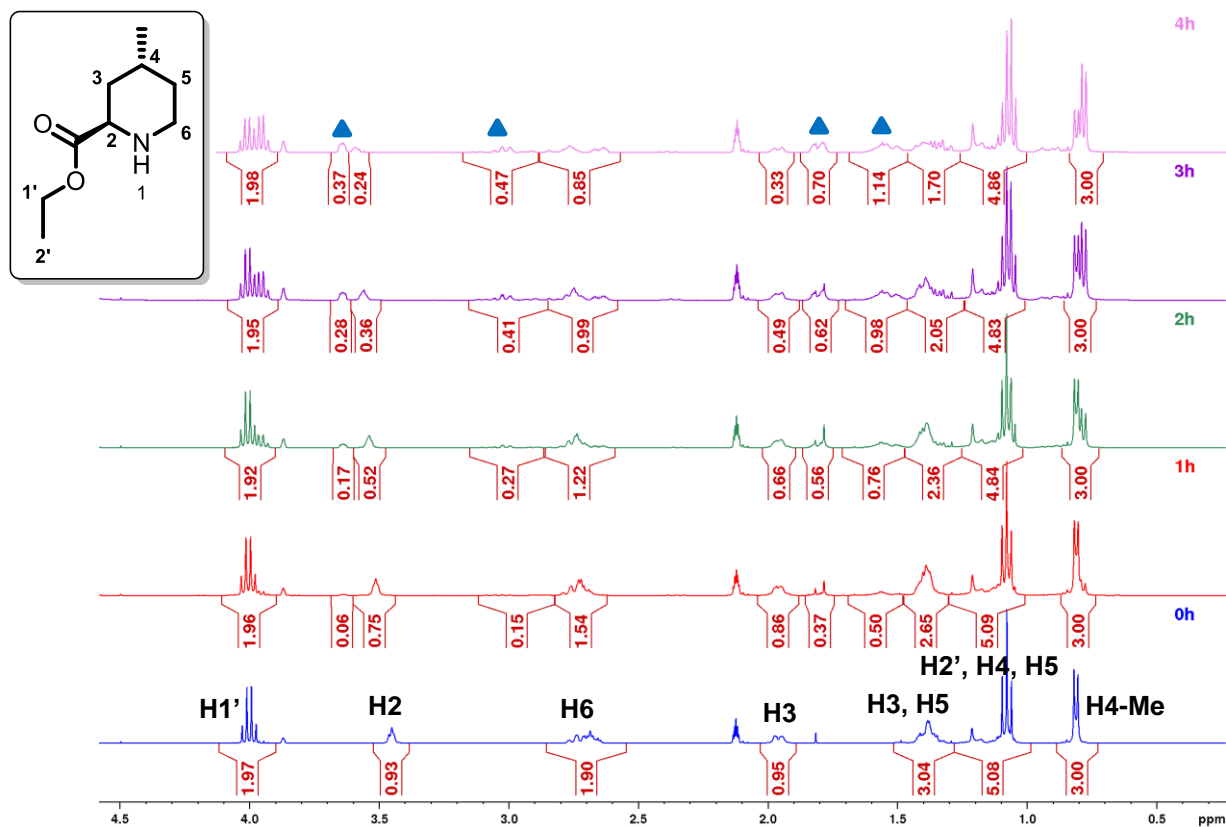
Figure 3.13. ^{1}H NMR spectra for the H/D exchange reaction of (2R, 4R)-**61** with d$_8$-IPA **47**, catalysed by SCRAM catalyst **13**. H4-Me protons used as internal standard. New signals indicated by blue triangle.
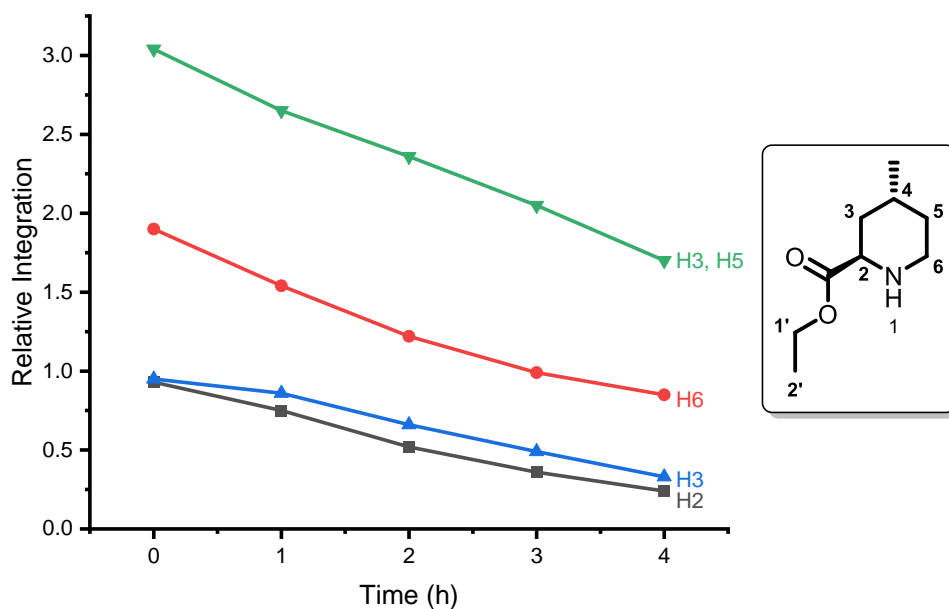
Figure 3.14. Decrease in ^{1}H NMR integration of (2R, 4R)-**61** for the H/D exchange reaction with d$_8$-IPA **47**, catalysed by SCRAM catalyst **13**

A corresponding increase in the new *cis* diastereomer proton signals, are shown in Figure 3.15. The increase in the integration values of the H1' and H4-Me quartet and doublet peaks respectively, is related directly to the evolution of the *cis* diastereomer, Figure 3.16.
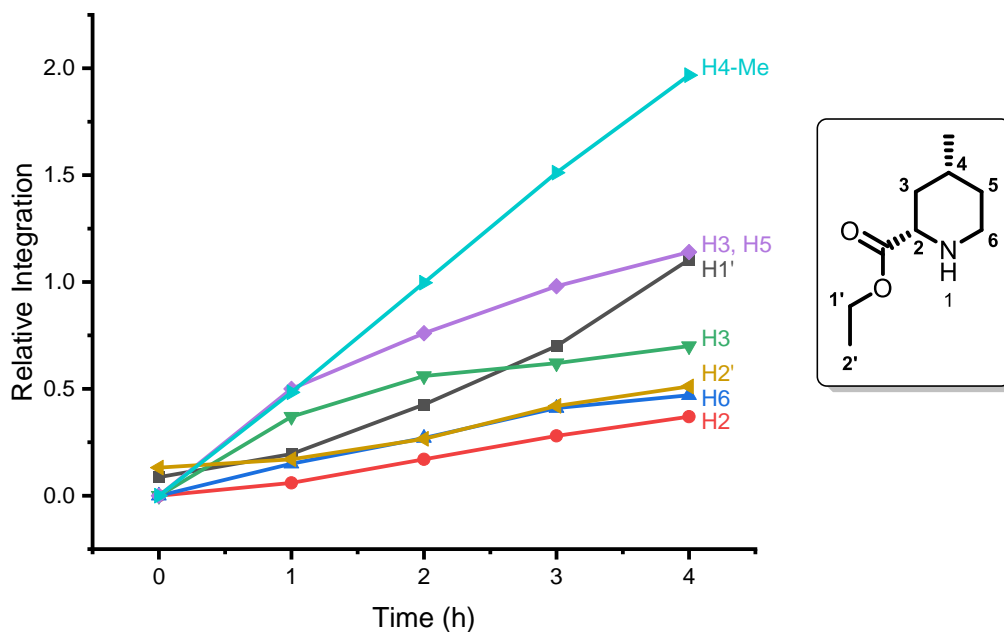
Figure 3.15. Increase in ^{1}H NMR integration of *cis*-**61** for the H/D exchange reaction with d$_8$-IPA **47**, catalysed by SCRAM catalyst **13**
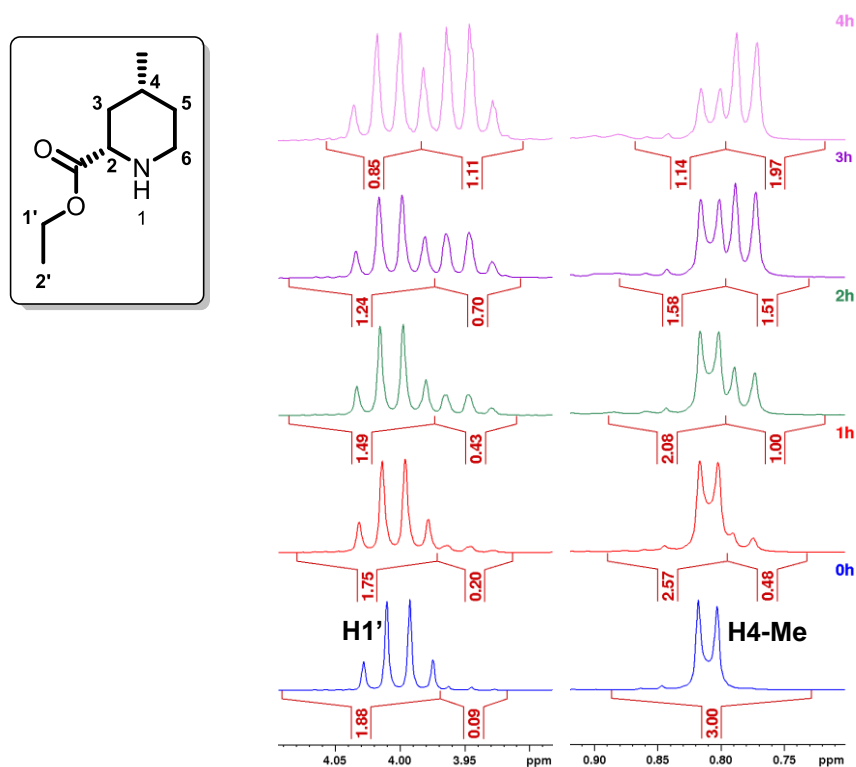
Figure 3.16. Expansion of H1' and H4-Me proton region in Figure 3.13, illustrating the decrease in the original H1' quartet and H4-Me doublet peaks due to the growth of *cis*-**61**

HRMS evidence of samples from this experiment provides further evidence for hydrogen-deuterium exchange, showing *M*+1 mass peaks, increasing in number of independent deuterated species as the reaction progresses, Figure 3.17.
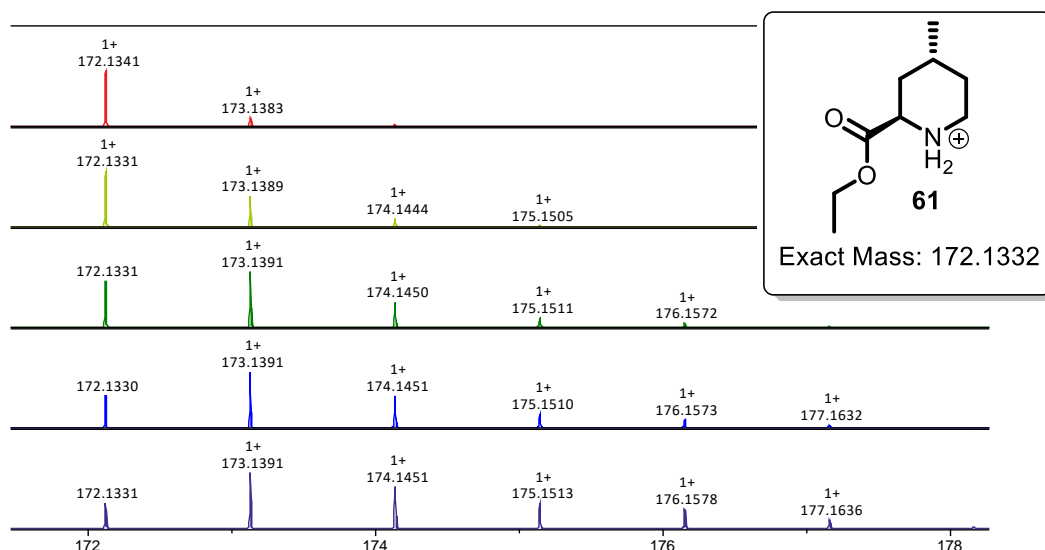
Figure 3.17. HRMS data indicating M+1 peaks of **61** in the H/D exchange reaction with d$_8$-IPA **47**, catalysed by SCRAM catalyst **13**. Top to bottom: 0 hours – 4 hours.

The appearance of a doublet adjacent to the original H4-Me peak would suggest the possibility of hydrogen-deuterium exchange at the C4 methine centre. This implies 1,4-isomerisation of the enamine. To ensure no epimerisation was occurring at this centre, a control reaction was conducted using protonated IPA and the *cis* diastereomer as starting material, depicted in Scheme 3.8.

Scheme 3.8. Reaction of **61** with hydrogenated IPA, catalysed by SCRAM catalyst **13**. Conducted to investigate stereochemistry at the 4*R* centre.

A comparison of the new ^{1}H NMR signals to pure (2*R*,4*R*)-**61**, in d^8-toluene **48**, expanded and visible in the fourth and final hour of heating (Figure 3.18a and b), provides support for the epimerisation of **61** in the presence of SCRAM catalyst **13**. Furthermore, there is no evidence of epimerisation at the C4 methine centre, as no additional doublet appears throughout the reaction, Figure 3.18c.

Figure 3.18. (a) Bottom blue ^{1}H NMR shows the amine, d$_8$-toluene **48**, IPA and SCRAM **13** catalyst prior to heating under microwave conditions. Top red ^{1}H NMR shows the amine, d$_8$-toluene **48**, IPA and SCRAM catalyst **13** after 4 hours of heating under microwave conditions. (b) Shows the ^{1}H NMR of pure (2*R*,4*R*)-**61** in d$_8$-toluene **48**. (c) Expansion of doublet region in (a)

The lack of doublet in the 4 hour control reaction, suggests that evolution of the doublet in Figure 3.13 is due to hydrogen-deuterium exchange and subsequent changes in proton-proton coupling rather than due to epimerisation at the C4 methine centre.

3.4.1.1 Diastereomeric salt investigation

a. *p*-Toluenesulfonic acid

An aim of this research is to investigate the separation of diastereomers through insoluble salt formation, and subsequent racemisation/epimerisation of the soluble mother liquor waste in a resolution, racemisation, recycle – R^3 process.[100] In this regard, epimerisation of the *p*-toluene sulfonic acid **62** (*p*-TSA) salt form of **61** was investigated. It was found that the sulfonic acid reacted with the amino ester to form a solid diastereomeric salt from isopropyl acetate, Scheme 3.9. Accordingly, the ability of SCRAM to epimerise the soluble amine salt diastereomer was investigated, Scheme 3.10.
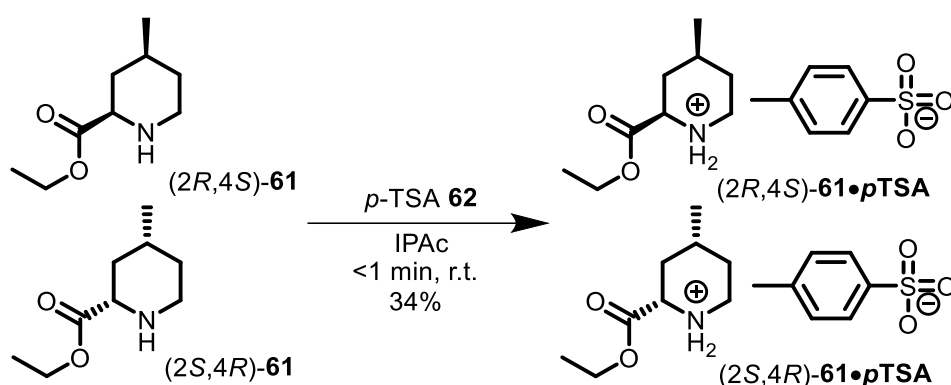
Scheme 3.9. A synthetic procedure for sulfonate crystals of **61** from a mixture of diastereomers. Diastereomeric excess was determined through NMR.
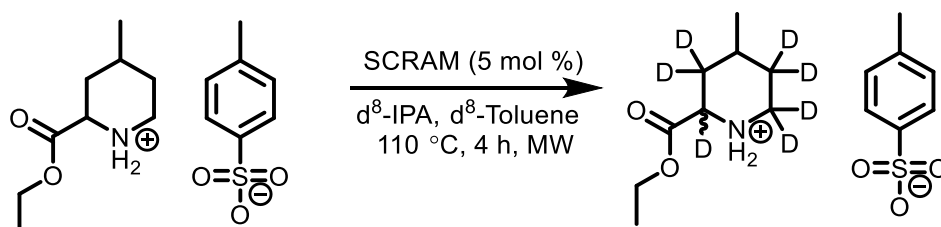
Scheme 3.10. Possible deuteration sites of **61**-*p*-toluenesulfonate in the H/D exchange reaction with d8-IPA **47**, catalysed by SCRAM catalyst **13**

Heating SCRAM catalyst **13** with the *cis p*-TSA salt of **61** in d8-IPA **47** produced a negligible change in the proton integration, and, in contrast to Figure 3.13, there were no signals to suggest epimerisation of the 2*R* centre. The only change observed, was for the H1, H2' signal, which is unsurprising due to uncatalysed hydrogen-deuterium exchange at the NH_2^+ centre. The NMR data is shown in Figure 3.19 and summarised graphically in Figure 3.20.
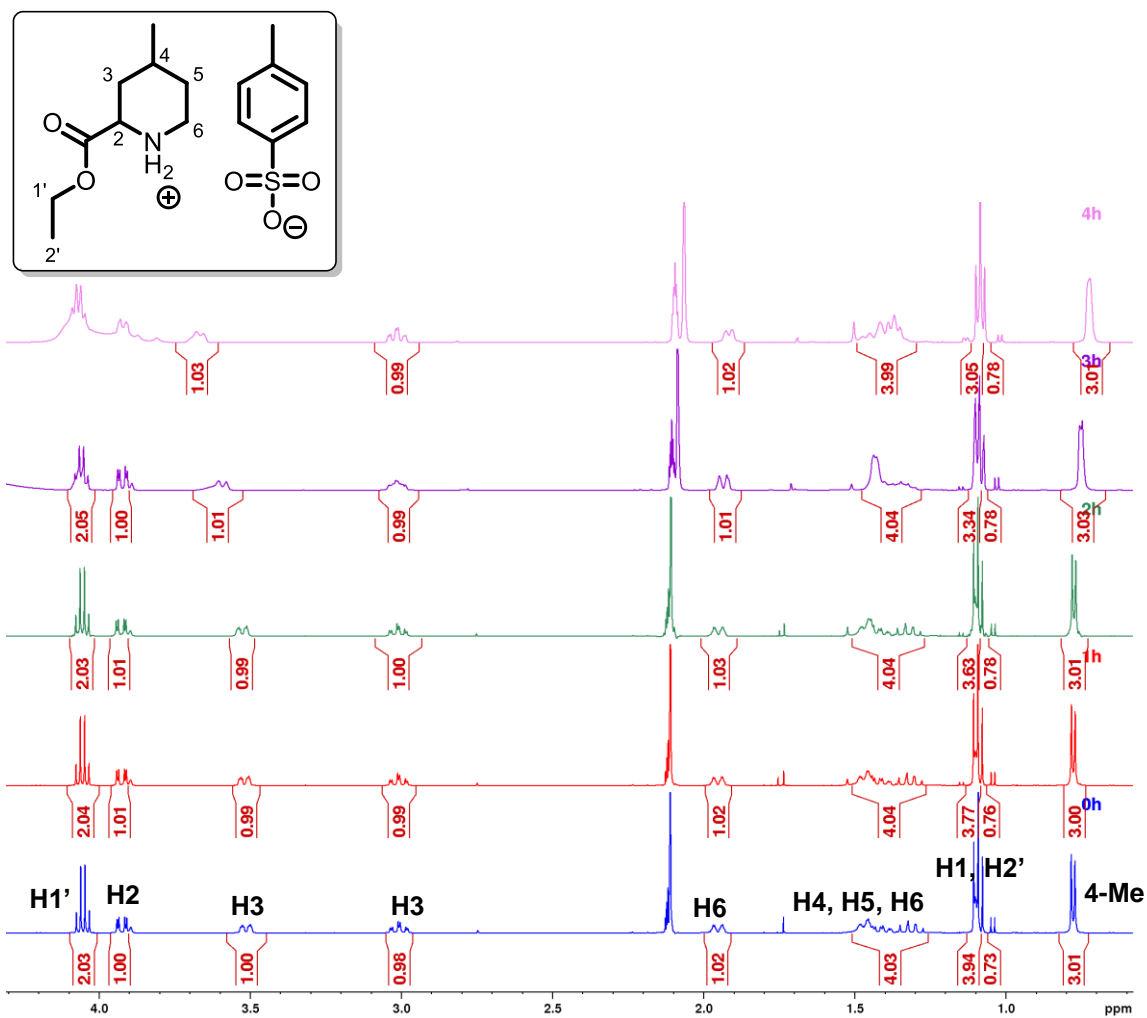
Figure 3.19. ^{1}H NMR spectra for the H/D exchange reaction of *cis*-**61**-*p*-toluenesulfonate with d$_8$-IPA **47**, catalysed by SCRAM catalyst **13**
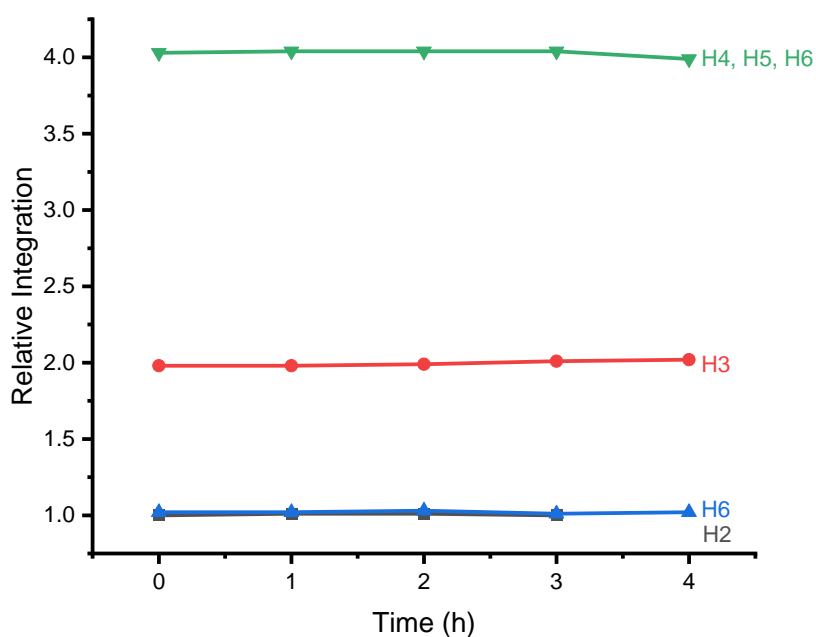
Figure 3.20. Change in ^{1}H NMR integration of *cis*-**61**-*p*-toluenesulfonate for the H/D exchange reaction with d_8-IPA **47**, catalysed by SCRAM catalyst **13**

HRMS evidence further supported this view, as no additional peaks appeared due to H/D exchange, Figure 3.21.
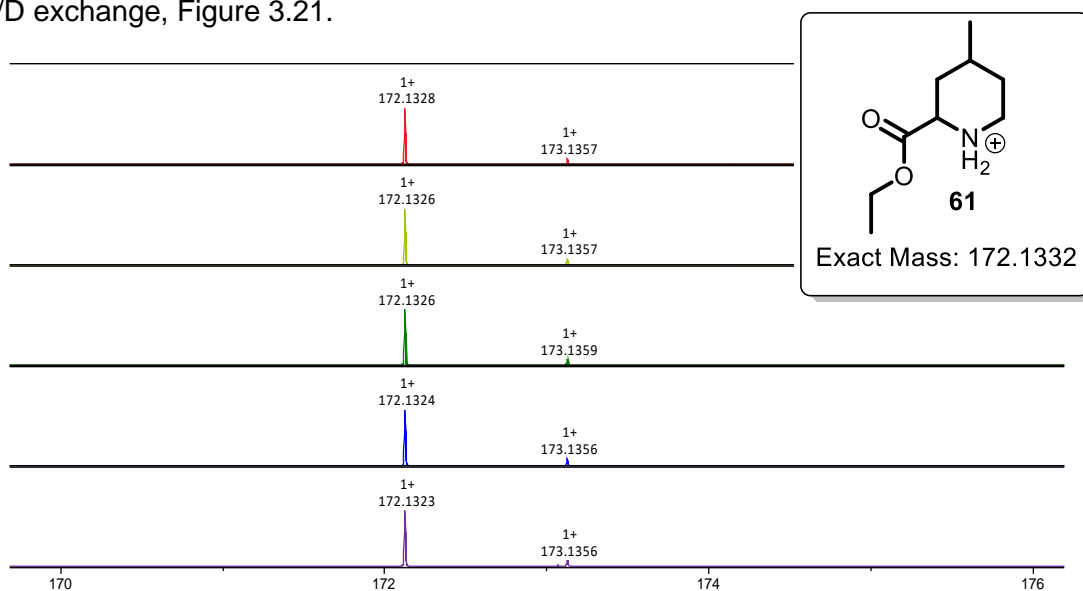
Figure 3.21. HRMS data indicating lack of M+1 peaks of *cis*-**61**-*p*TSA in the H/D exchange reaction with d_8-IPA **47**, catalysed by SCRAM catalyst **13**. Top to bottom: 0 hours – 4 hours.

The reason for this may be the low *p*Ka of *p*-toluene sulfonic acid **62** (-2.8), which means that the amine is fully protonated and there is very little free amine to bind with the

SCRAM catalyst, meaning epimerisation cannot take place. To investigate this, acetic acid **63** with a pKa of 4.76, was used instead.

b. Acetic acid

After reaction of *cis*-**61**-acetate salt with SCRAM catalyst **13**, the NMR spectrum, Figure 3.22, indicated epimerisation. A decrease in some proton signal integrations is apparent; a new quartet signal appears adjacent to and overlapping with the original H1' signal, other new quartet signals are shown appearing and demonstrated by the blue triangle. The sum integral of all signals is ~2, suggesting the appearance of these new signals is directly related to the formation of impurities, related to the ester H1' centre. HRMS data indicates that these additional peaks are likely due to transesterification with d_8-IPA **47**, Figure 3.25, and the amine's reaction with d_6-acetone, Figure 3.26. *M*+1 peaks are seen, which suggest these impurities have incorporated deuterium prior to, or after, their formation.

The α-H2 centre integration decreases by 57%, compared to the acid-free reaction, which by comparison, decreases by 34%, Figure 3.13. This is unsurprising given protonation of the amine decreases the pK_a of the α-H2 proton making it more susceptible to abstraction and therefore hydrogen-deuterium exchange. The H6 α-proton integration decreases by 60%, compared to the acid-free experiment where the same proton loses only half this. Integration of the β-H3 and H5 centres also decrease, in addition to the H4 and 4-Me centres, the latter declining due to the formation of impurities. The proton integration changes are summarised graphically in Figure 3.23.
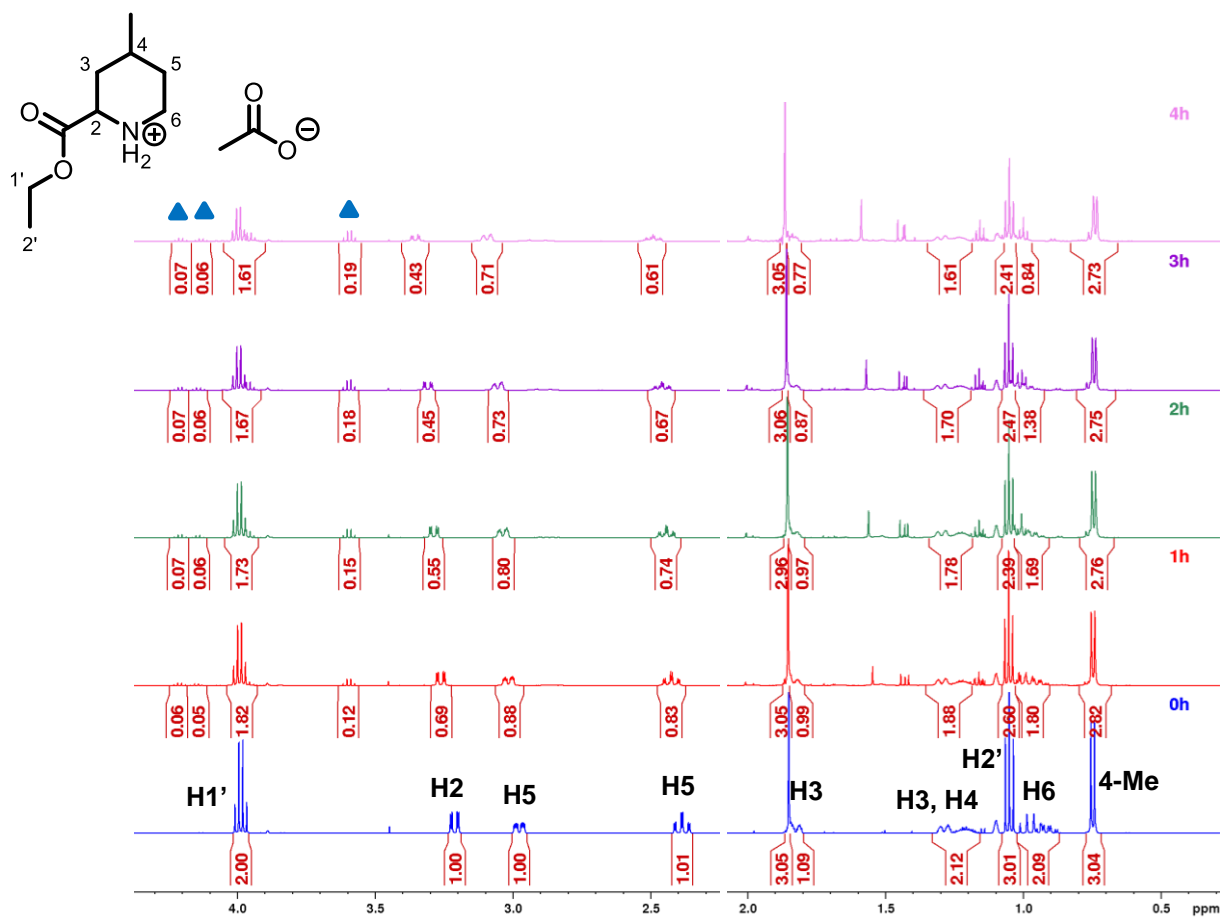
Figure 3.22. ^{1}H NMR spectra for the H/D exchange reaction of **33**-acetate with d$_8$-IPA **47**, catalysed by SCRAM catalyst **13**
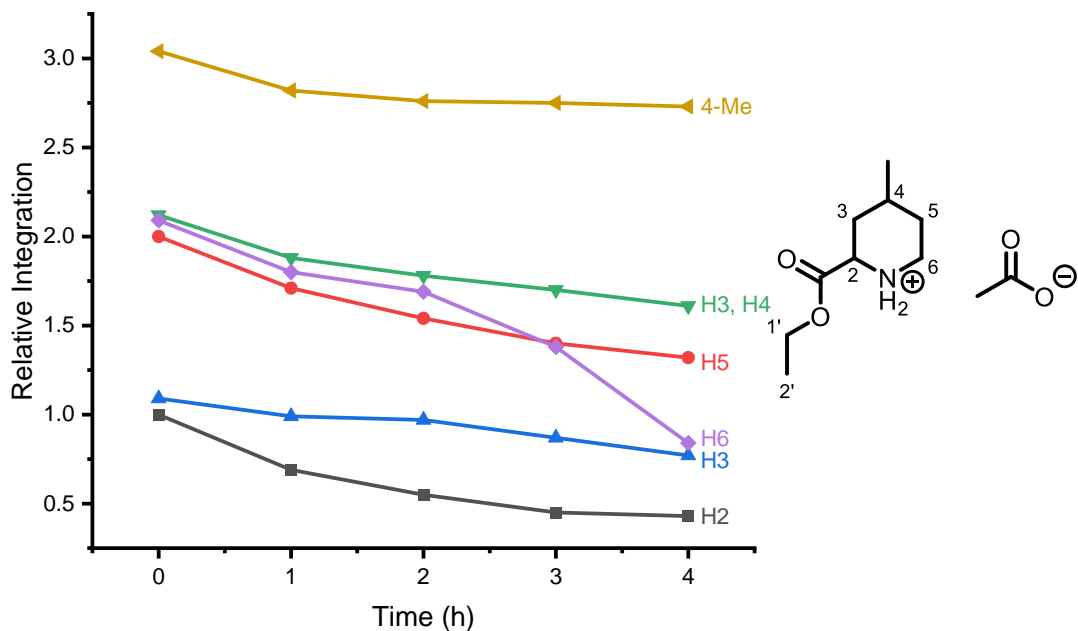
Figure 3.23. Decrease in ^{1}H NMR integration of **61**-acetate for the H/D exchange reaction with d$_8$-IPA **47**, catalysed by SCRAM catalyst **13**

In addition to NMR, HRMS data indicated M+1 peaks which further evidence hydrogen deuterium exchange, Figure 3.24. This confirmed the need for a weak acid salt of the amine to allow catalytic epimerisation with the SCRAM catalyst **13**. Peaks indicating the formation of deuterated transesterification impurity **64** and deuterated *N*-alkyl **65** were also evidenced, Figure 3.25 and Figure 3.26 respectively.
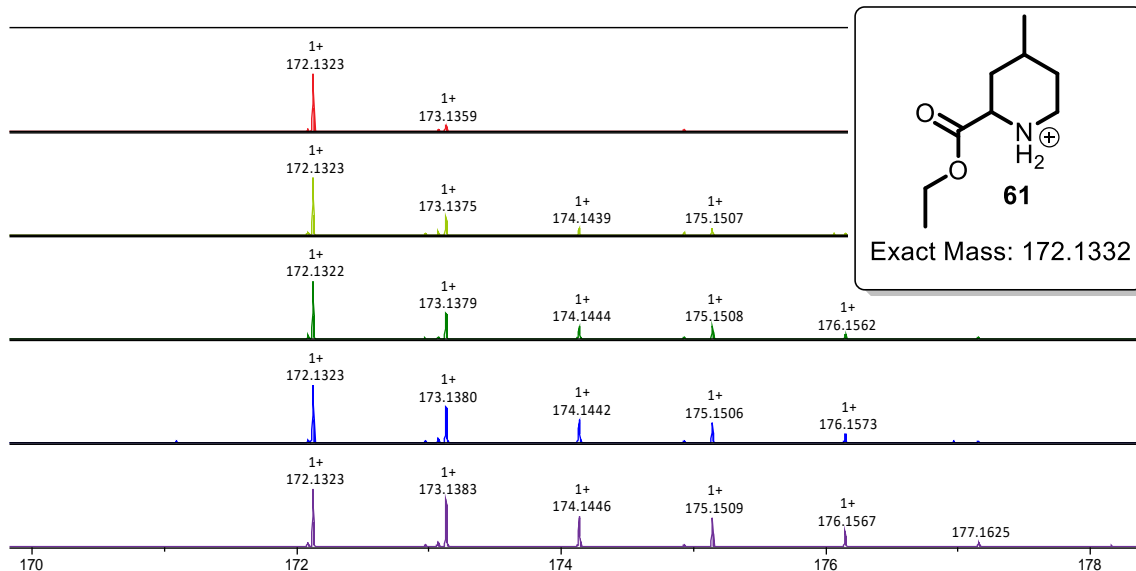
Figure 3.24 HRMS data indicating M+1 peaks of **61**-acetate in the H/D exchange reaction with d_8-IPA **47**, catalysed by SCRAM catalyst **13**. Top to bottom: 0 hours – 4 hours.
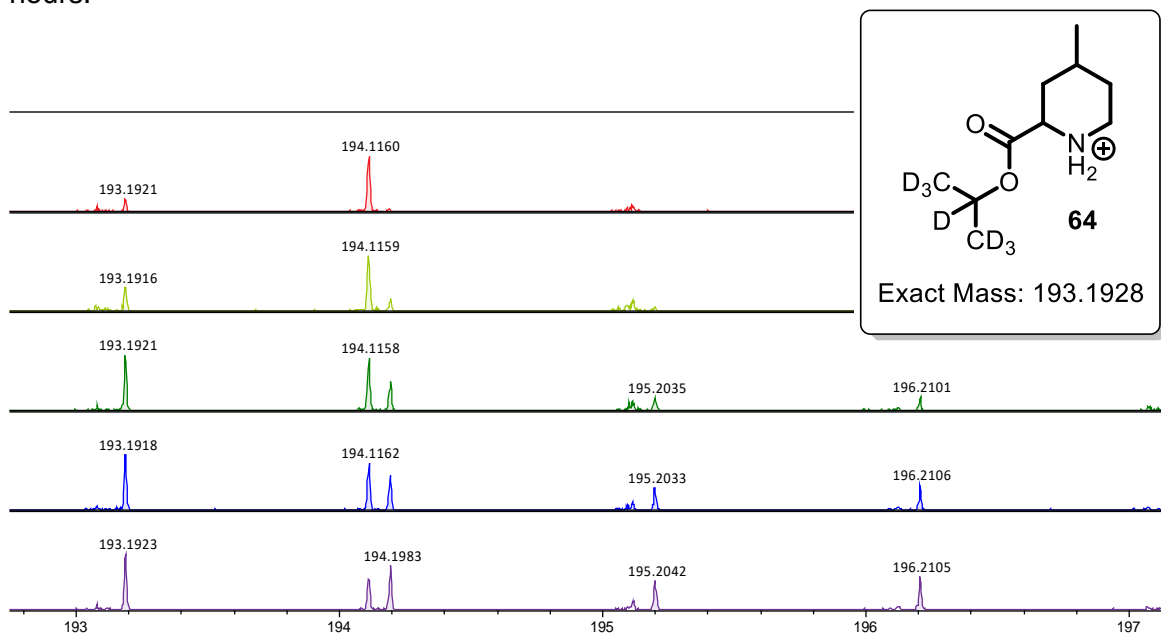
Figure 3.25. HRMS data indicating M+1 peaks of **64** in the H/D exchange reaction of **61**-acetate with d_8-IPA **47**, catalysed by SCRAM catalyst **13**. Top to bottom: 0 hours – 4 hours.
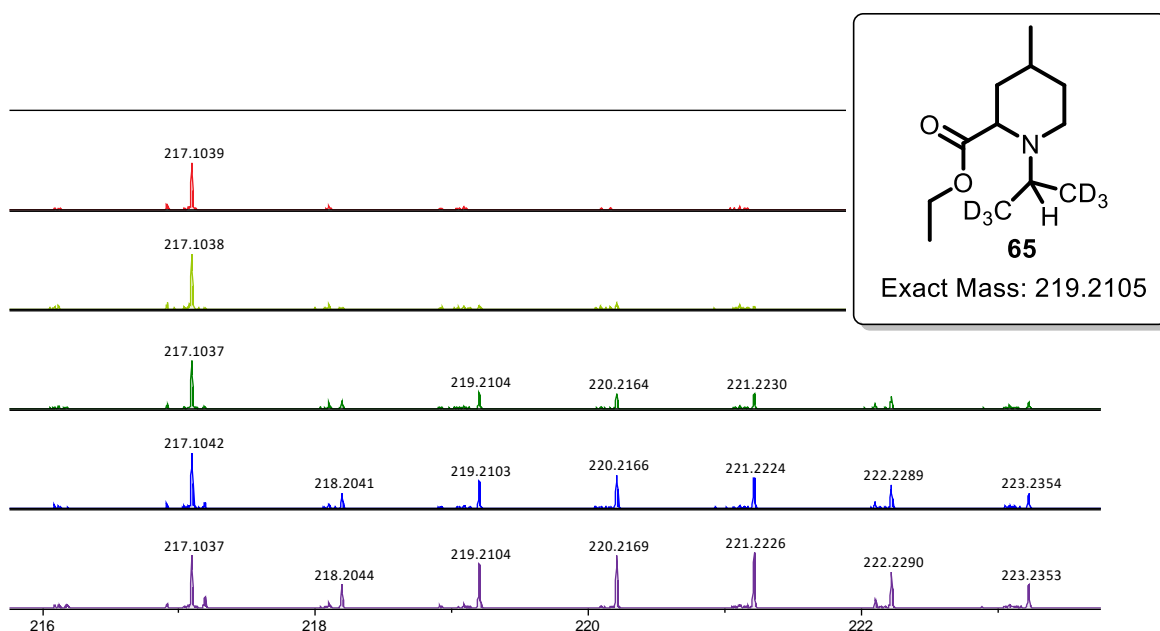
Figure 3.26. HRMS data indicating M+1 peaks of **65** in the H/D exchange reaction of **61**-acetate with d_8-IPA **47**, catalysed by SCRAM catalyst **13**. Top to bottom: 0 hours – 4 hours.

c. Benzoic acid

Benzoic acid **66** was investigated as an alternative diastereomeric resolving agent. The reaction is shown schematically in Figure 3.27
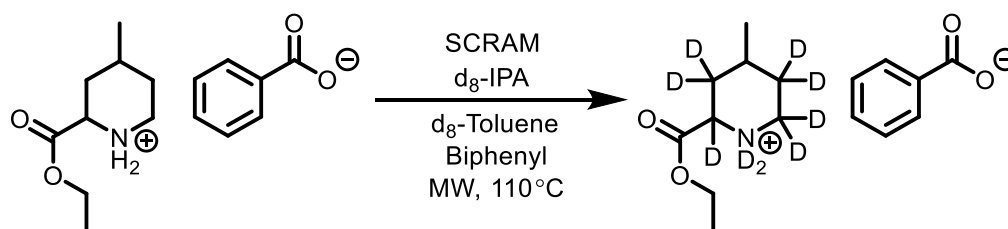
Figure 3.27. Possible deuteration sites of *cis*-**61**-benzoate in the H/D exchange reaction with d_8-IPA **47**, catalysed by SCRAM catalyst **13**.

Samples taken after the reaction, were analysed by ^{1}H NMR and selected regions are shown in Figure 3.28. The α-proton (H2) integration is shown to decrease throughout the reaction, by 86% after 4 hours, suggesting epimerisation. However, an interesting difference between the original reaction (Figure 3.13, no benzoic acid) and this one, is the absence of a new signal adjacent to the original H2 signal, indicating no epimerisation to the *cis*-diastereomer. Analysing the H3 and H6 protons, there is a ~6% decrease, which suggests there may be a small amount of proton-deuterium exchange in both H6^a, H6^b and H3^a, and increase in nearby signals. The appearance of new signals adjacent to H6 and H3 (indicated by the red circle and blue triangle respectively) does however indicate epimerisation. The H4 and H5 protons remain fairly consistent, despite the broadening and growth of tiny signals nearby. This may be due to the H4

85

proton position, which is unsusceptible to hydrogen-deuterium exchange, Figure 3.18. However, it may also be due to preferential formation of the C2-C3 enamine over the C5-C6 position, due to the former being more highly substituted, despite the destabilising, electron withdrawing ester. A small decrease in the 4-Me group is also seen, with the growth of a nearby doublet. This may be due to hydrogen-deuterium exchange, as it is visible when d^8-IPA is used, Figure 3.16, but not protonated IPA, Figure 3.18. The size of this, relative to that in Figure 3.16, suggests less hydrogen-deuterium exchange occurs when benzoic acid is used.

As in the original experiment, Figure 3.13, appearance of new and overlapping quartet and triplet signals, associated with the ester moiety of the molecule (Figure 3.28, labelled H1' and H2' respectively) provide further evidence for the formation of the opposite diastereomer. Interestingly, growth of new quartet and triplet signals are associated with an overall decrease in the integration of both the new and original signals, suggesting the formation of impurities. The integration decrease in the quartet is counterbalanced by an increase in a new nearby quartet and triplet (both indicated by the green square) whose true integration could not be determined due to the overlapping and broadening of nearby signals. The decrease in the H1' peak is mirrored by the increase in the new quartet peak, H1'', which is likely due to transesterification and subsequently the release of ethanol, Figure 3.30 and Scheme 3.11.
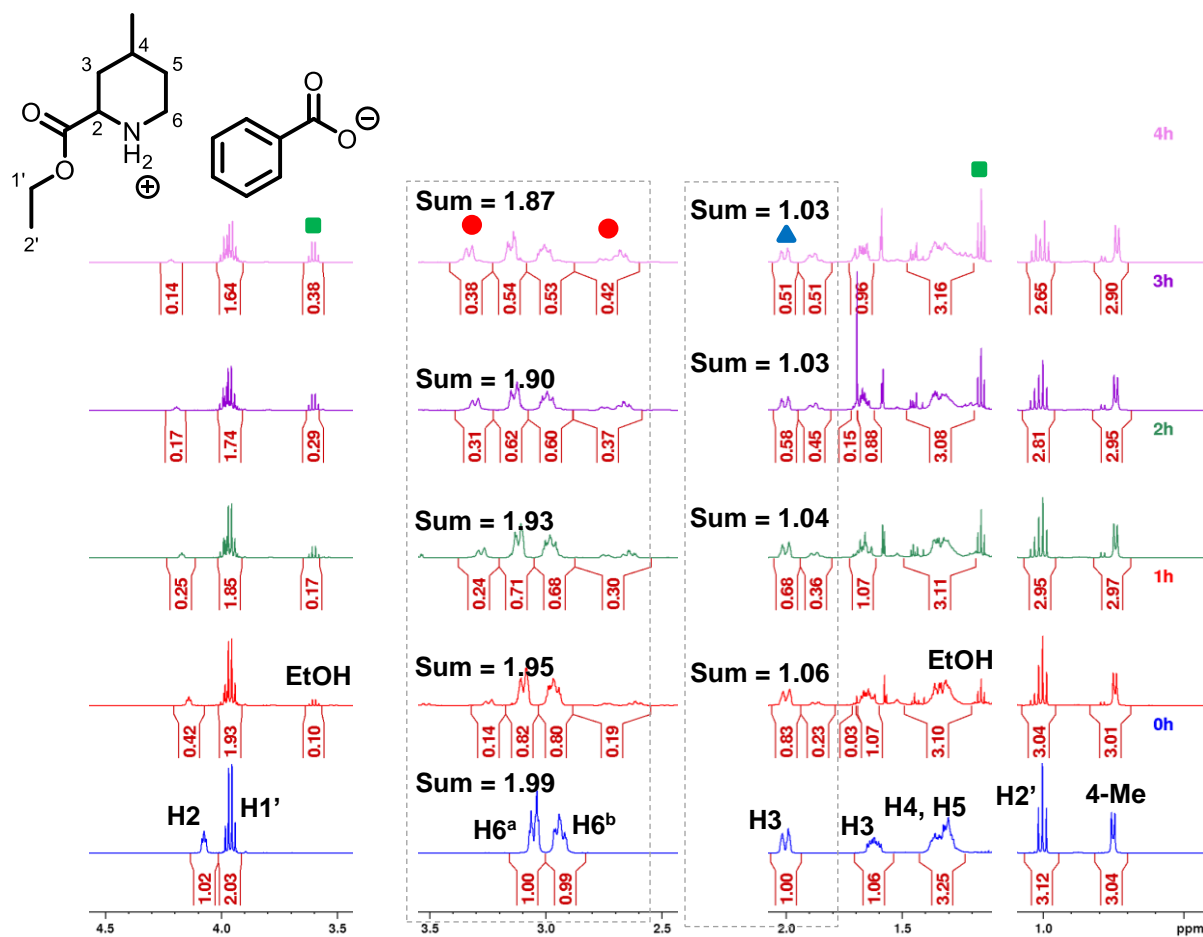
Figure 3.28. ¹H NMR spectra for the H/D exchange reaction of **61**-benzoate with d_8-IPA **47**, catalysed by SCRAM catalyst **13**. New peaks are indicated by the green square (EtOH), red circle (H6 protons) and blue triangle (H3 protons).
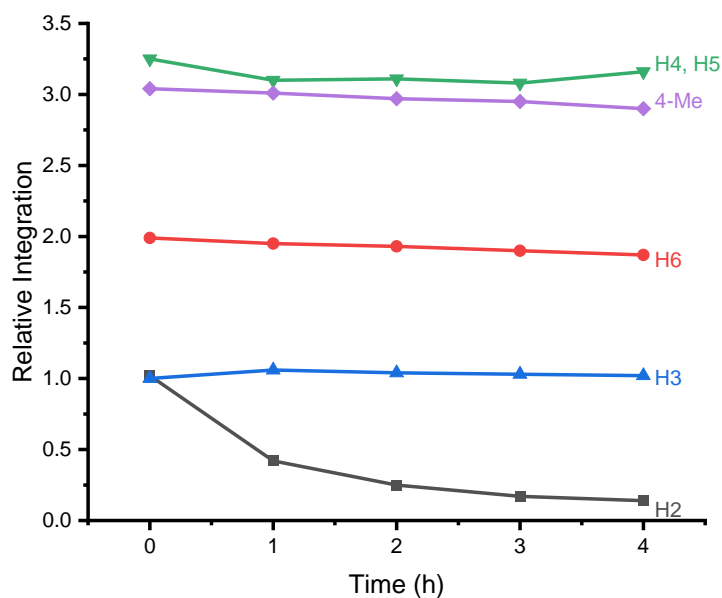
Figure 3.29. Decrease in ¹H NMR integration of **61**-benzoate for the H/D exchange reaction with d_8-IPA **47**, catalysed by SCRAM catalyst **13**
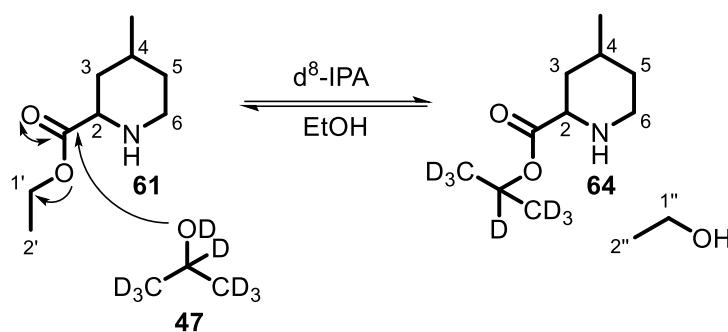
Scheme 3.11. Transesterification of **61** with **47** during H/D exchange reaction of **61**-benzoate.
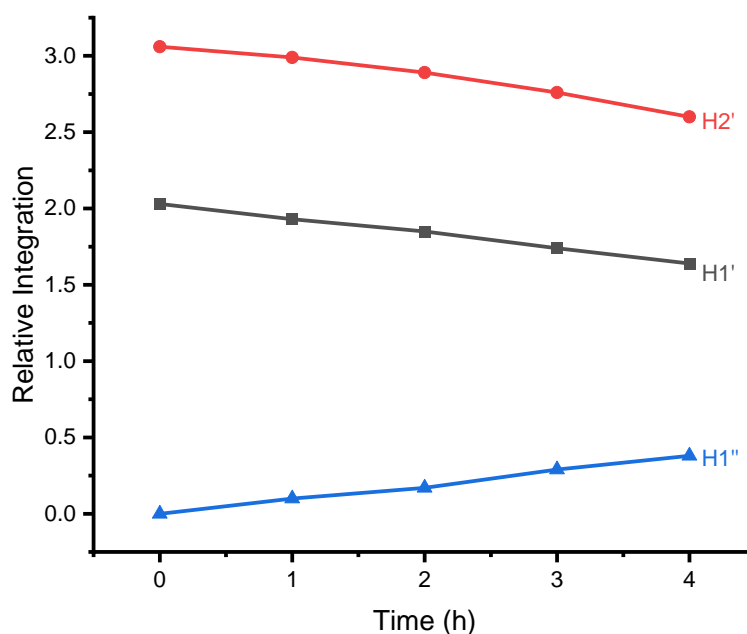
Figure 3.30. Decrease in ^{1}H NMR integration of ester functional group in **61**-benzoate, with corresponding increase in ethanol H1'' protons, for the H/D exchange reaction with d_8-IPA **47**, catalysed by SCRAM catalyst **13**

It is unclear why the benzoate mass spectrometry data differs from that of acetic acid, since the only difference is the substitution. When the reaction is conducted with benzoic acid, peaks at 170.1176 gmol^{-1} and 171.1206 gmol^{-1} are observed. These are absent from the reactions with and without acetic acid. These peaks may indicate the formation of an α-amino α,β-unsaturated ester **67**, Figure 3.31.

The parent ion MH$^+$ peak (172.1331 gmol^{-1}) is a fraction of the size of the protonated amine peak at 170.1176 gmol^{-1}. The peaks which appear after this are likely due to isotopes of carbon, based on the proximity of the peaks to each other. Also, there is no

appearance of peaks to suggest hydrogen-deuterium exchange, as is clear when no acid or acetic acid are used, Figure 3.17 and Figure 3.24 respectively. Together with the NMR data, this provides additional evidence that epimerisation may be occurring through an alternative mechanism, without hydrogen-deuterium exchange. This mechanism is discussed further in the following chapter.
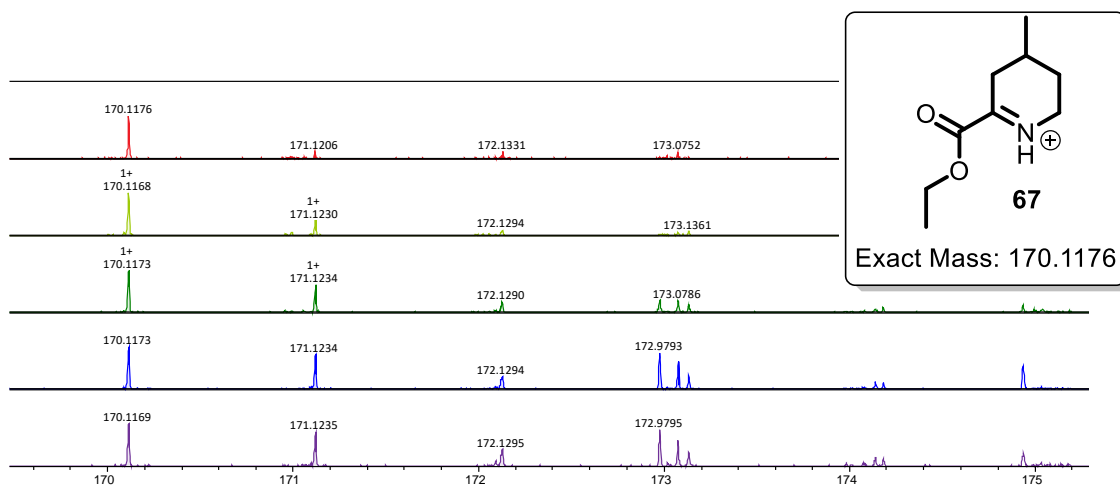
Figure 3.31. HRMS data indicating α-amino α,β-unsaturated ester **67** in the H/D exchange reaction of **61**-benzoate with d_8-IPA **47**, catalysed by SCRAM catalyst **13**. Top to bottom: 0 hours – 4 hours.

3.4.2 Proline Isopropyl Ester

Proline isopropyl ester **68** is an inexpensive starting material, and was selected for study due to its similarity to ethyl (2*R*,4*R*)-4-methylpiperidine-2-carboxylate **3**. Stirling *et al*. previously investigated the racemisation of proline methyl ester in toluene using SCRAM catalyst and found it racemised by 10% in 2 hours, possibly due to the electron withdrawing effect of the carbonyl group hindering hydride abstraction. Scheme 3.12 illustrates the reaction conditions and possible deuteration sites.[99]
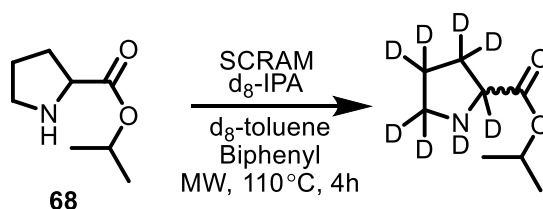
Scheme 3.12. Possible deuteration sites of **68** in the H/D exchange reaction with d_8-IPA **47**, catalysed by SCRAM catalyst **13**.

After the first hour of heating, a 15% decrease in H1' integration was seen, however a further 3 hours reaction gave no spectral change. Resolution of both the α-H2 and H5

protons is lost after the first hour of heating. Further reaction causes their integration to continue decreasing, suggesting hydrogen-deuterium exchange at both α-positions. Both H3 protons appear to decrease, whilst new signals appear adjacent, however, these may be associated with other species which are challenging to define. Similarly, the H4 protons also suggest hydrogen-deuterium exchange, however, the evolution of the large singlet signal (at around 1.50 ppm) makes integration and quantification of hydrogen-deuterium exchange in this instance difficult. The change in integration for this reaction is summarised graphically in Figure 3.33, where all α- and β-protons are demonstrated to decrease.
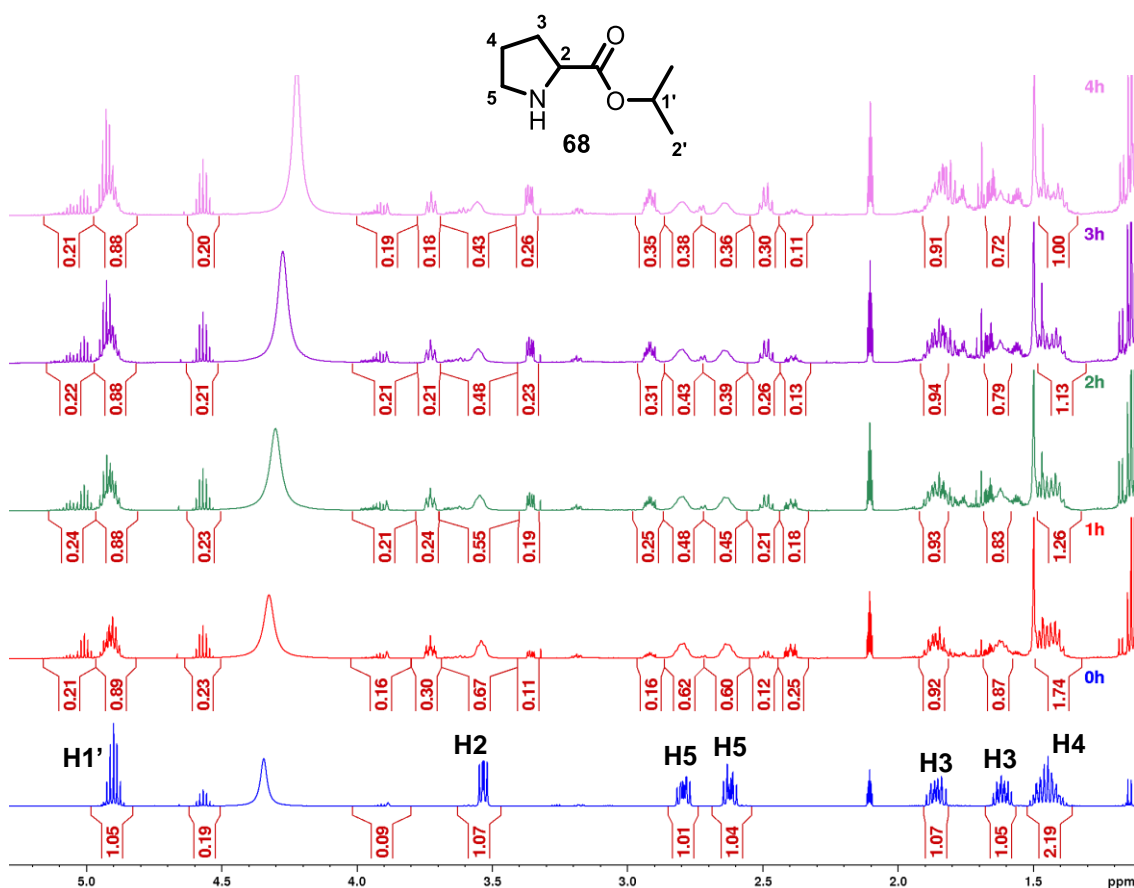
Figure 3.32. ^{1}H NMR spectra for the H/D exchange reaction of **68** with d$_8$-IPA **47**, catalysed by SCRAM catalyst **13**
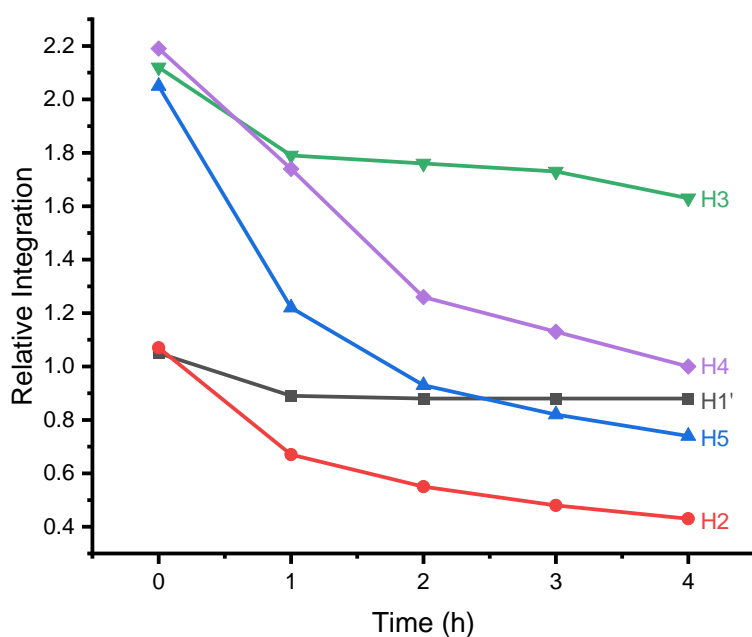
Figure 3.33. Decrease in ^{1}H NMR integration of **68** for the H/D exchange reaction with d$_8$-IPA **47**, catalysed by SCRAM catalyst **13**

HRMS data provides further evidence for **68** racemisation as demonstrated in Figure 3.34, where several M+1 peaks appear after the first hour of heating.
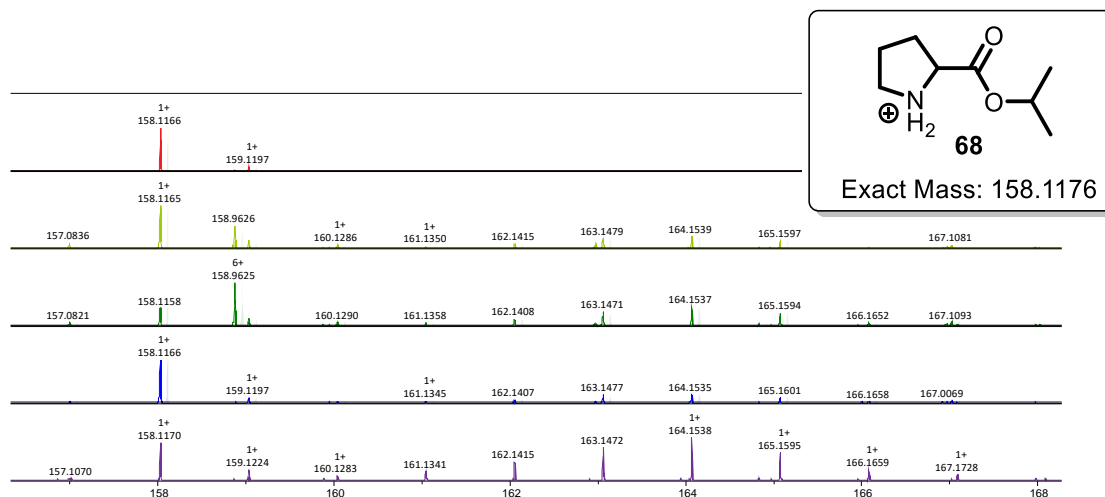
Figure 3.34. HRMS data indicating M+1 peaks of **68** in the H/D exchange reaction with d$_8$-IPA **47**, catalysed by SCRAM catalyst **13**. Top to bottom: 0 hours – 4 hours.

The same reaction was conducted with benzoic acid to produce a soluble benzoate salt of **68**. Compared to the reaction without benzoic acid **66**, the H1' proton integration decreased linearly throughout the reaction, with concomitant increase in a signal at 3.95 ppm, which may be the IPA released as a result of transesterification, Figure 3.36. The

α-H2 peak decreases more quickly than the reaction without benzoic acid. This is unsurprising since the ammonium cation lowers the H2 pK_a making it more susceptible to abstraction. Integration of the H5-proton, decreases more slowly than without acid, and may be due to exchange at the H2 centre, the proton of which has a lower pK_a that that of the H5 proton. The β-H3 and H4 protons also decrease through reaction, however, it is difficult to compare these to the results without acid, due to differences in chemical shift and therefore signal overlap and proton environment. Changes in integration are summarised in Figure 3.35.
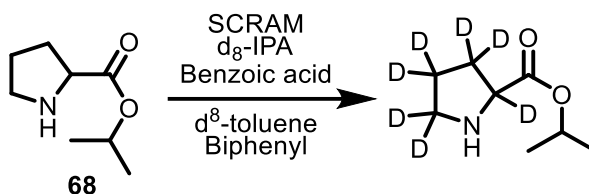
Scheme 3.13. Possible deuteration sites of **68**-benzoate in the H/D exchange reaction with d_8-IPA **47**, catalysed by SCRAM catalyst **13**.
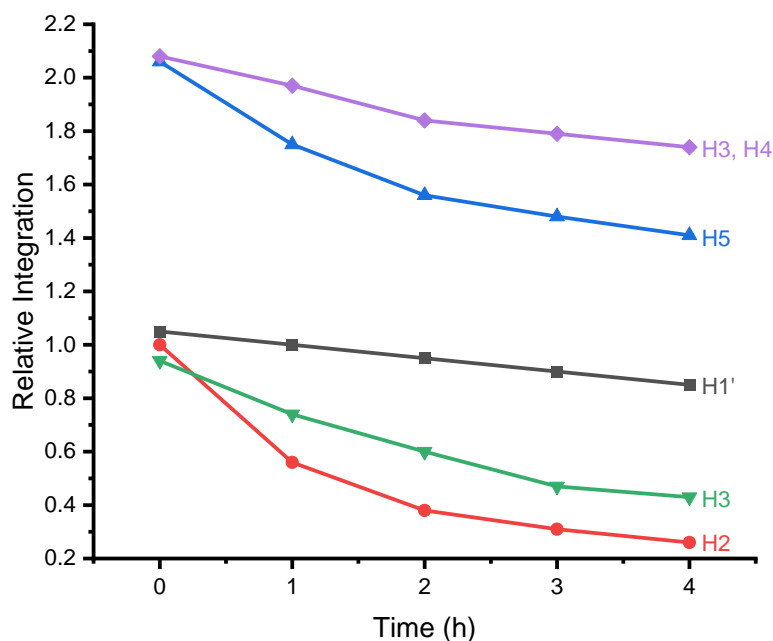
Figure 3.35. Decrease in ^{1}H NMR integration of **68**-benzoate for the H/D exchange reaction with d_8-IPA **47**, catalysed by SCRAM catalyst **13**
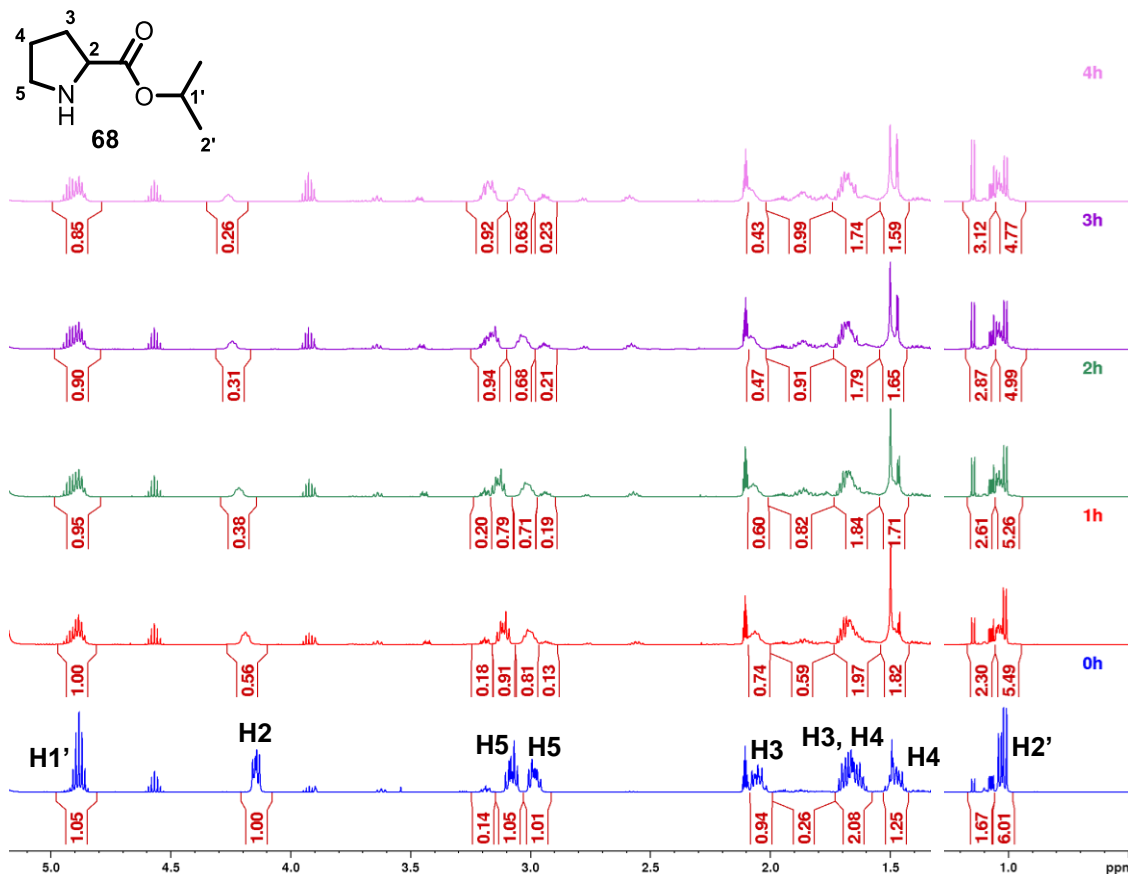
Figure 3.36. ^{1}H NMR spectra for the H/D exchange reaction of **68**-benzoate with d$_8$-IPA **47**, catalysed by SCRAM catalyst **13**

3.4.3 Ethyl (2R,4R)-1,4-dimethylpiperidine-2-carboxylate

The tertiary amine analogue of (2*R*,4*R*)-**61** was investigated, Scheme 3.14. Due to steric effects and formation of a higher energy quaternary iminium or enamine intermediate, it was unclear whether (2*R*, 4*R*)-**69** would epimerise.
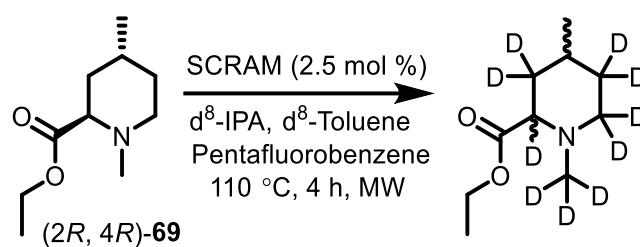
Scheme 3.14. Possible deuteration sites of **69** in the H/D exchange reaction with d$_8$-IPA **47**, catalysed by SCRAM catalyst **13**.

As shown in Figure 3.37 and Figure 3.38, the integration of all protons remained fairly constant. The initial fluctuation between 0 and 1 hours for H3/H4 can be attributed to an unknown peak appearing, slowly diminishing between 1 and 4 hours. A small percentage change is seen for both the H2 and H6 protons (8% and 9% respectively)

which is possible through imine-enamine tautomerisation, indicating some epimerisation. Mass spectrometry evidence shows some deuterated species, to support this, Figure 3.39. However, little epimerisation is occurring compared to the compound's secondary amine counterpart.
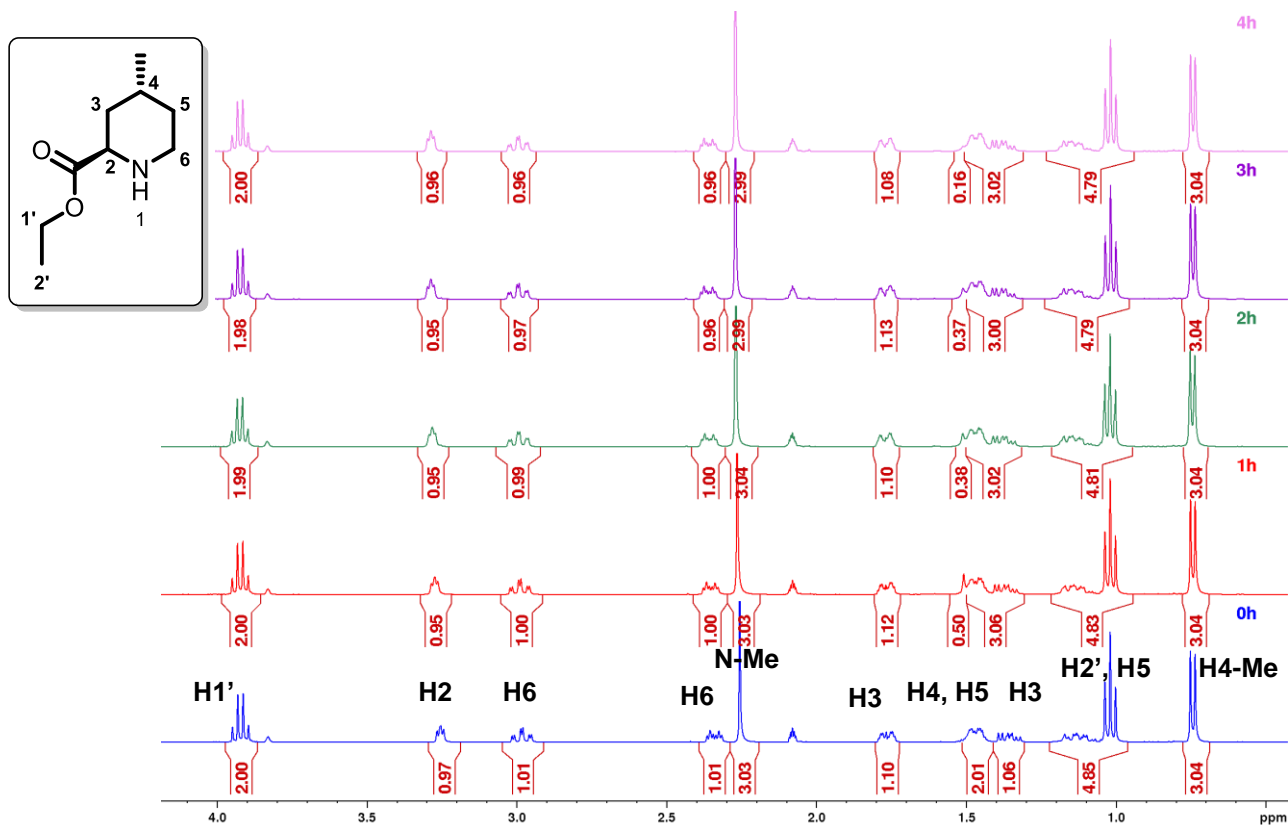
Figure 3.37. ¹H NMR spectra for the H/D exchange reaction of **69** with d₈-IPA **47**, catalysed by SCRAM catalyst **13**
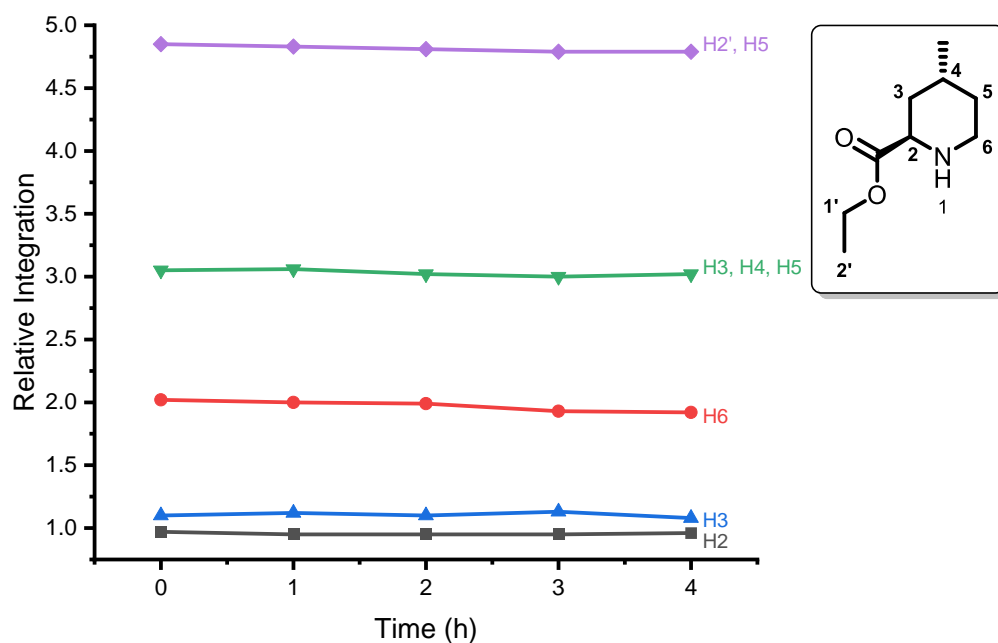
Figure 3.38. Decrease in ^{1}H NMR integration of **69** for the H/D exchange reaction with d$_8$-IPA **47**, catalysed by SCRAM catalyst **13**
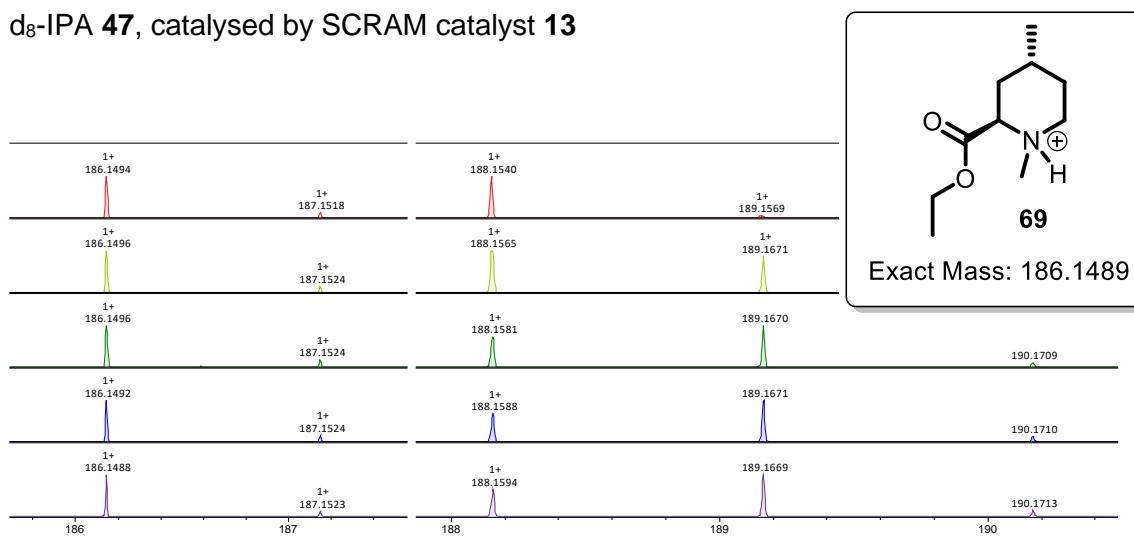
Figure 3.39. HRMS data indicating M+1 peaks of **69** in the H/D exchange reaction with d$_8$-IPA **47**, catalysed by SCRAM catalyst **13**. Top to bottom: 0 hours – 4 hours.

3.4.4 Sertraline

Sertraline **26** is an anti-depressant molecule first synthesised and patented by Pfizer, the synthesis and resolution of which will be described further in a subsequent section.[112] As the SCRAM **13** catalysed epimerisation of sertraline **26** had been investigated previously, it was selected as a substrate to investigate in this study.[50]

The reaction was conducted using d^{10}-o-xylene **70** as reaction solvent at 142 ºC, as an analogous experiment with d^8-toluene **48** conducted previously proved inconclusive.[101] The experiment is summarised in Scheme 3.15.
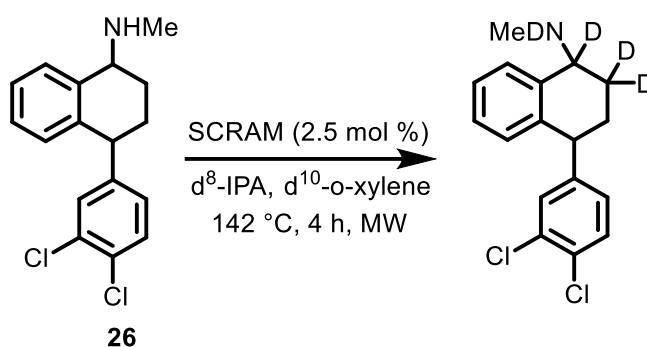
Scheme 3.15. Possible deuteration sites of **26** in the H/D exchange reaction with d_8-IPA **47**, catalysed by SCRAM catalyst **13**.

It is clear that most hydrogen-deuterium exchange occurs at the H1 centre in the first hour of heating (Figure 3.40, H1). The reaction starts with a 60% decrease in H1 integration in the first hour of heating, and is only 64% after 4 hours of heating. As expected, the δ chiral proton (H4) integration remains fairly consistent throughout reaction duration, in line with previous research which demonstrates the need for high temperature and strong base conditions for epimerisation at the methine centre.[50] The slight decrease might be hydrolysis of the intermediate imine to form the ketone.
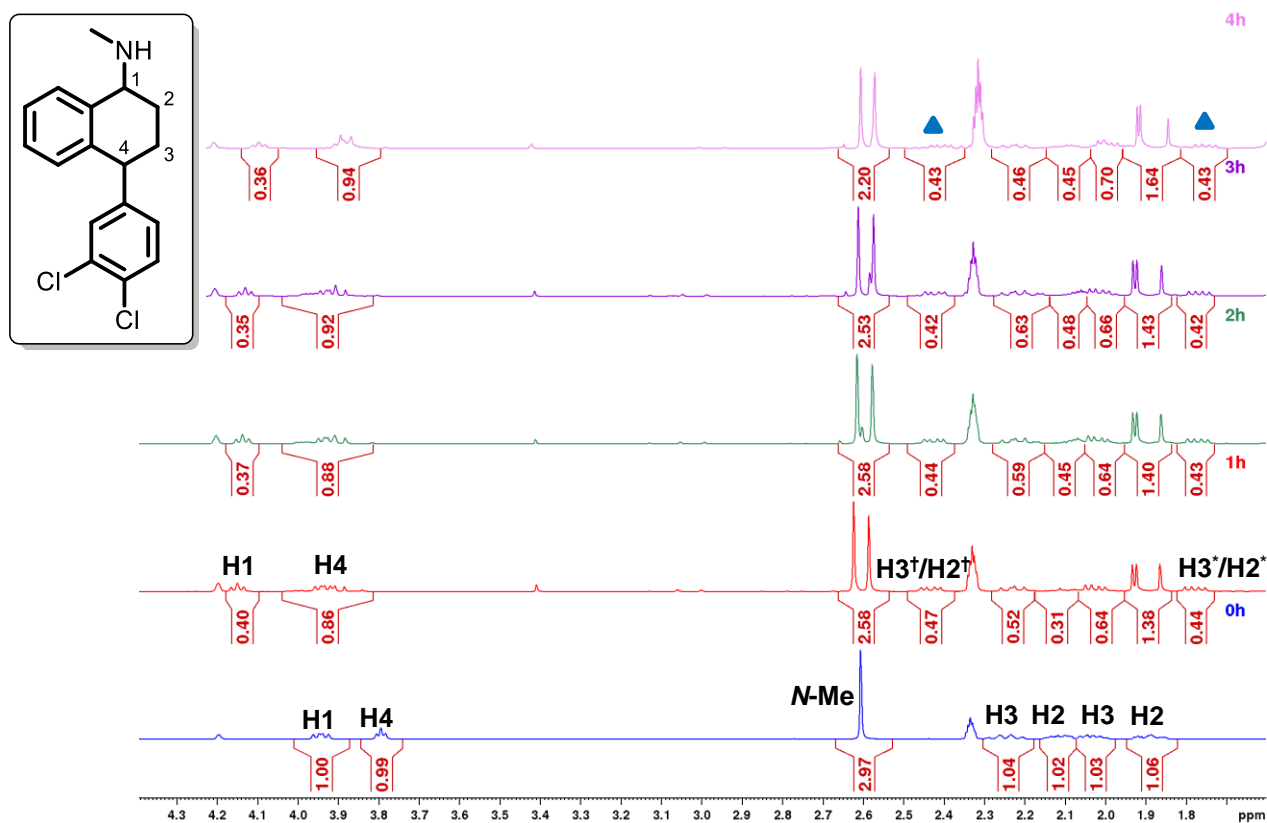
Figure 3.40. ^{1}H NMR spectra for the H/D exchange reaction of **26** with d$_8$-IPA **47**, catalysed by SCRAM catalyst **13**

The evolution of a singlet, adjacent to the *N*-Me peak, suggests formation of diastereomers through the epimerisation of the chiral amine centre. A decrease in integration suggests either hydrogen-deuterium exchange at this position and or the formation of methylamine through imine **71** hydrolysis to form sertralone **72** as shown in Scheme 3.16.
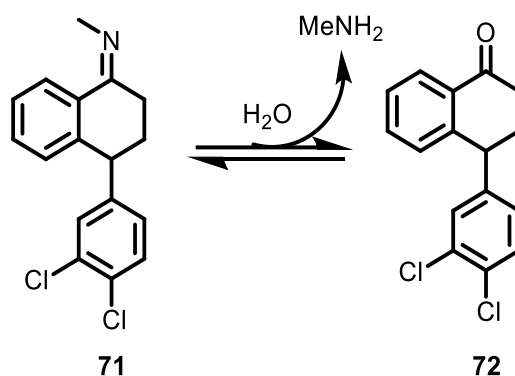
Scheme 3.16. Hydrolysis of sertraline's corresponding imine **71** to form the corresponding ketone, sertralone **72**

Additional peaks which appear at 1.75 ppm and 2.45 ppm (indicated by the blue triangles on Figure 3.40) after the first hour of heating, also suggest the formation of diastereomers, as they can be attributed to the formation of new diastereomeric protons. Analysis of the spectra suggests these peaks may be attributed to the H3 centre. The average integration of each H3 peaks is ~1 (Table 3.1), Hydrogen-deuterium exchange would not be expected at this centre because imine-enamine tautomerisation would affect only H1, H2 and *N*-Me positions, Scheme 3.17.

Time (hour)	Average of H3 peaks
0	1.04
1	1.05
2	1.06
3	1.06
4	1.01

Table 3.1. The average of all original and new H3 peaks (H3, H3', H3* and H3†)
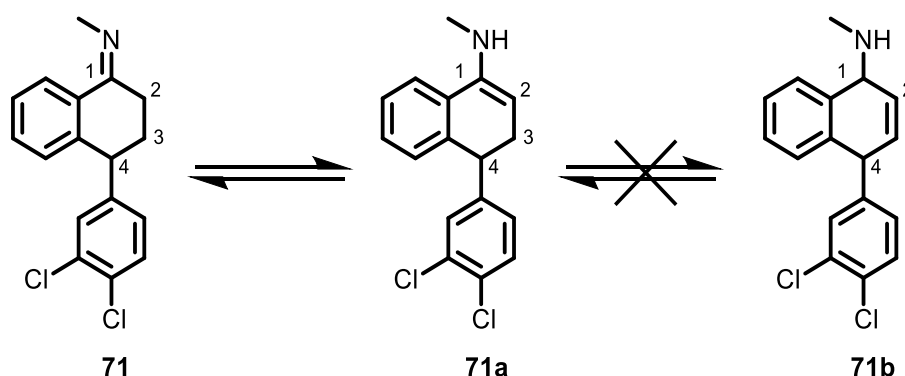
Scheme 3.17. Tautomerisation between imine **71** and enamine **71a**, formed through reaction with SCRAM catalyst **13**. Compound **71b** does not form.

If the new signal is the H3 centre, it does not explain the complete disappearance of the H2 proton peak. Whilst this could be due to complete deuteration, this seems unlikely due to the simultaneous exchange of hydrogen and deuterium atoms. One would expect a percent of deuteration, but not complete deuteration.

In place of the original H2 peak, a new doublet and singlet peak can be seen evolving. This region of the NMR spectrum is usually associated with the singlet peak(s) attributed to the Cp* protons of the SCRAM catalyst. It is sensible to suggest that the progressive increase in these peaks, accompanied by the plateau of proton integration decrease is due to the formation of methylamine deactivated SCRAM catalyst **73a**, **73b**, **73c**, the

equilibria for which can be seen in Scheme 3.18 where $K_1 = 0.16$ mM^{-1}, $K_2 = 17.31$ mM^{-1} and $K_3 = 0.046$ mM^{-1}. These specific equilibrium constant values were calculated previously by Kwan *et al.* through analysis of ^{1}H NMR titration data, where methylamine (2 M in MeOH) was added to a mixture of SCRAM catalyst in d$_6$-DMSO. Unfortunately, attempts to characterise and or isolate these methylamine bound species through crystallisation and mass spectrometry proved unsuccessful, however, the analogous IrCp*I$_2$NH$_3$ and IrCp*(NH$_3$)$_3$I$_2$ species have previously been reported.[98]
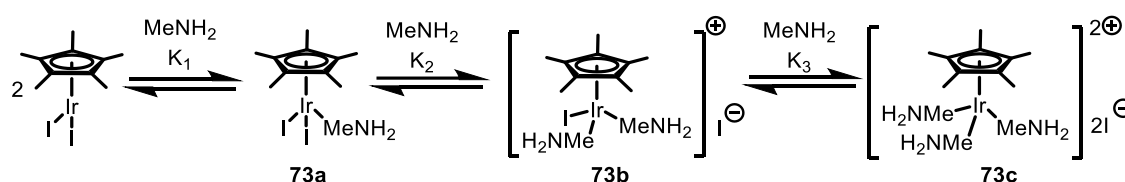
Scheme 3.18. Equilibrium to show methylamine deactivated SCRAM catalyst

Multiple signals would suggest several deactivated species of methylamine bound SCRAM, which is not unusual given that equilibrium constants (albeit obtained under different experimental conditions) suggest evidence for mono-, di- and tri- methylamine substituted SCRAM catalyst. The formation of these species has been described in a recent publication, and can be attributed to the hydrolysis of the intermediate imine as illustrated in Scheme 3.16.[98]

Evidence in the NMR spectrum also suggests that these new peaks are, in fact, attributed to the formation of methylamine bound SCRAM. [98] After the second and third hours of heating, the corresponding NMR shows a small signal overlapping with the *N*-methyl peak of sertraline, Figure 3.41. The integration of this peak, suggested to be methylamine bound to the iridium centre of SCRAM, is approximately a fifth the numerical quantity of the Cp* SCRAM peaks. As anticipated, the Cp* peaks equate to 15 protons, whilst that of the methylamine peak equates to 3 protons. The correlation of these peaks suggests that they are peak signals belonging to the same species, in this case, that of methylamine deactivated SCRAM catalyst.
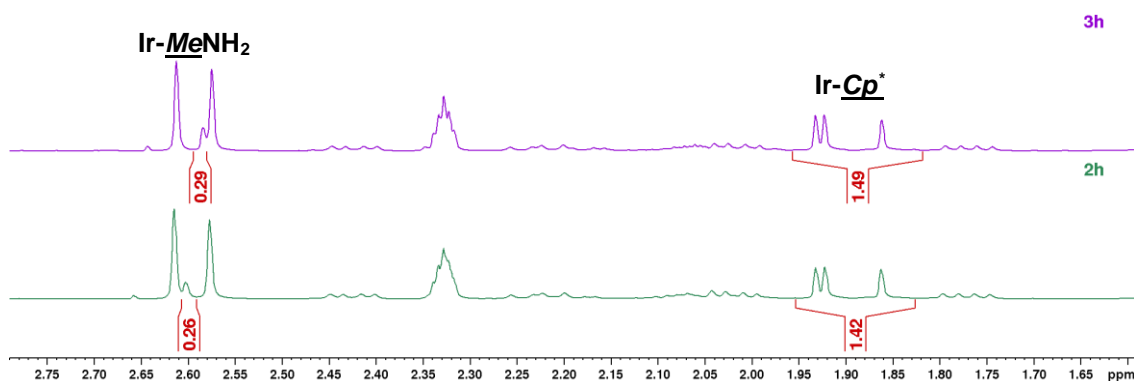
Figure 3.41 Comparison of methylamine (bound to iridium) and Cp* integrations to show a relationship of factor 5 in the second and third hour spectra for the H/D exchange investigation of sertraline

3.4.5 Diltiazem precursor

Diltiazem, a drug used to treat high blood pressure has an intermediate with two chiral centres (2S,2S)-**74**.[113] A similar diester intermediate (2S,2S)-**75** was available in copious quantity and was therefore utilised for hydrogen-deuterium exchange investigation.

(2S,2S)-**74**
acid intermediate

(2S,2S)-**75**
diester intermediate
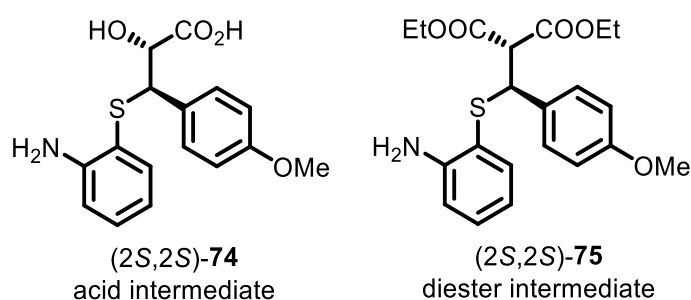
With respect to internal standard tetrakis(trimethylsilyl)silane, the integration of aromatic peaks decreased. This suggested either deuterium incorporation at these aromatic centres and or the formation of impurities. The growth of new peaks in the aromatic region could be seen in the spectra, with a singlet appearing at approximately 7.70 ppm and two doublets at around 6.60 ppm and 7.25 ppm, Figure 3.42, demonstrated by the red circle, green square and blue triangle respectively. This is in addition to other minor signals which can be seen appearing
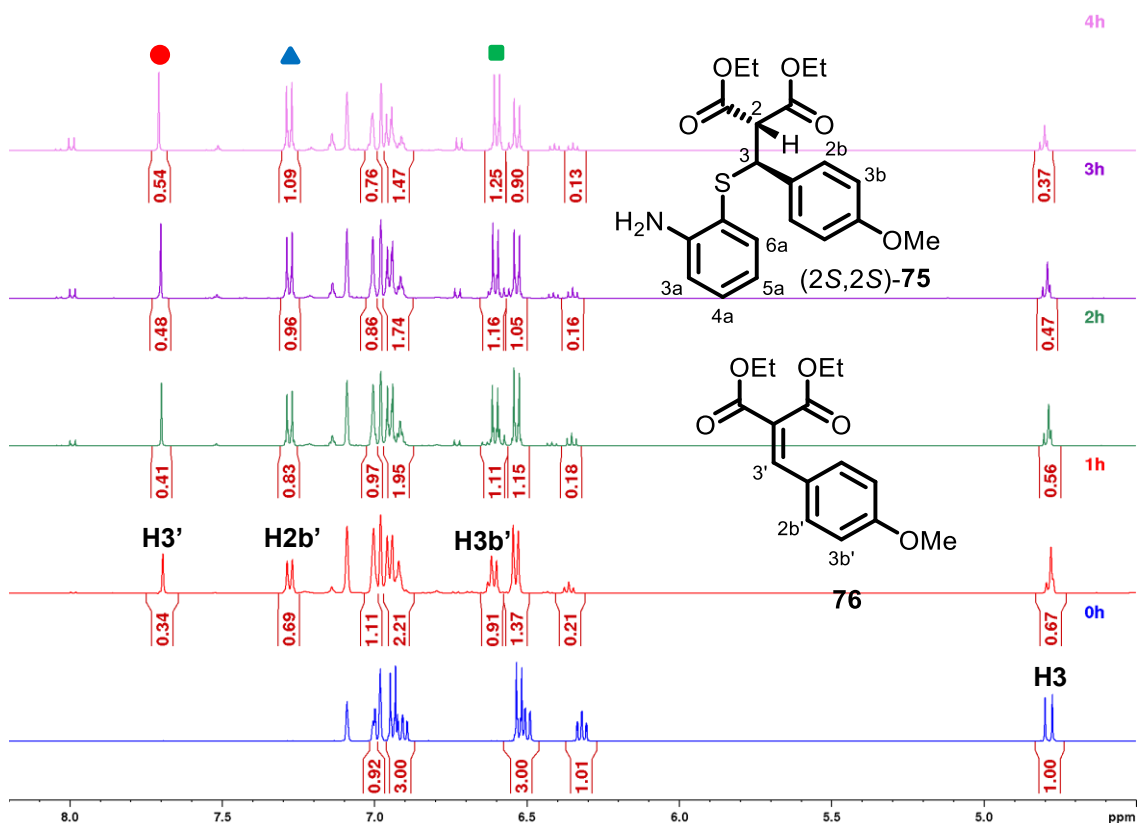
Figure 3.42. ^{1}H NMR spectra for the H/D exchange reaction of **75** with d$_8$-IPA **47**, catalysed by SCRAM catalyst **13**. New peaks of **76** indicated by red circle (H3'), blue triangle (H2b') and green square (H3b').

Due to the complex functionality of the diester compound, there are a few side reactions that may be occurring and therefore leading to the growth of additional aromatic peaks (as there is only one chiral centre, these peaks can't be due to the formation of diastereomers). The first possible mechanism involves the abstraction of the low pK_a β-diester proton. This is swiftly followed by the formation of a double bond and elimination of 2-aminothiophenol **77** along with the formation of **76**.[114] The alternative mechanism involves a cyclisation, whereby the aryl amine functionality attacks one of the esters, eliminating ethanol and forming a 7 membered ring **78**.[115] Both mechanisms can be seen summarised in Scheme 3.19
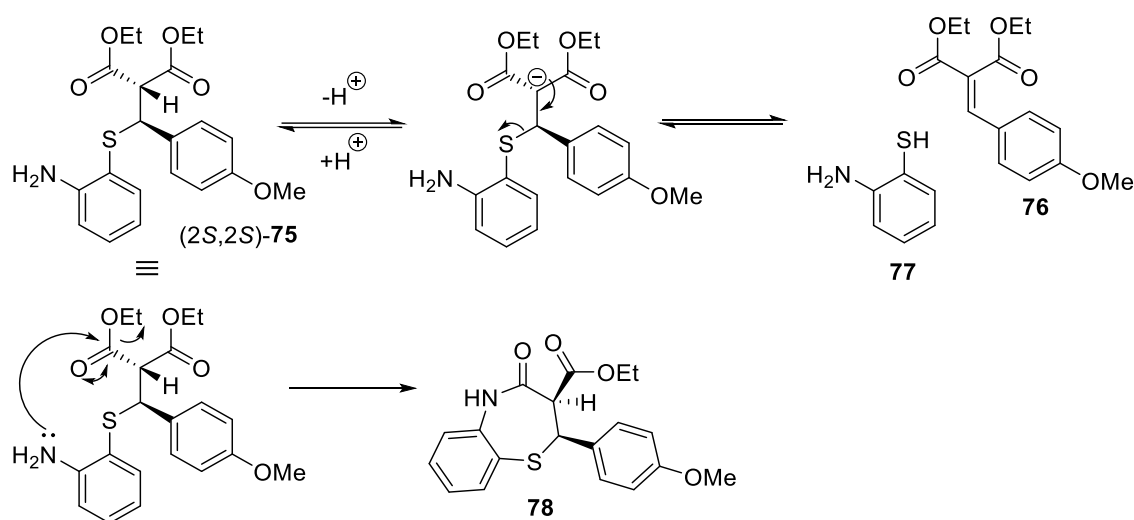
Scheme 3.19. Possible pathways of impurity formation from (2*S*,2*S*)-**75**

Interestingly, the decrease in H3 integration (which would otherwise indicate deuteration) is accompanied by a complimentary increase in the new singlet peak at around 7.70 ppm (Figure 3.42, labelled H3' with red circle). This is demonstrated in Table 3.2 where the sum of H3 and H3' peaks equates to approximately 1. The table also showcases the sum of these peaks in a control experiment to confirm the SCRAM catalyst was not involved in the formation of these impurities.

Time (hour)	Sum of H3 and H3' (SCRAM)	Sum of H3 and H3' (Control)
0	1.00	1.01
1	1.01	1.01
2	0.97	1.02
3	0.95	1.00
4	0.91	0.98

Table 3.2. The hourly sum of H3 and H3' proton peaks when (2*S*,2*S*)-**75** is reacted in the presence of and absence of SCRAM catalyst **13**

Whilst the integration of the control experiment stays fairly consistent, with a range of 0.03 ppm, that of the catalysed experiment is three times this value at 0.09 ppm. The steady 9% decrease in integration for the sum of both H3 and H3' suggests there may be some deuteration when SCRAM catalyst **13** is used. However, mass spectrometry evidence neither supports nor negates this theory of deuteration.

In addition to the vinyl H3' proton of **76**, two new doublet peaks can be seen appearing (Figure 3.43, labelled H2b' and H3b') which correspond to the *para* substituted aryl ring

of **76**. Additionally, the growth of a new double doublet and doublet of triplets likely corresponds to the aromatic protons of the 2-aminothiophenol compound **77** (Figure 3.43, labelled H3a', H6a' and H4a', H5a' respectively). As each signal is approximately in a 1:1 ratio with compound **76**, it is possible that each of these peaks corresponds to one proton, whilst the other two protons of 2-aminothiophenol **77** have evolved overlapping with the original peaks of the (2*S*,2*S*)-**75** starting material, therefore making the spectrum difficult to interpret.

Additionally, a methoxy group of compound **76** appears adjacent to the original compound's methoxy peak which has since decreased in intensity and integration (Figure 3.43, labelled and 4b'-OMe and 4b-OMe respectively). The 0 hour spectrum has been displayed to provide a direct comparison of both new and original ^{1}H NMR signals. The new ester signals appearing have also been integrated, however, due to their overlap with the original compound's ester peaks, their integrations do not give integer values.
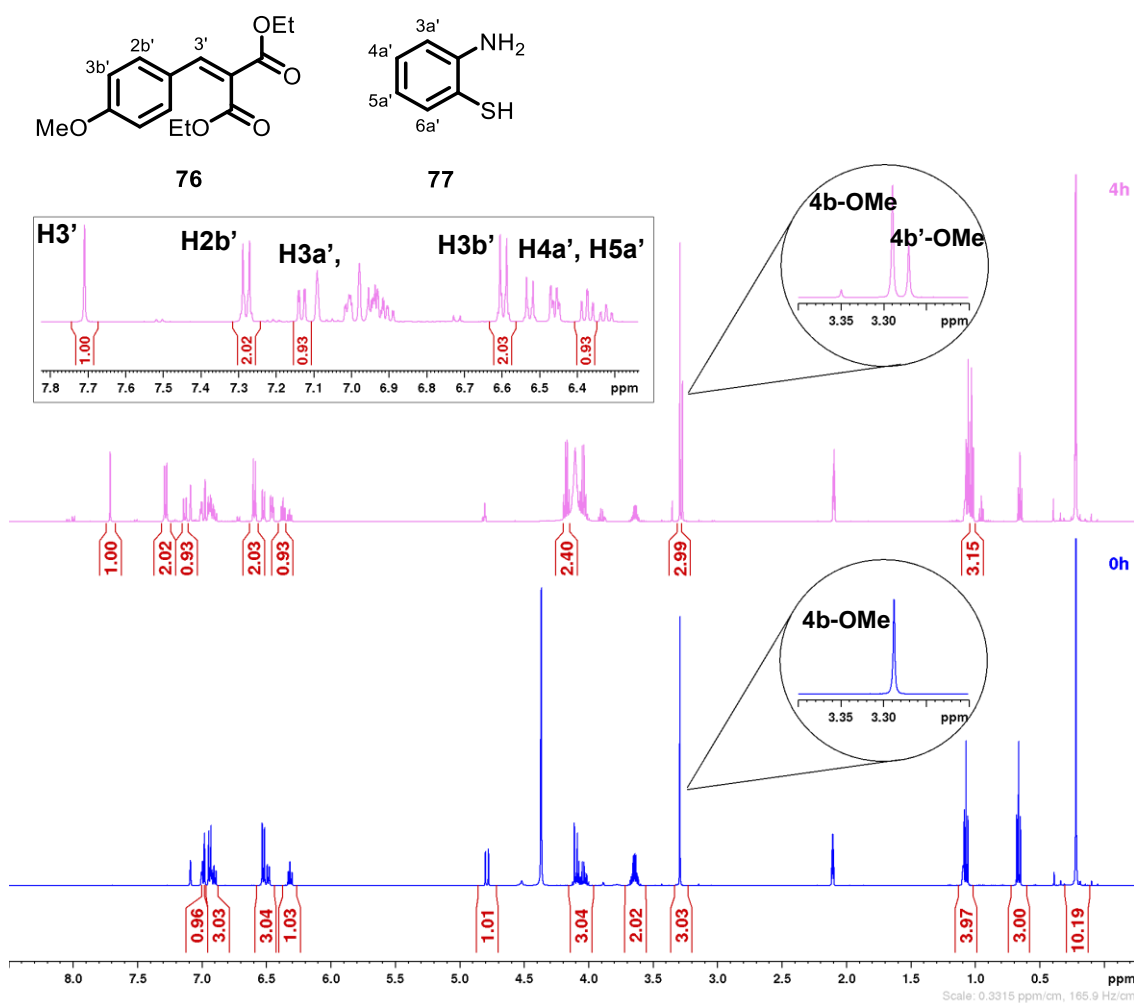
Figure 3.43. ^{1}H NMR spectra for the control reaction of **75** with d_8-IPA **47**, in absence of SCRAM catalyst **13**. Prime symbol has been used to distinguish impurities from original starting material.

3.4.6 1-{Imidazo[1,2-a]pyridin-6-yl}ethan-1-amine

Savolitinib, developed by AstraZeneca and HUTCHMED Ltd, has recently been approved in China for anti-cancer treatment.[116,117] An intermediate to this compound is a chiral amine **79** which formed a part of our study, Scheme 3.20.
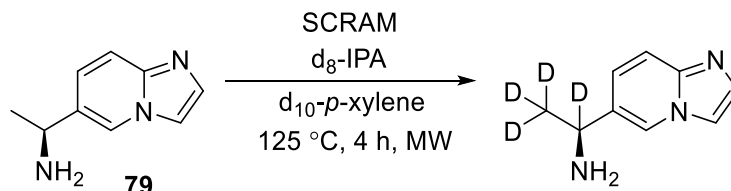
Scheme 3.20. Possible deuteration sites of **79** in the H/D exchange reaction with d_8-IPA **47**, catalysed by SCRAM catalyst **13**.

Following reaction, the data for this compound suggests there is little, if any, deuterium incorporation through the formation of the imine intermediate. Whilst the integration of

the α (H1') and β (H2') protons somewhat decreases throughout the reaction, there is a complimentary increase in new nearby signals, equating to the original integrations of 1 and 3 respectively. This is shown in Figure 3.44
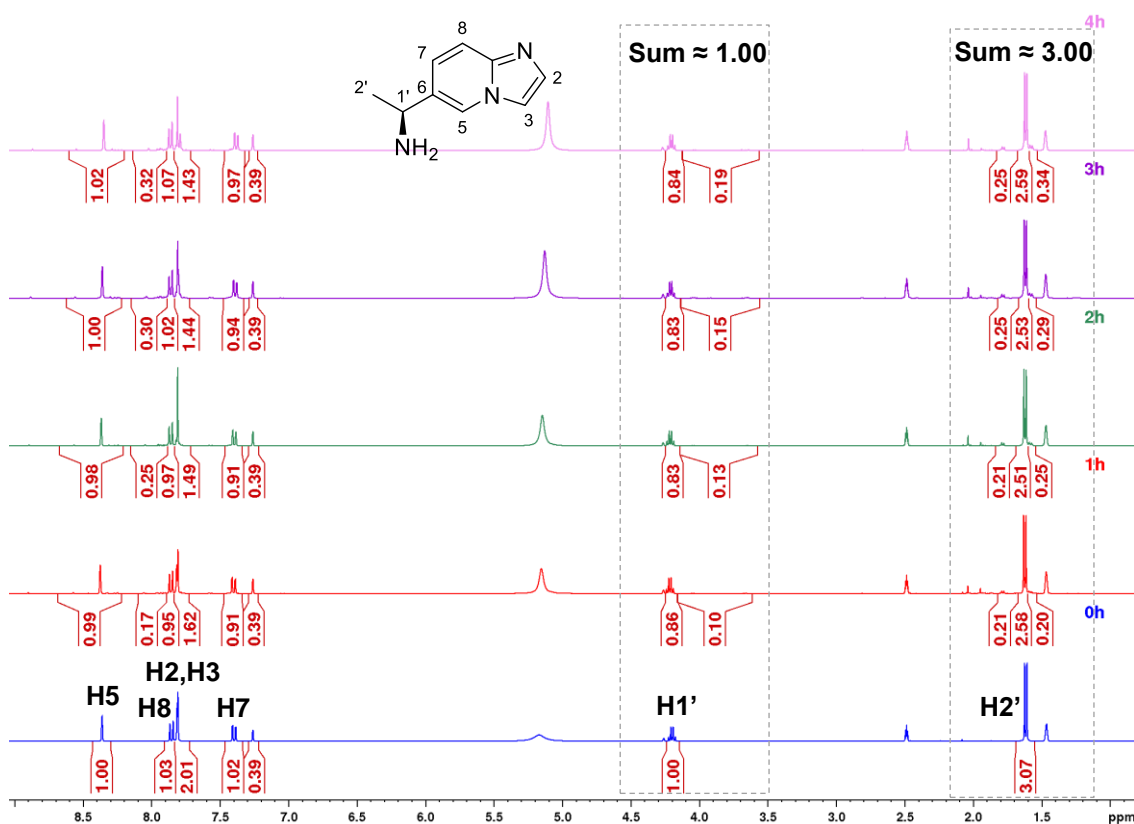
Figure 3.44. ^{1}H NMR spectra for the H/D exchange reaction of **79** with d$_8$-IPA **47**, catalysed by SCRAM catalyst **13**. Reaction conducted in d$_{10}$-p-xylene.

Whilst there is no evidence of deuterium incorporation through means of imine-enamine tautomerisation, evidence points to deuteration at the H2 and H3 centres through electrophilic substitution. The resonance structures in Scheme 3.21 show how electrophilic substitution at these centres may be favoured and why there is, therefore, a decrease in the corresponding ^{1}H NMR signal. HRMS data supports hydrogen-deuterium exchange, but to a smaller degree than other compounds in our study, Figure 3.45.
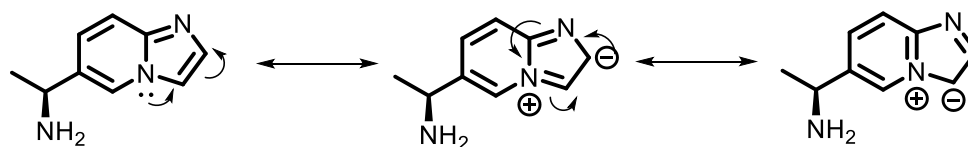
Scheme 3.21. Resonance structures showing the favourable placement of negative charge on **79**

In the case of **79**, it is possible that the formation of dimers is quicker than that of deuterium incorporation, which would explain the appearance of new NMR signals adjacent to the original H1' and H2' signals in the spectrum. Furthermore, the heterocyclic nitrogens may ligate to the catalytic iridium centre, reducing rate of racemisation.
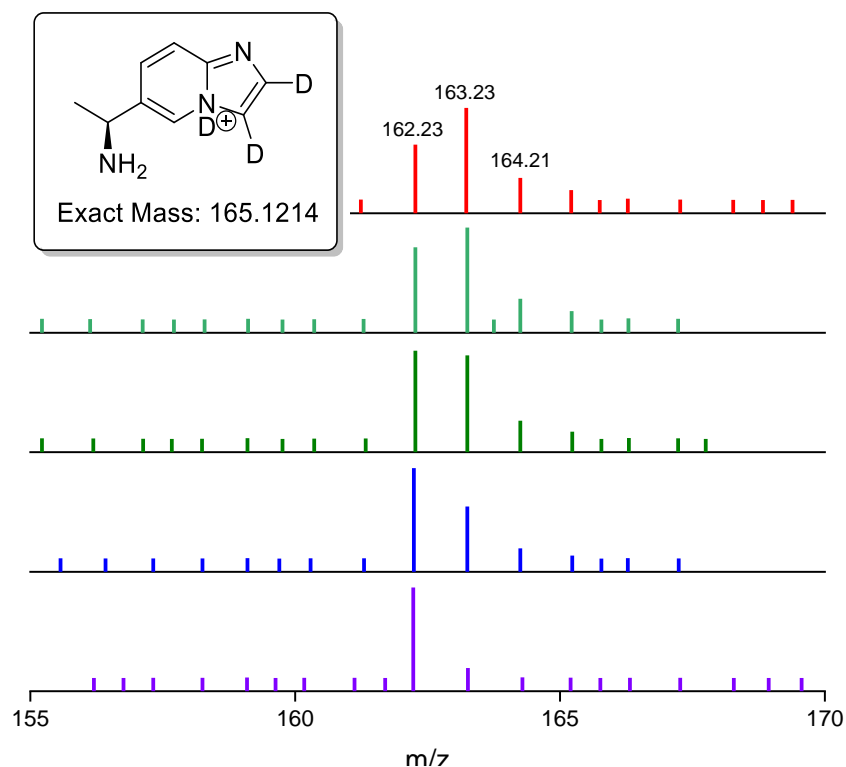
Figure 3.45. HRMS data indicating lack of M+1 peaks of **79** in the H/D exchange reaction with d_8-IPA **47**, catalysed by SCRAM catalyst **13**. Top to bottom: 0 hours – 4 hours.

3.4.7 (2*R*)-8-Bromo-5-methyl-1,2,3,4-tetrahydronaphthalen-2-yl)-(1*S*)-1-(phenylethyl)amine

A novel chiral aminotetralin, AR-A2 was previously investigated for central nervous system disorders at AstraZeneca. An intermediate in its synthesis, (2*R*,1*S*)-**80**, was investigated as part of our study.[118,119] Diastereomers of (2*R*,1*S*)-**80** have been studied and reported in the literature, making it a good candidate for further investigation.[120] This is a secondary amine with a chiral auxiliary which may induce stereochemistry during reduction of the intermediate imine, Scheme 3.22.
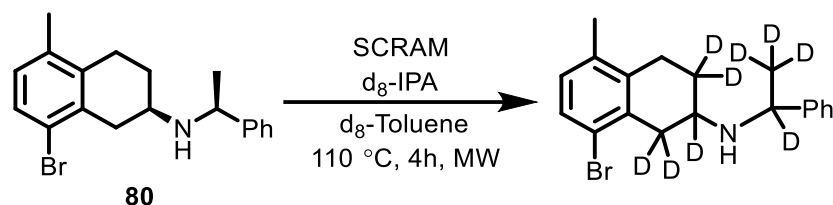
Scheme 3.22. Possible deuteration sites of **80** in the H/D exchange reaction with d_8-IPA **47**, catalysed by SCRAM catalyst **13**.

The data shows evolution of proton signals which correspond to the diastereomer of this amine. Diastereomeric proton peaks can be seen growing in for H1a (α), H1 (β), H5-Me and H2a the latter two of which correspond to the aromatic methyl and aliphatic methyl signals respectively, Figure 3.46.

The data suggests deuteration, but relatively more hydrogenation. At the H1 and H1a centres, there is an apparent decrease in integration of each peak, but also a complimentary increase of nearby diastereomeric proton peaks appearing (H1' and H1a' respectively, Figure 3.46). This data is summarised graphically in Figure 3.47 where the proton integration decrease of H1 and H1a is demonstrated to mirror that of the proton increase of H1' and H1a'.
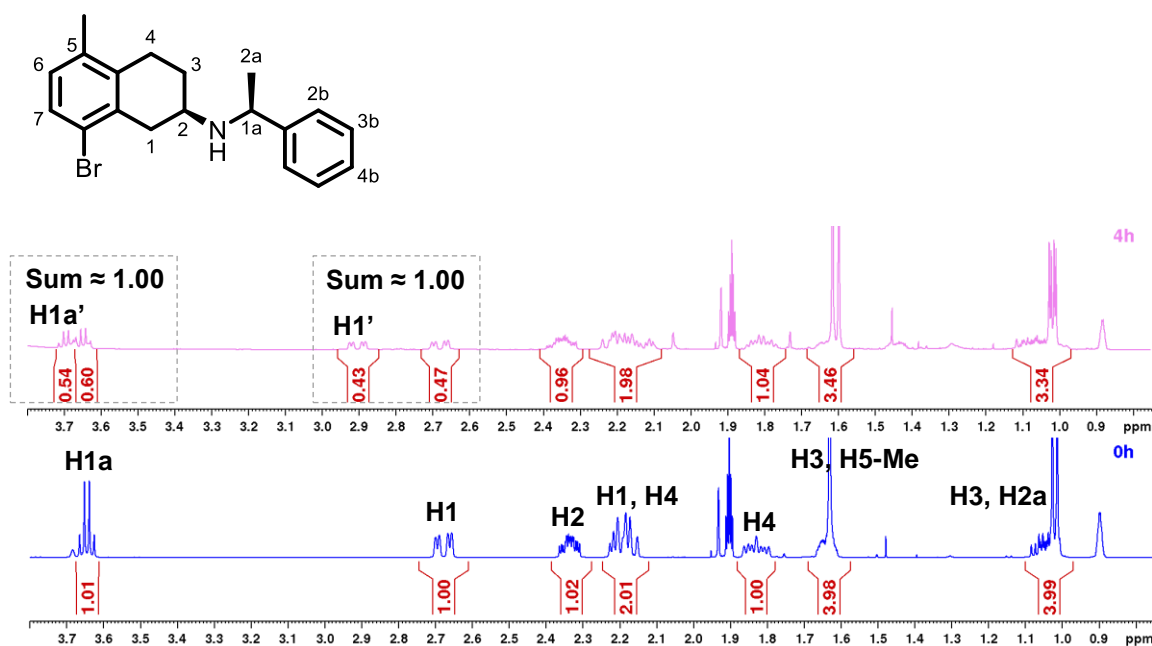
Figure 3.46. ^{1}H NMR spectra for the H/D exchange reaction of **80** with d_8-IPA **47**, catalysed by SCRAM catalyst **13**. Prime symbol has been used to distinguish diastereomeric protons.
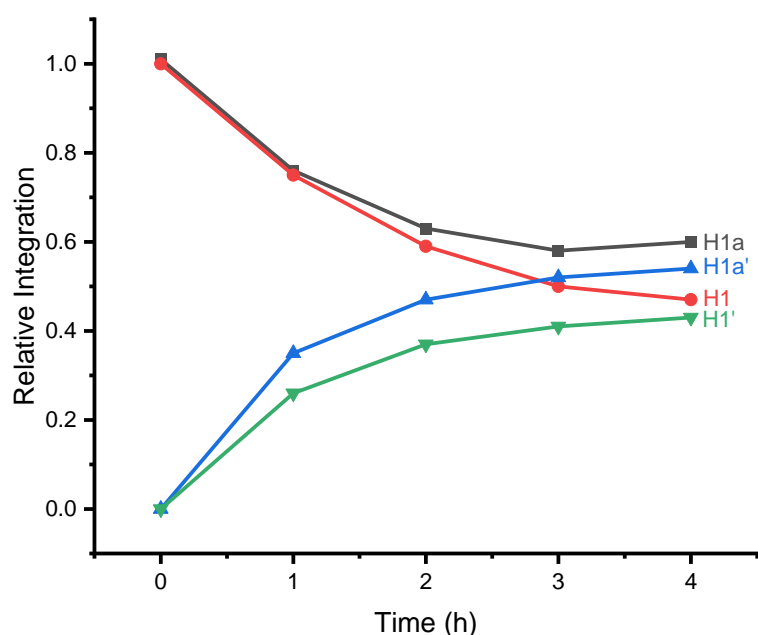
Figure 3.47. Decrease in ^{1}H NMR integration of α-H1 and α-H1a protons of **80**, with corresponding increase in ^{1}H NMR integration of α-H1' and α-H1a' for the H/D exchange reaction with d_8-IPA **47**, catalysed by SCRAM catalyst **13**. Prime symbol has been used to distinguish diastereomeric protons.

This would suggest the epimerisation at the H1a α centre occurs predominantly through hydrogenation as the peaks add up to approximately 1. The growth of H1' would also suggest epimerisation at either or both of the α centres (H1a and H2). Negligible decrease in integration at the α H2 centre (6% over the course of 4 hours) would suggest little incorporation of deuterium at this centre. However, in comparison to the H1a centre, it is possible that this centre is being hydrogenated as opposed to deuterated.

A possible explanation for this is that this imine in particular remains bound or associated to the iridium complex long enough to favour hydrogenation, as opposed to dissociation of the iridium-imine complex to then associate with an iridium-deuteride intermediate. The catalytically active iridium-deuteride species was shown being formed in Figure 3.13 from d_8-IPA **47**.[98]

As anticipated, there was no decrease in integration at the H4 position, as no imine or enamine forms at this centre. A decrease at the H3, H5-Me and H3, H2a centres suggests deuteration at the H3 and H2a centres through imine-enamine tautomerisation. This is in addition to the growth of a new singlet and doublet signal for H5-Me and H2a respectively, the former of which is unlikely to have experienced H/D

exchange due to it's position on an aromatic ring. The growth of the new H5-Me doublet will be due to the formation of diastereomers.

The hydrogen-deuterium exchange through integration decrease is summarised graphically in Figure 3.48. The graph demonstrates the relatively large integral decrease in H3, H5-Me and H3, H2a when compared to the negligible decrease in H1 (including new H1' peak) and H2. Mass spectrometry evidence also suggests deuterium exchange with the presence of +1 peaks, Figure 3.49.
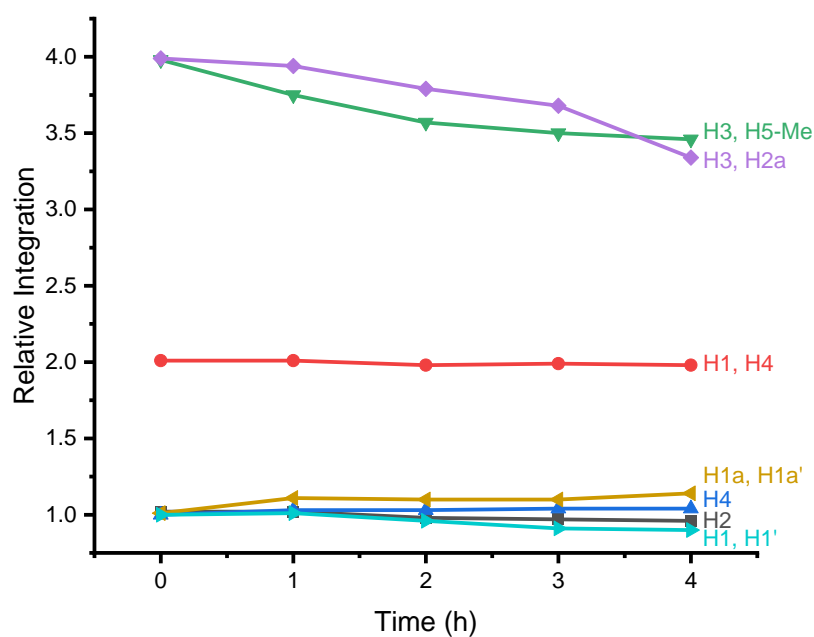
Figure 3.48. Decrease in ^{1}H NMR integration of **80** for the H/D exchange reaction with d_8-IPA **47**, catalysed by SCRAM catalyst **13**. Integration of both diastereomers has been combined for illustrative purposes.
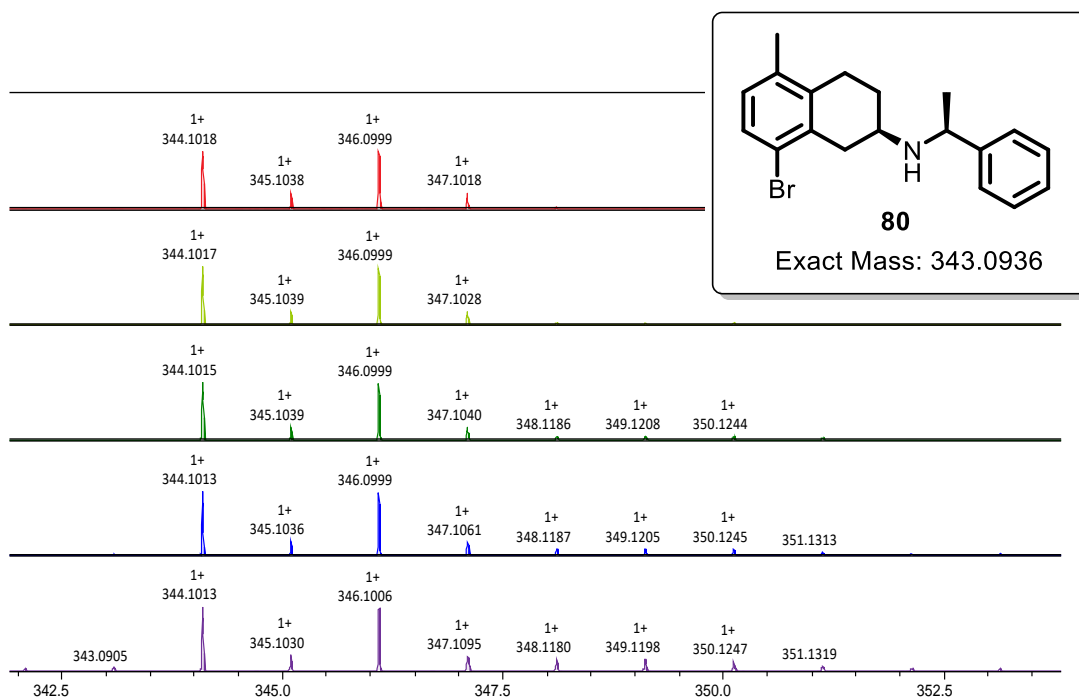
Figure 3.49. HRMS data indicating lack of M+1 peaks of **80** in the H/D exchange reaction with d₈-IPA **47**, catalysed by SCRAM catalyst **13**. Top to bottom: 0 hours – 4 hours.

The same reaction was also conducted without d₈-IPA to further confirm epimerisation was occurring, Scheme 3.23, as the opposite diastereomer was not available for comparison *via* NMR. One of the benefits of using a pure diastereomer is that d₈-IPA need not be used to confirm epimerisation, as the opposite diastereomer will visibly appear, ideally where original and new signals do not overlap for easy interpretation. Should the deuterated version of a solvent used for solid salt formation be available, it is also useful as one can investigate whether epimerisation may also occur under these conditions.
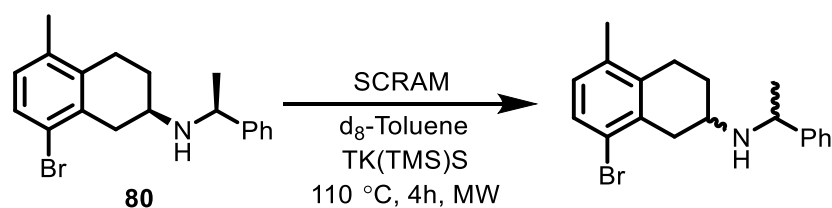
Scheme 3.23. Possible hydrogenation sites of **80** catalysed by SCRAM catalyst **13**.

It is clear from the hourly spectra, Figure 3.50, that epimerisation is taking place due to the appearance of a quartet peak adjacent to H1a, a double doublet peak adjacent to H1, a singlet peak adjacent to H5-Me and a doublet peak adjacent to H2a. As most of these peaks are close to the chiral centres, it is unsurprising that new peaks have evolved as a consequence.

However, for the new H1a and H1 peaks, it is clear from adding the two peaks together on an hourly basis that there is an extent of impurity formation. For the combined H1a peaks, there is a decrease in integration of 14% and a decrease of 9% for that of the combined H1 peaks. The integration of the H2 peak decreases by nearly 12%, the H1, H14 peak stays fairly consistent throughout the reaction until the final hour where the integration decreases, although it is unclear why.

Figure 3.50. ^{1}H NMR spectra for the hydrogenation reaction of **80**, catalysed by SCRAM catalyst **13**. Prime symbol has been used to distinguish diastereomeric protons.

3.4.7.1 Diastereomeric salt investigation

The epimerisation of **80** was investigated as before, without d$_8$-IPA, but with *S*-mandelic acid **25** added as an additional reagent to investigate epimerisation, Scheme 3.24.

Scheme 3.24. Possible hydrogenation sites of **80** in reaction with d$_8$-IPA **47**, catalysed by SCRAM catalyst **13**.

Unlike without *S*-**25**, addition of acid appears to prevent epimerisation from occurring, Figure 3.51. There are no additional peaks which appear attributed to the opposite diastereomer as in the experiment without **25**. There are, however, tiny signals which appear suggesting the formation of impurities. It is possible that these impurities are attributed to hydrolysis of the intermediate iminium ion which forms, supported by ^{13}C NMR data indicating a new peak in the carbonyl region of the NMR, 195.9 ppm. The iminium ion formed through (*S*)-**25** addition is more polarised than the regular imine, leading to a preference of hydrolysis over epimerisation.
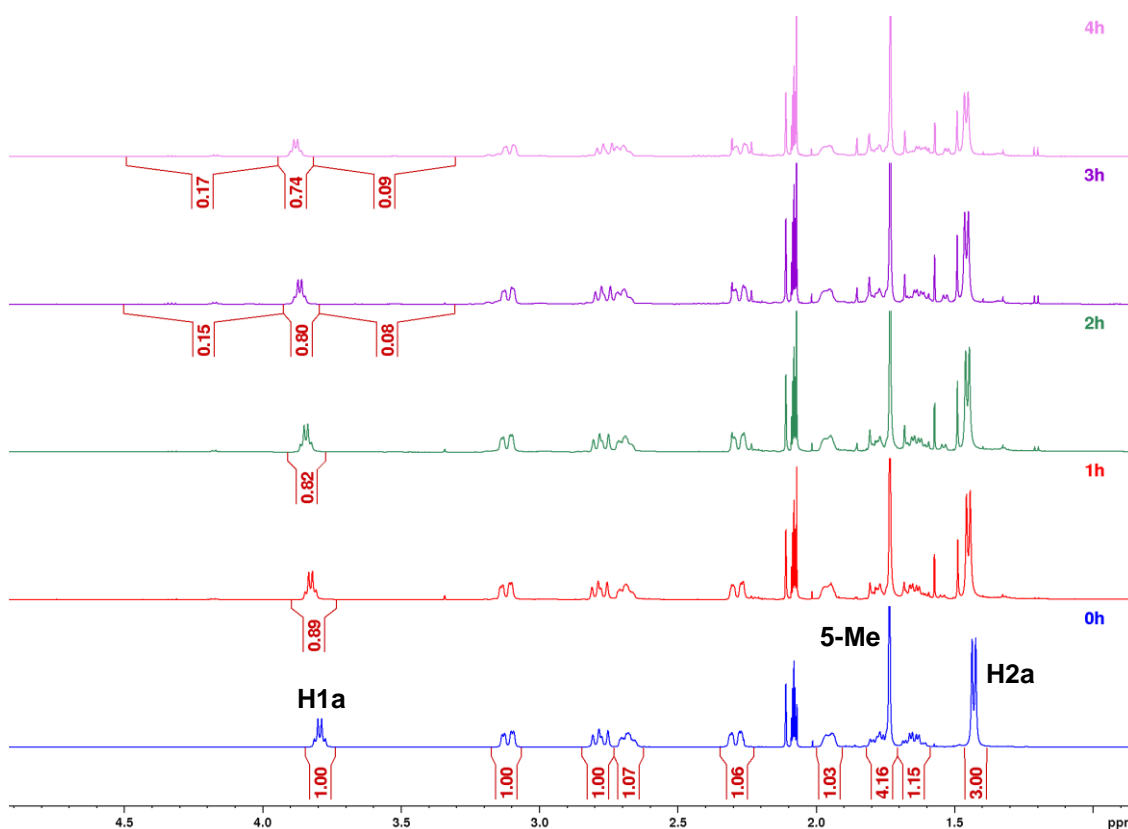
Figure 3.51. ^{1}H NMR spectra for the hydrogenation reaction of **80**-mandelate, catalysed by SCRAM catalyst **13**.

3.5 Limitations

The present study has indicated successful racemisation and epimerisation through catalysed hydrogen-deuterium incorporation. However, the methodology suffers from a number of limitations which must be acknowledged. For instance, the selected internal standard must not overlap with any substrate peaks, must be chemically inert towards catalysed hydrogen transfer or C-H activation, and is able to withstand and solubilise under reaction conditions. As ^{1}H NMR can only detect incorporation of deuterium and not hydrogen, the method is also unable to quantify rate of racemisation and is therefore qualitative. Furthermore, deuteration leads to changes in chemical shift, multiplicities and leads to signal broadening. As a result, interpretation of spectra can be difficult, and formation of unknown side-products can lead to misinterpretations of the data.

3.6 Conclusions and Future Work

A rapid screening methodology for determining chiral amine racemisation and epimerisation was developed. The method exploits ^{1}H NMR spectroscopy as a means to monitor location of deuterium incorporation, which is a result of catalysed imine formation and subsequent (deuterated) hydrogenation. Should this occur at the α-chiral centre, the amine is racemised through incorporation of deuterium. This novel methodology allows for circumvention of laborious syntheses and time-consuming analytical method development. Furthermore, the technique can be used with either enantiopure amine or racemic amine.

Investigation of (*S*)-1-cyclohexylethanamine provided evidence for amine dimerisation, and incorporation of deuterium into these dimers. The data suggests that the dimers, which cannot be formed without catalysed amine dehydrogenation, form at a rate faster than amine racemisation. The SCRAM catalysed racemisation of *N*-methyl-α-methylbenzylamine is already well-established,[75,100] and was supported by ^{1}H NMR data in this chapter. HRMS data did not reflect hydrogen-deuterium exchange when d_8-IPA or OD-IPA was used, suggesting further investigation, including validation using chiral GC, is required. Analysis using other selectively deuterated agents such as 2-propanol-1,1,1,3,3,3-d_6 and 2-propanol-2-d_1 is recommended to further understand this data. In contrast, investigation of 3-methylmorpholine demonstrates loss of ^{1}H NMR resolution, decrease in integration and presence of M+1 HRMS peaks. The reaction conducted without SCRAM catalyst confirmed impurity formation, however, there was no loss of ^{1}H NMR resolution, confirming loss of resolution was due to deuteration.

Through growth of new signals associated with the opposite diastereomer, investigation of ethyl-(2*R*,2*R*)-4-methylpiperidine-2-carboxylate **61** indicated epimerisation. New NMR signals were observed for the amine α-chiral centre and adjacent ester. Furthermore HRMS data indicated deuterated amine. Enantiomeric salts of **61** were investigated, and demonstrated the importance of their investigation using this rapid method. Addition of *p*-toluene sulfonic acid prevented amine epimerisation completely, whilst successful epimerisation was observed using acetic acid and benzoic acid. The findings suggest that lack of epimerisation with *p*-toluene sulfonic acid could be due to low pK_a, resulting in no free amine available for epimerisation. The tertiary amine analogue of **61** was investigated and showed no epimerisation, which may be due to steric hindrance of the *N*-Me group and or unfavourable formation of a high energy quaternary iminium. Investigation of a wide range of tertiary amines at higher temperatures is recommended to further expand study scope.

Proline isopropyl ester indicates racemisation due to the loss of resolution of ^{1}H NMR signals and HRMS data which shows deuterated amine. Appearance of new resolved signals adjacent to the α-chiral centre signals of the amine were not included in the analysis, demonstrating a limitation of the methodology. As ^{1}H NMR spectra become complicated, so does selection of NMR regions to include for analysis. Addition of benzoic acid reduces the number of resolved ^{1}H NMR signals which appear, suggesting its addition may reduce formation of protonated impurities.

Data for sertraline **26** epimerisation is consistent with previously reported data,[50] showing epimerisation as well as evidence for catalytic deactivation. Epimerisation of bromotetralin **80** is indicated through a mechanism consistent with hydrogenation rather than deuteration, and is confirmed through evolution of diastereomeric proton signals. Epimerisation is prevented upon addition of (*S*)-**25**, suggesting a weaker acid may need to be utilised for successful epimerisation, and illustrating the importance of investigating amine epimerisation with addition of chiral resolving acid.

4 Resolution-Racemisation-Recycle

4.1 Introduction

The maximum theoretical yield of a diastereomeric crystallisation of a racemic mixture is 50%. The yield can be increased by racemising the undesirable enantiomer and by resolving the resultant racemic solution through crystallisation, Figure 4.1.[121–125] This can be repeated iteratively by recycling the racemised mixture and resolving it in a process called R³, resolution-racemisation-recycle.[100] Crystallisation-Induced Diastereomeric Transformation (CIDT) can be used to form a pair of diastereomeric salts of differing solubilities. In-situ, catalysed or spontaneous epimerisation conditions, allow separation of the less soluble solid salt from the more soluble diastereomeric salt. In this way the yield can be increased beyond 50%.
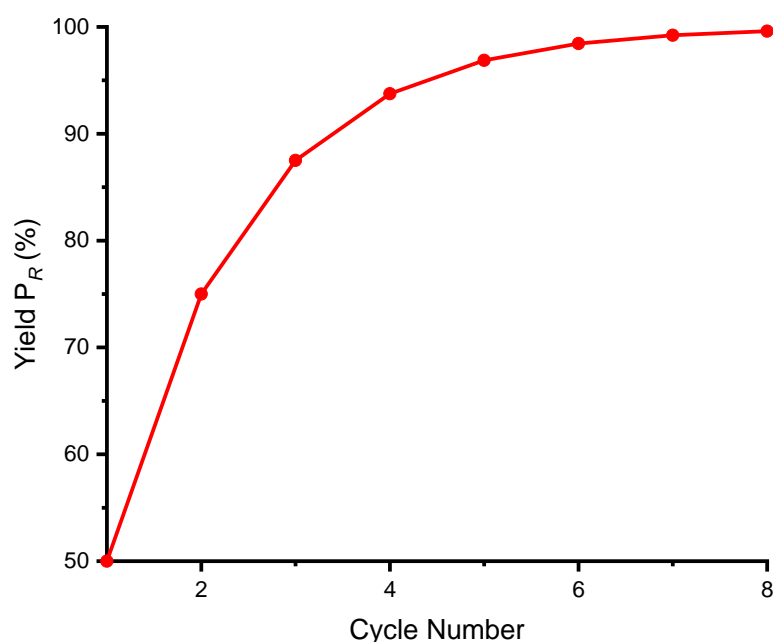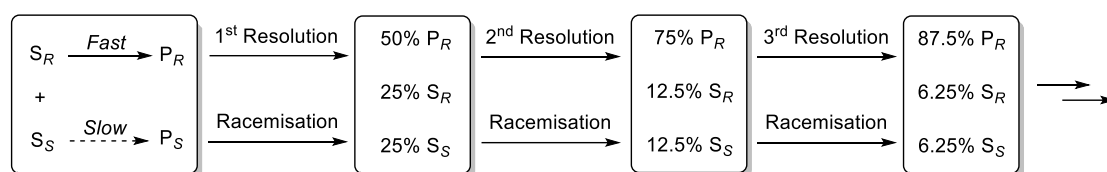
Figure 4.1. Depiction of iterative resolution and racemisation with subsequent effect on yield.[126]

Despite publications illustrating the use of CIDT in different processes, the incompatibility between resolution and racemisation conditions leads to an unfavourable compromise. Transition metal catalysed, or acid-base controlled, racemisation often requires harsh or high temperature conditions, whilst crystal resolution requires lower temperature to selectively dissolve one of the diastereomeric salts. The use of homogeneous catalysts leads to metal contamination of solid product, which can also affect the purity and yield of the desired salt.

As a result, the R^3 process was developed to spatially separate the resolution and racemisation. In this way, racemisation can occur under high temperature conditions, whilst the resolution can remain at room temperature conditions or below, promoting crystallisation. Combining these two processes through a continuous flow set-up allows for progress beyond traditional discrete single-step processes which require relatively more interaction from the user. Through catalyst immobilisation, the problem of metal contamination can be overcome in a way which allows for quicker and more facile recovery of catalyst.

In this chapter, the preparations and experiments which must be investigated prior to producing a successful R^3 process are discussed.

4.2 Experimental Set-Up

The R^3 process equipment consists of two continuous flow components, a diastereomeric crystallisation in continuously stirred tank reactor (CSTR) and racemisation in a tubular packed-bed reactor (PBR), Figure 4.2(a). A glass CSTR (50 cm^3) was used to carry out the diastereomeric crystallisation. The CSTR lid was made of polytetrafluoroethylene (PTFE) with two (3 mm I.D.) ports. Inside the CSTR, the chiral resolving acid (1.0 equiv.) was stirred with the racemic amine (1.0 equiv.) and the reaction solvent (20 cm^3), at ambient temperature. An in-line glass fritted filter (pore size 40 μm) was placed within the CSTR and was connected to the pump inlet using PTFE tubing to ensure only mother liquor (ML) was pumped out of the CSTR, while the solid remained in the CSTR. The pump outlet was connected to the packed-bed reactor (PBR) inlet, which consisted of a stainless steel HPLC column packed with immobilised SCRAM catalyst, which racemised or epimerised the circulating ML. The PBR was encapsulated in an aluminium block fitted with electrically controlled nickel heating cartridges. The PBR outlet was returned to the CSTR through one of the ports using PTFE tubing (1/16" O.D., 1/32" I.D.). The set-up included a priming union to expel any small particles or bubbles between reactions, and a back pressure regulator to modulate the upstream system pressure, Figure 4.2(b).
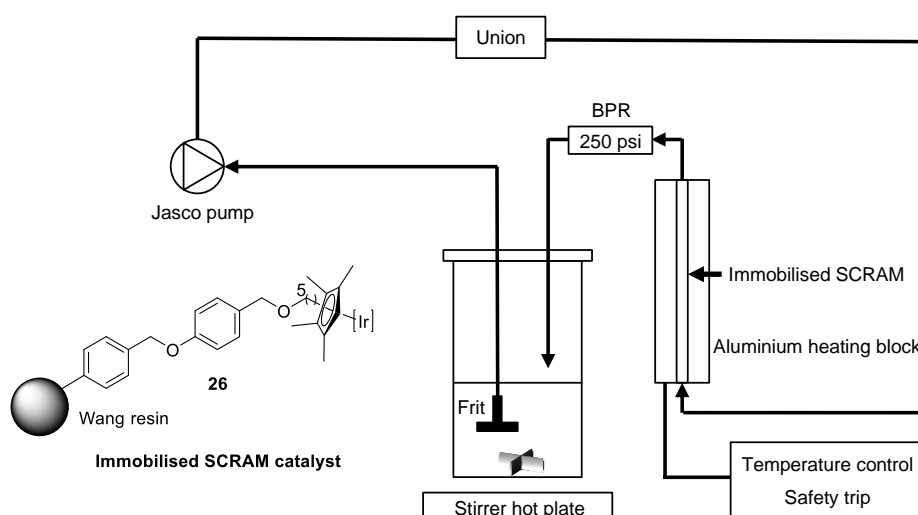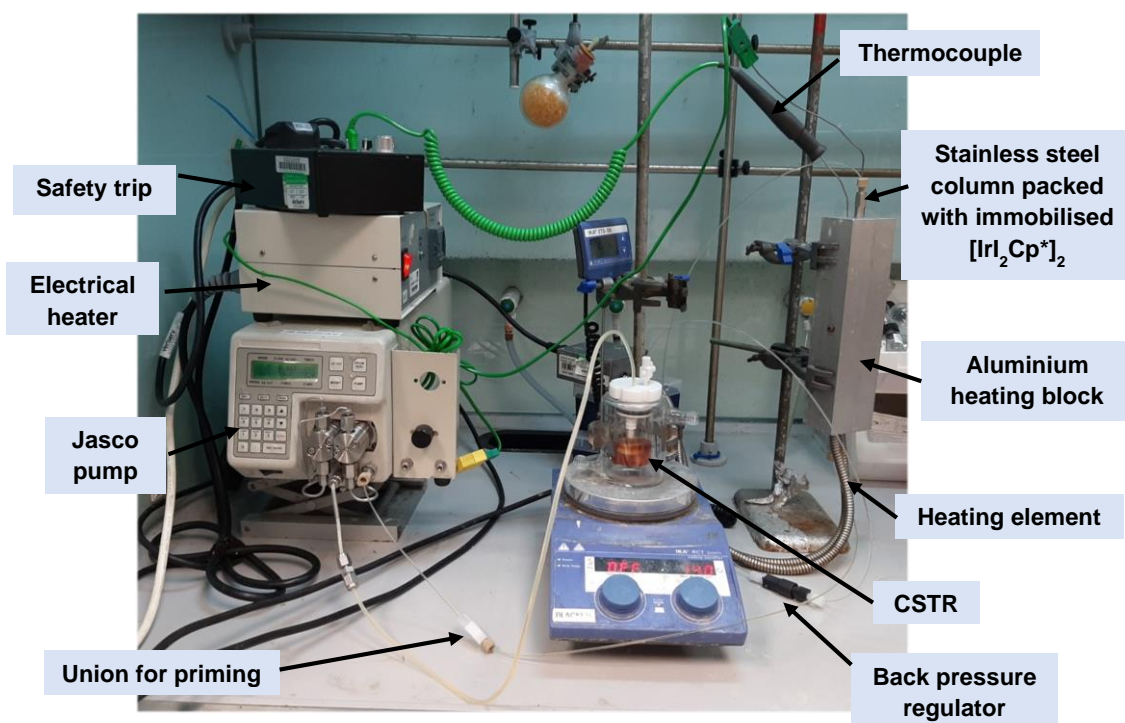
Figure 4.2. Experimental set-up for the R^3 process as shown by (a) photograph and (b) a schematic diagram

4.3 Sertraline Epimerisation

4.3.1 Introduction

Sertraline **26** was chosen as a substrate to investigate our R^3 process due to known resolution conditions and previous investigation of sertraline epimerisation using the SCRAM catalyst **13**. The original patent is reported to give sertraline in a 26% yield, which is environmentally and economically undesirable, as the remaining 74% isomers are treated as waste.

Blacker *et al.* have previously reported a semi-continuous process in the resolution racemisation and recycle of sertraline **26**. The selective crystallisation of (1*S*,4*S*)-**26** from a mixture of all 4 diastereomers was achieved in >99% ee and 90-98% de. Whilst the isolated yield of this isomer is 35%, the resolution yield is unimportant since the undesirable isomers can be recycled and transformed into the required (1*S*,4*S*)-diastereomer. A simplified scheme of this process is shown in Scheme 4.1 where (*S*)-Mandelic acid **25** is used as the resolving agent.[50]
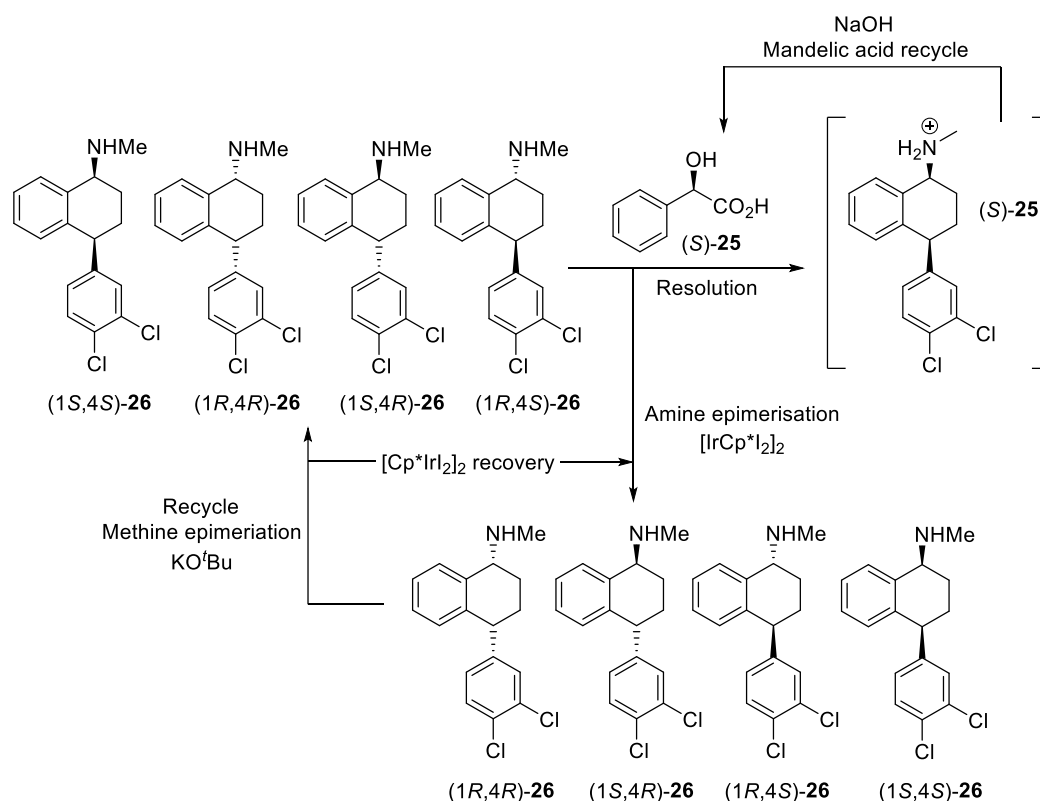
Scheme 4.1. Semi-continuous resolution-racemisation-recycle process of sertraline **26** reported by Blacker *et al.*[50]

As a result of this work, efforts were made to move towards a continuous epimerisation of the (1*S*)-centre of the amine. The original investigation into sertraline **26** epimerisation

using SCRAM catalyst **13** was conducted by Stirling *et al.*, Scheme 4.2, the results for which are summarised in Figure 4.3.[99]
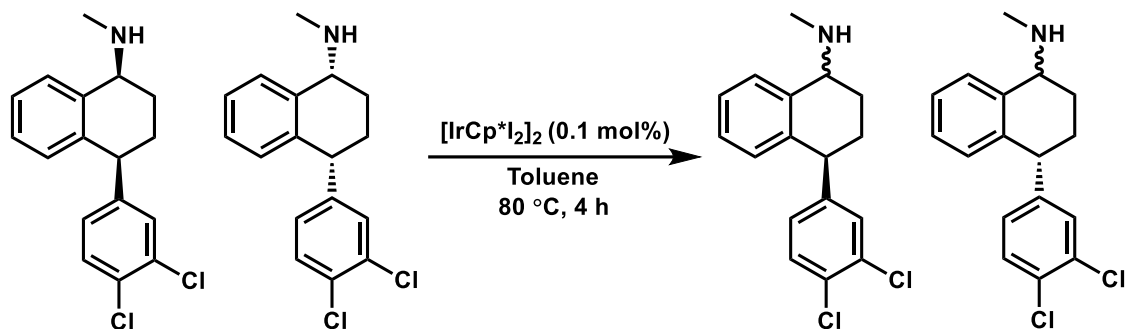
Scheme 4.2. Epimerisation of sertraline **26** and its diastereomer (0.5 M) using SCRAM catalyst **13** (0.1 mol%) in toluene at 80 °C. Original experiment conducted by Stirling *et al.*[99]
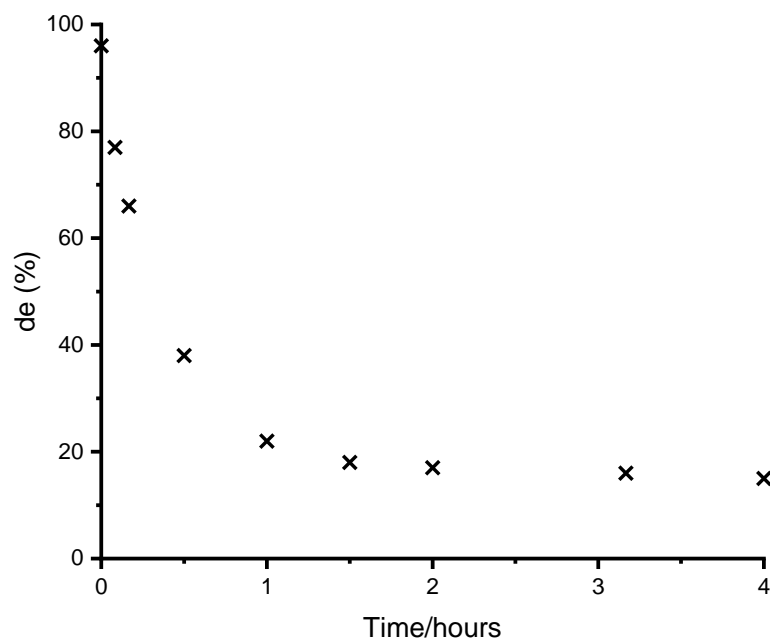
Figure 4.3. The result of sertraline **26** (0.5 M) epimerisation using SCRAM catalyst **13** (0.1 mol%) in toluene at 80 °C. Original experiment conducted by Stirling *et al.*[99]

After approximately 2 hours, the epimerisation of sertraline reaches a plateau at ~14% de. This was thought to be the thermodynamic equilibrium endpoint of the reaction, due to stereo-control of the 4S centre. However, this work has shown that methylamine, which is released from sertraline during the epimerisation, poisons the catalyst. To explain further, previous work in the group by Kwan *at al.* demonstrated that racemisation of the secondary amine (*S*)-*N*,α-Dimethylbenzylamine **33** by SCRAM

catalyst **13**, fails to completely racemise and only reaches a minimum of 6% ee, Figure 1.3.[75,98,100]

It was shown that spiking a partially racemised mixture with additional (*S*)-*N*,α-Dimethylbenzylamine **33** at around 24 hours, gave little further racemisation, showing the catalyst had been fully deactivated, Figure 4.4.
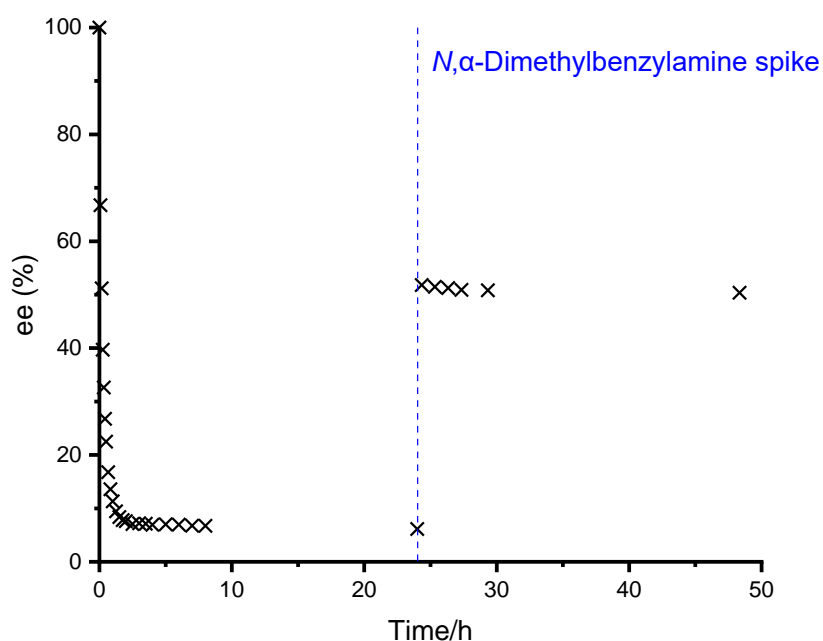
Figure 4.4. Racemisation of (*S*)-*N*,α-Dimethylbenzylamine **33** (0.5 M) with SCRAM catalyst **13** (0.2 mol%) at 105 ºC in toluene with an additional (*S*)-*N*,α-Dimethylbenzylamine **33** (0.5 M) spike at around 28.5 hours.

This was found to be due to hydrolysis of the intermediate imine **81** liberating methylamine which complexes irreversibly with the iridium centre to poison the catalyst, Scheme 4.3.
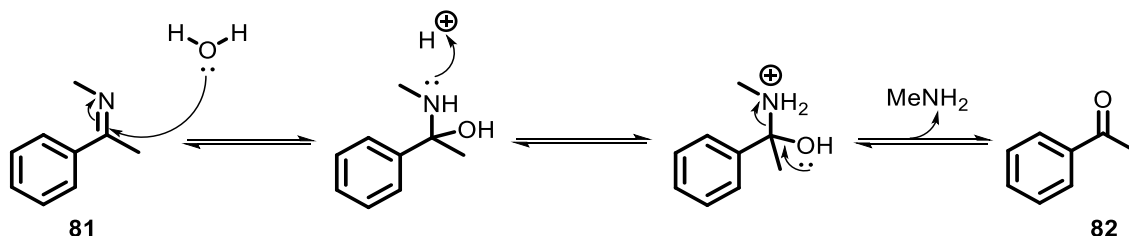
Scheme 4.3. Side reaction to show hydrolysis of **81** to form of acetophenone **82** and catalyst poison, methylamine

The results of further experiments with (S)-N,α-Dimethylbenzylamine **33** and SCRAM catalyst **13** (1 mol%) in THF at 60 ⁰C are shown in Figure 4.5.[75] Whilst one experiment was used as a control, the other two experiments were spiked with 2 and 20 equivalents of methylamine (with respect to iridium) respectively. Spiking with 2 equivalents of methylamine halted the reaction, but it resumed approximately an hour later and was able to reach 15% ee. This is in comparison to 20 equivalents of methylamine which seemed to stop the reaction completely at ~48% ee, Figure 4.5. The data suggests that presence of methylamine decreases the rate of **33** racemisation.
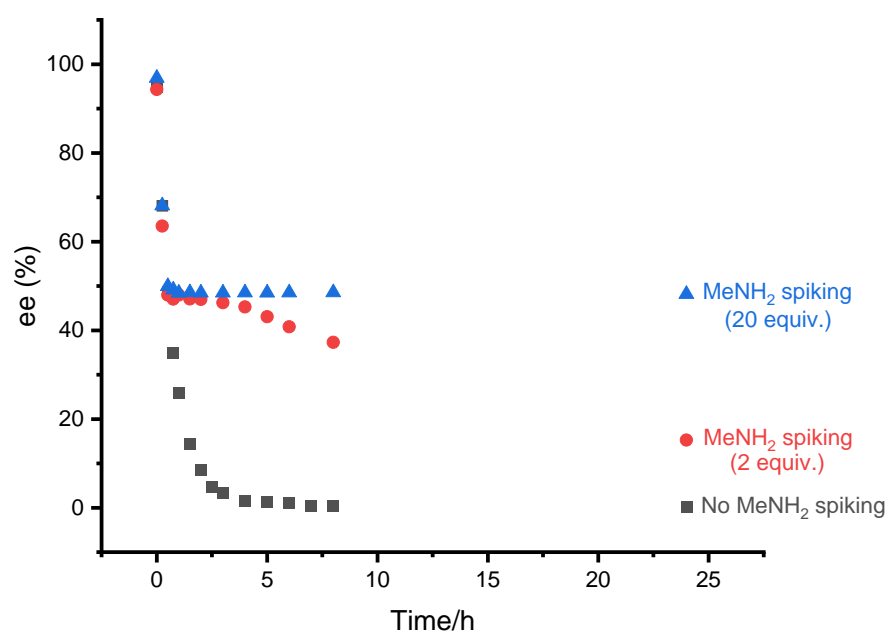
Figure 4.5. Racemisation of (S)-N,α-Dimethylbenzylamine **33** (0.5 M) at 60 ⁰C with SCRAM catalyst **13** (1 mol%) in THF with spiking of $MeNH_2$ (2 and 20 equiv. with respect to Ir) after 30 minutes.[75]

Since sertraline **26** also has an N-methyl group, the hypothesis tested was that the intermediate imine was hydrolysed to release methylamine, which deactivated the catalyst and prevented its complete epimerisation, Scheme 4.3.

A spiking experiment, similar to Figure 4.4, was performed. After the sertraline **26** (0.5 M) was epimerised using SCRAM catalyst **13** (1 mol%) in toluene at 80 ⁰C for 28.5 hours, an additional aliquot of sertraline **26** (0.5 M) was added. The epimerisation of sertraline **26** decreased in rate markedly from the original $t_{1/2}$ value of 0.25 hours to 88.5 hours, confirming catalyst poisoning, Figure 4.6.
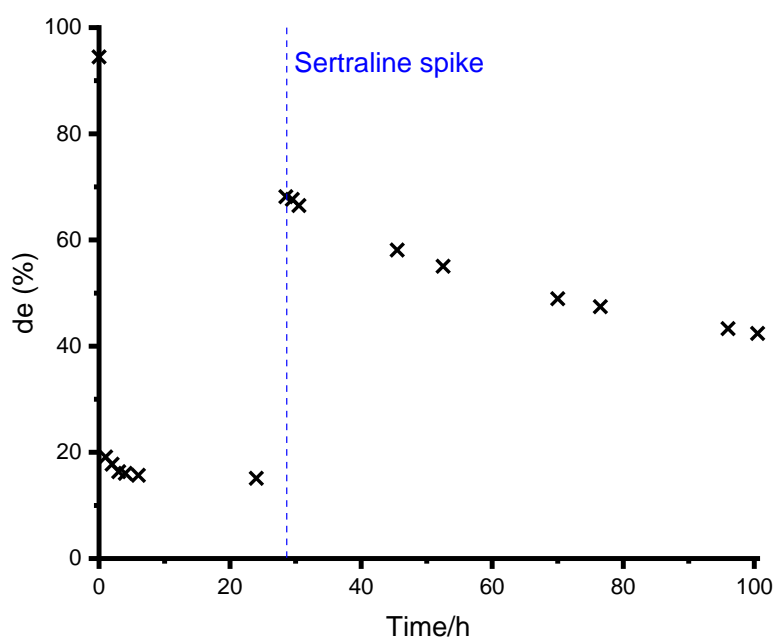
Figure 4.6. Epimerisation of sertraline **26** (0.5 M) with SCRAM catalyst **13** (1 mol%) at 80 °C in toluene with an additional sertraline **26** (0.5 M) spike at around 28.5 hours.

Additional evidence was found by GC when the ketone precursor **72** was spiked into the epimerisation mixture, Figure 4.7. This increased the intensity of the sertralone **72** peaks at 76.1 and 77.3 minutes showing that this was formed during the reaction and indicating methylamine must be formed as a by-product.
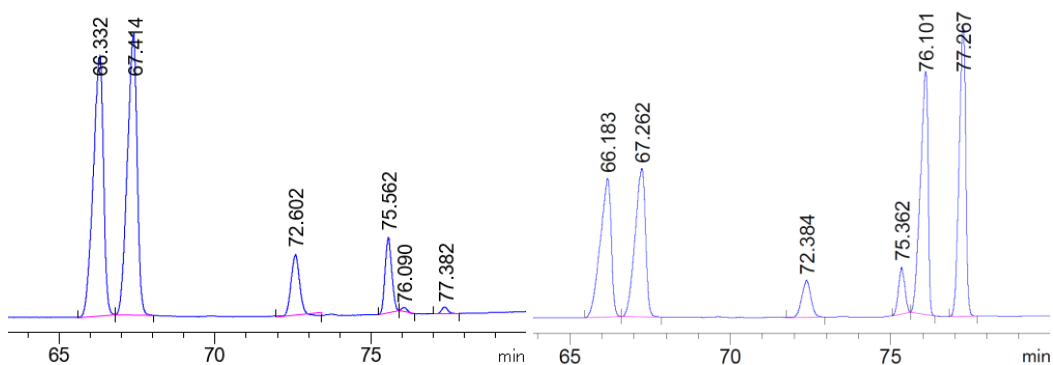
Figure 4.7. Left: chromatogram after sertraline (0.5 M) spike but before sertralone **72** spike. Right: After both sertraline (0.5M) and **72** spike. Numbers shown above peaks correspond to GC retention time in minutes.

The hydrolysis reaction requires water, and moisture levels in the batch reaction may differ from those in continuous flow used in the R^3 process. The equipment was set up as shown in Figure 4.8
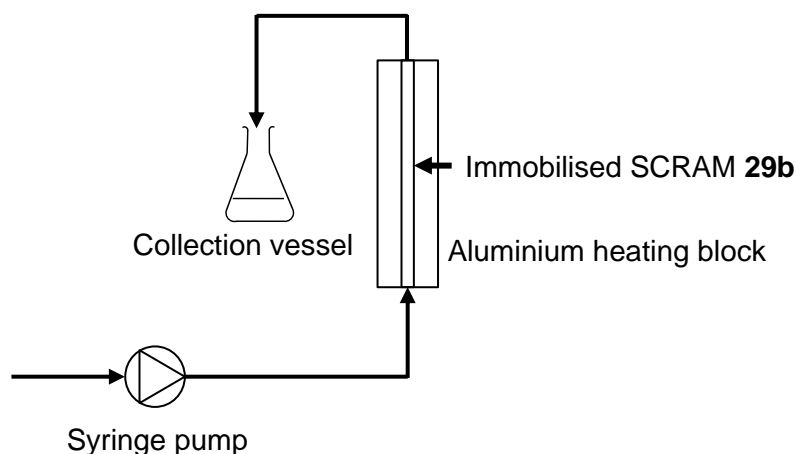
Figure 4.8. Reaction set-up for investigation of sertraline epimerisation under flow conditions using **29b** as epimerisation catalyst.

Based on similar experimental conditions to Stirling *et al.*, the results are shown in Figure 4.9, where the rate of catalyst deactivation is approximately 5% per reactor volume. Complete catalyst deactivation would be anticipated at around 10-12 reactor volumes. The rapid deactivation may be attributed to the catalyst to amine ratio of 12.7%, which indicates that at any one moment in time, there is a larger quantity of amine in the packed bed reactor than there is catalyst. This is in comparison to a similar experiment conducted with (*S*)-**33** where catalyst deactivation was 1.3% per reactor volume with a catalyst to amine ratio of 112%, Figure 4.10.[100]

Solvent:	Toluene
Temperature:	80 ºC
Residence time:	15 min
Catalyst:	125 uM
Substrate:	500 mM
Column volume:	1.97 mL
Flow rate:	0.131 mL/min
Total volume:	40 mL
Catalyst to resident amine ratio:	12.7%
Catalyst to total amine ratio:	5.0%
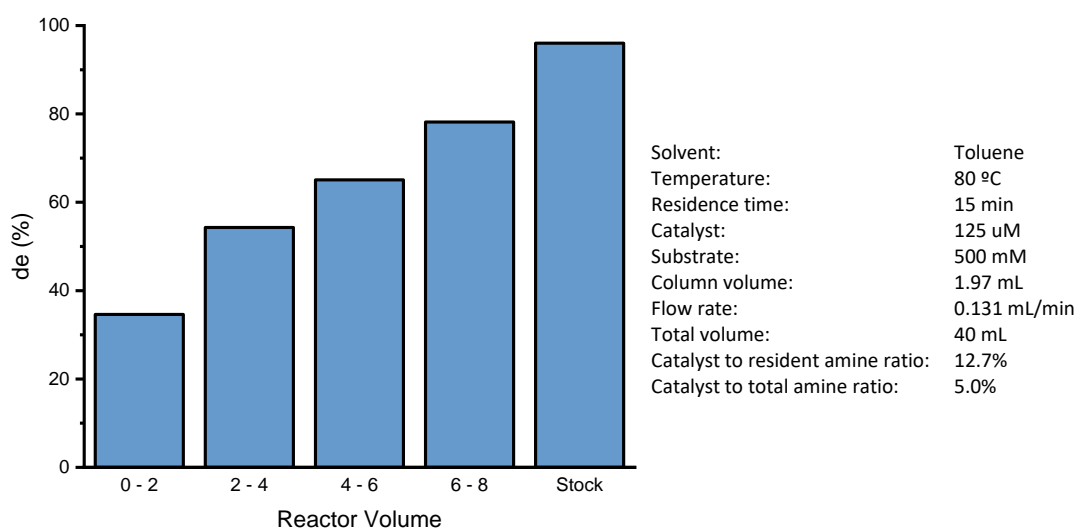
Figure 4.9. Deactivation study of immobilised SCRAM catalyst **29b** via flow epimerisation of sertraline **26**, where 0-2 is the average of the first two reactor volumes, 2-4 the average of the third and fourth and so forth.
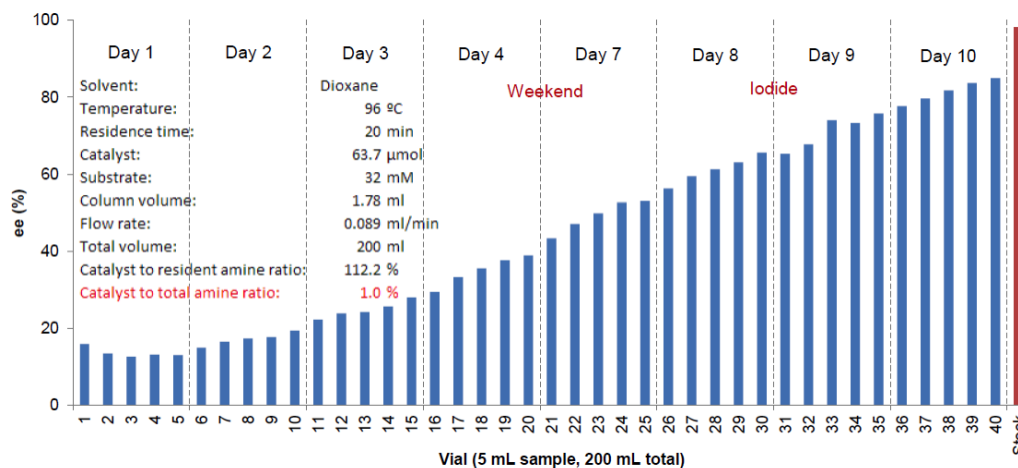
Figure 4.10. Deactivation study of immobilised SCRAM catalyst **29b** *via* flow racemisation of (*S*)-**33**.[100]

With this information in hand, the R³ process was tried with sertraline. In a CSTR, a mixture of sertraline **26** diastereomers of 2.6% de were dissolved in toluene and (*S*)-mandelic acid **25** (1 equiv.) was added as the resolving agent with biphenyl as the internal standard. The mixture was stirred at ambient temperature, and the ML was recirculated to the heated column containing immobilised SCRAM catalyst **29b**, and then deposited back into the CSTR. This was continued for 10 reactor volumes, equating to a process time of approximately 25 hours. The solid was isolated from the CSTR, dried, weighed and found to be 41% yield of 45% de, equating to 28% (1*S*,4*S*)-**26** and 9% of (1R,4S)-**26**. Whilst the result yield of solid is disappointing, the fact that ¾ of the solid is the desired diastereomer is encouraging. The reason for the low yield might be that the optimum concentration was not found, meaning that too much of the sertraline was still dissolved.

The changes in *cis* and *trans* diastereomer concentration, in both the mother liquor and solid phase, are shown in Figure 4.11. In the starting material, the *cis* and *trans* diastereomers are each 250 mM and upon addition of (*S*)-**25** the solid is 22% of the mass of 78% d.e. Over 7.5 reactor volumes the solid is 71% of the reaction mass of 12% d.e. The data suggests that the majority of the change occurs prior to the first reactor volume, which may be due to amine resolution or could be due to sertraline epimerisation which is fast.[99]
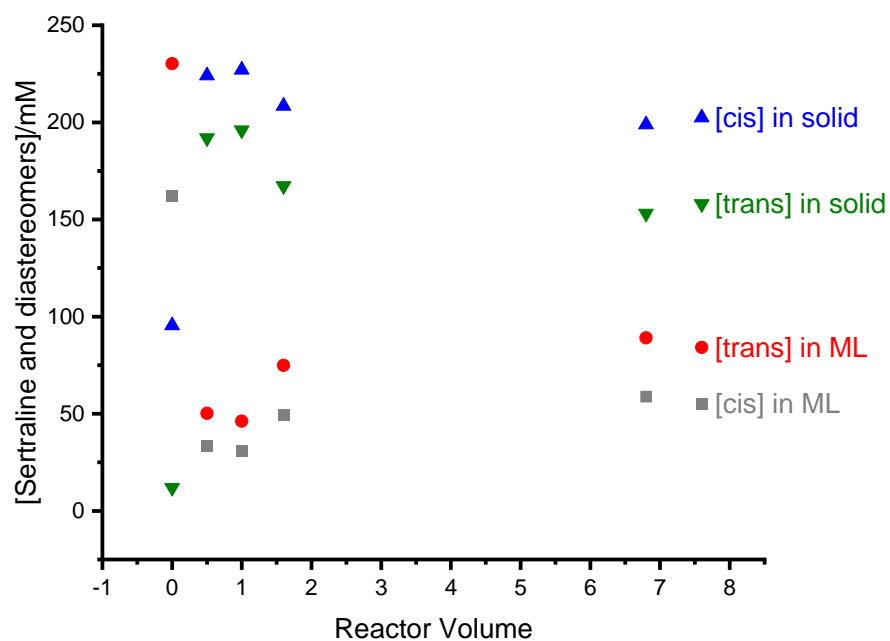
Figure 4.11. Concentration change of *cis* and *trans* diastereomers of sertraline **26** throughout the R³ process. Reactor volume 10 is omitted due to sampling error.

A problem encountered is that, despite best efforts taking a representative sample of solid and mother liquor, the sampling of solid during the reaction is challenging. Whilst it is relatively easy to sample consistent quantities of mother liquor which reflects the initial input of internal standard, this is quite the challenge for the solid. Despite trialling the reaction with the addition of an external standard, concentration values calculated from the initial quantity of amine placed into the system, and the concentration in the mother liquor proved to give more sensible values.

4.4 Dynamic resolution of ethyl-4-methylpiperidine-2-carboxylate in the R³ process

To test the dynamic resolution of ethyl-4-methylpiperidine-2-carboxylate **61** in the R³ process, the epimerisation of salt forms was investigated. Formation of a solid salt was successful upon the addition of benzoic acid, whereby the *cis* diastereomers of **61** crystallised out and the *trans* diastereomers remained soluble, Scheme 4.4.
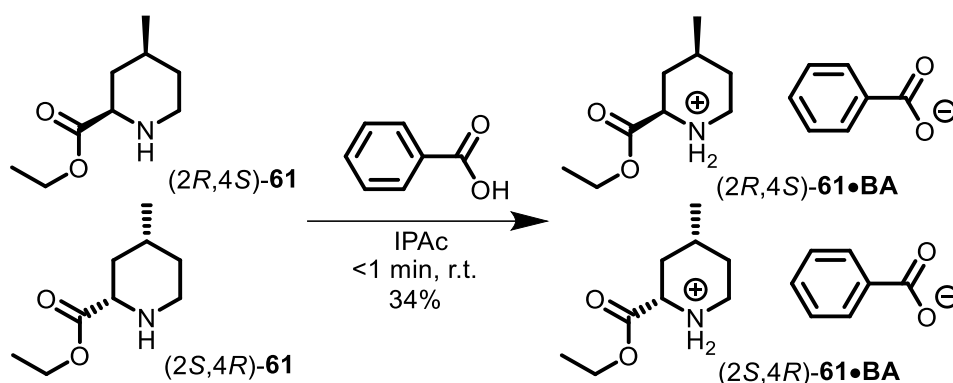
Scheme 4.4. The synthesis of *cis* **61**-benzoate from (2*R*,4*S*)-**61** and (2*S*,4*R*)-**61** in isopropyl acetate.

As the salt was formed in isopropyl acetate, the epimerisation of diastereomers of **61** were investigated using SCRAM catalyst **13** in isopropyl acetate. The conditions are shown are shown below in Table 4.1, with accompanying scheme.
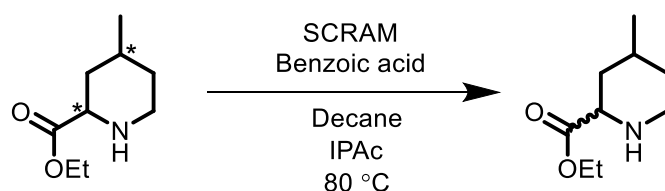
Entry [a]	Diastereomer [b]	13 (mol%)	66 (equiv.)	Time (h)	Amine (%)	de (%)
1	(2R,4R)	0.2	-	24	99%	76%
2	(2R,4R)	0.2	1	26	84%	-28%
3	(2R,4S), (2S,4R)	0.2	-	26	94%	88%
4	(2R,4S), (2S,4R)	0.2	1	22	98%	52%
5	(2R,4R)	0.2	1	30	97%	94%
6	(2R,4R)	1.0	1	32	85%	93%
7	(2R,4R)	1.0	1	26	82%	-35%
8	(2R,4R)	-	1	26	97%	-37%
9	(2R,4R)	1.0	1	26	91%	-28%
10	(2R,4R)	-	1	24	95%	-1%

Table 4.1. Epimerisation of ethyl-4-methylpiperidine-2-carboxylate **61** diastereomers under various conditions. [a] Entries **1-4**, **7,8** were run under batch conditions. Entries **5** and **6** were run under flow (R^3) conditions. Samples from entries **2,4-6**, **9**, **10** were worked up with $NaHCO_3$ (aq) prior to analysis. Entries **7,8** were worked up with NaOH (aq) prior to analysis [b] Entries **3** and **4** were run using an equimolar mixture of *cis* amine

Entries **1** and **3** were investigated under similar conditions, however, the former with *trans* (2R,4R)-**61** and the latter with an equimolar mixture of *cis* diastereomers (2R,4S)-**61** and (2S,4R)-**61**. The diastereomeric excess decreases only to 76% and 88% respectively, however, when each reaction was conducted with an equivalent of benzoic acid, the d.e. decreased to -28% and 52% respectively (entries **2** and **4**), suggesting that addition of benzoic acid increases the rate of epimerisation at the α-centre. The change in rate of epimerisation between these reactions is shown in Figure 4.12. Formation of the ammonium salt lowers the energy for epimerisation by changing the dehydrogenation/reduction equilibrium. It is apparent from the data that epimerisation of the *trans* diastereomer to the *cis* is favoured over that of the *cis* diastereomer to the *trans* diastereomer. This is likely because the *cis* diastereomer is able to exist with two

equatorial substituents rather than one equatorial and one axial in the case of the *trans* diastereomer, as shown in Figure 4.13.
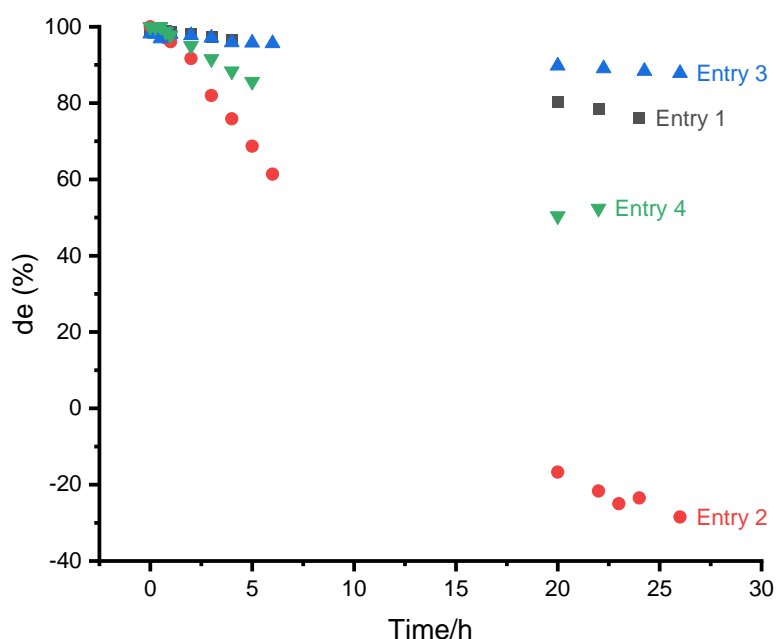
Figure 4.12. Change in diastereomeric excess of entries **1-4** in Table 4.1
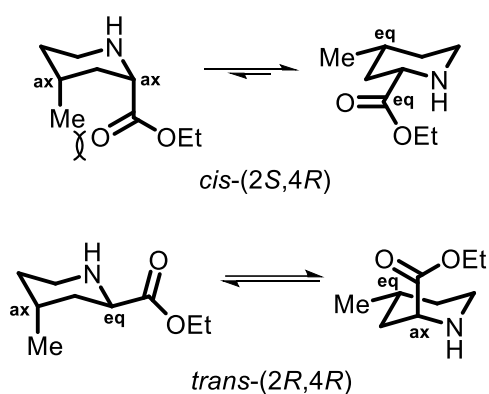
Figure 4.13. Equilibrium of chair conformers for (2*S*,4*R*)-**61** and (2*R*,4*R*)-**61** illustrating distribution of axial and equatorial positions of substituents.

With promising (2*R*,4*R*)-**61** epimerisation under batch conditions, the reaction was repeated under R³ process conditions, entries 5 and 6. The set-up used was the same as earlier, shown in Figure 4.2, however homogeneous **13**, rather than immobilised SCRAM catalyst **29b**, was employed, due the unavailability of the latter. Despite using 0.2 mol% and 1.0 mol% catalyst, the d.e. remained high at 94% and 93% after 30 and

32 hours of mother liquor circulation respectively. The amine **61** concentration remained at 97% in the former reaction, but dropped to 85% in the latter reaction, which may be attributable to ester hydrolysis. With this disappointing result the reaction with 1 mol% catalyst **13** was repeated under batch conditions (Table 4.1, entries 7 and 9) using NaOH $_{(aq)}$ or NaHCO$_3$ $_{(aq)}$ to work up the samples prior to analysis. As in entry 2, the d.e. was seen to decrease to -35% entry 7, and -28% entry 9. The lack of epimerisation in the continuous flow R^3 process entry may be due to the dispersion of homogenous catalyst **13** throughout the flow system meaning its effective concentration is much lower, whilst in the case of immobilised SCRAM **29b**, catalyst is concentrated within the heated column. The data suggests the use of immobilised catalyst is essential in developing an R^3 process.

A control reaction was run to confirm that impurity formation (Table 4.1, entries 6 and 7) was unrelated to benzoic acid **66** addition. A reaction without SCRAM catalyst **13** was conducted (Table 4.1, entry 8 and 10 with NaOH $_{(aq)}$ and NaHCO$_3$ $_{(aq)}$ work up respectively). With NaOH $_{(aq)}$ work-up the d.e. decreases to -37% whilst with NaHCO$_3$ $_{(aq)}$ it decreases to -1%. The difference is larger than when SCRAM catalyst **13** was used (Table 4.1, entries 7 and 9). The result suggests that the base may be epimerising the α-centre, Figure 4.14. Epimerisation occurs to a lesser extent when using the milder bicarbonate base, entry 10, but addition of SCRAM catalyst also causes epimerisation, entry 9.
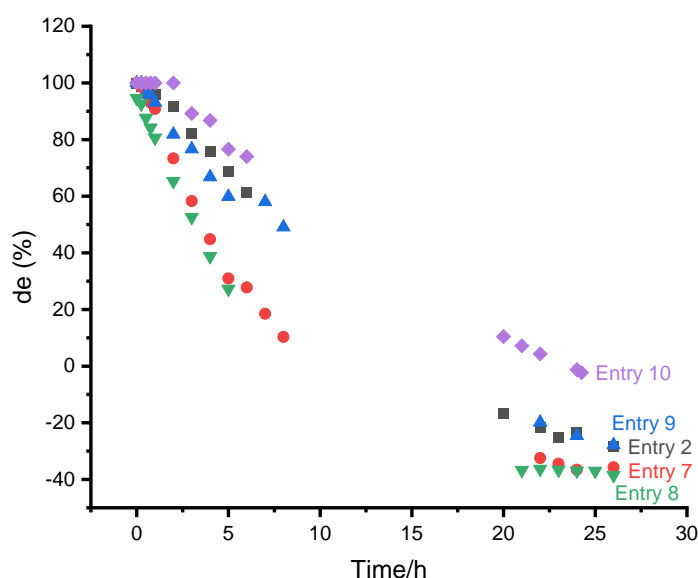
Figure 4.14. Change in diastereomeric excess of entries **2**, **7-10** in Table 4.1

Interestingly, each data set showed the appearance of a peak in the GC where the *cis-***61** was expected. Based on HRMS data, this was initially thought to be due to transesterification with isopropyl alcohol to form (2*R*,4*R*)-**83**, Scheme 4.5. However, spiking and observation of GC data indicated a new peak at 58.9 minutes, Figure 4.15. The data suggested the peak at 61.1 minutes may indeed be due to epimerisation of (2*R*,4*R*)-**61** in the absence of SCRAM catalyst.

Scheme 4.5. Initial proposition for the compound (2*R*,4*R*)-**83** formed upon (2*R*,4*R*)-**61** reaction with benzoic acid **66** in isopropyl acetate.

Figure 4.15. GC chromatogram showing elution times for trifluoroacetylated (2*R*,4*R*)-**61** (58.7 min), trifluoroacetylated (2*R*,4*R*)-**83** (58.9 min), trifluoroacetylated (2*R*,4*S*)-**61** (60.9 min), trifluoroacetylated (2*S*,4*R*)-**61** (61.1 min)

To investigate this hypothesis, benzoic acid was placed in a d_8-toluene solution containing *cis* diastereomers (2*R*, 4*S*)-**61** and (2*S*, 4*R*)-**61** (reaction a), and a similar solution containing *trans* (2*R*, 4*R*)-**61** (reaction b). An NMR was taken of each solution prior to heating (110 ºC) for 4 hours, and another was taken after this period of time. Comparing each NMR prior to and after heating, it was apparent that new signals had appeared in each 4 hour NMR, Figure 4.16. Each 4 hour NMR indicated signals which were present in the opposite reaction 0 hour NMR, and were comparable in chemical shift and multiplicity. The new peaks in reaction a are indicated by green circles, Figure 4.16a, and can be compared with the analogous green circles in the opposite reaction b, Figure 4.16b. Similarly, reaction b has new peaks indicated by yellow squares, Figure 4.16b, which can be compared to the yellow squares in reaction a, Figure 4.16a.

Figure 4.16. Reaction of (a) *cis* diastereomers (2*R*,4*S*)-**61**, (2*S*,4*R*)-**61** and (b) (2*R*,4*R*)-**61** *trans* diastereomer with benzoic acid **66** in d⁸-toluene **48** at 110 °C for a total of 4 hours. In each 4 hour spectrum, green circles/ orange squares represent new signals which can be compared to the same corresponding shape in the 0 hour spectrum of the opposite reaction. TK(TMS)S is internal standard tetrakis(trimethylsilyl)silane.

Due to the ability of *trans*-**61** to epimerise well in the presence of benzoic acid and *cis*-**61** ability to form solid with benzoic acid **66** at standard temperature conditions, a successful CIDT reaction was conducted whereby (2*R*,4*R*)-**61** was epimerised with **66** to (2*S*,4*R*)-**61**, which was able to crystallise out to form pure solid crystals. The *cis* arrangement of these atoms were confirmed through single crystal x-ray diffraction.

The mechanism by which this epimerisation was able to take place is unclear, however, a form of hydrogen abstraction to form enol **84** or α,β-unsaturated ester **85** followed by reincorporation of hydrogen, resulting in epimerisation was proposed. This is summarised in Scheme 4.6.
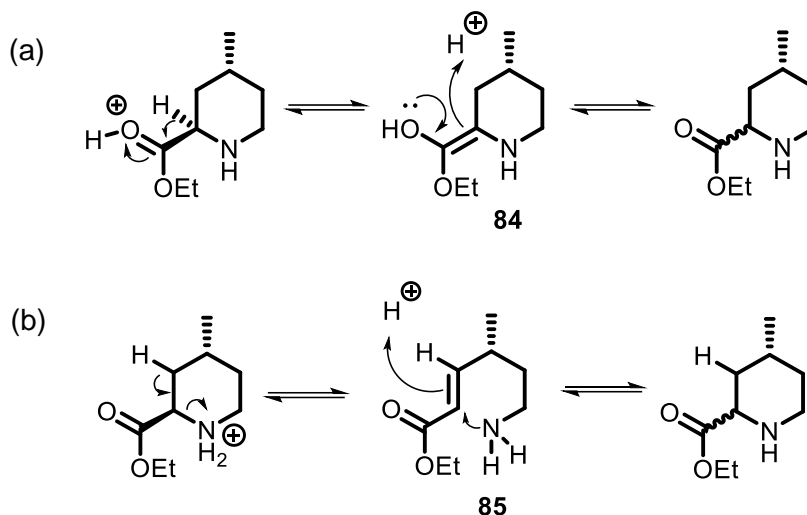
Scheme 4.6. Proposed mechanisms for epimerisation at the 2*R* centre of **61** involving the formation of (a) an enol **84** or (b) an α,β-unsaturated ester **85** followed by epimerisation

4.5 Conclusions and Future Work

To find conditions most suited for the R^3 process, both resolution and racemisation must be investigated separately. The possibility of racemisation was investigated using hydrogen-deuterium exchange experiments as described in Chapter 3. In addition to this, racemisation must also be investigated under conditions intended for amine resolution to ensure compatibility of solvent and resolving acid. Finding ideal conditions can be time consuming, however, once ideal conditions are found it is possible to increase yield to a theoretical maximum of 100% depending on racemisation conditions.

The investigation into sertraline **26** epimerisation allowed study into the previous observation that it fails to reach 0% d.e. and instead reaches a minimum of ~14% d.e., thought to be the thermodynamic equilibrium endpoint. Through spiking experiments, like those conducted by Kwan *et al.*, our investigation showed that SCRAM **13** catalysed sertraline epimerisation failed to reach 0% d.e. due to catalytic deactivation. The release of methylamine by hydrolysis of the imine intermediate, acts as catalyst poison. This was supported by GC data which indicated the formation of the hydrolysis product, sertralone, the formation of which is accompanied by methylamine. In continuous flow,

the immobilised catalyst **29b** was found to deactivate by approximately 5.4% per reactor volume, suggesting that complete deactivation would take only 10 reactor volumes.

Translating this approach to our R^3 process, sertraline and impurities formed alongside its synthesis were placed into the R^3 system. The initial diastereomeric excess of 2.6% increased to approximately 45% de with a solid yield of 41% (27% of which was attributed to (1*S*,4*S*)-**26**) showing the ability of the R^3 process to improve the level of diastereomeric purity under unoptimised conditions. To progress further, the solubility of each mandelate diastereomer in the reaction solvent should be investigated. In this way the optimal concentration would provide conditions where (1*S*,4*S*)-**26** is insoluble and the other diastereomers soluble.

In the case of ethyl-4-methylpiperidine-2-carboxylate **61**, enantiomeric resolution conditions were established, whereby the *cis* diastereomers of a benzoate salt were able to crystallise, whilst *trans*-**61** remained in the isopropyl acetate solution. Investigation found that *cis*-**61** and *trans*-**61** diastereomeric benzoate salts could be epimerised. Epimerisation of *trans*-**61** to *cis*-**61** was more favourable than the opposite reaction, likely due to the number of stable equatorial substituents on the *cis* diastereomer relative to the *trans* diastereomer.

Upon investigation of the reaction in absence of SCRAM **13** catalyst, it became apparent that epimerisation can occur without the catalyst. Rapid NMR studies confirmed this observation. It is unclear how this is occurring, however some mechanisms have been proposed.

To conclude this work, a CIDT reaction was conducted whereby (2*R*,4*R*)-**61** diastereomer was epimerised with benzoic acid under reflux conditions, and the resultant (2*S*,4*R*)-**61** diastereomer was left to crystallise as the benzoate salt. Despite the low yield of this reaction (3.2%), future investigation of this reaction under R^3 conditions with immobilised SCRAM catalyst has the potential to increase the yield.

Due to the relative difficulty in synthesising the (2*R*,4*R*)-**61**, future work should investigate epimerisation of the *cis* diastereomer to allow crystallisation of the *trans* diastereomer. Given that literature data suggests the *trans* diastereomer is able to crystallise with tartaric acid in butanone, it may be useful to investigate similar conditions as a starting point.[127] It would be interesting to see whether tartaric acid is able to epimerise the amine in the same way as benzoic acid, though previous use of diacids to resolve amines has highlighted unusual and complex metastable crystal forms.[100]

5 Experimental

Unless otherwise stated, all chemicals were obtained from Fluorochem, Alfa Aesar, Fischer Scientific or Sigma-Aldrich, and were subsequently used without further purification. The immobilised SCRAM **29b** was obtained from Yorkshire Process Technology and was also used without further purification. Nuclear Magnetic Resonance spectra were recorded on Bruker 500 UltraShield Spectrometer at 500 MHz for 1H NMR and 126 MHz for 13C NMR, Bruker ADVANCE III HD-400 Spectrometer at 400 HMz for 1H NMR and 100 MHz for 13C NMR, or Bruker DX300 Spectrometer at 300 MHz for 1H NMR and 75 MHz for 13C NMR. Infrared (IR) spectra were recorded on a Perkin Elmer Spectrum One Fourier Transform-Infra Red (FT-IR) spectrometer or on a Bruker Alpha Platinum Attenuated Total Reflection (ATR). Vibrational frequencies are reported in wavenumbers, cm-1. Melting points were determined using Reichert Hot Stage apparatus or using Differential Scanning Calorimetry (DSC) Q20, TA Instruments (0°C to 300°C, Heating rate / 10°C per minute, Inert gas / Nitrogen, Gas flow / 50mL per minute). High-resolution mass spectrometry (HRMS) was carried out using a Bruker MaXis Impact Spectrometer with electrospray ionisation (ESI) in positive mode. Cationic and anionic fragments were assigned as X and Y respectively for the MS peaks of amine salts. Optical rotation ([α]D) was measured using Polartronic H532 at 589 nm and was calculated using the following equation

$$[\alpha]_D^T = \frac{Rotation \times 100}{c \times l}$$

Where T = temperature; c = concentration of the sample in grams per 100 mL; l = path length which refers to the length of the cell in dm (1 dm in this case).

Single crystal structures were obtained at 120 K on an Agilent SuperNova diffractometer equipped with an Atlas CCD detector and connected to an Oxford Cryostream low temperature device using mirror monochromated Cu Kα radiation (λ = 1.54184 Å) from a Microfocus X-ray source. The structure was solved by intrinsic phasing SHELXT174 and refined by a full matrix least squares technique based on F2 using SHELXL2014.175

5.1 NMR Abbreviations

Abbreviations: br, broad; m, multiplet; s, singlet; d, doublet; t, triplet, q, quartet, qu, quintet; sept, septet; m [t, dd, q, tt, sext]. Notation in brackets describes overall appearance of the multiplet (e.g. m[d] represents a multiplet with the appearance of a doublet, m[dd, dq] represents a multiplet with the appearance of a structurally different doublet doublet and doublet quartet signal).

5.2 Synthesis of starting materials

5.2.1 Ethyl (2R,4R)-4-methylpiperidine-2-carboxylate[128]
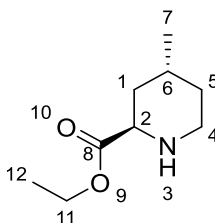
(2*R*,4*R*)-4-Methyl-2-piperidine-carboxylic acid (2 g, 11.7 mmol) was stirred with anhydrous ethanol (100 cm^3) under nitrogen conditions for 24 hours. The subsequent solution was concentrated and the oily yellow residue was suspended in aqueous NaHCO$_3$ (100 cm^3) with effervescence. The solution was extracted with CHCl$_3$ (100 cm^3 x 4), dried (MgSO$_4$) and concentrated in *vacuo* and dried under high vacuum. The title compound was isolated (2.20 g, 12.8 mmol, 91%) as a yellow oil. **[α]$_D^{20}$** = -19.8° (*c* 5, ethanol); **^{1}H NMR (400 MHz, CDCl$_3$)**; δ 4.20 (2 H, q, *J* 7.2, H-11), 3.65 (1 H, t, *J* 4.5, H-2), 2.96 – 2.76 (2 H, m, H-4), 2.22 – 1.97 (2 H, m, H-1 and NH), 1.68 – 1.50 (1 H, m, H-5 and H-6), 1.50 – 1.38 (1 H, m, H-1), 1.30 (1 H, t, *J* 7.2, H-12), 1.25 – 1.11 (1 H, m, H-5), 0.96 (1 H, d, *J* 6.4, H-7); **^{13}C{^{1}H} NMR (100 MHz, CDCl$_3$);** δ 174.40 (C-8), 60.67 (C-11), 55.56 (C-2), 42.28 (C-4), 34.96 (C-1), 33.72 (C-5), 27.63 (C-6), 21.58 (C-7), 14.33 (C-12); **v_{max}/cm^{-1}**; 2952, 2919, 2871, 1729, 1457, 1370, 1204; **m/z (ES)**; (Found MH$^+$, 172.1334. C$_9$H$_{17}$NO$_2$ requires MH$^+$, 172.1338)

Spectroscopic data was consistent with literature values.[129]

5.2.2 Ethyl 4-methylpyridine-2-carboxylate[128]
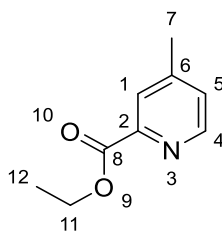
Under nitrogen conditions, 4-methyl-pyridine-2-carboxylic acid (19.90 g, 145.1 mmol) was stirred with dry ethanol (200 cm^3). Thionyl chloride (32 cm^3) was slowly syringed in and the mixture was stirred under reflux overnight. The mixture was concentrated in vacuo and NaHCO$_3$ solution (250 cm^3) was added to neutralise the mixture and DCM (250 cm^3) was used for extraction. The DCM solution was concentrated and the product was placed under high vacuum. The title compound was isolated (14.8 g, 89.3 mmol, 62%) as a yellow oil. **^{1}H NMR (400 MHz, CDCl$_3$)**; δ 8.61 (1 H, d, J 5.0, H-4), 7.97 (1 H, d, J 1.4, H-1), 7.29 (1 H, d, J 5.0, H-5), 4.48 (2 H, q, J 7.1, H-11), 2.44 (3 H, s, H-7), 1.45 (3 H, t, J 7.1, H-12); **^{13}C{^{1}H} NMR (100 MHz, CDCl$_3$)**; δ 165.52 (C-8), 149.64 (C-4), 148.41 (C-6), 148.12 (C-2), 127.65 (C-5), 126.02 (C-1), 61.89 (C-11), 21.03 (C-7), 14.35 (C-12); **v$_{max}$/cm^{-1}**; 2936, 1739, 1714, 1601, 1366, 1203; **m/z (ES)**; (Found MNa$^+$, 188.0680. C$_9$H$_{17}$NO$_2$ requires MNa$^+$, 188.0687)

5.2.3 *Cis*-ethyl-4-methylpiperidine-2-carboxylate[130]
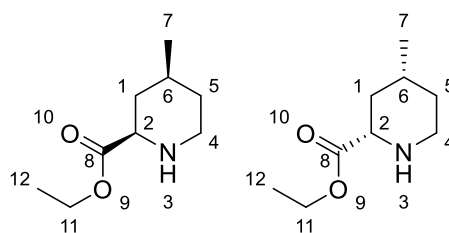
Ethyl-4-methylpyridine-2-carboxylate (5 g, 30.3 mmol), methane sulfonic acid (2 cm^3) and dry ethanol (10 cm^3) were placed together and the reaction mixture was stirred for 30 minutes whilst a hydrogen balloon was collected. Prior to this, the reaction vessel was evacuated and subsequently filled with nitrogen a total of three times. PtO$_2$ (489 mg, 2.15 mmol) was placed in a similarly evacuated vessel and the ethanol solution was syringed in, with an additional amount of dry ethanol (30 cm^3). The hydrogen gas balloon was attached with a reverse bubbler to confirm hydrogen uptake. The reaction was stirred for a period of around 4 days, with regular replacement of the hydrogen balloon.

PtO$_2$ was separated through reduced pressure filtration using celite and the subsequent reaction mixture was concentrated in *vacuo*. Chloroform (40 cm^3) and NaHCO$_3$ solution (40 cm^3) were added and the mixture was stirred to allow effervescence. The mixture was extracted with additional chloroform (2 x 40 cm^3). The organic layer was dried with MgSO$_4$ and the solution was concentrated in *vacuo*. The <u>title compound</u> was isolated (4.25 g, 24.8 mmol, 82%) as a yellow liquid. **^{1}H NMR (400 MHz, CDCl$_3$)**; 4.16 (2 H, q, *J* 7.1, H-11), 3.28 (1 H, dd, *J* 11.7, 2.5, H-2), 3.13 (1 H, ddd, *J* 12.4, 4.3, 2.5, H-4), 2.61 (1 H, td, *J* 12.4, 2.5, H-4), 2.06 – 1.91 (1 H, m, H-1), 1.80 (1 H, br s, NH), 1.63 – 1.39 (2 H, m, H-5 and H-6), 1.25 (3 H, t, *J* 7.1, H-12), 1.11 – 0.96 (2 H, m, H-1 and H-5), 0.93 (3 H, d, *J* 6.4, H-7); **^{13}C{^{1}H} NMR (100 MHz, CDCl$_3$)**; δ 173.44 (C-8), 60.72 (C-11), 59.09 (C-2), 45.90 (C-4), 38.01 (C-1), 34.61 (C-5), 31.29 (C-6), 22.40 (C-7), 14.20 (C-12); **v_{max}/cm^{-1}**; 2950, 2914, 2870, 2798, 1734, 1446, 1242; **m/z (ES)**; (Found MH$^+$, 172.1331. C$_9$H$_{17}$NO$_2$ requires MH$^+$, 172.1338)

Spectroscopic data was consistent with literature values.[131]

5.2.4 Ethyl (2*R*,4*R*)-1,4-dimethylpiperidine-2-carboxylate[128]
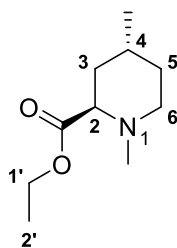
(2*R*,4*R*)-1,4-dimethyl-2-piperidine-carboxylic acid (2 g, 12.7 mmol) was stirred with anhydrous ethanol (100 cm^3) under nitrogen conditions for 16 hours. The subsequent solution was concentrated and the residue was suspended in aqueous NaHCO$_3$ (100 cm^3) with effervescence. The solution was extracted with CHCl$_3$ (100 cm^3 x 3), dried (MgSO$_4$) and concentrated in *vacuo* and dried under high vacuum. The <u>title compound</u> was isolated (0.80 g, 4.32 mmmol, 40%) as a yellow oil. **[α]$_D^{20}$** = 32.9° (*c* 0.1, ethanol); **^{1}H NMR (500 MHz, CDCl$_3$)**; δ 4.15 (2 H, q, *J* 7.1, H-1'), 3.33 (1 H, t, *J* 4.9, H-2), 2.98 (1 H, ddd, *J* 3.3, 10.0, 11.6, H-6), 2.49 (1 H, dt, *J* 4.9, 11.6, H-6), 2.40 (3 H, s, *N*-Me), 1.88 (1 H, m[dd, dq], *J* 1.6, 7.0, 13.2, H-3), 1.68 (2 H, m, H-4, H-5), 1.49 (1 H, dq, *J* 4.9, 13.2, H-3), 1.26 (3 H, t, *J* 7.1,H-2'), 1.19 – 1.34 (1 H, m, H-5) 0.91 (3 H, d, *J* 7.0, 4-Me); **^{13}C{^{1}H} NMR (125 MHz, CDCl$_3$)**; δ 173.36 (C=O), 62.12 (C-2'), 59.98 (C-2), 49.14 (C-6), 43.42 (*N*-Me), 36.16 (C-3), 33.11 (C-5), 25.46 (C-4), 20.72 (4-Me), 14.35 (C-1'); **v$_{max}$/cm^{-1}**; 2951, 2952, 2871, 2848, 2813, 1731, 1446, 1377, 1348, 1295, 1282, 1260, 1235, 1219; **m/z (ES)**; (Found MH$^+$, 186.1489. C$_{10}$H$_{19}$NO$_2$ requires MH$^+$, 186.1489)

138

5.2.5 Sertraline[112]
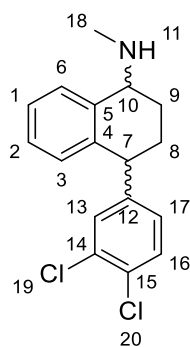
Under nitrogen, $MeNH_2$ (2 M) in tetrahydrofuran (800 cm^3) was cooled to 0 – 5 ºC. Sertralone (50 g, 0.172 mmol) was added to the solution and $TiCl_4$ (10 cm^3) was added with stirring. Misty fumes of HCl could be seen. The reaction was stirred under nitrogen for 17 hours. A sintered funnel was used to remove the solid in the reaction and the solids were washed with THF to give an imine containing solution of THF. Additional THF was added to the mixture to maintain a volume of 600 cm^3. A vessel containing Pd/C (5 g) was evacuated and purged with nitrogen several times and the reaction mixture was filtered in. A hydrogen balloon with a reverse bubbler confirmed hydrogen uptake of the reaction mixture. TLC (1% TEA, 1:1 Petrol:DCM) confirmed reaction completion. The mixture was concentrated *in vacuo* and placed under high vacuum. HCl (2 M) in ethanol was added to the residue and sertraline hydrochloride precipitated as a white solid. It was washed with ethanol and or petroleum ether. The hydrochloride salt was converted to its freebase, the subsequent organic layer dried ($MgSO_4$) and concentrated *in vacuo*. A yellow oil was obtained which later solidified. The <u>title compound</u> was isolated (11.1 g, 36.4 mmol, 21%) as a yellow solid. **[α]$_D^{20}$** = 54.5° (*c* 0.1, ethanol); M.p. = 60.46 ºC {lit.[132] m.p. 65.58 - 67.25 ºC}; **^{1}H NMR (500 MHz, CDCl$_3$)**; δ 7.36 (2 H, m, H-6, H-13), 7.24 (1 H, d, *J* 2.1, H-16), 7.20 (1 H, t, *J* 7.2, H-1), 7.10 (1 H, td, *J* 7.4, 1.4, H-2), 6.97 (1 H, dd, *J* 2.0, 8.2, H-17), 6.81 (1 H, d, *J* 7.8, H-3), 3.98 (1 H, dd, *J* 5.4, 9.1, H-10), 3.74 (1 H, at, *J* 4.0, H-7), 2.54 (3 H, s, H-18), 2.04 (3 H, m, H-8 & H-9), 1.82 (1 H, td, *J* 4.4, 11.0, H-9); **^{13}C{^{1}H} NMR (125 MHz, CDCl$_3$)**; δ 147.64 (C-12), 139.60 (C-5) 138.84 (C-4), 132.44 (C-14), 130.86 (C-6), 130.45 (C-17), 130.22 (C-15), 129.96 (C-16), 129.34 (C-13), 128.42 (C-3), 127.40 (C-2), 126.76 (C-1), 57.46 (C-7), 45.52 (C-10), 34.46 (C-18), 28.62 (C-8), 25.82 (C-9); **v_{max}/cm^{-1}**; 3061, 3017, 2975, 2938, 2854, 2784, 2104, 1925, 1822, 1684, 1662, 1589, 1559, 1487, 1470, 1435, 1394, 1342, 1322, 1263; **m/z (ES)**; (Found MH$^+$, 306.0807. $C_{17}H_{17}Cl_2N$ requires MH$^+$, 306.0811)

5.2.6 Ethyl-4-methylpiperidine-2-carboxylate *p*-toluenesulfonate
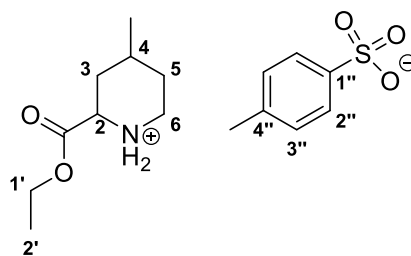
A racemic mixture of ethyl (2*R*,4*S*)-1,4-dimethylpiperidine-2-carboxylate and ethyl (2*S*,4*R*)-1,4-dimethylpiperidine-2-carboxylate (50.0 mg, 0.292 mmol) was added to isopropyl acetate (1.5 cm^3). Subsequently, an aliquot of *p*-toluene sulfonic acid (55.2 mg, 0.292 mmol) was added. Solid precipitate of salt formed within minutes and was isolated using reduced pressure filtration and was washed with petroleum ether. The <u>title compound</u> was isolated (71 mg, 0.206 mmol, 70%) as a white powdery solid. M.p. = 156.74 °C; **^{1}H NMR (500 MHz, CDCl$_3$)**; δ 7.71 (2 H, d, *J* 8.1, H-2''), 7.15 (2 H, d, *J* 8.1, H-3''), 4.17 (2 H, qd, *J* 7.1, 5.3, H-1'), 3.83 (1 H, dd, *J* 3.0, 13.0, H-2), 3.69 (1 H, qd, *J* 1.9, 13.0, H-6), 3.02 (1 H, dt, *J* 3.0, 19.5, H-6), 2.35 (1 H, s, H-4''), 2.12 (1 H, dd, *J* 1.9, 13.0, H-3), 1.74 – 1.46 (4 H, m, H-3, H-4, H-5), 1.24 (3 H, t, *J* 7.1, H-2'), 0.96 (3 H, d, *J* 6.1, 4-Me); **^{13}C{^{1}H} NMR (125 MHz, CDCl$_3$)**; δ 168.3472 (C=O), 141.7136 (C-1''), 140.3323 (C-4''), 128.7690 (C-2''), 125.9828 (C-3''), 62.4628 (C-1'), 57.3209 (C-2), 44.4171 (C-6), 33.3886 (C-3), 29.6035 (C-5), 29.5780 (C-4), 21.3389 (4''-Me), 21.1911 (4-Me), 13.9143 (C-2'); **v_{max}/cm^{-1}**; 2966, 2930, 2872, 2809, 2743, 2467, 1737, 1598, 1496, 1457, 1401, 1375, 1348, 1313, 1267, 1254, 1227; **m/z (ES)**; (calculated for C$_9$H$_{18}$NO$_2^+$ [M−**Y**]$^+$: 172.1332, found: 172.1331; calculated for C$_7$H$_7$O$_3$S$^-$ [M−**X**]$^-$: 171.0121, found: 171.0115)

5.2.7 Ethyl-4-methylpiperidine-2-carboxylate benzoate
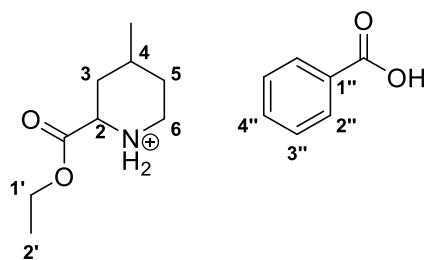
A racemic mixture of ethyl (2*R*,4*S*)-1,4-dimethylpiperidine-2-carboxylate and ethyl (2*S*,4*R*)-1,4-dimethylpiperidine-2-carboxylate (49.9 mg, 0.292 mmol) was added to isopropyl acetate (1.5 cm³). Addition of benzoic acid followed (35.9 mg, 0.294 mmol) and the homogeneous solution was left to stand. Subsequent crystals were isolated after 24 hours and washed with hexane. The title compound was isolated as a colourless solid (53.6 mg, 0.182 mmol, 63%). M.p. = 107.53 °C; **¹H NMR (500 MHz, D₂O)**; δ 7.86 (2 H, dd, *J* 1.4, 7.7, H-2''), 7.54 (1 H, tt, *J* 1.4, 7.7, H-4''), 7.47 (2 H, at, *J* 7.7, H-3''), 4.28 (2 H, dq, *J* 2.3, 7.2, H-1'), 3.98 (1 H, dd, *J* 3.2, 12.9, H-2), 3.48 (1 H, dq, *J* 2.1, 12.9, H-6), 3.02 (1 H, td, *J* 3.2, 13.1, H-6), 2.31 (1 H, dq, *J* 3.2, 14.2, H-3), 1.89 (1 H, dm, *J* 14.2, H-5), 1.79 (1 H, m, H-4), 1.32 (2 H, qm, *J* 13.1, H-3, H-5), 1.28 (3 H, t, *J* 7.2, H-2'), 0.99 (3 H, d, *J* 6.5, 4-Me); **¹³C{¹H} NMR (125 MHz, D₂O)**; δ 175.67 (C=O, ester), 169.64 (C=O, acid), 136.18 (C-1''), 131.20 (C-4''), 128.74 (C-2''), 128.25 (C-3''), 63.42 (C-1'), 57.02 (C-2), 43.86 (C-6), 33.35 (C-3), 29.34 (C-5), 28.58 (C-4), 20.37 (4-Me), 13.08 (C-2') **v$_{max}$/cm⁻¹**; 2959, 2930, 2873, 2326, 2164, 2125, 1981, 1744, 1705, 1594, 1540, 1458, 1444, 1425, 1367, 1317, 1268, 1254, 1205; **m/z (ES);** (calculated for $C_9H_{18}NO_2^+$ [M−Y]⁺: 172.1332, found: 172.1331; calculated for $C_7H_5O_2^-$ [M−X]⁻: 121.0295, found: 121.0292)

5.2.8 DL-Proline Isopropyl Ester
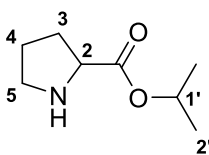
To a solution of DL-proline (4.01 g, 34.7 mmol) and isopropyl alcohol (120 cm^3), thionyl chloride (12 cm^3) was added slowly. The resultant mixture was stirred for 24 hours. The concentrated crude sample was dissolved into dichloromethane (100 cm^3) and the solution treated with NH$_3$ (aq) (100 cm^3). The mixture was stirred for a further 24 hours. The phases were separated and the aqueous layer was extracted with additional dichloromethane (100 cm^3) and the organic phase filtered through an alumina pad. The mixture was concentrated in *vacuo*. The title compound was isolated (4.49 g, 25.9 mmmol, 75%) as an orange liquid. **^{1}H NMR (500 MHz, CDCl$_3$)**; δ 5.04 (1 H, sept, *J* 6.3, H-1'), 3.77 (1 H, dd, *J* 5.6, 8.6, H-2), 3.12 (1 H, dt, *J* 6.6, 10.4, H-5), 2.95 (1 H, dt, *J* 6.6, 10.4, H-5), 2.89 (br s, N*H*), 2.15 (1 H, m, H-3), 1.80 (3 H, m, H-3, H-4), 1.25 (6 H, dd, *J* 4.5, 6.3, H-2'); **^{13}C{^{1}H} NMR (125 MHz, D$_2$O)**; δ 174.48 (C=O), 68.76 (C-1'), 59.97 (C-2), 47.09 (C-5), 30.36 (C-3), 25.44 (C-4), 21.90 (C-2'), 21.88 (C-2'); **m/z (ES);** (Found MH$^+$, 158.1166. C$_8$H$_{15}$NO$_2$ requires MH$^+$, 158.1176)

Spectroscopic data was consistent with literature values.[133]

5.3 Dynamic Reaction Monitoring (DReaM) Facility

5.3.1 DReaM Facility Equipment

The reaction was carried out under an inert atmosphere of argon in a standard glass round-bottomed flask, a Vapourtec SF-10 peristaltic pump was used to circulate the reaction mixture around the system to a Bruker InsightMR flow tube located within the NMR spectrometer (Bruker 500 MHz Avance III HD equipped with a nitrogen cooled Prodigy CryoProbe).

The tubing between the InsightMR flow tube in the NMR spectrometer and the reaction mixture was narrow diameter polyetheretherketone (PEEK) tubing (0.762 mm ID, Upchurch Scientific) was used. Tubing inside the InsightMR flow tube was PEEK (0.125 mm ID, Upchurch Scientific). All other connections were made using standard HPLC-type PEEK connectors (Upchurch Scientific), allowing apparatus to be purged with inert gases as required.

Mass spectrometry samples were taken from the reaction flow path into a 50 uL injection loop. This sample was transferred to the mass spectrometer using an Agilent 1260 Infinity II HPLC system to trigger valve openings and closings, and a Knauer P4.1S to further dilute the 50uL sample with VWR HPLC grade IPA. The samples were taken every 15 minutes and were samples into the mass spectrometer (Bruker MicrOTOF-Q, positive ionisation mode) for 5 minutes.

An Anton Parr MCP 100 polarimeter was used for optical rotation measurements. The polarimeter flow cells were placed within the flow pathway, allowing the reaction mixture to pass through for analysis after time in the NMR flow cell.

5.3.2 Experimental Procedure

SCRAM catalyst **13** (58.1 mg) was added to a mixture of ethyl acetate (16 cm^3) and isopropyl alcohol (4 cm^3) which contained 1,3,5-trimethoxybezene (0.1 M) as internal standard. The mixture was heated to 70 ⁰C in an attempt to form a homogenous mixture. After 1 hour, (*S*)-(−)-*N*,α-Dimethylbenzylamine **33** (0.7 cm^3) was added and a filter was placed onto the PEEK tubing to allow circulation of the heterogeneous reaction mixture. The filter was removed 3.5 hours later when the reaction homogenised. In total, the reaction mixture was circulated for 6 hours.

5.3.3 NMR Acquisition Parameters

Non-selective ^{1}H NMR spectra were gained using pulse sequence zg30 where the acquisition time was 1.64 seconds with a total number of 8 scans.

Selective excitation ^{1}H NMR spectra were gained using pulse sequence seldpfgse_calc.ptg, with a 2.0 second acquisition time and a total number of 16 scans. The -5 to -25 ppm region of the spectrum was excited.

A static ^{1}H NMR spectra was recorded at the end of the experiment to allow calculation of flow correction factors. For the selective excitation spectra, a static spectrum focussing on the 1,3,5-trimethoxybenzene internal standard signal was also recorded.

5.3.4 NMR Data Processing

Batch processing of NMR data was carried out using Bruker TopSpin 4.1.3. The integration of relevant peaks were saved as integral regions and the "multi_integ3" command in TopSpin was employed to integrate a set number of spectra in accordance with the initial integral regions specified. Flow correction factors were applied to the data to account for the difference between static and flowing NMR spectra.

5.3.5 Mass Spectrometry Data Processing

Mass spectrometry data was batch processed using a unique script (Bruker Compass DataAnalysis 4.3) which created an average spectrum across all data timepoints between m/z 50 and 2000.

5.3.6 General Procedure for Rapid Chiral Amine Racemisation

Experiments were performed using a CEM Discover SP microwave synthesiser or an Anton-Paar Monowave 50 synthesis reactor.

SCRAM catalyst **13** was added to a microwave or monowave tube with magnetic stirrer bar. Chiral amine was dissolved into a mixture of d_8-toluene **48** and d_8-isopropyl alcohol **47**, and suitable internal standard was added if required. The mixture was added to the tube containing SCRAM, and a sample was taken for ^{1}H NMR and HRMS. The ^{1}H NMR sample was poured back into the tube and sealed with a silicon cap, and PTFE septum if using the Monowave 50. The mixture was heated to 110 ºC for an hour, and another sample was taken for ^{1}H NMR and HRMS. The ^{1}H NMR sample was poured back into the tube, sealed and placed for heating again. The heating and sampling process was repeated for 4 hours. Specific quantities are detailed in Table 5.1, where all experiments

were conducted with corresponding amine (50 mg), SCRAM catalyst **13** (2.5 mol%) and d_8-IPA, unless stated otherwise.

Entry [a-g]	Amine	d_8-toluene/ μL	d-IPA/ μL	Internal standard[h]
1	26	600	700	-
2	33	1000	400	-
3	33	1000	400	-
4	58	1000	400	Biphenyl
5	55	1000	400	Biphenyl
6	58	600	378	Biphenyl
7	61	600	700	-
8	61	600	400	-
9	61	1000	400	Biphenyl
10	61	1000	400	Biphenyl
11	61	1000	400	TK(TMS)S
12	68	1000	400	Biphenyl
13	68	1000	400	Biphenyl
14	69	600	700	-
15	75	1000	400	TK(TMS)S
16	75	1000	400	TK(TMS)S
17	79	1000	1200	-
18	80	1000	380	-
19	80	1400	-	TK(TMS)S
20	80	1400	-	-

Table 5.1. Conditions used for H/D exchange experiments. [a] Entries **1,7,8,10,14** were conducted with 30 mg amine, [b] Entries **7,8,10** were conducted with 5 mol% SCRAM catalyst **13**, [c] Entry **3** was conducted with OD-IPA **54**, [d] Entries **4** and **9** were conducted with hydrogenated IPA, [e] Entry **17** was conducted in d_{10}-*p*-xylene at 125 ºC, [f] Entry **1** was conducted in d_{10}-*o*-xylene at 142 ºC. [g] An equimolar quantity of acid was added to entries **8** (*p*-toluene sulfonic acid), **10** (acetic acid), **11**, **13** (benzoic acid) and **20** (*S*-mandelic acid). [h] TK(TMS)S =

tetrakistrimethylsilylsilane. Where an internal standard isn't detailed, protons resistant to H/D exchange were used as an internal standard.

5.4 Gas Chromatography Traces and Methods

5.4.1 Ethyl-4-methylpiperidine-2-carboxylate
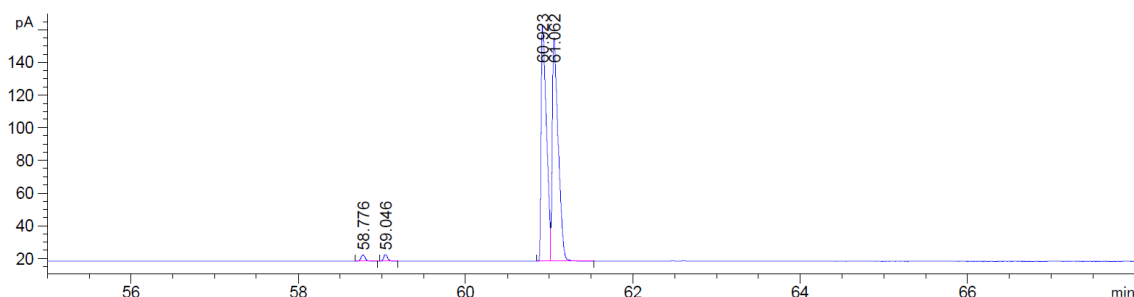
Figure 5.1. Chiral GC trace of trifluoroacetylated **61**. Method, column = CP-CHIRASIL-DEX column (25 m × 0.25 mm × 0.25 µm); oven temperature = 50 °C isothermal for 5 min, 5 °C min^{-1} ramped to 65 °C and isothermal for 40 minutes, 5 °C min^{-1} ramped to 200 °C; inlet pressure = 15 psi. GC elution time; trifluoroacetylated (2*R*,4*R*)-**61** (58.8 min), trifluoroacetylated (2*S*,4*S*)-**61** (59.0 min), trifluoroacetylated (2*R*,4*S*)-**61** (60.9 min), trifluoroacetylated (2*S*,4*R*)-**61** (61.1 min)
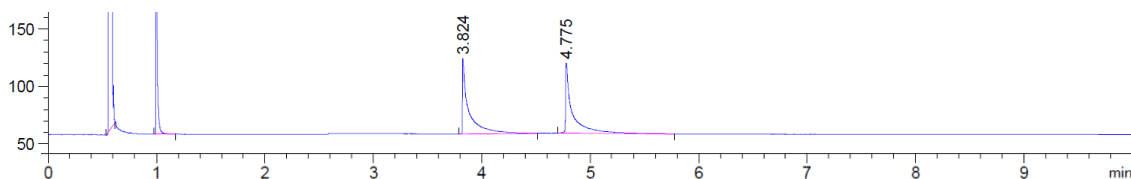
Figure 5.2. Achiral GC trace of *cis*- and *trans*-ethyl-4-methylpiperidine-2-carboxylate **61**. Method, column = HP-5 column (5% phenyl methyl siloxane; 30 m × 0.32 mm × 0.25 µm); oven temperature = 35 °C isothermal for 10 min, 10 °C min^{-1} ramped to 300 °C and isothermal for 5 min; inlet pressure = 9.38 psi. GC elution time; *trans*-**61** (3.8 min), c*is*-**61** (4.8 min)

5.4.2 Sertraline
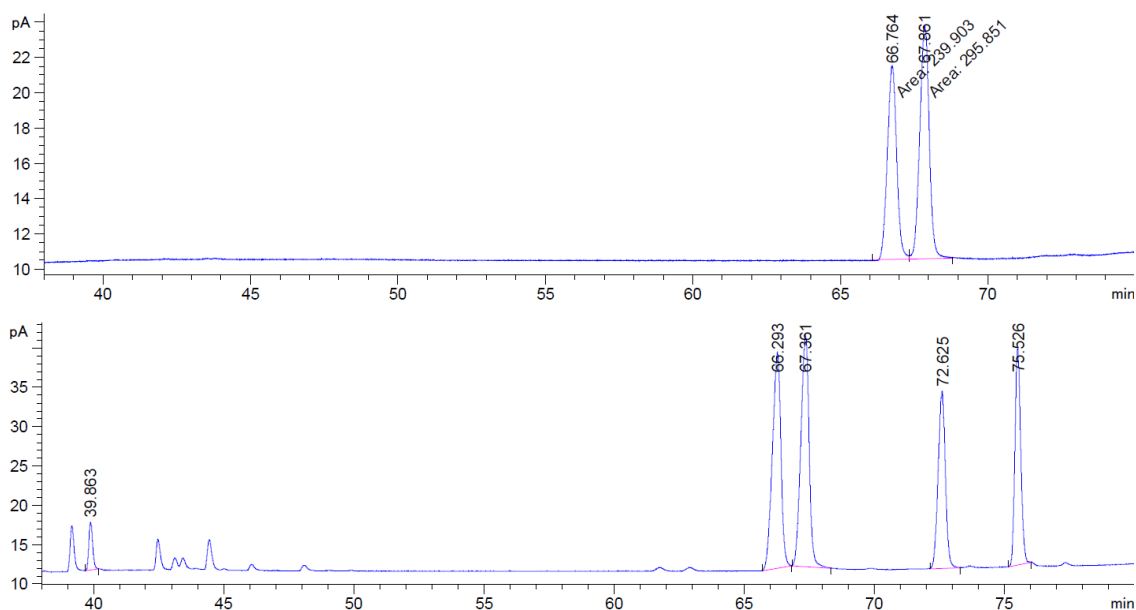
Chiral GC traces of sertraline **26**. Method, column = CP-CHIRASIL-DEX column (25 m × 0.25 mm × 0.25 μm); oven temperature = 100 °C isothermal for 0 min, 10 °C min^{-1} ramped to 150 °C, 2 °C min^{-1} ramped to 170 °C and isothermal for 20 minutes, 2 °C min^{-1} ramped to 180 °C and isothermal for 30 minutes, 2 °C min^{-1} ramped to 200 °C; inlet pressure = 15 psi. (1*S*,4*S*)-**26** (66.3 min), (1*R*,4*R*)-**26** (67.4 min), (1*R*,4*S*)-**26** (72.6 min), (1*S*,4*R*)-**26** (75.5 min)
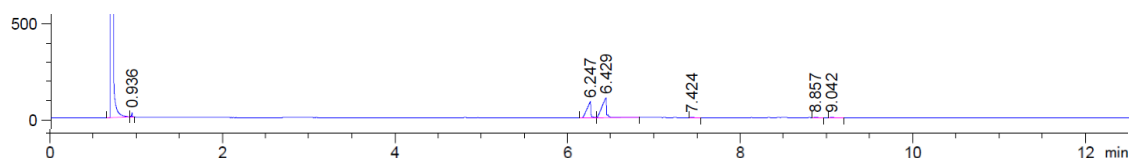
Achiral GC traces of sertraline **26**. Method, column = HP-5 column (5% phenyl methyl siloxane; 30 m × 0.32 mm × 0.25 μm); oven temperature = 100 °C isothermal for 0 min, 10 °C min^{-1} ramped to 250 °C and isothermal for 5 minutes, 20 °C min^{-1} ramped to 290 °C; inlet pressure = 8.25 psi. *Cis*-**26** (6.2 min), *trans*-**26** (6.4 min)

5.5   Resolution-Racemisation-Recycle

5.5.1 Experimental set-up

The experimental set-up for the R^3 process, summarised in consisted of a glass CSTR (50 cm^3) with a gas tight PTFE lid and two ports (3 mm I.D.). An in-line frit (40 μm pore size) inside the CSTR was connected to the inlet of a Jasco pump *via* PTFE tubing

(1/16" O.D., 1/32" I.D.). The pump outlet was connected to the inlet of a PBR through a priming union. The stainless steel PBR was enclosed by an aluminium heating block, and the outlet of the column was fed back into the CSTR with passage through a 250 psi BPR.
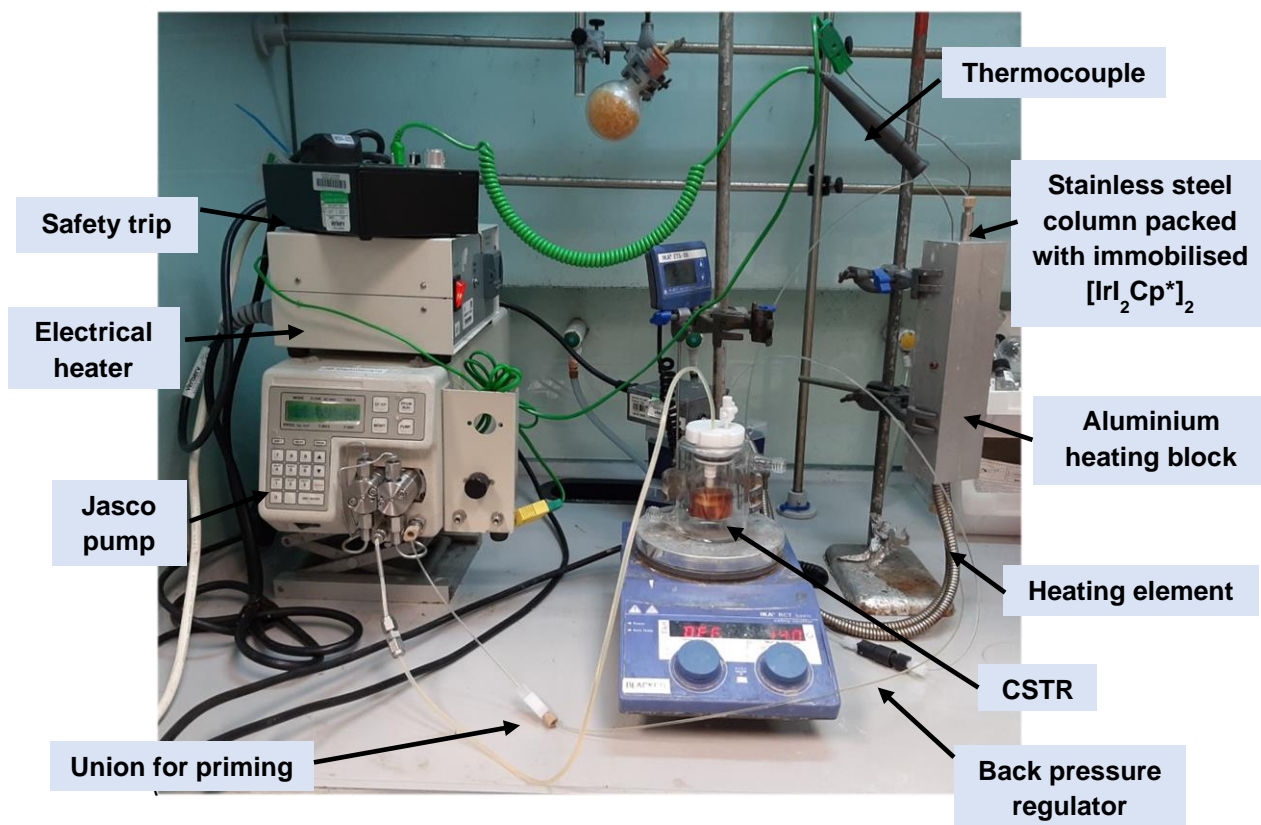
Figure 5.3. Experimental set-up for the R^3 process

The reactor volume of the system varied with replacement of tubing, and was calculated by pumping a known quantity of solvent through the set-up until the CSTR contained 20 cm^3 of solvent. The difference between the initial known quantity of solvent and final quantity of solvent gave the reactor volume for the system.

5.5.2 Sertraline

For the R^3 investigation of sertraline **26**, residence times were determined as follows,

$$Flow\ rate = \frac{Packed\ Bed\ Reactor\ Volume}{t_{res}(racemisation)} = \frac{1.97\ mL}{15\ min} = 0.131\ mL/min$$

$$t_{res}(overall) = \frac{Reactor\ Volume}{Flow\ Rate} = \frac{20\ mL}{0.131\ mL/min} \approx 2.5\ hours$$

The PBR was filled with sand (5.7 g), immobilised SCRAM (ICP 7.73% Ir, 0.252g, 0.10 mmol iridium) and was wet with IPA. A racemic mixture of sertraline (3.108 g, 0.5 M) was added to a solution of biphenyl (20 mM) in toluene (20 cm^3). *R*-mandelic acid **25** (1.550 g, 0.5 M) was added and the resultant slurry was stirred for 60 minutes. During stirring, the R^3 system was purged with stock solution of biphenyl in toluene, and the column was heated to 80 °C.

Samples were taken prior to and during circulation of the mother liquor. Each 100 μL sample containing a mixture of solid and mother liquor was separated using a PTFE syringe filter (0.45 μm). Prior to mother liquor and solid sample work up, the solid sample was treated as follows,

1. The solid in the syringe filter was washed with hexane to remove any residual surface mother liquor
2. The syringe filter contents were dissolved through sonication using DCM
3. The solid containing solvent was concentrated under vacuum and weight of solid recorded
4. Stock solution of biphenyl in toluene (100 μL) was added to the concentrated solid as an external standard

After independent treatment of solid, each solid and mother liquor sample was treated as follows,

1. Ethyl acetate (2000 μL) and NaOH (2.5 M, 2000 μL) were added
2. The shaken samples were allowed to separate, and ethyl acetate was pipetted into a new sample vial
3. The contents of each sample vial were dried using magnesium sulfate
4. The magnesium sulfate was removed using a combination of wool and celite within a Pasteur pipette
5. The residual solution for each sample was placed for achiral and chiral GC

5.5.3 Ethyl-4-methylpiperidine-2-carboxylate

(a) 0.2 mol% SCRAM

For ethyl-4-methylpiperidine-2-carboxylate **61** using SCRAM catalyst **13** (0.2 mol%) residence times were determined as follows,

$$Flow\ rate = \frac{Packed\ Bed\ Reactor\ Volume}{t_{res}(racemisation)} = \frac{1.97\ mL}{65.6\ min} = 0.03\ mL/min$$

$$t_{res}(overall) = \frac{Reactor\ Volume}{Flow\ Rate} = \frac{13.5\ mL}{0.03\ mL/min} \approx 7.5\ hours$$

The PBR was filled with sand (5.57 g) and wet with isopropyl acetate. (2R,4R)-**61** (1.25 g, 7.30 mmol) was added to a mixture of isopropyl acetate (12.5 cm^3), decane (612.5 µL) and homogeneous SCRAM catalyst **13** (17.0 mg, 14.6 µmol). A sample (20 µL) was taken prior to benzoic acid **66** (891.8 mg, 7.30 mmol) addition and after **66** dissolution. After column heating (80 ºC), the mixture was circulated through the R^3 set up. Samples were taken at 0.25, 0.5, 0.75, 1, 3, 3.25, 3.5, 3.75 and 4 RV where one reactor volume was 13.5 cm^3, and at a flow rate of 0.03 mLmin^{-1} equating to 7.5 hours. Homogeneous samples were worked up as follows,

1. Ethyl acetate (2000 µL) and NaOH (2.5 M, 2000 µL) were added
2. The shaken samples were allowed to separate, and ethyl acetate was pipetted into a new sample vial
3. The contents of each sample vial were dried using magnesium sulfate
4. The magnesium sulfate was removed using a combination of wool and celite within a Pasteur pipette
5. The residual solution for each sample was placed for achiral and chiral GC, where the latter sample was derivatised using trifluoroacetic anhydride (30 µL) prior to analysis

(b) 1 mol% SCRAM

For ethyl-4-methylpiperidine-2-carboxylate **61** using SCRAM catalyst **13** (1 mol%) residence times were determined as follows,

$$Flow\ rate = \frac{Packed\ Bed\ Reactor\ Volume}{t_{\ res}(racemisation)} = \frac{1.97\ mL}{65.6\ min} = 0.03\ mL/min$$

$$t_{res}(overall) = \frac{Reactor\ Volume}{Flow\ Rate} = \frac{12.5\ mL}{0.03\ mL/min} \approx 7\ hours$$

The reaction was carried out and sampled as in **(a) 0.2 mol% SCRAM**, where samples were taken at 0, 0.25, 0.5, 0.75, 1, 3.25, 3.75, 4, 4.25 RV.

5.5.4 Sertraline epimerisation in batch

Sertraline **26** (619.2 mg, 2.02 mmol) was added to a mixture of toluene (4 cm^3) and SCRAM **13** (23.7 mg, 0.02 mmol) and refluxed at 80 ºC. Samples (100 µL) were taken

after 0, 1, 2, 3, 4, 6 and 24 hours and quenched in ethyl acetate (2 cm^3) and 2.5 M sodium hydroxide solution (2 cm^3). The samples were separated, the organic layer dried (MgSO$_4$), separated and placed for GC analysis. At 28.5 hours an additional aliquot of sertraline **26** was added (0.5 equiv.) and after dissolution another sample was taken. Subsequent samples were taken at 29.5, 30.5, 45.5, 52.5, 70, 96 and 100.5 hours and quenched as described above.

5.5.5 Sertraline epimerisation in flow

The epimerisation of sertraline **26** was studied in flow,

Figure 5.4. The tubular stainless steel column was loaded with a mixture of sand (5.5 g) and immobilsed SCRAM catalyst **29b** (ICP 7.73% Ir, 310 mg, 0.12 mmol iridium). The column contents were wet using toluene and the column slowly heated to 80 ºC. A stock solution of sertraline **26** (7.63 g, 2.5 mmol) and biphenyl (388.6 mg) in toluene (50 cm^3) was prepared and 10 reactor volumes (1 RV = 5 cm^3) were collected at 0.131 mLmin^{-1} and analysed using chiral GC.
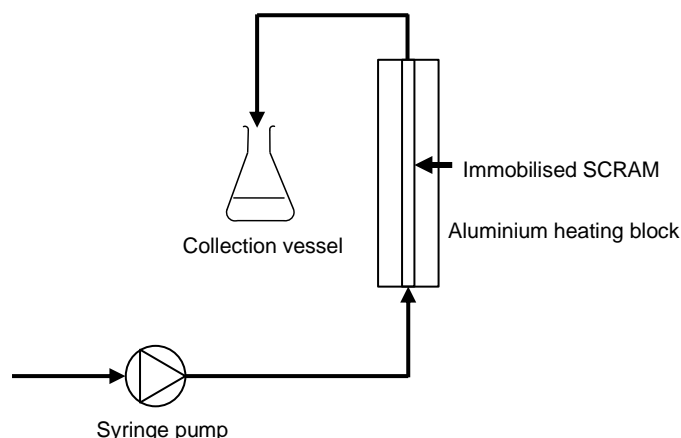
Figure 5.4. Experimental set-up for sertraline epimerisation under flow conditions

5.5.6 Ethyl-4-methylpiperidine-2-carboxylate epimerisation in batch

A general epimerisation of ethyl-4-methylpiperidine-2-carboxylate **61** under batch conditions described in Table 4.1, Chapter 4 is as follows,
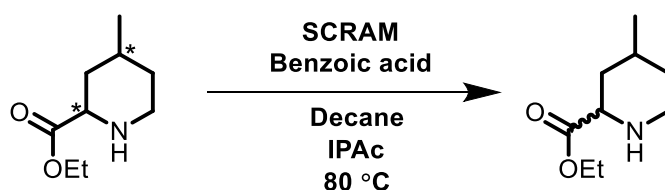
Ethyl-4-methylpiperidine-2-carboxylate (407 mg, 2.38 mmol) was added to a mixture of isopropyl acetate (4 cm^3), benzoic acid (289.4 mg, 2.37 mmol) and *n*-decane (196 μL). SCRAM catalyst (5.4 mg, 4.64 μmol) was added and the reaction mixture was refluxed at 80 ⁰C for 24 hours.

For mixtures containing benzoic acid, samples (20 μL) were worked up as follows,

1. Ethyl acetate (2000 μL) and base, either NaOH (2.5 M, 2000 μL), or NaHCO$_3$ (1 M, 2000 μL) were added
2. The shaken samples were allowed to separate, and ethyl acetate was pipetted into a new sample vial
3. The contents of each sample vial were dried using magnesium sulfate
4. The magnesium sulfate was removed using a combination of wool and celite within a Pasteur pipette
5. The residual solution for each sample was separated into two equal aliquots and each placed for chiral or achiral GC. The former sample was derivatised with trifluoroacetic anhydride (30 μL) prior to analysis

To samples without benzoic acid, ethyl acetate (980 μL) was added and achiral GC samples were analysed without further manipulation. Chiral GC samples were derivatised with trifluoroacetic anhydride (30 μL) prior to analysis.

5.5.7 Ethyl-4-methylpiperidine-2-carboxylate dynamic resolution

(2*R*,4*R*)-Ethyl-4-methylpiperidine-2-carboxylate (407 mg, 2.38 mmol) was added to a mixture of isopropyl acetate (4 cm^3), benzoic acid (289.4 mg, 2.37 mmol) and *n*-decane (196 μL). SCRAM catalyst (5.4 mg, 4.64 μmol) was added and the reaction mixture was refluxed at 80 ⁰C for 24 hours. The mixture was placed in the fridge, left over the weekend and colourless platelet-like crystals of (2*S*,4*R*)-ethyl-4-methylpiperidine-2-carboxylate benzoate salt (22.2 mg, 76 μmol, 3.2%) were isolated

6 References

1   T. C. Nugent, *Chiral Amine Synthesis: Methods, Developments and Applications*, Wiley-VCH, Weinheim, 1st edn., 2010.

2   D. Ghislieri and N. J. Turner, *Top. Catal.*, 2014, **57**, 284–300.

3   N. Chhabra, M. L. Aseri and D. Padmanabhan, *Int. J. Appl. Basic Med. Res.*, 2013, **3**, 16–18.

4   S. Ghosh, Y. Chisti and U. C. Banerjee, *Biotechnol. Adv.*, 2012, **30**, 1425–1431.

5   J. Clayden, N. Greeves and S. Warren, in *Organic Chemistry*, Oxford University Press, New York, 2nd edn., 2012, pp. 1102–1133.

6   G. Liu, D. A. Cogan and J. A. Ellman, *J. Am. Chem. Soc*, 1997, **119**, 9913–9914.

7   J. A. Ellman, T. D. Owens and T. P. Tang, *Acc. Chem. Res.*, 2002, **35**, 984–995.

8   Z. Han, S. G. Koenig, H. Zhao, X. Su, S. P. Singh and R. P. Bakale, *Org. Process. Res. Dev.*, 2007, **11**, 726–730.

9   A. Grajewska and M. D. Rozwadowska, *Tetrahedron Asymmetry*, 2007, **18**, 557–561.

10   V. R. Arava, L. Gorentla and P. K. Dubey, *J. Org. Chem.*, 2011, **1**, 26–32.

11   R. Dorta, D. Broggini, R. Kissner and A. Togni, *Chem. Eur. J.*, 2004, **10**, 4546–4555.

12   H. Blaser, W. Brieden, B. Pugin, F. Spindler, M. Studer and A. Togni, *Top. Catal.*, 2002, **19**, 3–16.

13   C. Blanc, F. Agbossou-Niedercorn and G. Nowogrocki, *Tetrahedron Asymmetry*, 2004, **15**, 2159–2163.

14   H. U. Blaser, *Adv. Synth. Catal.*, 2002, **344**, 17–31.

15   J. M. Mwansa, M. J. Stirling and M. I. Page, *Pure Appl. Chem.*, 2020, **92**, 107–121.

16   J. M. Mwansa, M. J. Stirling, G. Sweeney, J. Hanusek, J. Váňa and M. I. Page, *Dalton Trans.*, 2022, **51**, 2696–2707.

17   S. Bellemin-Laponnaz, T. Achard, D. Bissessar, Y. Geiger and A. Maisse-François, *Coord. Chem. Rev.*, 2017, **332**, 38–47.

18   G. Ma and M. P. Sibi, *Chem. Eur. J.*, 2015, **21**, 11644 – 11657.

19   E. Vedejs and M. Jure, *Angew. Chem. Int. Ed.*, 2005, **44**, 3974–4001.

20   J. M. Keith, J. F. Larrow and E. N. Jacobsen, *Adv. Synth. Catal.*, 2001, **343**, 5–26.

21   H. Lorenz and A. Seidel-Morgenstern, *Angew. Chem., Int. Ed.*, 2014, **53**, 1218–1250.

22   F. Darvas, G. Dormán and V. Hessel, *Flow Chemistry Volume 2*, Walter de Gruyter, Berlin, 2014.

23   R. A. Sheldon, *Chirotechnology: Industrial Synthesis of Optically Active Compounds*, Marcel Dekker, New York, 1st edn., 1993.

24   J. Mullin, *Crystallization*, Reed Educational and Professional Publishing Ltd, Oxford, 4th edn., 2001.

25   K. M. J. Brands and A. J. Davies, *Chem. Rev.*, 2006, **106**, 2711–2733.

26   C. Rougeot and J. E. Hein, *Org. Process Res. Dev.*, 2015, **19**, 1809–1819.

27   G. Levilain and G. Coquerel, *CrystEngComm*, 2010, **12**, 1983–1992.

28   C. Brandel, Y. Amharar, J. M. Rollinger, U. J. Griesser, Y. Cartigny, S. Petit and G. Coquerel, *Mol. Pharm.*, 2013, **10**, 3850−3861.

29   S. Gonella, J. Mahieux, M. Sanselme and G. Coquerel, *Org. Process Res. Dev.*, 2012, **16**, 286–293.

30   J. B. Crawford, R. T. Skerlj and G. J. Bridger, *J. Org. Chem.*, 2007, **72**, 669–671.

31   E. J. Ebbers, G. J. A. Ariaans, J. P. M. Houbiers, A. Bruggink and B. Zwanenburg, *Tetrahedron*, 1997, **53**, 9417–9476.

32   A. J. Blacker, M. J. Stirling and M. I. Page, *Org. Process Res. Dev.*, 2007, **11**, 642–648.

33   M. J. Stirling, J. M. Mwansa, G. Sweeney, A. J. Blacker and M. I. Page, *Org. Biomol. Chem.*, 2016, **14**, 7092–7098.

34   G. Csjernyik, K. Bogár and J. E. Bäckvall, *Tetrahedron Lett.*, 2004, **45**, 6799–6802.

35   N. Y. Shin, J. M. Ryss, X. Zhang, S. J. Miller and R. R. Knowles, *Science*, 2019, **366**, 364–369.

36   C. Viedma, *Am. Phys. Soc.*, 2005, **94**, 1–4.

37   L.-C. Sö, G. Toglu, R. R. E. Steendam, H. Meekes, E. Vlieg and F. P. J. T. Rutjes,

Chem. Soc. Rev., 2015, **44**, 6723–6732.

38   J. E. Hein, B. Huynh Cao, C. Viedma, R. M. Kellogg and D. G. Blackmond, *J. Am. Chem. Soc.*, 2012, **134**, 12629–12636.

39   A. R. A. Palmans, *Mol. Syst. Des. Eng.*, 2017, **2**, 34–46.

40   T. Noël and E. Zysman-Colman, *Chem Catal.*, 2022, **2**, 468–476.

41   B. König, *European J. Org. Chem.*, 2017, **2017**, 1979–1981.

42   J. Großkopf, M. Plaza, A. Seitz, S. Breitenlechner, G. Storch and T. Bach, *J. Am. Chem. Soc*, 2021, **143**, 21241–21245.

43   J. H. Choi, Y. H. Kim, S. H. Nam, S. T. Shin, M. J. Kim and J. Park, *Angew. Chem. Int. Ed.*, 2002, **41**, 2373–2376.

44   J. H. Choi, Y. K. Choi, Y. H. Kim, E. S. Park, E. J. Kim, M.-J. Kim and J. Park, *J. Org. Chem.*, 2004, **69**, 1972–1977.

45   B. Martín-Matute, M. Edin, K. Bogár and J. E. Bäckvall, *Angew. Chem. Int. Ed.*, 2004, **43**, 6535–6539.

46   S.-B. Ko, B. Baburaj, M.-J. Kim and J. Park, *J. Org. Chem.*, 2007, **72**, 6860–6864.

47   O. Verho and J.-E. Bäckvall, *J. Am. Chem. Soc.*, 2015, **137**, 3996−4009.

48   M. Stirling, J. Blacker and M. I. Page, *Tetrahedron Lett.*, 2007, **48**, 1247–1250.

49   Y. Fujima, M. Ikunaka, T. Inoue and J. Matsumoto, *Org. Process Res. Dev.*, 2006, **10**, 905–913.

50   A. J. Blacker, S. Brown, B. Clique, B. Gourlay, C. E. Headley, S. Ingham, D. Ritson, T. Screen, M. J. Stirling, D. Taylor and G. Thompson, *Org. Process Res. Dev.*, 2009, **13**, 1370–1378.

51   S. J. Lucas, B. D. Crossley, A. J. Pettman, A. D. Vassileiou, T. E. O. Screen, A. J. Blacker and P. C. McGowan, *Chem. Commun.*, 2013, **49**, 5562.

52   G. J. Sherborne, M. R. Chapman, A. J. Blacker, R. A. Bourne, T. W. Chamberlain, B. D. Crossley, S. J. Lucas, P. C. Mcgowan, M. A. Newton, T. E. O. Screen, P. Thompson, C. E. Willans and B. N. Nguyen, *J. Am. Chem. Soc.*, 2015, **137**, 4151–4157.

53   A. S. Burange, S. M. Osman and R. Luque, *iScience*, 2022, **25**, 1–22.

54   G. Bolla, B. Sarma and A. K. Nangia, *Chem. Rev.*, 2022, **122**, 11514−11603.

55   H. Zhang, R. Lakerveld, P. L. Heider, M. Tao, M. Su, C. J. Testa, A. N. D. Antonio,

P. I. Barton, R. D. Braatz, B. L. Trout, A. S. Myerson, K. F. Jensen and J. M. B. Evans, *Cryst. Growth Des.*, 2014, **14**, 2148−2157.

56   S. Mascia, P. L. Heider, H. Zhang, R. Lakerveld, B. Benyahia, P. I. Barton, R. D. Braatz, C. L. Cooney, J. M. B. Evans, T. F. Jamison, K. F. Jensen, A. S. Myerson and B. L. Trout, *Angew. Chem. Int. Ed.*, 2013, **52**, 12359–12363.

57   J. L. Quon, H. Zhang, A. Alvarez, J. Evans, A. S. Myerson and B. L. Trout, *Cryst. Growth Des.*, 2012, **12**, 3036–3044.

58   M. B. Plutschack, B. Pieber, K. Gilmore and P. H. Seeberger, *Chem. Rev.*, 2017, **117**, 11796–11893.

59   M. R. Chapman, M. H. T. Kwan, G. King, K. E. Jolley, M. Hussain, S. Hussain, I. E. Salama, C. Gonzaíez Niñ, L. A. Thompson, M. E. Bayana, A. D. Clayton, B. N. Nguyen, N. J. Turner, N. Kapur and A. J. Blacker, *Org. Process Res. Dev.*, 2017, **21**, 1294−1301.

60   A. J. Alvarez, A. Singh and A. S. Myerson, *Cryst. Growth Des.*, 2011, **11**, 4392–4400.

61   S. Qamar, K. Galan, M. Peter Elsner, I. Hussain and A. Seidel-Morgenstern, *Chem. Eng. Sci.*, 2013, **98**, 25–39.

62   K. Galan, M. J. Eicke, M. P. Elsner, H. Lorenz, A. Seidel-Morgenstern and G. Simon, *Cryst. Growth Des.*, 2015, **15**, 1808–1818.

63   D. Zhang, S. Xu, S. Du, J. Wang and J. Gong, *Engineering*, 2017, **3**, 354–364.

64   A. Puglisi, M. Benaglia and V. Chiroli, *Green Chem.*, 2013, **15**, 1790–1813.

65   M. B. Plutschack, B. Us Pieber, K. Gilmore and P. H. Seeberger, *Chem. Rev.*, 2017, **117**, 11796–11893.

66   I. Atodiresei, C. Vila and M. Rueping, *ACS Catal.*, 2015, **5**, 1972−1985.

67   D. Zhao and K. Ding, *ACS Catal.*, 2013, **3**, 928–944.

68   D. L. Hughes, *Org. Process Res. Dev.*, 2018, **22**, 13–20.

69   D. A. Foley, A. L. Dunn and M. T. Zell, *Magn. Reson. Chem.*, 2016, **54**, 451–456.

70   A. M. R. Hall, J. C. Chouler, A. Codina, P. T. Gierth, J. P. Lowe and U. Hintermair, *Catal. Sci. Technol*, 2016, **6**, 8406.

71   A. M. R. Hall, R. Broomfield-Tagg, M. Camilleri, D. R. Carbery, A. Codina, D. T. E. Whittaker, S. Coombes, J. P. Lowe and U. Hintermair, *Chem. Commun.*, 2017,

54, 30–33.

72 A. M. R. Hall, P. Dong, A. Codina, J. P. Lowe and U. Hintermair, *ACS Catal.*, 2019, **9**, 2079–2090.

73 D. B. G. Berry, A. Codina, I. Clegg, C. L. Lyall, J. P. Lowe and U. Hintermair, *Faraday Discuss.*, 2019, **220**, 45–57.

74 J. H. Vrijsen, I. A. Thomlinson, M. E. Levere, C. L. Lyall, M. G. Davidson, U. Hintermair and T. Junkers, *Polym. Chem.*, 2020, **11**, 3546–3550.

75 M. H. T. Kwan, Ph.D. Thesis, University of Leeds, 2018.

76 D. G. Hamilton and R. H. Crabtree, *J. Am. Chem. Soc.*, 1988, **110**, 4126–4133.

77 R. H. Crabtree, *Acc. Chem. Res.*, 1990, **23**, 95–101.

78 J. M. Goldberg, Ph.D. Thesis, University of Washington, 2017.

79 C. Ammann, F. Isaia and P. S. Pregosin, *Magn. Reson. Chem.*, 1988, **26**, 236–238.

80 R. H. Crabtree, B. E. Segmuller and R. J. Uriarte, *Inorg. Chem.*, 1985, **24**, 1949–1950.

81 D. G. Hamilton and R. H. Crabtree, *J. Am. Chem. Soc.*, 1988, **110**, 4126–4133.

82 G. E. Dobereiner, N. Hazari and N. D. Schley, *Organometallics*, 2021, **40**, 295–301.

83 D. Schröder, *Acc. Chem. Res.*, 2012, **45**, 1521–1532.

84 G.-J. Cheng, X.-M. Zhong, Y.-D. Wu and X. Zhang, *Chem. Commun.*, 2019, **55**, 12749–12764.

85 X. Yan, E. Sokol, X. Li, G. Li, S. Xu and R. Graham Cooks, *Angew. Chem. Int. Ed.*, 2014, **53**, 5931–5935.

86 G. E. Dobereiner, A. Nova, N. D. Schley, N. Hazari, S. J. Miller, O. Eisenstein and R. H. Crabtree, *J. Am. Chem. Soc*, 2011, **133**, 7547–7562.

87 N. Phillips, L. Treasure, N. H. Rees, R. Tirfoin, J. E. McGrady and S. Aldridge, *Eur. J. Inorg. Chem.*, 2014, **2014**, 4877–4885.

88 R. Corberá, M. Sanaú, E. Peris and S. Baynat, *J. Am. Chem. Soc.*, 2006, **128**, 3974–3979.

89 R. Corberán and E. Peris, *J. Am. Chem. Soc.*, 2008, **27**, 1954–1958.

90 R. H. Crabtree, H. Felkin and G. E. Morris, *J. Organomet. Chem.*, 1977, **141**, 205–215.

91 R. H. Crabtree, H. Felkin, G. E. Morris, T. J. King and J. A. Richards, *J. Organomet. Chem.*, 1976, **113**, C7–C9.

92 R. H. Crabtree, P. C. Demou, D. Eden, J. M. Mihelcic, C. A. Parnell, J. M. Quirk and G. E. Morris, *J. Am. Chem. Soc*, 1982, **104**, 82963–87.

93 D. M. Heinekey, J. M. Millar, T. F. Koetzle, N. G. Payne and K. W. Zilm, *J. Am. Chem. Soc.*, 1990, **112**, 909–919.

94 D. M. Heinekey, A. S. Hinkle and J. D. Close, *J. Am. Chem. Soc.*, 1996, **118**, 5353–5361.

95 T. Yamagata, H. Tadaoka, M. Nagata, T. Hirao, Y. Kataoka, V. Ratovelomanana-Vidal, J. P. Genet and K. Mashima, *Am. Chem. Soc.*, 2006, **25**, 2505–2513.

96 T. Nagano, A. Iimuro, R. Schwenk, T. Ohshima, Y. Kita, A. Togni and K. Mashima, *Chem. Eur. J.*, 2012, **18**, 11578–11592.

97 K. Mashima, K. Higashida, A. Iimuro, H. Nagae and Y. Kita, *Chem. Rec.*, 2016, **16**, 2585–2594.

98 M. H. T. Kwan, N. P. B. Pokar, C. Good, M. F. Jones, R. Munday, T. Screen and A. J. Blacker, *Tetrahedron*, 2021, **80**, 131823.

99 M. J. Stirling, Ph.D. Thesis, University of Leeds, 2006.

100 M. H. T. Kwan, J. Breen, M. Bowden, L. Conway, B. Crossley, M. F. Jones, R. Munday, N. P. B. Pokar, T. Screen and A. J. Blacker, *J. Org. Chem.*, 2021, **86**, 2458–2473.

101 C. Davies, Master's Report, University of Leeds, 2017.

102 L. Neubert, D. Michalik, S. Bä, S. Imm, H. Neumann, J. Atzrodt, V. Derdau, W. Holla and M. Beller, *J. Am. Chem. Soc.*, 2012, **134**, 12239−12244.

103 P. S. Kiuru and K. Wähälä, *Tetrahedron Lett.*, 2002, **43**, 3411–3412.

104 M. Zhan, R. Xu, Y. Tian, H. Jiang, L. Zhao, Y. Xie and Y. Chen, *Eur. J. Org. Chem.*, 2015, **2015**, 3370–3373.

105 C. S. Donald, T. A. Moss, G. M. Noonan, B. Roberts and E. C. Durham, *Tetrahedron Lett.*, 2014, **55**, 3305–3307.

106 A. P. Kourounakis, D. Xanthopoulos and A. Tzara, *Med. Res. Rev.*, 2020, **40**,

709–752.

107   C. Agami, F. Bisaro, S. Comesse, S. Guesné, C. Kadouri-Puchot and R. Morgentin, *European J. Org. Chem.*, 2001, **12**, 2385–2389.

108   C. Alegret, F. Santacana and A. Riera, *J. Org. Chem.*, 2007, **72**, 7688–7692.

109   R. Sablong and J. A. Osborn, *Tetrahedron Asymmetry*, 1996, **7**, 3059–3062.

110   N. Tamosiunaite, L. C. Logie, S. E. Neale, K. Singh, D. L. Davies and S. A. Macgregor, *J. Org. Chem*, 2022, **87**, 1445–1456.

111   T. Zhang, X. Hu, Z. Wang, T. Yang, H. Sun, G. Li and H. Lu, *Chem. Eur. J*, 2016, **22**, 2920–2924.

112   *US Pat.*, 4 536 518, 1985.

113   S. E. O'Connor, A. Grosset and P. Janiak, *Fundam. Clin. Pharmacol.*, 1999, **13**, 145–153.

114   C. F. Bernasconi, R. J. Ketner, S. D. Brown, X. Chen and Z. Rappoport, *J. Org. Chem.*, 1999, **64**, 8829–8839.

115   S. Ohno, K. Mizukoshi, K. Izumi, K. Kato and M. Hori, *Chem. Pharm. Bull.*, 1988, 551–562.

116   A. Markham, *Drugs*, 2021, **81**, 1665–1670.

117   N. K. Adlington, L. R. Agnew, A. D. Campbell, R. J. Cox, A. Dobson, C. Fernandez Barrat, M. A. Y. Gall, W. Hicks, G. P. Howell, A. Jawor-Baczynska, L. Miller-Potucka, M. Pilling, K. Shepherd, R. Tassone, B. A. Taylor and A. Williams, *J. Org. Chem.*, 2019, **84**, 4735–4747.

118   H. J. Federsel, M. Hedberg, F. R. Qvarnström and W. Tian, *Org. Process Res. Dev.*, 2008, **12**, 512–521.

119   A. Chartoire, C. Claver, M. Corpet, J. Krinsky, J. Mayen, D. Nelson, S. P. Nolan, I. Pen Afiel, R. Woodward and R. E. Meadows, *Org. Process Res. Dev.*, 2016, **20**, 551–557.

120   P. Schuisky, H. J. Federsel and W. Tian, *J. Org. Chem.*, 2012, **77**, 5503–5514.

121   X. X. Shi, F. Ni, H.-X. Shang, M.-L. Yan and J.-Q. Su, *Tetrahedron Asymmetry*, 2006, **17**, 2210–2215.

122   L. Chen, E. Dovalsantos, J. Yu, S. Lee, S. O'Neill-Slawecki, M. Mitchell, S. Sakata and B. Borer, *Org. Process Res. Dev.*, 2006, **10**, 838–840.

123   S. Koul, R. Parshad, S. C. Taneja and G. N. Qazi, *Tetrahedron Asymmetry*, 2003, **14**, 2459–2465.

124   R. Zhu, Z. Xu, W. Ding, S. Liu, X. Shi and X. Lu, *Chinese J. Chem.*, 2014, **32**, 1039–1048.

125   M. Woods, U. C. Dyer, J. F. Andrews, C. N. Morfitt, R. Valentine and J. Sanderson, *Org. Process Res. Dev.*, 2000, **4**, 418–426.

126   U. T. Strauss, U. Felfer and K. Faber, *Tetrahedron: Asymmetry*, 1999, **10**, 107–117.

127   R. Ren, D. Sun, T. Wei, S. Zhang and J. Gong, *Org. Process Res. Dev.*, 2014, **18**, 709–716.

128   *Canadian Pat.*, 2960667, 2017.

129   P. Ferraboschi, M. De Mieri, P. Grisenti, M. Lotz and U. Nettekoven, *Tetrahedron Asymmetry*, 2011, **22**, 1626–1631.

130   G. Lunn and E. B. Sansone, *J. Org. Chem.*, 1986, **51**, 513–517.

131   P. D. Bailey, G. R. Brown, P. Korber, A. Reed and R. D. Wilson, *Tetrahedron: Asymmetry*, 1991, **2**, 1263–1282.

132   Q. H. Sohrab Rohani, J. Zhu and H. Gomaa, *Am. Chem. Soc.*, 2010, **10**, 1633–1645.

133   L. Biancalana, M. Bortoluzzi, E. Ferretti, M. Hayatifar, F. Marchetti, G. Pampaloni and S. Zacchini, *RSC Adv.*, 2017, **7**, 10158–10174.

7 Appendix

7.1 X-Ray Crystallography Data

(a) Ethyl-4-methylpiperidine-2-carboxylate p-toluenesulfonate
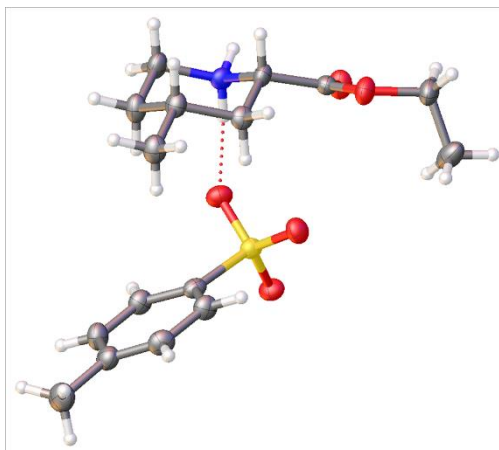
Identification code	NP82B
Empirical formula	$C_{16}H_{25}NO_5S$
Formula weight	343.43
Temperature/K	125.01(10)
Crystal system	orthorhombic
Space group	$P2_12_12_1$
a/Å	8.5547(4)
b/Å	11.0863(5)
c/Å	18.1594(10)
α/°	90
β/°	90
γ/°	90
Volume/Å^3	1722.23(15)
Z	4
ρ_{calc}g/cm^3	1.325
μ/mm^{-1}	1.885
F(000)	736.0
Crystal size/mm^3	0.12 × 0.04 × 0.02
Radiation	CuKα (λ = 1.54184)
2Θ range for data collection/°	9.346 to 147.246
Index ranges	-10 ≤ h ≤ 9, -13 ≤ k ≤ 12, -15 ≤ l ≤ 21
Reflections collected	6618
Independent reflections	3354 [R_{int} = 0.0570, R_{sigma} = 0.0798]
Data/restraints/parameters	3354/0/220
Goodness-of-fit on F^2	1.049
Final R indexes [I>=2σ (I)]	R_1 = 0.0504, wR_2 = 0.1091
Final R indexes [all data]	R_1 = 0.0649, wR_2 = 0.1159
Largest diff. peak/hole / e Å^{-3}	0.22/-0.53

(b) Ethyl-4-methylpiperidine-2-carboxylate benzoate
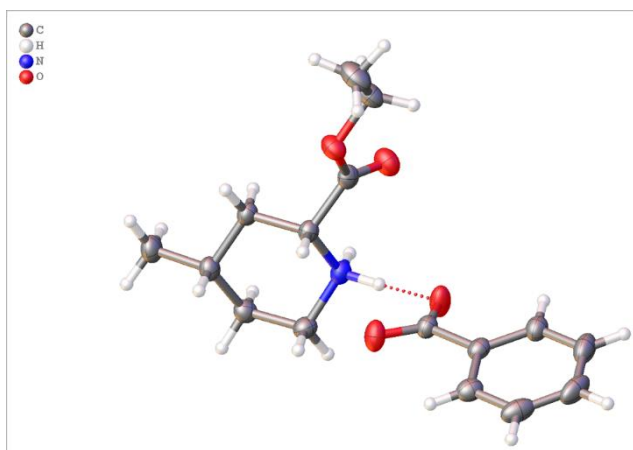
Identification code	NP2_180d
Empirical formula	$C_{16}H_{23}NO_4$
Formula weight	293.35
Temperature/K	130.01(10)
Crystal system	monoclinic
Space group	$P2_1/n$
a/Å	11.9712(2)
b/Å	9.29500(10)
c/Å	14.1933(2)
α/°	90
β/°	92.6770(10)
γ/°	90
Volume/Å^3	1577.60(4)
Z	4
ρ_{calc}g/cm^3	1.235
µ/mm^{-1}	0.721
F(000)	632.0
Crystal size/mm^3	0.44 × 0.37 × 0.34
Radiation	Cu Kα (λ = 1.54184)
2Θ range for data collection/°	11.384 to 145.516
Index ranges	-14 ≤ h ≤ 14, -11 ≤ k ≤ 10, -15 ≤ l ≤ 17
Reflections collected	13422
Independent reflections	3044 [R_{int} = 0.0243, R_{sigma} = 0.0167]
Data/restraints/parameters	3044/0/200
Goodness-of-fit on F^2	1.040
Final R indexes [I>=2σ (I)]	R_1 = 0.0395, wR_2 = 0.0990
Final R indexes [all data]	R_1 = 0.0423, wR_2 = 0.1012
Largest diff. peak/hole / e Å^{-3}	0.23/-0.17